Springer Theses
Recognizing Outstanding Ph.D. Research

Anja Schmidt

Modelling Tropospheric Volcanic Aerosol

From Aerosol Microphysical Processes to Earth System Impacts

Springer

Springer Theses

Recognizing Outstanding Ph.D. Research

For further volumes:
http://www.springer.com/series/8790

Aims and Scope

The series "Springer Theses" brings together a selection of the very best Ph.D. theses from around the world and across the physical sciences. Nominated and endorsed by two recognized specialists, each published volume has been selected for its scientific excellence and the high impact of its contents for the pertinent field of research. For greater accessibility to non-specialists, the published versions include an extended introduction, as well as a foreword by the student's supervisor explaining the special relevance of the work for the field. As a whole, the series will provide a valuable resource both for newcomers to the research fields described, and for other scientists seeking detailed background information on special questions. Finally, it provides an accredited documentation of the valuable contributions made by today's younger generation of scientists.

Theses are accepted into the series by invited nomination only and must fulfill all of the following criteria

- They must be written in good English.
- The topic should fall within the confines of Chemistry, Physics, Earth Sciences, Engineering and related interdisciplinary fields such as Materials, Nanoscience, Chemical Engineering, Complex Systems and Biophysics.
- The work reported in the thesis must represent a significant scientific advance.
- If the thesis includes previously published material, permission to reproduce this must be gained from the respective copyright holder.
- They must have been examined and passed during the 12 months prior to nomination.
- Each thesis should include a foreword by the supervisor outlining the significance of its content.
- The theses should have a clearly defined structure including an introduction accessible to scientists not expert in that particular field.

Anja Schmidt

Modelling Tropospheric Volcanic Aerosol

From Aerosol Microphysical Processes to Earth System Impacts

Doctoral Thesis accepted by
the University of Leeds, United Kingdom

Springer

Author
Dr. Anja Schmidt
School of Earth and Environment
University of Leeds
Leeds
UK

Supervisors
Prof. Dr. Ken Carslaw
School of Earth and Environment
University of Leeds
Leeds
UK

Prof. Dr. Marge Wilson
School of Earth and Environment
University of Leeds
Leeds
UK

Prof. Dr. Thor Thordarson
School of GeoSciences
Grant Institute University of Edinburgh
Edinburgh
UK

ISSN 2190-5053 ISSN 2190-5061 (electronic)
ISBN 978-3-642-34838-9 ISBN 978-3-642-34839-6 (eBook)
DOI 10.1007/978-3-642-34839-6
Springer Heidelberg New York Dordrecht London

Library of Congress Control Number: 2012952685

Printed on acid-free paper

Springer is part of Springer Science+Business Media (www.springer.com)

Parts of this thesis have been published in the following journal articles:

Schmidt A; Carslaw KS; Mann GW; Wilson M; Breider TJ; Pickering SJ; Thordarson T (2010) The impact of the 1783-1784 AD Laki eruption on global aerosol formation processes and cloud condensation nuclei, ATMOSPHERIC CHEMISTRY AND PHYSICS, 10, pp. 6025–6041. doi: 10.5194/acp-10-6025-2010

Schmidt A; Ostro B; Carslaw KS; Wilson M; Thordarson T; Mann GW; Simmons AJ (2011) Excess mortality in Europe following a future Laki-style Icelandic eruption, PROCEEDINGS OF THE NATIONAL ACADEMY OF SCIENCES OF THE UNITED STATES OF AMERICA, 108, pp.15710–15715. doi: 10.1073/pnas.1108569108

Schmidt, A; Carslaw, KS; Mann, GW; Rap, A; Pringle, KJ; Spracklen, DV; Wilson, M; and Forster, PM (2012): Importance of tropospheric volcanic aerosol for indirect radiative forcing of climate, ATMOSPHERIC CHEMISTRY AND PHYSICS, 12, 7321–7339, doi:10.5194/acp-12-7321-2012, 2012

Supervisor's Foreword

Lítilla sanda lítilla sæva;	A little sand has a little sea,
lítil eru geð guma;	And small are the minds of men;
því allir men urðu-t jafnspakir;	Though all men are not equal in wisdom,
hálf er öld hvar.	Yet half-wise only are all.
Hávamál	Translated by Henry Adams Bellows

It seems appropriate to begin my introduction of this thesis on Icelandic volcanism with some wise words from Icelandic poetry. There are several translations of the Hávamál, all with slightly different interpretations. My intention is to highlight the gains in knowledge that can be made when students set out to tackle a scientific question that requires collaboration across traditional scientific disciplines. In the study of volcanic effects on the environment and society, one scientific discipline can take you only so far. To fully understand the impact requires collaboration, in this case among the author (by training a geologist, but through her Ph.D. now also an atmospheric scientist), volcanologists, climate scientists, and even epidemiologists. In the words of Hávamál, each is only half-wise, but together, and with Anja's vision, it has been possible to form a more complete and fascinating picture of how volcanism impacts our climate and ourselves.

Anja Schmidt's thesis is a unique and comprehensive evaluation of the impacts of tropospheric volcanic aerosol on the atmosphere, climate, air quality, and human health. Using a state-of-the-art global aerosol model, the thesis describes and quantifies the impact of volcanic sulfur emissions on global aerosol properties, clouds, and the radiative forcing of climate. The advanced model enables an estimate of the impact of the emissions on aerosol microphysical properties such as particle number concentrations and sizes. The result is an improved ability to quantify the climate and air quality effects of volcanic emissions.

There are several important advances made in this thesis. First, it is shown that worldwide continuously degassing volcanoes exert a major effect on global clouds and climate. In a follow up paper, the results have been extended to show that degassing volcanoes are a major source of uncertainty in our estimates of

human-induced climate change. Second, the impact of the 1783 Laki eruption in Iceland is re-examined to show that this long-lasting flood lava eruption would have had major effects on clouds and climate. Third, by combining the research on volcanism, atmospheric science, and epidemiology, it is shown that a present-day Laki-style eruption would seriously affect European air quality and cause over 100,000 premature deaths in the first year. As a result, future large eruptions are being considered seriously as a major public health hazard.

This thesis will be of interest to scientists from the geological, atmospheric, health, and policy communities. With these audiences in mind, the introductory material and explanations of specialist terms are presented in such a way as to be accessible to a wide range of readers. As a result of this thesis one more scientist has learned the ability to work across disciplines. Hopefully, by reading this thesis many more scientists will see the importance of the connections.

As Anja Schmidt's supervisor I would like to personally thank colleagues who provided the necessary interdisciplinary expertise, but especially Marjorie Wilson, Thorvaldur Thordarson, Bart Ostro, and Piers Forster. We are each half-wise, but together, through a good student, we get closer to being fully wise.

Leeds, UK, 2012 Ken Carslaw

Acknowledgments

First and foremost I would like to express my most sincere gratitude to my supervisors, Ken Carslaw and Marge Wilson, whose willingness to supervise across the disciplines made pursuing such a project a highly valuable and enjoyable experience for me. I highly value their supportive, motivating, and direct way of supervision which allowed me to work freely and creatively knowing that I would receive their full support and guidance whenever needed. Also, I would like to express my special thanks to Marge who, following my Erasmus year, strongly encouraged me to outline my own Ph.D. project and compete for a University of Leeds Research Scholarship.

Second, I would like to express my gratitude to Thor Thordarson who has shown great interest in this project ever since the 2008 Laki field trip in Iceland. I am utmost grateful for his guidance regarding the Laki model set-up and many in-depth discussions about Laki and the wealth of contemporary accounts. Moreover, I owe him the pleasure of spending hours right in front of Fimmvörduháls, which was highly inspiring and educational.

Furthermore, I would like to extend my most sincere gratitude to Graham Mann who patiently guided me through "the world of pain" (aka IDL). I highly value his support in running GLOMAP and our many fruitful discussions regarding my results.

Kirsty Pringle, Steven Pickering, and Matt Woodhouse have been great in providing support in running GLOMAP-mode. Moreover, I am grateful to Tom Breider who developed the coupled chemistry version of TOMCAT and provided helpful insights during the early stages of running the model. Both Matt and Nigel Richards deserve a big thanks for their help with IDL.

This project benefited a lot from the fact that people such as Bart Ostro readily showed an interest in my work and shared their expert knowledge. I am utmost thankful to Bart, who patiently answered many questions I had regarding the Laki mortality study. I would also like to express my gratitude to Adrian Simmons who also readily provided meteorological datasets for the Laki mortality study.

I am also grateful to Piers Forster, Joonas Merikanto, Alan Haywood, Martyn Chipperfield, Bernd Kärcher, Gera Stenchikov, Hans Graf, Bob Andres,

and Peter Baxter, who showed great interest in my research and with whom I had some really fruitful discussions.

Pursuing this Ph.D. would have been only half the fun without my colleagues at ICAS and my friends. A special mention to my best mates and partners in crime Jon Poulter, Matt Woodhouse, and Eimear Dunne, who shared the ups and downs of life as a Ph.D. student.

Besonderer Dank gilt meinen Eltern, Elvira und Peter, für ihre Unterstützung, Ermutigung und die zahlreichen Kehrpakete.

Last but not least I would like to express my special thanks to Kay for his incredible patience and selfless support throughout.

Contents

Abbreviations

AIE	Aerosol Indirect Effect
AF	Attributable Fraction
AK1998	Andres & Kasgnoc (1998) emission inventory
CDNC	Cloud Drop Number Concentration(s)
CI	Confidence Interval
C-R functions	Concentration-Response functions
DJF	December–January–February
ECMWF	European Centre for Medium-Range Weather Forecasts
ER	Excess Risk
GISS modelE	Goddard Institute for Space Studies modelE
GLOMAP	GLObal Model of Aerosol Processes
IPCC	Intergovernmental Panel on Climate Change
ISCCP	International Satellite Cloud Climatology Project
JAS	July–August–September
JFM	January–February–March
JJA	June–July–August
L-s	Summertime Laki eruption
L-w	Wintertime Laki eruption
NH	Northern Hemisphere
PM2.5	Particulate Matter with diameters smaller than 2.5 micrometres
RR	Relative Risk
SH	Southern Hemisphere
STOCHEM model	STOchastic CHEMistry model
UK	United Kingdom
UKCA model	United Kingdom Chemistry-Aerosol-climate model
WHO	World Health Organization

Chapter 1
Motivation and Background

" ... the sun appeared as a red ball of fire,
the moon was as red as blood, and when rays of their
light fell upon the earth it took on the same colour."
Jón Steingrímsson, 1783

1.1 Motivation

In summer 1783 the French naturalist M. Mourgue de Montredon was the first to link the presence of a sulphurous aerosol cloud in the atmosphere over Europe to volcanic activity in Iceland. Shortly thereafter B. Franklin, J. L. Christ and C. G. Kratzenstein drew similar conclusions independently from each other (Thordarson and Self 2003 and references therein). Meanwhile, the Icelandic priest Jón Steingrímsson documented the eruption in question—the 1783–1784 AD Laki eruption—in extensive detail (Steingrímsson 1788, 1998). Modern "Volcanology" itself is a young science with the atmospheric phenomena observed during the summer of 1783 being considered as the starting point for scientific documentation of the effects of volcanic activity on atmospheric composition, climate and society.

Volcanic activity provides a natural source of pollutants such as sulphur dioxide (SO_2) or hydrogen sulphide (H_2S) to the atmosphere and thus has the potential to impact atmospheric composition and chemistry. In particular, since the 1991 explosive eruption of Mt. Pinatubo the scientific understanding of volcanic activity and its effects on the atmosphere and environment has advanced greatly. The Intergovernmental Panel on Climate Change (IPCC) recognises short-lived explosive volcanic activity as an important episodic source of natural pollutants and as a potential driver of climate change. However, the level of scientific understanding of more ancient volcanic eruptions is rated by the IPCC to be low (Forster et al. 2007).

A. Schmidt, *Modelling Tropospheric Volcanic Aerosol*, Springer Theses,
DOI: 10.1007/978-3-642-34839-6_1, © Springer-Verlag Berlin Heidelberg 2013

To date, it is stratospheric volcanic aerosol formed following short-lived explosive eruptions that has been studied the most, mainly due to theoretical work and the unique observational records gathered following the 1963 Agung, the 1980 Mt. St. Helens, the 1982 El Chichón and the 1991 Mt. Pinatubo eruptions (e.g., Lamb 1970; Pollack et al. 1976; Toon and Pollack 1980; Pollack and Ackerman 1983; Rampino and Self 1984; Robock and Mao 1992; Robock 2000). Moreover, Graf et al. (1997) among others recognised that volcanic SO_2 injected into the troposphere by continuously degassing and sporadically erupting volcanoes has a higher efficiency to form sulphate (SO_4) aerosol when compared to anthropogenic SO_2 emissions. Thus, continuously degassing and sporadically erupting volcanoes also have a great potential to affect atmospheric composition, atmospheric chemistry and the Earth's climate system (e.g., Mather 2008).

The 2010 eruption of the ice-capped Eyjafjallajökull volcano created awareness about the potential of volcanic activity in Iceland to impact Europe on a scale that not only has an economic impact but also affects people's day to day lives. In terms of both eruption size and duration the Eyjafjallajökull eruption can be considered as small and short-lived. However, its impact on the global economy and society was significant. Thordarson and Larsen (2007) have studied the recurrence frequency of Icelandic volcanic eruptions and found that there are on average 20–25 eruptions per century. Thus, studying high-latitude Icelandic eruptions is vital for hazard mitigation as these events will happen again.

The 1783–1784 AD Icelandic Laki eruption is the prime and best documented example of a long-lasting flood lava event which injected volcanic gases into the upper troposphere and lower stratosphere. Thordarson et al. (1996) and Thordarson and Self (1993, 2003) provided the first comprehensive review of the Laki eruption in a form that enables numerical studies to be conducted. Numerical simulations of volcanic eruptions are one of the key tools for assessing the cause-and-effect mechanisms induced by volcanic eruptions. Furthermore, simulating volcanic eruptions tests and advances the capabilities of the numerical models employed, which is regarded as vital for evaluating the effects of man-made climate change using these same models (e.g., Robock 2000).

Despite recent advances (e.g., Robock 2000; Mather et al. 2003; Textor et al. 2004; Timmreck et al. 2009, 2010), there is a clear need to better understand the microphysical processes driving the formation and removal of volcanic aerosol and ash in general, and of tropospheric volcanic aerosol in particular. Moreover, little research has been done to quantify the potential health hazards and impact on society arising from, for example, a future Laki-style eruption. In order to enhance our understanding of man-made climate change there is a need to better quantify and separate the natural direct and indirect effects on the radiation balance of the atmosphere from those that are anthropogenically induced. Employing a sophisticated global aerosol microphysics model in order to investigate the atmospheric, climatic, environmental and societal effects induced by long-lasting flood lava volcanism thus tests and advances current understanding. Such a study further creates awareness of the potential Earth

Fig. 1.1 Distribution of active and dormant volcanoes (*red dots*) on Earth in relation to the major tectonic plates. Figure from Schmincke (2004)

system effects caused by these natural hazards which is vital for mitigating the effects of future eruptions.

A glossary explaining the most relevant terminology across the disciplines is provided at the end of this thesis.

1.2 Volcanic Activity on Earth

Volcanic activity on Earth varies in time, space and eruption style. Some 218 subaerial volcanoes have been active at least once since 1964 (Andres and Kasgnoc 1998), 380 volcanoes are known to have erupted in the last century and more than 1,500 volcanoes are known to have erupted during the last 10,000 years (McClelland et al. 1989). According to the Smithsonian's Global Volcanism Program[1] 62 volcanic eruptions occurred between January and September 2010. Figure 1.1 shows the spatial distribution of volcanoes on Earth, which is not random but strongly correlated with plate tectonics, allowing one to distinguish three volcano-tectonic settings:

(a) **subduction zone volcanism** (convergent plate boundary): eruptions are often explosive in nature due to the high volatile content of the predominantly andesitic or dacitic magmas;
(b) **intraplate volcanism** (hot-spot or mantle plume volcanism): areas of anomalously high magma production that are pre-dominantly associated with basaltic magmas and their differentiates;

[1] http://www.volcano.si.edu/world/find_eruptions.cfm

(c) **mid-ocean ridge or rifting area volcanism** (divergent boundary): representing, volumetrically, the dominant type of magmatism on Earth, accounting for around 70 % of global magma production (McBirney 1984) dominated by submarine outpourings of volatile-poor basaltic magma.

Depending on their tectonic setting volcanoes are often characterised by a particular volcanic eruption style. A volcanic eruption can consist of single or multiple short-lived (i.e. days) explosive phases (referred to as an "explosive eruption") during which the magma is violently fragmented (due to the expansion of dissolved gases or the interaction of the magma with water) or it can exhibit longer-lived (i.e. months to years), more quiet, outpourings of magma forming lava flows (referred to as an "effusive eruption"). However, volcanic eruptions often comprise a mixture of both effusive and explosive styles (often referred to as "mixed eruptions"). It is the volatiles released during explosive volcanic eruptions that are most likely to reach the stratosphere. Moreover, explosive volcanic activity often produces large quantities of volcanic ash due to the violent fragmentation of volatile-rich magma. Effusive volcanic eruptions on the contrary are characterised by more quiescent outpourings of predominantly mafic lava that typically has a high sulphur content (e.g., Haughton et al. 1974; Wallace and Carmichael 1992). The size of a volcanic eruption is usually expressed in terms of the volume (km^3) or the mass (kg) of magma produced during an eruption. In Iceland, an effusive eruption that yields a large magma volume ($>1\,km^3$) is referred to as a "flood lava eruption" (Thordarson and Larsen 2007)—an eruption type that often exhibits "fire fountaining" along a "fissure" or "fissure system". A fire fountain is created when basaltic magma exiting a fissure is disrupted into a spray, and a volcanic fissure is a fracture or crack at the surface along which the lava spray is ejected.

1.2.1 1783–1784 AD Laki Flood Lava Eruption

In Iceland, the 1783–1784 AD Laki flood lava eruption is also known as "Skaftáreldar" which translates to "Skaftár Fires" with "Skaftár" denoting the fact that the Laki lava flooded into the Skaftár-river gorge (Thordarson and Self 1993). The Laki eruption is by far the best documented historic flood lava eruption with key parameters such as duration, onset of explosive activity phases, eruption column heights and amount of volatiles released into the atmosphere well constrained (Thordarson and Self 2003). Thordarson and Larsen (2007) have found that at least four volcanic events which produced magma volumes characteristic of Icelandic flood lava eruptions have taken place in Iceland (1783–1784 AD Laki, 12th Century Frambruni, 934–40 Eldgjá and ~900 AD Hallmundarhraun). Two of these events (i.e. 1783–1784 AD Laki and 934–40 Eldgjá) featured distinctive explosive episodes of sub-Plinian intensity.

The Laki fissure system is 27 km long and is part of the Grímsvötn volcanic system (Fig. 1.2) in southern Iceland (Jakobsson 1979). Since the beginning of the Holocene, the Grímsvötn volcanic system has yielded a total eruptive magma volume of around

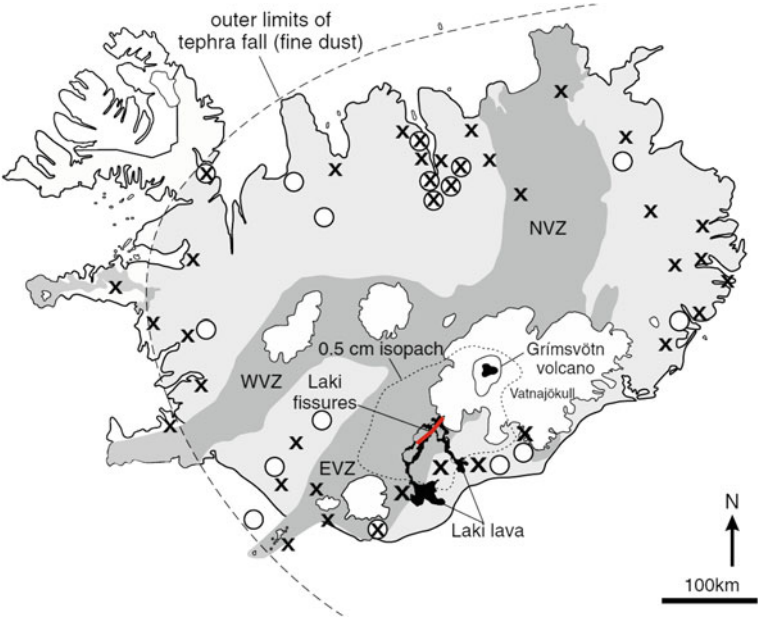

Fig. 1.2 Geological setting of the 1783–1784 AD Laki fissures (*red line*) and lava flow (*black*) with active volcanic zones in Iceland shown in *dark grey* (with WVZ = Western Volcanic Zone, EVZ = Eastern Volcanic Zone, and NVZ = Northern Volcanic Zone). Also shown are the outer limits and the 0.5 cm isopach (i.e. line of equal *thickness*) of the Laki tephra fall with *open circles* indicating locations where the fall of fine tephra was reported. Large crosses indicate locations where the loss of large amounts of livestock (within 2–14 days of the onset of the eruption) was reported. Figure from Thordarson and Self (2003)

55 km^3. Half of that volume was produced by six fissure eruptions which took place in the ice-free part of the volcanic system. Of these six fissure eruptions, Laki yielded a total eruptive volume of 15.1 km^3 (Thordarson and Self 1993); i.e. 30 % of the total Holocene eruptive magma volume. Out of the total eruptive volume of 15.1 km^3, lava flows account for 14.7 $km^3 \pm 1$ km^3 with the remainder (0.4 km^3) being tephra fall. For comparison, the 1991 Mt. Pinatubo eruption produced a tephra volume of around 5 km^3 (dense-rock equivalent) (e.g., Gerlach et al. 1996). The composition of the lava erupted during Laki was predominantly a quartz-tholeiite basalt (Sigmarsson et al. 1991; Thordarson et al. 1996).

Thordarson and Self (1993) have reconstructed the course of the Laki eruption using contemporary descriptions of the eruption combined with tephra stratigraphy. The eruption commenced on 8th June 1783 and lasted for eight months until 7th February 1784. The eruption featured episodic activity with ten so-called "eruption episodes" occurring during the first five months of activity (Thordarson and Self 1993, 2003). Each of these ten eruption episodes (indicated by the numerals I–X in Fig. 1.3) was associated with the opening of a new fissure segment which was

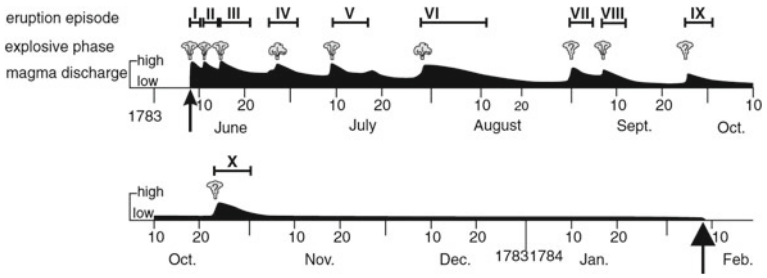

Fig. 1.3 Sequence of events during the 1783–1784 AD Laki eruption with eruption episodes indicated by the numerals I–X (with *horizontal bars* indicating the duration of each eruption episode). The occurrence of explosive phases is indicated by *eruption clouds* and the magma discharge rate is represented by the *black curve*. Figure from Thordarson and Self (2003)

accompanied by a short-lived (0.5–4 days) explosive phase followed by a longer-lived phase of Hawaiian-type fire fountaining and degassing from the lava flows. The explosive phases featured violent Strombolian to sub-Plinian-type activity during which volcanic gases were lofted high into the upper troposphere and lower stratosphere. During peak activity, the eruption column above the vents reached heights of between 9 and 13 km (Thordarson and Self 1993), thus reaching the lower stratosphere above Iceland (the tropopause in Iceland is situated at around 11 km during summer). The estimates of the eruption column heights are in agreement with eruption column models (e.g., Woods 1993); however it is important to note that the injection height is important for determining the lifetime of both the gaseous SO_2 released and the SO_4 aerosol formed. Stevenson et al. (2003b) simulated the Laki eruption using three different assumptions about the SO_2 injection height (and about the split between the amount of volatiles released from the vents and lava flows) and found differences in the annual mean lifetimes of around ten days for SO_2 and around three days for SO_4. Volatiles released from the Laki lava flows are considered to have been confined to the boundary layer, consistent with the pattern of volatile release from lava flows on Hawaii. The height of the fire fountains reached up to 1450 m during peak activity phases as opposed to 200–600 m during repose phases (Thordarson and Self 1993; Thordarson et al. 1996).

Figure 1.3 also shows that the temporal spacing between each successive eruption episode increased during the course of the eruption. During the first 1.5 months the eruption was most vigorous yielding around 60 % of the total eruptive volume by the end of eruption episode V. By the end of eruption episode X in October 1783, around 93 % of the total eruptive volume had been expelled. The remaining three months of the eruption did not feature any explosive phases, but rather quiescent degassing from the lava flows.

In order to constrain a volatile release budget, Thordarson et al. (1996) studied the major element and volatile composition of glass inclusions and groundmass glass in the quenched products of the Laki eruption—a method referred to as “the

petrological method". Thordarson et al. (1996) estimated the total volatile release of the Laki eruption as follows: ~122 Tg of SO_2, 235 Tg of H_2O, 15 Tg of Cl, and 7 Tg of HF. Around 80 % of the total SO_2 mass was released at the vents, equating to ~98.5 Tg of SO_4, with the remainder of ~23.5 Tg SO_2 being released from the lava flows (Table 1.1 for details), which is referred to as "two-stage degassing model" (Thordarson et al. 1996; Thordarson and Self 2003). The strength of the SO_2 venting correlates with peak activity phases at the onset of each of the ten eruption episodes during which the bulk of the volatiles was released (Fig. 1.3). Around 96 % of the total volatile mass was released by the end of the fifth month of the eruption. It is worth noting that eruption episodes I to III released a total of around 40 Tg of SO_2 during the course of eight to ten days, whereas only about 4 Tg of SO_2 in total was released from the vents during the last three months of the eruption. Further details on the temporal resolution of the volatile release for each eruption episode are shown in Table 1.1. T. Thordarson (pers. communication, 2008) compiled and provided the volatile release data set used in this thesis on the basis of the studies by Thordarson et al. (1996) and Thordarson and Self (1993, 2003). Table 1.1 lists the best estimate available for the purpose of a modelling study; however it should be noted that uncertainties of ±20 % are commonly associated with that estimate.

Thordarson and Self (2003) estimated (on a theoretical basis) that the total of 122 Tg of SO_2 emitted would yield an SO_4 aerosol mass of around 200 Tg, assuming that all of the SO_2 is converted to SO_4 and a composition of 75 wt% of H_2SO_4 and 25 wt% of H_2O which is commonly assumed for stratospheric volcanic SO_4 aerosol (Hamill et al. 1977, see also Sect. 1.4.3).

Table 1.1 Overview of 1783–1784 AD Laki eruption episodes, duration of eruption episodes, timing of the peak and total SO_2 release (in Tg of SO_2), and total SO_2 release from the Laki vents as reconstructed by Thordarson et al. (1996)

Eruption episode	Episode duration	Timing of peak SO_2 emission	Total SO_2 released, Tg	SO_2 released at vents, Tg
I	8–10 Jun	8 Jun	10.3	8.3
II	11–13 Jun	11–12 Jun	16.7	13.5
III	14–21 Jun	14–15 Jun	23.2	18.7
IV	25 Jun–1 Jul	26–28 Jun	13.4	10.8
V	9–21 Jul	9–10 Jul	11.0	8.9
VI	29 Jul–9 Aug	29–30 Jul	16.3	13.2
VII	31 Aug–4 Sep	31 Aug?	9.6	7.7
VIII	7–14 Sep	7 Sep	7.3	5.9
IX	24–29 Sep	24–25 Sep	5.4	4.4
X	25–30 Oct	25 Oct	3.6	2.9
last 3 months	1 Nov 1783 – 7 Feb 1784	–	5.1	4.1
total			**121.9**	**98.4**

Table modified after Thordarson and Self (2003)

Thordarson and Self (2003) not only provided a detailed analysis and quantification of the volatiles released during the Laki eruption but also a comprehensive review of the first and last occurrence, transport and physical properties of the volcanic SO_4 aerosol haze reviewing more than 130 contemporary documents. Chapter 4 will also examine how well the modelled spatial and temporal distribution of the Laki SO_4 aerosol compares to the observational record compiled by Thordarson (1995) and Thordarson and Self (2003).

1.3 Volcanic Gases

The abundances of gaseous species released during a volcanic eruption vary from volcano to volcano and often also during a volcanic eruption or between subsequent eruptions of the same volcano. The most abundant volatile species released during a volcanic eruption is water vapour (H_2O), contributing between 50 % and 90 % by volume of the gas phase (Textor et al. 2004 and references therein). The second most abundant species is carbon dioxide (CO_2), contributing between 1 % and 40 % by volume of the gas phase. Despite H_2O and CO_2 being the most abundant volatiles during volcanic eruptions their impact on atmospheric composition is thought to be negligible because of their insignificant relative contribution to the (high) atmospheric background concentrations of those two species. It is worth noting that a recent study by Joshi and Jones (2009) suggested that very large volcanic eruptions could inject sufficient quantities of H_2O into the lower stratosphere to cause a warming of the troposphere which outlasts the cooling induced by the stratospheric volcanic SO_4 aerosol. However, whether sufficient quantities of H_2O are indeed injected into the stratosphere during a volcanic eruption remains a matter of debate (Self 2009).

Sulphur (S) species contribute between 2 % and 35 % by volume of the gas phase and are typically most abundant in form of SO_2 and H_2S, with much lower abundances of molecular sulphur (S), carbonyl sulphide (COS) and carbon disulphide (CS_2) (Textor et al. 2004 and references therein). H_2S oxidises to SO_2 within a few hours to days; thus for most applications it is acceptable to consider SO_2 only. SO_2 is the sole species emitted by volcanoes which has clearly been demonstrated to have the potential to affect the climate system and to be an important oxidant in volcanic plumes (e.g., Robock 2000). However, since the detection of bromine oxide (BrO) radicals at Soufriéré Hills volcano on Montserrat (Bobrowski et al. 2003), halogens are also considered to also play an important role in volcanic plume chemistry (for a review see von Glasow et al. 2009). The main halogen compounds released during volcanic eruptions are hydrogen chloride (HCl) contributing 1–10 % by volume of the gas phase, hydrogen bromide (HBr) (contributing 10^{-3} % by volume of the gas phase), and hydrogen fluoride (HF) (contributing less than 10^{-3} % by volume of the gas phase) (Textor et al. 2004 and references therein). A number of other species such as nitrogen oxides and mercury are emitted during volcanic eruptions; however, there are only a few measurements of these compounds and their relevance for volcanic

plume chemistry and impact on atmospheric composition and chemistry is still under investigation (von Glasow et al. 2009 and references therein).

1.3.1 Time-Averaged Volcanic Sulphur Emissions

Subaerial volcanism is an important source of sulphur species to the atmosphere with estimates of the annual volcanic sulphur flux ranging from 0.75 Tg(S) per year (Kellogg et al. 1972) to 25.0 Tg(S) per year (Lambert et al. 1988) (see also review by Textor et al. 2004, Table 2). This compares to a sulphur flux of 13–36 Tg(S) per year from other natural sources such as dimethylsulphide (DMS), 1–6 Tg(S) from biomass burning and 0.4–5.6 Tg(S) from land biota and soils (Penner et al. 2001 and references therein). For comparison, the current anthropogenic sulphur flux is estimated to be around 58 Tg(S) per year (Smith et al. 2010).

Generally, subaerial volcanic sulphur fluxes vary temporally and spatially and two distinct volcanic activity states contribute to the total flux:

(a) **continuously degassing volcanoes** such as Mt. Etna in Italy or Mt. Erebus in Antarctica; and
(b) **sporadically erupting volcanoes** such as Popocatépetl in Mexico or Mt. Pinatubo in the Philippines.

Averaged over long time-scales (e.g. one year) it is the continuously degassing volcanoes that contribute most to the total volcanic sulphur flux to the troposphere, with an estimated 1 % contribution from sporadically erupting subaerial volcanoes (Andres and Kasgnoc 1998). It is important to note that volcanic sulphur emissions are often spatially distinct from major anthropogenic sulphur source regions (e.g., Graf et al. 1997); thus continuously degassing volcanoes often affect pristine atmospheric regions that are unaffected by anthropogenic SO_2 emissions.

Generally, there is great uncertainty regarding the magnitude of the volcanic sulphur flux, mainly a result of the differences in extrapolating and accounting for volcanoes that are not monitored (Textor et al. 2004). Nonetheless, time-averaged volcanic sulphur emission inventories are a useful tool for assessing the impact of volcanic sulphur emissions on tropospheric chemistry, composition and climate which subsequently allows distinguishing between the natural forcing and the anthropogenic forcing component.

Only a handful of studies (Chin and Jacob 1996; Graf et al. 1997; Stevenson et al. 2003a) have investigated how time-averaged volcanic sulphur emissions affect tropospheric chemistry and composition using General Circulation Models (GCMs) and Chemical Transport Models (CTMs), but have neglected aerosol microphysical processes.

1.4 Tropospheric Volcanic Aerosol

An "aerosol" is a suspension of solid or liquid particles in the air ranging in size from a few nanometres (nm) to around 100 micrometers (μm) in diameter (Seinfeld and Pandis 1998). In the atmosphere, aerosol particle number concentrations typically range from 130 particles per cubic centimetre (cm^3) in marine regions to 100,000 particles per cm^3 in urban areas (Seinfeld and Pandis 1998). Both natural and anthropogenic sources contribute to atmospheric aerosol concentrations. Aerosol that is injected directly into the atmosphere through mechanical processes (e.g. sea spray or soil dust) is termed "primary aerosol". In contrast, aerosol that is formed via the chemical conversion of gaseous precursors into liquid or solid particles (i.e. a process termed "gas-to-particle conversion") is referred to as "secondary aerosol".

Volcanic activity contributes to the total aerosol particle number concentration of the atmosphere in two ways: firstly, through gas-to-particle conversion of precursor species such as H_2SO_4 formed from SO_2 and secondly, through the direct emission of aerosol particles (mostly consisting of sulphuric acid, often called SO_4 aerosol) from the volcanic vent into the atmosphere (Allen et al. 2002). Once aerosol is present in the atmosphere it plays a key role in influencing the Earth's climate system due to the ability of particles to scatter and absorb solar radiation (e.g., Haywood and Boucher 2000; Carslaw et al. 2010) and to alter cloud microphysical properties (see Sect. 1.5.1 for more details). Volcanic aerosol can also affect marine and terrestrial ecosystems (e.g., Robock 2000; Carslaw et al. 2010 and references therein) and can pose a health hazard to humans when inhaled (e.g., Delmelle et al. 2002). Moreover, volcanic aerosol also plays an important role in global chemical cycles such as the sulphur cycle.

1.4.1 Tropospheric Sulphur Cycle

Sulphur compounds are emitted in gaseous form or as aerosol from natural sources such as marine phytoplankton, biomass burning, land biota and soils, and from anthropogenic sources such as fossil fuel burning and aircraft exhausts (Penner et al. 2001). In the troposphere, SO_2 commonly has a chemical lifetime of hours to a few days and if released into the stratosphere the chemical lifetime of SO_2 increases to several weeks (e.g., Bluth et al. 1992). Once in the atmosphere, SO_2 is removed via dry deposition or oxidised to form SO_4 aerosol. SO_2 can be oxidised by the OH radical (dry oxidation or gas-phase oxidation) to form sulphuric acid (H_2SO_4) vapour via a series of reactions (Pham et al. 1995):

$$SO_2 + OH + M \longrightarrow HSO_3 + M \tag{1.1}$$

$$HSO_3 + OH \longrightarrow SO_3 + H_2O \tag{1.2}$$

$$HSO_3 + O_2 \longrightarrow SO_3 + HO_2 \tag{1.3}$$

$$SO_3 + H_2O \longrightarrow H_2SO_4 \tag{1.4}$$

As H_2SO_4 is a low volatility compound it rapidly nucleates to form new aerosol or condenses onto existing aerosol.

Moreover, aqueous phase oxidation of SO_2 in cloud droplets or pre-existing aerosol forms SO_4 aerosol by reacting with dissolved hydrogen peroxide (H_2O_2) or ozone (O_3) (Seinfeld and Pandis 1998):

$$SO_2 + H_2O_2 \xrightarrow{(aq)} S(IV) + H_2O \tag{1.5}$$

$$SO_2 + O_3 \xrightarrow{(aq)} S(IV) + O_2 \tag{1.6}$$

Furthermore, existing aerosol such as volcanic ash particles can provide a surface for SO_2 to react onto—this process is referred to as "heterogeneous reaction" (Eatough et al. 1994). The heterogeneous uptake of SO_2 is an important oxidation pathway to consider for explosive, ash-producing volcanic eruptions (Eatough et al. 1994; Mather et al. 2003); however it is rarely treated in global models simulating volcanic eruptions.

Model calculations of the present-day sulphur cycle suggest that aqueous phase oxidation is the dominant oxidation pathway for anthropogenic SO_2 emissions (Penner et al. 2001). Stevenson et al. (2003a) have shown that aqueous phase oxidation of SO_2 by H_2O_2 dominates the gas-phase oxidation pathway when considering time-averaged volcanic sulphur emissions. Chapters 3 and 4 will explore the dominant oxidation pathways and their change when considering SO_2 emissions from continuously degassing and sporadically erupting volcanoes and large SO_2 perturbations following the onset of the 1783–1784 AD Laki eruption.

Sulphate aerosol commonly has an atmospheric residence time of 4.9 days under present-day atmospheric conditions (Penner et al. 2001). In comparison, Stevenson et al. (2003a) have found that the residence time of volcanic SO_4 in the troposphere is on the order of six days. For comparison, volcanic SO_4 aerosol has a chemical lifetime of around one year in the stratosphere (e.g., Barnes and Hofmann 1997; Robock 2000).

The main sink for SO_4 aerosol is wet deposition which—at high concentrations referred to as "acid rain"—can have a profound effect on the environment.

1.4.2 Aerosol Particle Size Distribution

One of the most important characteristics of any aerosol population is the particle size distribution, which ultimately determines how aerosol will be cycled through

the atmosphere and how it will scatter solar radiation and affect clouds. Moreover, the particle size distribution allows us to draw conclusions on the processes involved in the formation of the aerosol population. Figure 1.4 shows typical size ranges of volcanic aerosol with respect to its volume distribution (Durant et al. 2010). Measurements of volcanic particle size distributions reveal a multi-modal shape of the size distribution, suggesting that several microphysical processes play a role in forming volcanic aerosol (Watson and Oppenheimer 2001 and references therein). Thus, in order to assess the full complexity of the evolution of a volcanic aerosol cloud, numerical models need to allow for the size distribution to evolve freely instead of prescribing it. For example, Timmreck et al. (2009) have shown that following very large volcanic eruptions the aerosol optical properties (thus the impact on climate) will differ depending on the assumption made for the initial size distribution of stratospheric volcanic aerosol. Earlier numerical studies of volcanic aerosol (Pinto et al. 1989; Bekki et al. 1996) show that non-linear microphysical processes drive the temporal evolution of the size distribution emphasising the need for studies of microphysical processes following volcanic eruptions. Chapter 4 will explore the impact of the 1783–1784 AD Laki eruption on microphysical processes in the troposphere and additionally discuss the role of the season in which such an eruption commences.

Generally, the aerosol size distribution can be described by four so-called modes which are best represented by a log-normal distribution (Whitby 1978). As shown in Fig. 1.4 each mode is defined according to certain particle diameter (d_p) range with:

$d_p < 0.01\,\mu\text{m}$ = "nucleation" mode

$0.01 < d_p < 0.1\,\mu\text{m}$ = "Aitken" mode

$0.1 < d_p < 1.0\,\mu\text{m}$ = "accumulation" mode

$d_p > 1.0\,\mu\text{m}$ = "coarse" mode

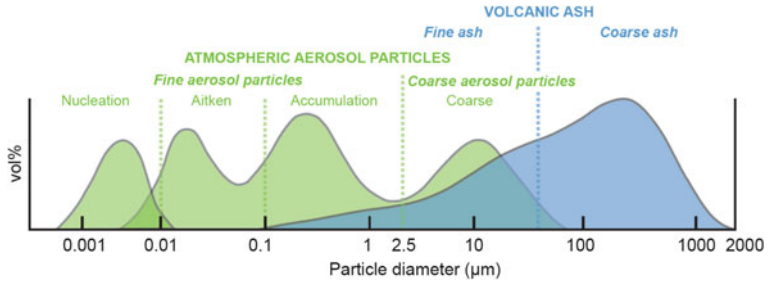

Fig. 1.4 Size range of volcanic particles with typical aerosol modes shown in *green*, and volcanic ash-sized particles shown in *blue*. Figure from Durant et al. (2010)

New particle formation (i.e. nucleation) produces particles with diameters smaller than 0.01 μm and occurs when the concentration of a volatile species such as H_2SO_4 vapour exceeds its equilibrium vapour pressure (Whitby 1978). Favourable conditions for nucleation are low ambient temperatures (reducing the equilibrium vapour pressure), low ambient surface area and high concentrations of condensibles (e.g., review by Kulmala et al. 2004). In volcanic plumes, Aitken and accumulation mode particles form due to the condensation of volatile species released from the magma and due to coagulation and condensation of nucleation mode-sized particles (Mather et al. 2003). Coarse mode particles result from the fragmentation of magma and erosion of lithic fragments from the vent wall—these particles are most commonly associated with explosive volcanic activity (Mather et al. 2003). However, for example, Rose et al. (1980) have reported a bimodal size distribution for airborne ash samples collected from three active volcanoes (Pacaya, Fuego and Santiaguito) with numerous sub-micron-sized crystal fragments being present.

Moreover, with distance from the vent the shape of the aerosol size distribution evolves as particles are cycled through the atmosphere (Hobbs et al. 1982; Rose et al. 1982). For example, particles in the coarse mode tend to be efficiently removed by gravitational settling (Raes et al. 2000), while high concentrations of nucleation and Aitken mode particles grow and coagulate to form larger accumulation mode particles. Particles in the accumulation mode are most relevant to climate as particles in this size range not only have a high scattering efficiency but also the longest atmospheric residence times. Moreover, accumulation mode particles are in the size range that poses the greatest risk to human health as such particles can penetrate deep into the lungs (e.g., Pope and Dockery 2006).

1.4.3 Particle Composition and Morphology

Chemical composition is another important aerosol property as it determines particle density and particle water uptake—atributes which ultimately control particle residence times in the atmosphere. Size-resolved chemical composition measurements of volcanic aerosol at, for example, Masaya volcano (Nicaragua) indicate highly acidic accumulation mode-sized aerosol consisting of soluble ions such as SO_4^{2-}, H^+, Na^+, K^+ and NH_4^+ (Mather et al. 2003). Information on particle composition is also vital for assessing the adverse health effect from volcanic particulates.

Commonly, the composition of volcanic SO_4 aerosol is assumed to comprise 75 wt% H_2SO_4 and 25 wt% H_2O (Hamill et al. 1977) which is in good agreement with infrared absorption measurements of the Mt. Pinatubo aerosol (Grainger et al. 1993). Throughout this thesis it is assumed that the volcanic aerosol exists as $H_2SO_4 \cdot 2\,H_2O$ which is equivalent to 73 wt% of H_2SO_4 and 27 wt% of H_2O.

The morphology of particles controls the efficiency of removal processes; for example Rose et al. (1983) have shown that glass-shards with sizes smaller than 50 μm from

the 1980 Mt. St. Helens eruption were rapidly removed by particle aggregation due to a high area-to-mass ratio.

1.4.4 Particle Activation

A subset of the entire aerosol population acts as "cloud condensation nuclei" (CCN)—the effectiveness of which is determined by the particle size, chemical composition, mixing state and ambient environment (e.g., Penner et al. 2001). Cloud condensation nuclei play an important role for cloud formation as they provide a surface for atmospheric water vapour to condense onto in order to from cloud droplets. Sulphates are water-soluble salts that are known to serve as CCN at low supersaturations (Penner et al. 2001); thus volcanic sulphur emissions likely provide an important source of climate-relevant CCN-sized particles in the atmosphere. However, the quantification of which is still very limited. Thus, numerical models such as GLOMAP-mode (Mann et al. 2010) used for this thesis provide an ideal tool for investigating the impact of volcanic sulphur emissions on the global CCN number concentration budget.

1.5 Impact of Volcanic Activity on the Earth System

Volcanic activity affects the Earth system in a variety of ways and on many different time-scales. The most profound effects concern the impact on weather, climate, environment and society. The 1963 Agung, 1980 Mt. St. Helens, 1982 El Chichón and 1991 Mt. Pinatubo eruptions greatly stimulated research to advance the understanding of short-lived explosive volcanic eruptions. However, we are only beginning to understand the role of longer-lived flood lava events and effusive volcanic eruptions injecting gases into the troposphere and/or lower stratosphere. The following section provides an overview of the current knowledge of the impact of volcanic emissions on the troposphere and of long-lived flood lava eruptions on the Earth system. A comprehensive review on short-lived explosive volcanic eruptions and stratospheric volcanic aerosol (not discussed in extensive detail within this thesis) is provided by Robock (2000).

1.5.1 Impact on Climate and Dynamics

As shown in Fig. 1.5, natural and anthropogenic aerosol influence the radiation budget of the Earth in two ways:

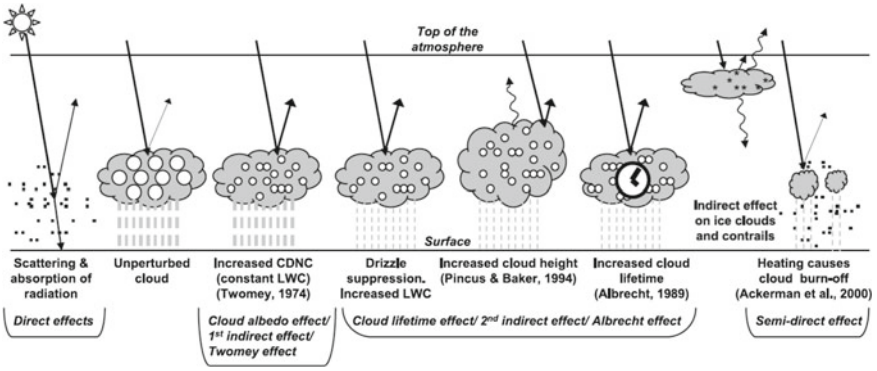

Fig. 1.5 Schematic representation of the aerosol direct and indirect effects. Aerosol are represented by the *small black dots* and cloud droplets are represented by different-sized *open circles*. *Straight lines* represent incoming and backscattered solar radiation, and *wavy lines* represent terrestrial radiation. *Vertical grey dashes* represent rainfall and LWC refers to liquid water content. Figure from Forster et al. (2007)

1. directly by scattering and absorbing incoming solar and thermal infrared radiation, which is referred to as the "**aerosol direct effect**" (e.g., Haywood and Boucher 2000)
2. indirectly by altering cloud microphysical properties thus modifying the optical properties and the lifetime of clouds, which is referred to as the "**aerosol indirect effects**" (e.g., Penner et al. 2001).

Sulphate aerosol essentially scatters across the entire solar spectrum with a small degree of absorption in the near-infrared spectrum due to its optical properties and typical particle radius of 0.5 μm (Penner et al. 2001 and references therein). Following a volcanic eruption SO_4 aerosol scatters incoming solar radiation back into space thereby exerting a negative top-of-the-atmosphere direct radiative effect which is expressed as cooling at the surface (see Fig. 1.6).

Graf et al. (1997) have investigated the effects of time-averaged tropospheric volcanic sulphur emissions on the atmospheric sulphur budget. Graf et al. (1997) showed that despite volcanic sulphur emissions being a factor of 4.5 lower than anthropogenic sulphur emissions, their contribution to the atmospheric SO_2 burden (i.e. the amount of a gaseous substance or particulates in the atmosphere at a given time) is only around 24 % less when compared to anthropogenic SO_2 emissions. This fractional contribution of volcanic sulphur emissions to the SO_2 burden can be explained with longer SO_2 lifetimes due to injection at higher altitudes compared to anthropogenic SO_2 emissions. Moreover, Graf et al. (1997) have shown that volcanic sulphur emissions have a factor of 4.7 higher SO_4 burden efficiency[2] when compared to anthropogenic sulphur emissions. Overall, the work by Graf et al. (1997) implies

[2] Graf et al. (1997) defined "SO_4 burden efficiency" as the fractional contribution of a sulphur source to the SO_4 burden divided by the fractional source strength.

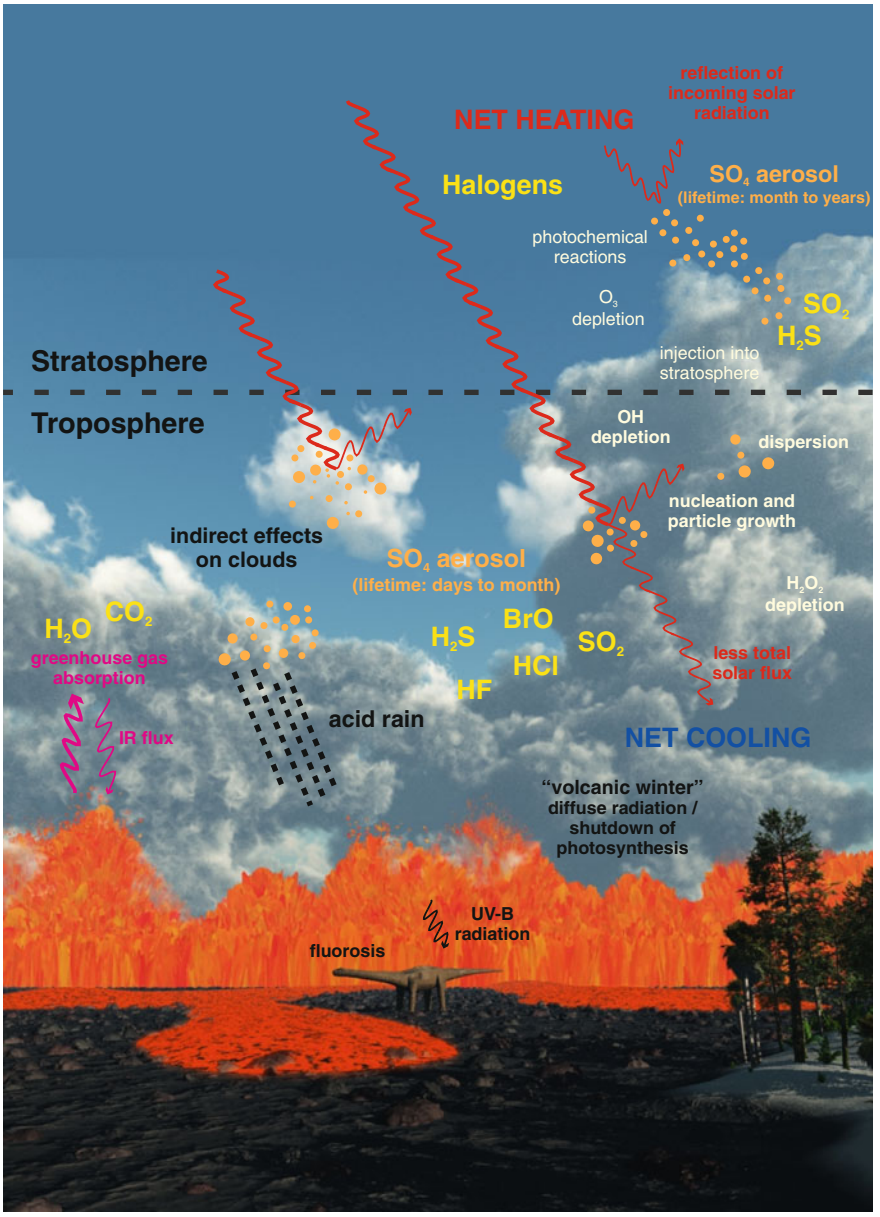

Fig. 1.6 Schematic presentation of the impacts of volcanic activity on atmospheric composition and chemistry, climate and the environment. Annotations made by the author, and underlying image drawn by Jonathan Poulter, Ph.D. student, University of Leeds

that the relative effect on radiation is greater for volcanic sulphur emissions compared to anthropogenic sulphur emissions. An earlier study by Chin and Jacob (1996) found a similarly high SO_4 burden efficiency for volcanic sulphur. Stevenson et al. (2003a) reported a similarly high SO_4 burden potential from volcanic sulphur emissions; however these authors found a lower contribution of volcanic sulphur to the atmospheric SO_4 burden compared to the studies of Chin and Jacob (1996) and Graf et al. (1997). The findings presented in Stevenson et al. (2003a) highlight a strong model-dependence of the results which is especially true for the parameterisation of vertical transport and aerosol-cloud interactions.

During the last decade, high-latitude flood lava eruptions have been recognised as having the potential to profoundly affect the climate system and the environment. Historic records of, for example, surface temperature changes following the 1783–1784 AD Laki eruption imply substantial effects on climate and atmospheric dynamics (Thordarson and Self 2003 and references therein). Reports from Iceland imply a severe 1783/84 winter with surface temperatures persistently below −15° C in western and northern Iceland. There are also indications that the summer of 1784 in Iceland was cold with overnight temperatures often dropping below freezing, and that the cold winter weather in Iceland prevailed until 1786 (Thordarson and Self 2003 and references therein).

Angell and Korshover (1985) used temperature records dating back to 1781 and found a NH annual mean temperature anomaly of −0.14° C relative to the five-year intervals before and after the Laki eruption. In Europe and North America, the winter of 1783/84 was one of the longest and coldest for 250 years according to several historical chronicles (Thordarson and Self 2003). Thordarson and Self (2003) investigated 29 weather station records from Europe and the north-eastern United States. These authors found, compared to the 31-year period from 1768 to 1798, a sharp cooling event of around −3° C during 1783–1784 followed by a 4-year-long, gradual recovery of the temperatures back to the mean state. The three years following the Laki eruption exhibit temperatures that are 1.3–1.4° C cooler than the 31-year mean. Further investigations of the weather station records also imply a high frequency of colder than average summers in Europe and the north-eastern United States for the years 1784, 1785, and 1786 (Thordarson and Self 2003). These findings are supported by results from the analysis of temperature-sensitive tree-ring density records from Alaska (D'Arrigo and Jacoby 1999). When reconstructing summer temperatures for 1783, Jacoby et al. (1999) found that the summer of 1783 was the coldest summer in over 400 years. An earlier study by Briffa et al. (1998) investigating tree-ring density changes found a less profound NH-mean cooling of -0.27 ± 0.3° C for 1783. Moreover, accounts from the Alaska Inuit community also imply unusual cold temperatures, noting that "summer did not arrive" and that the "big winter" lasted until April (i.e. most likely April 1784) (D'Arrigo and Jacoby 1999; Jacoby et al. 1999). Overall, the differences in temperature anomalies reported in the studies mentioned above imply that the surface temperature response following Laki was spatially not uniform. Thus, it might not be straightforward to use historical records of surface temperature changes for evaluating hemispheric mean surface temperature

changes simulated by means of numerical models. Recently, D'Arrigo et al. (2011) attributed the anomalously cold 1783/4 winter to natural variability (rather than Laki) namely to the occurrence of a negative North Atlantic Oscillation combined with an El Niño event in the Pacific (which is a similar meteorological situation to that during the winter of 2009/10). However, whether D'Arrigo et al. (2011)'s hypothesis holds, remains to be tested—ideally by means of an aerosol-chemistry-climate model such as UKCA.

Kington (1988) noted that July 1783 temperatures were above average in north, west and central Europe. Overall, there are implications that the unusual temperatures in July 1783 were caused by a persistent anticyclonic weather system affecting central and northern Europe (Kington 1988; Thordarson and Self 2003). Nonetheless, there is still some debate as to whether the onset of the Laki eruption on 8 June 1783 played a role in affecting temperatures during July 1783 (Thordarson and Self 2003).

To date, the impact of the Laki eruption on atmospheric chemistry and climate has been investigated using CTMs and GCMs. Stevenson et al. (2003b) were the first to study the atmospheric impact of the Laki eruption using the STOCHEM-ed CTM in the Hadley Centre's Unified Model GCM. Stevenson et al. (2003b) estimated that the eruption produced a total of 17–22 Tg(S) of SO_4 aerosol (=71–92 Tg of volcanic SO_4 aerosol assuming that the volcanic aerosol exists as $H_2SO_4 \cdot 2\,H_2O$). In a follow-up study, Highwood and Stevenson (2003) used the Reading Intermediate GCM in order to assess the direct radiative effects induced by the Laki SO_4 aerosol by using the SO_4 output fields from the Stevenson et al. (2003b) study. In the Highwood and Stevenson (2003) study, the Laki SO_4 aerosol affects the general atmospheric circulation due to changes in surface temperatures induced by the eruption; however, the changes in circulation are not fed back on to the aerosol distribution itself. Highwood and Stevenson (2003) calculated a relatively moderate mean northern hemisphere temperature anomaly of -0.21 K for the year 1783, which is slightly lower than the observations indicate. However, Highwood and Stevenson (2003) stressed that when considering the uncertainties and limitations of their study, the radiative effect following Laki could have been up to 1.6 times greater than predicted by their model. Chenet et al. (2005) modelled the spatial and temporal distribution of 200 Tg of SO_4 aerosol (a theoretical value of the SO_4 aerosol yield derived from Stothers (1996) and Thordarson and Self (2003)) using the LMDZT-INCA GCM and found general agreement with historic records of the first and last appearance of the Laki SO_4 aerosol haze as compiled by Thordarson and Self (2003). However, Chenet et al. (2005) did not reproduce the actual course of the eruption and simplified the SO_2 emission scenario; thus a detailed comparison with the aforementioned historical records is not possible. Oman et al. (2006a) used the Goddard Institute for Space Studies (GISS) modelE GCM coupled to an on-line sulphur CTM (Koch et al. 2006) in order to model the chemical transformation of around 122 Tg of SO_2 and the subsequent distribution of the Laki SO_4 aerosol. Oman et al. (2006a) estimated that the Laki eruption yielded between 163 and 166 Tg of volcanic SO_4 aerosol (assuming that the volcanic aerosol exists as $H_2SO_4 \cdot 2\,H_2O$) and calculated a substantial radiative perturbation with a peak top-of-atmosphere net radiative forcing of $-27\,W\,m^{-2}$

in August. Oman et al. (2006a) also calculated a peak in the global mean direct forcing of $-4\,\mathrm{W\,m^{-2}}$ for August 1783.

In an accompanying study, Oman et al. (2006b) assessed the climatic impact (i.e. by means of calculating the direct effect) of the Laki SO_4 aerosol and found a significant cooling of -1 to -3° C over most of the northern hemisphere (NH) during summer 1783. Moreover, as a result of the significant cooling induced by the eruption, Oman et al. (2006b) found a weakening of the Indian and African monsoon system, which in turn is associated with a significant warming of $+1$ to $+2^\circ$ C and precipitation anomalies of -1 to -3 mm per day (due to changes in cloud cover) over the Sahel of Africa. Oman et al. (2006b) also examined a long-term Nile river level record (Kondrashov et al. 2005) and concluded that high-latitude eruptions such as Laki and the 1912 Katmai eruption have the potential to induce precipitation anomalies resulting in anomalous low water discharge rates of the Nile and Niger rivers. Overall, the findings presented by Oman et al. (2006b) confirm the results of a study presented by Graf (1992) who investigated the effects of reduced incoming solar radiation north of 50° N which is likely to represent the aftermath of a strong volcanic eruption and found a weakening of the Asian summer monsoon. Moreover, by reviewing historical records of the aftermath of the Laki eruption, Thordarson (1995) and Thordarson and Self (2003) have found evidence that high-latitude eruptions may exert a very far-reaching impact on both the environment and the climate system. For example, these authors reported evidence for unusually cold summer temperatures as far away as China and Japan during 1783.

Robock (2002) highlighted the assessment of the indirect effects of volcanic aerosol on clouds as a research priority in a report for the 2002 AGU Chapman conference on "Volcanism and the Earth's atmosphere". As shown in Fig. 1.5, the aerosol indirect effects denote the ability of aerosol to induce changes in the microphysical properties of clouds. An increase in CCN number concentrations results (under the assumption that the liquid water content of a cloud is fixed) in cloud droplets to increase in their number concentration but to decrease in their size. This results in an overall increase in surface area, thereby reflecting incoming short-wave radiation more efficiently (because a larger cloud drop surface area increases the albedo of a cloud). This microphysically induced effect is referred to as the "first aerosol indirect effect" (Twomey 1974, 1977) or "cloud albedo effect" (e.g., Forster et al. 2007). Albrecht (1989) hypothesised that an increase in ambient aerosol concentrations leads to an increase in the lifetime of a cloud as the precipitation of smaller cloud drops is less efficient when compared to larger cloud drops—this effect is referred to as the "cloud lifetime effect" or "second aerosol indirect effect".

There are already several indications that volcanically derived particles act as CCN in the troposphere (e.g., Mather et al. 2004; Mather 2008), thus potentially altering cloud microphysical properties. Gassó (2008) noted that volcanic emissions injected into the lowermost troposphere during weak volcanic eruptions are "underreported", despite the fact that these emissions may exert a significant indirect radiative effect on low-level clouds. Gassó (2008) also presented the first observational evidence of

the impact of weak explosive volcanic eruptions on marine boundary layer clouds using satellite-retrieved microphysical properties of these volcano-clouds. Gassó (2008) showed that the volcanically-induced changes in cloud microphysical properties strongly depend on ambient conditions and the composition of the volcanic emissions, and concludes that the magnitude of the indirect effects induced by such eruptions remains to be assessed.

Highwood and Stevenson (2003) noted that the aerosol indirect effects induced by the Laki eruption were "potentially large", and assessed the indirect forcing for the first month following the onset of the eruption using an empirical calculation of the cloud drop number concentrations (CDNC). However, Highwood and Stevenson (2003) noted that at the time of their study the uncertainties were such that the indirect forcing was "unquantifiable". Assessing the aerosol indirect effects using numerical models is subject to a large uncertainty (Forster et al. 2007)—most GCMs use an observationally derived empirical relationship between CDNC and SO_4 mass (Boucher and Lohmann 1995; Feichter et al. 1997; Lohmann and Feichter 1997) or SO_4 number (Jones et al. 1994). Using empirical relationships between SO_4 mass and CDNC is suitable for overcoming computational limits. However, Ramanathan et al. (2001) have shown that the number of cloud drops varies spatially for a given aerosol number concentration, thus introducing large uncertainties when calculating global CDNC. Moreover, employing observed sulphate-CDNC relationships does not allow to quantify uncertainties in CDNC due to aerosol processes or aerosol size distribution. More recently, physically-based parameterisations have been introduced to calculate CDNC based on the Köhler theory using aerosol size distribution and chemical composition (Abdul-Razzak and Ghan 2002; Nenes and Seinfeld 2003). Overall, physically-based aerosol activation schemes are regarded as superior to mass-based relationships, as the former mechanistically account for the physical and chemical properties of the aerosol size distribution when deriving CDNC. The treatment of both aerosol microphysics and aerosol activation has now improved in models, allowing for a physically-based assessment of the first aerosol indirect effect induced by the Laki SO_4 aerosol. The results of employing a physically-based aerosol activation scheme together with a radiative transfer code will be presented in Chap. 5.

1.5.2 Impact on Environment and Society

Volcanic eruptions are a major natural hazard to life on Earth and the environment, thus monitoring volcanoes, predicting volcanic eruptions and mitigating volcanic hazards is important. The environmental hazards posed by volcanic eruptions include acid damage to crops and vegetation (e.g., Delmelle et al. 2002; Delmelle 2003) and fluorine poisoning of livestock and humans (e.g., Thorarinsson and Sigvaldason 1972; Hansell et al. 2006). For example, Grattan and Pyatt (1994) and Grattan (1998)

reported that the acidic air pollution following the Laki eruption posed a serious threat to remote ecosystems and vegetation, including crops and trees.

The presence of volcanic aerosol in the atmosphere can not only exert a climatic impact but also impact the environment. Gauci et al. (2008) investigated the combined impact of the surface cooling induced by the Laki SO_4 aerosol and the intensification of sulphur deposition during the eruption on the methane (CH_4) flux from wetlands. Gauci et al. (2008) found that the NH wetland CH_4 flux halved for the first twelve months of the eruption. It is also known that, under high atmospheric aerosol loadings, a large fraction of the incoming solar radiation is forward-scattered which results in enhanced downward diffuse radiation. For example, Mercado et al. (2009) used the JULES land-surface scheme in the Hadley Centre climate model and showed that following the 1991 Mt. Pinatubo eruption the terrestrial carbon sink was enhanced for around 2–3 years as a result of enhanced diffuse radiation increasing plant photosynthesis. Moreover, as discussed in Sect. 1.5.1, volcanic eruptions can induce changes in atmospheric circulation, which in turn can lead to droughts and crop failure in regions far away from the source of the eruption. For example, there are a number of reports of a severe droughts in China (Wang and Zhao 1981), Egypt (Hassan 1998) and India (e.g., Mooley and Pant 1981), and a severe famine in Japan (which, however, apparently started in 1782 AD) (e.g., Arakawa 1955), linked to the 1783–1784 AD Laki eruption.

The geological record reveals that the impact of very large-scale volcanic eruptions may even induce major cultural changes in a society. The prime example is the Thera eruption of Santorini (Greece, 3620 B.P.), which coincides with the end of the Minoan culture (e.g., Bond and Sparks 1976). Moreover, volcanic eruptions have the potential to threaten life to such a degree that species become extinct or come close to extinction. There are suggestions that the Toba eruption (Indonesia, ~74,000 B.P.) and the subsequently induced volcanic winter (Rampino et al. 1988) caused a so-called "bottleneck" in the human population count with only 4,000–10,000 individuals remaining for ~20,000 years (Rampino and Ambrose 2000, and references therein). Proposed volcanism-induced extinction mechanisms (see Fig. 1.6) are mainly based on the release of large amounts of volcanic gases over short time-scales (i.e. atmospheric loadings of > 1,000 Tg of SO_2 over a decade) (e.g., Thordarson and Self 1996; Self et al. 2008; Thordarson et al. 2009). The most commonly proposed volcanism-induced extinction mechanism is global surface cooling (following the conversion of 1,000–10,000 Tg of volcanic sulphur to SO_4 aerosol) coinciding with global darkness due to the presence of large amounts of volcanic aerosol. This scenario is known as "volcanic winter" (e.g., Rampino et al. 1988) and is thought to exert high levels of stress on the biosphere (e.g., Thordarson et al. 2009). Moreover, increased acid precipitation due to the presence of large amounts of SO_4 aerosol has been linked to severe ecosystem damage and ocean acidification (Wignall 2001 and references therein). Furthermore, there are suggestions that the depletion of oxidants such as OH, H_2O and O_3 induce complex atmospheric chemistry feedbacks (e.g., Pinto et al. 1989; Bekki 1995). The depletion of O_3 is thought to result in increased ultraviolet-B (UV-B) radiation which in turn induces damage to pollen to a

degree that germination is impaired (Visscher et al. 2004; Koti et al. 2005). McLean (1985) suggested that CO_2 released during the Cretaceous-Tertiary Deccan Trap flood basalt volcanism in India led to global warming which subsequently decreased the pH in the marine mixed layer, thus driving planktonic organisms into extinction by affecting a vital part of the food chain. However, Caldeira and Rampino (1990) used a global biochemical carbon-cycle model and estimated a long-term warming trend of less than 1° C resulting from the CO_2 emitted during the Deccan eruptions. Thus, Caldeira and Rampino (1990) concluded that CO_2 induced warming is too weak to cause a pH decrease in the mixed layer of the oceans. Beerling et al. (2007) used a 2-D Chemical Transport Model to suggest that the release of HCl and methyl chloride (CH_3Cl) during the 250 Ma Siberian Traps flood basalt volcanism caused mutagenic effects on plants through increased UV-B radiation resulting from O_3 depletion. However, the model used in their study does not account for the complexity of chemical feedbacks that play a role when SO_2 and SO_4 aerosol loadings are elevated (i.e. both species have the potential to absorb UV, thus limiting the radiative impact caused by O_3 depletion).

Nowadays, the impact of volcanic gases and particulates on human health is a major concern (e.g., Baxter et al. 1981; Baxter 1990; Delmelle et al. 2002; Hansell et al. 2006). It is well-known that volcanic eruptions can increase pollutant concentrations close to the source (e.g., Delmelle et al. 2002) which in turn can have a negative impact on health, as for example shown in a study in Hawaii (Hansell and Oppenheimer 2004 and references therein). Despite a range of pollutant measurements at several active volcanoes around the world there is little quantification of the disease burden associated with exposure to volcanic air pollution (Hansell and Oppenheimer 2004). Nonetheless, there is compelling evidence that the 1783–1784 AD Laki eruption not only caused environmental stress but also posed a health hazard far beyond the borders of Iceland (e.g., Thordarson and Self 2003; Grattan et al. 2003). Around 21 % of the human population and 75 % of the livestock perished in Iceland (Thordarson and Self 2003) as a consequence of the eruption. Grattan et al. (2003) compiled English parish mortality records and suggested that mortality in England in the summer of 1783 was 10–20 % above the 51-year moving mean (Wrigley and Schofield 1989). Furthermore, several historical accounts of increased mortality rates and/or respiratory disorders during the summer of 1783 are also found in France, the Netherlands, Italy and Sweden (Durand and Grattan 1999; Grattan et al. 2003; Grattan 2005; Witham and Oppenheimer 2005). A Laki-style eruption is likely to recur, thus Chap. 6 investigates the impact of such an eruption on air pollution and mortality in Europe.

Volcanoes are not only agents of destruction but also enrich and benefit life on Earth and the environment in a variety of ways. Iceland serves as a prime example of the ambivalence of living with volcanic activity by exploiting geothermal resources closely related to its volcano-tectonic setting. In Iceland geothermal resources provide for around 50 % of the country's annual energy requirements (Arnórsson 2000). The great fertility of volcanic soils is another example of how volcanoes are beneficial to the environment; however fertile volcanic soils often lure humans into (too) close

proximity of the volcano itself which is a great hazard if the volcano becomes active. Apart from volcanic products being used as materials in commerce and in industry, volcanic regions have a great economical potential in terms of tourism. Moreover, over the course of many centuries, volcanism has found its way into the literature and arts, which greatly enriches human culture (Sigurdsson 2000; Sigurdsson and Lopes-Gautier 2000).

1.6 Thesis Aims

Firstly, this thesis will investigate the impact of time-averaged volcanic sulphur emissions on the global cloud condensation nuclei budget and the sulphur cycle using a global aerosol microphysics model (GLOMAP-mode). Secondly, this thesis will examine the impact of the large-scale, 1783–1784 AD Laki flood lava eruption on aerosol microphysical processes and changes in cloud properties using GLOMAP-mode. In contrast, previous studies have investigated the impact of volcanic eruptions on the climate system, atmospheric dynamics and the environment employing General Circulation Models (GCMs) or Chemistry Transport Models (CTMs)—these particular model frameworks did not account for detailed microphysics. Timmreck et al. (2009) highlighted that in order to simulate the impact of stratospheric volcanic aerosol on the climate system it is important for the aerosol size distribution to evolve freely instead of prescribing it. Using a comprehensive global aerosol microphysics model such as GLOMAP-mode allows studying the aerosol microphysical processes that drive the evolution of the aerosol size distribution in the troposphere and the subsequent impact of a volcanic eruption on the Earth system. The work presented here will also provide a physically-based estimate of the first aerosol indirect effect following the 1783–1784 AD Laki eruption. Moreover, this work will assess the potential impact of a future Laki-style eruption on society by adopting a inter-disciplinary approach that quantifies the health effects that could arise if a Laki-style eruption were to occur under present-day conditions.

In particular, this thesis examines:

1. **The role of time-averaged volcanic sulphur emissions in the pre-industrial era** (**Chap.** 3):
   (a) What can be learned from explicitly accounting for microphysical processes when studying time-averaged volcanic sulphur emissions?
   (b) Are time-averaged volcanic sulphur emissions an important source of CCN?
   (c) How sensitive are CCN number concentrations to changes in the volcanic sulphur source strength?
   (d) How much do sulphur emissions from continuously degassing and sporadically erupting volcanoes contribute to the first aerosol indirect effect?

2. **The impact of the 1783–1784 AD Laki eruption on microphysical processes and global CCN number concentrations** (**Chap.** 4):
   (a) How much do chemical and microphysical processes change following the Laki eruption when compared to the unperturbed pre-industrial atmosphere?
   (b) Was the Laki eruption an important source of CCN?
   (c) What role does the season in which such an eruption commences play in determining microphysical processes and CCN number concentrations?
   (d) How well does GLOMAP-mode compare to historical and observational records of the Laki sulphate aerosol?
3. **The impact of the 1783–1784 AD Laki eruption on cloud drop number concentrations (CDNC) and the magnitude of the first aerosol indirect effect** (**Chap.** 5):
   (a) Did the Laki eruption impact CDNC at low-level cloud altitude?
   (b) What difference arises from employing a physically-based aerosol activation scheme versus empirical estimates of CDNC?
   (c) What is the magnitude of the first aerosol indirect effect following the Laki eruption?
   (d) How does the first aerosol indirect effect following Laki compare to previous estimates of the direct effect?
   (e) Does the magnitude of the first aerosol indirect effect differ depending on which season the Laki eruption commences?
4. **What if a Laki-style eruption were to happen tomorrow?** (**Chap.** 6):
   (a) Would a Laki-style eruption under present-day conditions be a severe air pollution event in Europe?
   (b) Would a Laki-style eruption pose a severe hazard to human health and increase excess mortality in present-day Europe?

References

Abdul-Razzak H, Ghan SJ (2002) A parameterization of aerosol activation 3. Sectional representation. J Geophys Res 107(D3):4026 doi:10.1029/2001JD000483

Albrecht BA (1989) Aerosols, cloud microphysics, and fractional cloudiness. Science 245:1227–1230

Allen AG, Oppenheimer C, Ferm M, Baxter PJ, Horrocks LA, Galle B, McGonigle AJS, Duffell HJ (2002) Primary sulfate aerosol and associated emissions from Masaya Volcano, Nicaragua. J Geophys Res 107(D23):4682 doi:10.1029/2002JD002120

Andres RJ, Kasgnoc AD (1998) A time-averaged inventory of subaerial volcanic sulfur emissions. J Geophys Res 103:25251–25262

Angell JK, Korshover J (1985) Surface temperature changes following the six major volcanic episodes between 1780 and 1980. J Climate Appl Meteorol 24:937–951

Arakawa H (1955) Meteorological conditions of the great famines in the last half of the Tokugawa period. Jpn Meteorol Geophys 6:3–68

Arnórsson S (2000) Exploitation of geothermal resources. In: Sigurdsson H, Houghton BF, McNutt SR, Rymer H, Stix J (eds) Encyclopedia of volcanoes. Academic press, San Diego, pp 1243–1258

Barnes JE, Hofmann DJ (1997) Lidar measurements of stratospheric aerosol over Mauna Loa observatory. Geophys Res Lett 24:1923–1926

Baxter PJ (1990) Medical effects of volcanic eruptions. Bull Volcanol 52:532–544. doi:10.1007/BF00301534

Baxter PJ, Ing R, Falk H, French J, Stein GF, Bernstein RS, Merchant JA, Allard J (1981) Mount St Helens eruptions, May 18 to June 12, 1980: an overview of the acute health impact. JAMA 246:2585–2589

Beerling DJ, Harfoot M, Lomax B, Pyle JA (2007) The stability of the stratospheric ozone layer during the end-Permian eruption of the siberian traps. Philos Trans R Soc A: Math Phys Eng Sci 365:1843–1866

Bekki S (1995) Oxidation of volcanic SO_2—a sink for stratospheric OH and H_2O. Geophys Res Lett 22:913–916

Bekki S, Pyle JA, Zhong W, Toumi R, Haigh JD, Pyle DM (1996) The role of microphysical and chemical processes in prolonging the climate forcing of the Toba eruption. Geophys Res Lett 23:2669–2672

Bluth G, Doiron S, Schnetzler C, Krueger A, Walters L (1992) Global tracking of the SO_2 clouds from the June, 1991 Mount Pinatubo eruptions. Geophys Res Lett 19:151–154

Bobrowski N, Honninger G, Galle B, Platt U (2003) Detection of bromine monoxide in a volcanic plume. Nature 423:273–276

Bond A, Sparks RSJ (1976) The Minoan eruption of santorini, Greece. J Geol Soc 132:1–16

Boucher O, Lohmann U (1995) The sulfate-CCN-cloud albedo effect, a sensitivity study with two general circulation models. Tellus Ser B 47:281–300

Briffa KR, Jones PD, Schweingruber FH, Osborn TJ (1998) Influence of volcanic eruptions on northern hemisphere summer temperature over the past 600 years. Nature 393:450–455

Caldeira K, Rampino MR (1990) Carbon dioxide emissions from deccan volcanism and a K/T boundary greenhouse effect. Geophys Res Lett 17(9):1299–1302. doi:10.1029/GL017i009p01299

Carslaw KS, Boucher O, Spracklen DV, Mann GW, Rae JGL, Woodward S, Kulmala M (2010) A review of natural aerosol interactions and feedbacks within the Earth system. Atmos Chem Phys 10:1701–1737

Chenet AL, Fluteau F, Courtillot V (2005) Modelling massive sulphate aerosol pollution, following the large 1783 Laki basalticeruption. Earth Planet Sci Lett 236:721–731

Chin M, Jacob DJ (1996) Anthropogenic and natural contributions to tropospheric sulfate: a global model analysis. J Geophys Res 101:18691–18699

D'Arrigo RD, Jacoby GC (1999) Northern North American tree-ring evidence for regional temperature changes after major volcanic events. Clim Change 41:1–15. doi:10.1023/A:1005370210796

D'Arrigo R, Seager R, Smerdon JE, LeGrande AN, Cook ER (2011) The anomalous winter of 1783–1784: was the Laki eruption or an analog of the 2009–2010 winter to blame? Geophys Res Lett 38:L05706

Delmelle P (2003) Environmental impacts of tropospheric volcanic gas plumes. Geol Soc London Spec Publ 213:381–399. doi:10.1144/GSL.SP.2003.213.01.23

Delmelle P, Stix J, Baxter P, Garcia-Alvarez J, Barquero J (2002) Atmospheric dispersion, environmental effects and potential health hazard associated with the low-altitude gas plume of Masaya volcano, Nicaragua. Bull Volcan 64:423–434. doi:10.1007/s00445-002-0221-6

Durand M, Grattan J (1999) Extensive respiratory health effects of volcanogenic dry fog in 1783 inferred from european documentary sources. Environ Geochem Health 21:371–376. doi:10.1023/A:1006700921208

Durant AJ, Bonadonna C, Horwell CJ (2010) Atmospheric and environmental impacts of volcanic particulates. Elements 6:235–240

Eatough D, Caka F, Farber R (1994) The conversion of SO_2 to sulfate in the atmosphere. Isr J Chem 34:301–314

Feichter J, Lohmann U, Schult I (1997) The atmospheric sulfur cycle and its impact on the shortwave radiation. Clim Dyn 13:235–246

Forster P, Ramaswamy V, Artaxo P, Berntsen T, Betts R, Fahey D, Haywood J, Lean J, Lowe D, Myhre G, Nganga J, Prinn R, Raga G, Schulz M, Van Dorland R (2007) Changes in atmospheric constituents and in radiative forcing. In: Solomon S, Qin D, Chen Z, Manning, M, Marquis M, Averyt KB, Tignor M, Miller H (eds) Climate change 2007: the physical science basis. Contribution of working group I to the fourth assessment report of the intergovernmental panel on climate change, Cambridge University Press, Cambridge, pp 129–234

Gassó S (2008) Satellite observations of the impact of weak volcanic activity on marine clouds. J Geophys Res 113:D14S19

Gauci V, Blake S, Stevenson DS, Highwood EJ (2008) Halving of the northern wetland CH4 source by a large Icelandic volcanic eruption. J Geophys Res 113:G00A11

Gerlach T, Westrich H, Symonds R (1996) Pre-eruption vapor in Magma of the climatic Mount Pinatubo eruption: source of the giant stratospheric Sulfur Dioxide cloud. In: Newhall C, Punongbayan R (eds) Fire and mud: eruptions and lahars of Mount Pinatubo, Philippines, 1126, Philippine Institute of Volcanology and Seismology, Quezon City and University of Washington Press, Seattle

Graf HF (1992) Arctic radiation deficit and climate variability. Clim Dyn 7:19–28

Graf HF, Feichter J, Langmann B (1997) Volcanic sulfur emissions: estimates of source strength and its contribution to the global sulfate distribution. J Geophys Res 102:727–738

Grainger RG, Lambert A, Taylor FW, Remedios JJ, Rodgers CD, Corney M, Kerridge BJ (1993) Infrared absorption by volcanic stratospheric aerosols observed by ISAMS. Geophys Res Lett 20:1283–1286

Grattan JP, Pyatt FB (1994) Acid damage to vegetation following the Laki fissure eruption in 1783—an historical review. Sci Total Environ 151:241–247

Grattan J (1998) The distal impact of Icelandic volcanic gases and aerosols in Europe: a review of the 1783 Laki fissure eruption and environmental vulnerability in the late 20th century. Geol Soc London Eng Geol Spec Publ 15:97–103

Grattan J (2005) Pollution and paradigms: lessons from Icelandic volcanism for continental flood basalt studies. Lithos 79:343–353

Grattan J, Durand M, Taylor S (2003) Illness and elevated human mortality in Europe coincident with the Laki fissure eruption. Volcanic Degassing, In: Oppenheimer C, Pyle D.M, Barclay J (eds) Geological society london special publications, vol. 213, pp 401–414

Hamill P, Toon OB, Kiang CS (1977) Microphysical processes affecting stratospheric aerosol particles. J Atmos Sci 34:1104–1119

Hansell A, Oppenheimer C (2004) Health hazards from volcanic gases: a systematic literature review. Arch. Environ. Health 59:628–639

Hansell AL, Horwell CJ, Oppenheimer C (2006) The health hazards of volcanoes and geothermal areas. Occup Environ Med 63:149–156

Hassan FA (1998) Climatic change, Nile floods and civilization. NatResour 34:34–40

Haughton DR, Roeder PL, Skinner BJ (1974) Solubility of Sulfur in mafic magmas. Econ Geol 69:451–467

Haywood J, Boucher O (2000) Estimates of the direct and indirect radiative forcing due to tropospheric aerosols: a review. Rev Geophys 38:513–543

Highwood EJ, Stevenson DS (2003) Atmospheric impact of the 1783–1784 Laki eruption: part II—climatic effect of sulphate aerosol. Atmos Chem Phys 3:1177–1189

Hobbs P, Tuell J, Hegg D, Radke L, Eltgroth M (1982) Particles and gases in the emissions from the 1980–1981 volcanic eruptions of Mt. St. Helens. JGR-Atmos 87:1062–1086

Jacoby GC, Workman KW, D'Arrigo RD (1999) Laki eruption of 1783, tree rings, and disaster for northwest Alaska Inuit. Quat Sci Rev 18:1365–1371

Jakobsson SP (1979) Petrology of recent basalts from the Eastern volcanic zone, Iceland. Acta Naturalia Islandica 26:1–103

Jones A, Roberts D, Slingo A (1994) A climate model study of indirect radiative forcing by anthropogenic sulfate aerosols. Nature 370:450–453
Joshi MM, Jones GS (2009) The climatic effects of the direct injection of water vapour into the stratosphere by large volcanic eruptions. Atmos Chem Phys 9:6109–6118
Kellogg WW, Cadle RD, Allen ER, Lazrus AL, Martell EA (1972) The Sulfur cycle. Science 175:587–596
Kington JA (1988) The weather of the 1780's over Europe. Cambridge University Press, New York, pp 180
Koch D, Schmidt G, Field C (2006) Sulfur, sea salt and radionuclide aerosols in GISS Model. J Geophys Res 111:D06206
Kondrashov D, Feliks Y, Ghil M (2005) Oscillatory modes of extended Nile River records (A.D. 622–1922). Geophys Res Lett 32:L10702
Koti S, Reddy KR, Reddy VR, Kakani VG, Zhao D (2005) Interactive effects of carbon dioxide, temperature, and ultraviolet-B radiation on soybean (Glycine max L.) flower and pollen morphology, pollen production, germination, and tube lengths. J Exp Bot 56:725–736
Kulmala M, VehkamÃki H, PetÃjÃ T, Lauri A, Kerminen VM, Birmili W, McMurry PH (2004) Formation and growth rates of ultrafine atmospheric particles: a review of observations. J Aerosol Sci 35:143–176
Lamb HH (1970) Volcanic dust in the atmosphere; with a chronology and assessment of its meteorological significance. Proc R Soc Lond A: Math Phys Sci 266:425–533
Lambert G, Le Cloarec MF, Pennisi M (1988) Volcanic output of SO_2 and trace metals: a new approach. Geochim Cosmochim Acta 52:39–42
Lohmann U, Feichter J (1997) Impact of sulfate aerosols on albedo and lifetime of clouds: a sensitivity study with the ECHAM4 GCM. J Geophys Res 102(D12):13685–13700
Mann GW, Carslaw KS, Spracklen DV, Ridley DA, Manktelow PT, Chipperfield MP, Pickering SJ, Johnson CE (2010) Description and evaluation of GLOMAP-mode: a modal global aerosol microphysics model for the UKCA composition-climate model. Geosci Model Dev 3:519–551
Mather TA (2008) Volcanism and the atmosphere: the potential role of the atmosphere in unlocking the reactivity of volcanic emissions. Philos Trans R Soc A: Math Phys Eng Sci 366:4581–4595
Mather T, Pyle DM, Oppenheimer C (2003) Tropospheric volcanic aerosol. In: Volcanism and the Earth's atmosphere, of geophysical monograph, vol 139. American Geophysical Union (AGU), Washington, pp 189–212
Mather TA, Tsanev VI, Pyle DM, McGonigle AJS, Oppenheimer C, Allen AG (2004) Characterization and evolution of tropospheric plumes from Lascar and Villarrica volcanoes. Chile J Geophys Res 109:D21303
McBirney A (1984) Igneous petrology. Freeman Cooper, San Francisco, p 504
McClelland L, Simkin T, Summers M, Nielsen E, Stein TC (eds) (1989) Global volcanism 1975–1985. Prentice-Hall, Englewood Cliffs
McLean DM (1985) Deccan traps mantle degassing in the terminal cretaceous marine extinctions. Cretac Res 6:235–259
Mercado LM, Bellouin N, Sitch S, Boucher O, Huntingford C, Wild M, Cox PM (2009) Impact of changes in diffuse radiation on the global land carbon sink. Nature 458:1014–1017
Mooley DA, Pant GB (1981) Droughts in India over the last 200 years, their socio-economic impacts and remedial measures for them. In: Wigley TML, Ingram MJ, Farmer G (eds) Climate and history: studies in past climates and their impact on man. Cambridge University Press, New York, pp 465–478
Nenes A, Seinfeld JH (2003) Parameterization of cloud droplet formation in global climate models. J Geophys Res 108(D14):4415. doi:10.1029/2002JD002911
Oman L, Robock A, Stenchikov GL, Thordarson T, Koch D, Shindell DT, Gao C (2006a) Modeling the distribution of the volcanic aerosol cloud from the 1783–1784 Laki eruption. J Geophys Res 111:D12209. doi:10.1029/2005JD006899

Oman L, Robock A, Stenchikov GL, Thordarson T (2006b) High-latitude eruptions cast shadow over the African monsoon and the flow of the Nile. Geophys Res Lett 33:L18711. doi:10.1029/2006GL027665
Penner JE, Andrea M, Annegarn H, Barrie L, Feichter J, Hegg D, Jayaraman A, Leaitch R, Murphy D, Nganga J, Pitari GEA (2001). The scientific basis. Contribution of working group I to the third assessment report of the intergovernmental panel on climate change. In: Houghton JT, Ding YEA (eds) Climate change 2001. Cambridge University Press, Cambridge, New York
Pham M, Mueller JF, Brasseur GP, Granier C, Megie G (1995) A three-dimensional study of the tropospheric sulfur cycle. J Geophys Res 100(D12):26061–26092
Pinto JP, Turco RP, Toon OB (1989) Self-limiting physical and chemical effects in volcanic eruption clouds. J Geophys Res 94(D8): 11165–11174 doi:10.1029/JD094iD08p11165
Pollack JB, Ackerman TP (1983) Possible effects of the El chichon volcanic cloud on the radiation budget of the northern tropics. Geophys Res Lett 10:1057–1060
Pollack JB, Toon OB, Sagan C, Summers A, Baldwin B, Van Camp W (1976) Volcanic explosions and climatic change: a theoretical assessment. J Geophys Res 81:1071–1083
Pope CA, Dockery DW (2006) Health effects of fine particulate air pollution: lines that connect. J Air Waste Manag Assoc 56:709–742
Raes F, Dingenen RV, Vignati E, Wilson J, Putaud JP, Seinfeld JH, Adams P (2000) Formation and cycling of aerosols in the global troposphere. Atmos Environ 34:4215–4240
Ramanathan V, Crutzen PJ, Kiehl JT, Rosenfeld D (2001) Aerosols, climate, and the hydrological cycle. Science 294:2119–2124
Rampino MR, Ambrose SH (2000) Volcanic winter in the garden of Eden: the Toba supereruption and the late pleistocene human population crash. Geol Soc Am Spec Pap 345:71–82
Rampino MR, Self S (1984) Sulphur-rich volcanic eruptions and stratospheric aerosols. Nature 310:677–679
Rampino MR, Self S, Stothers RB (1988) Volcanic winters. Ann Rev Earth Planet Sci 16:73–99
Robock A (2000) Volcanic eruptions and climate. Rev Geophys 38:191–219
Robock A (2002) Blowin' in the wind: research priorities for climate effects of volcanic eruptions. Eos Trans AGU 83(42):472
Robock A, Mao J (1992) Winter warming from large volcanic eruptions. Geophys Res Lett 19:2405–2408
Rose WI, Chuan RL, Cadle RD, Woods DC (1980) Small particles in volcanic eruption clouds. Am J Sci 280:671–696
Rose WI, Chuan RL, Woods DC (1982) Smal particles in plumes of Mount St Helens. J Geophys Res 87:4956–4962
Rose WI, Wunderman RL, Hoffman MF, Gale L (1983) A volcanologist's review of atmospheric hazards of volcanic activity: fuego and Mount St. Helens. J Volcanol Geoth Res 17:133–157
Schmincke HU (2004) Volcanism. Springer, Heidelberg, p 324
Seinfeld J, Pandis S (1998) Atmospheric chemistry and physics: from air pollution to climate change. Wiley, New York, pp 1326
Self S (2009) Interactive comment on "The climatic effects of the direct injection of water vapour into the stratosphere by large volcanic eruptions". In: Joshi MM, Jones GS (eds) Atmospheric Chemistry and Physics Discuss, vol 9, pp C216–C219
Self S, Blake S, Sharma K, Widdowson M, Sephton S (2008) Sulfur and chlorine in late cretaceous deccan Magmas and eruptive gas release. Science 319:1654–1657
Sigmarsson O, Condomines M, Grõnvold K, Thordarson T (1991) Extreme magma homogeneity in the 1783–84 Lakagigar eruption: origin of a large volume of evolved basalt in Iceland. Geophys Res Lett 18:2229–2232
Sigurdsson H (2000) Volcanoes in article. In: Sigurdsson H, Houghton BF, McNutt SR, Rymer H, Stix J (eds) Encyclopedia of volcanoes. Academic Press, San Diego, pp 1315–1338
Sigurdsson H, Lopes-Gautier R (2000) Volcanoes in literature and film. In: Sigurdsson H, Houghton BF, McNutt SR, Rymer H, Stix J (eds) Encyclopedia of Volcanoes. Academic Press, San Diego, pp 1339–1360

Smith SJ, van Aardenne J, Klimont Z, Andres R, Volke A (2010) Anthropogenic sulfur dioxide emissions: 1850âĂş2005. Atmos Chem Phys Discuss 10:16111–16151
Steingrímsson J (1788) Fullkomid skrif um Sídueld (A complete description on the Sída volcanic fire). Safn til Sögu íslands. Copenhagen, 1907–1915
Steingrímsson J (1998) Fires of the Earth. The Laki eruption 1783–1784. Nordic Volcanological Institute and University of Iceland Press, Reykjavík, p 95
Stevenson DS, Johnson CE, Collins WJ, Derwent RG (2003a) The tropospheric sulphur cycle and the role of volcanic SO_2, Volcanic Degassing, pp 295–305
Stevenson DS, Johnson CE, Highwood EJ, Gauci V, Collins WJ, Derwent RG (2003b) Atmospheric impact of the 1783–1784 Laki eruption: part I chemistry modelling. Atmos Chem Phys 3:487–507
Stothers RB (1996) Major optical depth perturbations to the stratosphere from volcanic eruptions: pyrheliometric period, 1881–1960. J Geophys Res [Atmos] 101:3901–3920
Textor C, Graf C, Timmreck HF, Robock A (2004) Emissions from volcanoes. In: Granier C, Artaxo P, Reeves C (eds) Emissions of chemical compounds and aerosols in the atmosphere. Kluwer, Dordrecht, pp 269–303
Thorarinsson S, Sigvaldason G (1972) The Hekla eruption of 1970. Bull Volcan 36:269–288. doi:10.1007/BF02596870
Thordarson T (1995) Volatile release and atmospheric effects of basaltic fissure eruptions. Ph.D. thesis, University of Hawaii, Honolulu
Thordarson T, Self S (1993) The Laki (Skaftar Fires) and Grimsvatn eruptions in 1783–1785. Bull Volcanol 55:233–263
Thordarson T, Self S (1996) Sulfur, chlorine and fluorine degassing and atmospheric loading by the Roza eruption, Columbia river basalt group, Washington. J Volcanol Geoth Res 74:49–73
Thordarson T, Self S, Oskarsson N, Hulsebosch T (1996) Sulfur, chlorine, and fluorine degassing and atmospheric loading by the 1783–1784 AD Laki (Skaftar fires) eruption in Iceland. Bull Volcanol 58:205–222
Thordarson T, Larsen G (2007) Volcanism in Iceland in historical time: volcano types, eruption styles and eruptive history. J Geodyn 43:118–152
Thordarson T, Rampino M, Keszthelyi LP, Self S (2009) Effects of megascale eruptions on Earth and Mars. Geol Soc Am Spec Pap 453:37–53
Thordarson T, Self S (2003) Atmospheric and environmental effects of the 1783–1784 Laki eruption: a review and reassessment. J Geophys Res [Atmos] 108(D1):4011. doi:10.1029/2001JD002042
Timmreck C, Lorenz SJ, Crowley TJ, Kinne S, Raddatz TJ, Thomas MA, Jungclaus JH (2009) Limited temperature response to the very large AD 1258 volcanic eruption. Geophys Res Lett 36:L21708
Timmreck C, Graf HF, Lorenz SJ, Niemeier U, Zanchettin D, Matei D, Jungclaus JH, Crowley TJ (2010) Aerosol size confines climate response to volcanic super-eruptions. Geophys Res Lett 37:L24705
Toon OB, Pollack JB (1980) Atmospheric aerosols and climate. Am Sci 68:268–278
Twomey S (1974) Pollution and the planetary albedo. Atmos Environ 41:120–125
Twomey S (1977) Influence of pollution on shortwave Albedo of clouds. J Atmos Sci 34:1149–1152
Visscher H, Looy CV, Collinson ME, Brinkhuis H, van Konijnenburg-van Cittert JHA, Kãijrschner WM, Sephton MA (2004) Environmental mutagenesis during the end-Permian ecological crisis. Proc Natl Acad Sci USA 101:12952–12956
von Glasow R, Bobrowski N, Kern C (2009) The effects of volcanic eruptions on atmospheric chemistry. Chem Geol 263:131–142
Wallace P, Carmichael IS (1992) Sulfur in basaltic magmas. Geochim Cosmochim Acta 56:1863–1874
Wang SW, Zhao ZC (1981) Droughts and floods in China, 1470–1979. In: Wigley TML, Ingram MJ, Farmer G (eds) Climate and history studies in past climates and their impact on man. Cambridge University Press, New York, pp 271–288
Watson IM, Oppenheimer C (2001) Photometric observations of Mt. Etna's different aerosol plumes. Atmos Environ 35:3561–3572

Whitby K (1978) The physical characteristics of sulfur aerosols. Atmos Environ 12:135–159. Proceedings of the international symposium
Wignall PB (2001) Large igneous provinces and mass extinctions. Earth Sci Rev 53:1–33
Witham CS, Oppenheimer C (2005) Mortality in England during the 1783–1784 Laki craters eruption. Bull Volcanol 67:15–26. doi:10.1007/s00445-004-0357-7
Woods AW (1993) A model of the plumes above basaltic fissure eruptions. Geophys Res Lett 20:1115–1118
Wrigley EA, Schofield RS (1989) The population history of England 1541–1871: a reconstruction. Cambridge University Press, Cambridge 794 pp

Chapter 2
GLOMAP-Mode Overview

2.1 Introduction

The GLObal Model of Aerosol Processes (GLOMAP) is a comprehensive size-resolving global aerosol model which is embedded in the Toulouse Offline Model of Chemistry and Transport (TOMCAT, Stockwell and Chipperfield 1999; Chipperfield 2006). GLOMAP was initially developed using a two-moment (i.e. carrying information on particle number concentration and on particle mass concentration) bin scheme (GLOMAP-bin; Spracklen et al. 2005a,b). GLOMAP-bin has been used in numerous studies (e.g., Spracklen et al. 2008a,b; Merikanto et al. 2009; Pringle et al. 2009), and shown to perform well when compared to observational data sets of, for example, particle number concentrations and SO_2 mass concentrations (e.g. Spracklen et al. 2005a).

Mann et al. (2010) presented a full description and evaluation of a version of GLOMAP that uses a two-moment modal scheme (GLOMAP-mode). GLOMAP-mode treats the same aerosol microphysical processes as GLOMAP-bin but at greatly reduced computational cost. Throughout this thesis GLOMAP-mode has been used. GLOMAP-mode treats microphysical processes such as binary homogeneous nucleation, hygroscopic growth, coagulation, condensation, cloud processing (oxidation of dissolved SO_2 to SO_4 in cloud droplets), as well as dry and wet deposition.

GLOMAP-mode is benchmarked against the AEROCOM model inter-comparison data set (Textor et al. 2006) and several other observational data sets such as for example EMEP (European Monitoring and Evaluation Programme, Loevblad et al. 2004) or IMPROVE (Interagency Monitoring of Protected Visual Environments, Malm et al. 2002). Mann et al. (2010) have shown that the model is capable of simulating realistic present-day aerosol mass concentrations, number concentrations, particle size distributions, and CCN concentrations in both marine and continental locations.

GLOMAP-mode has been used in several previous studies. Manktelow et al. (2007) have investigated regional and global changes in the sulphur cycle between the years

A. Schmidt, *Modelling Tropospheric Volcanic Aerosol*, Springer Theses,
DOI: 10.1007/978-3-642-34839-6_2, © Springer-Verlag Berlin Heidelberg 2013

1985 and 2000. Woodhouse et al. (2008) have investigated the response of CCN number concentrations to a regional, fivefold increase in DMS concentrations, and found only modest changes in CCN number concentrations. In a follow-up study, Woodhouse et al. (2010) have shown that, on a global scale, the sensitivity of CCN to changes in DMS is too low for future changes in DMS to be climatically relevant.

2.2 TOMCAT Chemical Transport Model

GLOMAP-mode is run as an extension to the TOMCAT global three-dimensional CTM (Stockwell and Chipperfield 1999; Chipperfield 2006) using a horizontal resolution of $2.8° \times 2.8°$ and 31 hybrid σ-p levels extending from the surface to 10 hPa in the vertical. Below about 100 hPa, the vertical σ levels are purely terrain-following whereas above ~100 hPa they are pure pressure levels. The model is driven by meteorological fields specified from European Centre for Medium-Range Weather Forecasts (ECMWF) analyses at 6-h intervals. TOMCAT uses the tracer advection scheme of Prather (1986) which preserves sharp gradients and minimises numerical diffusion due to the conservation of second-order moments of the spatial distribution of the advected tracers. In order to calculate sub-grid scale moist convection in cumulus clouds, TOMCAT uses the mass flux scheme of Tiedtke (1989).

2.3 Gas-Phase Species and Chemistry

Trace Gas Emissions
Depending on the aim of the study, different combinations of emission inventories have been used throughout this thesis. Each results chapter includes a statement as to what emissions have been used.

Oceanic DMS emissions have been calculated from monthly mean seawater DMS concentrations from Kettle and Andreae (2000) using the sea-air flux parameterisation of Nightingale et al. (2000). According to Kettle and Andreae (2000), DMS fluxes range from 13 to 37 Tg (S) per year depending on the gas flux parameterisations and wind speed prognostics. GLOMAP-mode predicts an annual mean DMS flux of 18.6 Tg(S) (Woodhouse et al. 2010).

In GLOMAP-mode, SO_2 is emitted from anthropogenic, biomass burning and volcanic sources. Anthropogenic SO_2 emissions are from Cofala et al. (2005) and account for 52.4 Tg (S) per year (with 24.1 Tg(S) per year from power stations, 19.6 Tg (S) per year from industrial processes, 5.7 Tg (S) per year from transportation, and 4.6 Tg (S) per year from domestic consumption). Anthropogenic SO_2 emissions used in this thesis are assumed to be constant throughout the year. Monthly varying SO_2 emission from biomass burning sources are from Van der Werf et al. (2003) and account for 2.1 Tg (S) per year. Depending on the vegetation type that is burning, the injection height ranges from 0 to 6 km which follows recommendations by Dentener et al. (2006).

The volcanic SO_2 emission inventory used in GLOMAP-mode is based on data sets by Andres and Kasgnoc (1998) and Halmer et al. (2002). The data set provided by Andres and Kasgnoc (1998) takes into account both continuously erupting volcanoes and sporadically erupting volcanoes and accounts for 10.4 Tg(S) per year. Following recommendations of Dentener et al. (2006) sulphur emissions from continuously erupting volcanoes are released into grid boxes between the height of the volcano and one third below that height in order to account for degassing along the flanks of the volcano. It should be noted, that the Andres and Kasgnoc (1998) data set (also referred to as the GEIA inventory, which includes information on the spatial distribution of the sources required for global modelling studies) is scaled by a factor 1.21 (Dentener et al. 2006, following recommendations of Graf et al. (1998) and Textor et al. (2004))[1] when referred to as AEROCOM data set with the latter being used throughout this thesis. Halmer et al. (2002) estimated that explosive volcanic activity averaged over the last 100 years accounts for 2.0 Tg(S) per year. In GLOMAP-mode sulphur emissions from explosively erupting volcanoes are released into grid boxes between 500 and 1500 m above the height of each volcano that has been active over the last 100 years. In order to account for gas-to-particle conversion in the volcanic plume, 2.5 % of the total sulphur flux is assumed to be emitted as primary sulphate into the accumulation and coarse mode (see also Sect. 2.5). Note that, this partitioning follows Stier et al. (2005) based on observations of anthropogenic sulphur emissions from power plants. In GLOMAP-mode, the total volcanic sulphur flux (i.e. using the inventories of Andres and Kasgnoc (1998) and Halmer et al. (2002)) equates to 14.22 Tg(S) per year; that is after partitioning into SO_2 and primary SO_4. For the purpose of the study presented in Chap. 3 the Halmer et al. (2002) inventory was excluded whereas all remaining chapters used both the Andres and Kasgnoc (1998) and Halmer et al. (2002) inventories.

Monthly mean emission of monoterpenes are from Guenther et al. (1995) which is the only source of secondary organic carbon treated in this work.

Gas Phase Chemistry

The sulphur chemistry scheme in GLOMAP-mode includes eight sulphur species: DMS, DMSO (dimethyl sulphoxide), MSA (methane sulphonic acid), SO_2, H_2S, H_2SO_4, COS (carbonyl sulphide), and CS_2 (carbon disulphide). The original sulphur reaction scheme was based on Pham et al. (1995) and used "offline oxidant fields" (i.e. by means of a look-up table) (e.g., Manktelow et al. 2007; Woodhouse et al. 2010). This "offline-scheme" has been updated as part of a PhD project in order to fully couple the oxidants and sulphur species (i.e. allowing for interactions between the sulphur species and oxidants) which is referred to as "coupled-chemistry scheme" (Breider et al. 2010; Breider 2010). Using a fully coupled chemistry scheme is crucial when simulating volcanic eruptions as high concentrations of SO_2 significantly impact oxidant concentrations which in turn feeds back onto the chemistry. For the work presented in this thesis the coupled chemistry version of GLOMAP-mode has been used which is coupled to the full background chemistry

[1] Dentener et al. (2006) wrongly stated that the GEIA data set is scaled using a factor 1.5.

Table 2.1 Sulphur reaction scheme in the coupled TOMCAT-GLOMAP-mode model

Reactants		Products	Reference
$DMS + OH$	$\rightarrow$	$SO_2 + CH_3O_2 + HCHO$	Atkinson (2000)
$DMS + OH$	$\rightarrow$	$0.6\,SO_2 + 0.4\,DMSO + 0.6\,CH_3O_2 + 0.4\,HO_2$	Pham et al. (1995)
$DMSO + OH$	$\rightarrow$	$0.6\,SO_2 + 0.4\,MSA + 0.6\,CH_3O_2$	Pham et al. (1995)
$DMS + NO_3$	$\rightarrow$	$SO_2 + HNO_3 + CH_3O_2 + HCHO$	Atkinson (2000)
$H_2S + OH$	$\rightarrow$	$SO_2 + OH$	Pham et al. (1995)
$CS_2 + OH$	$\rightarrow$	$SO_2 + COS + OH$	Pham et al. (1995)
$COS + OH$	$\rightarrow$	$SO_2 + OH$	Pham et al. (1995)
$SO_2 + OH + M$	$\rightarrow$	$H_2SO_4 + HO_2 + M$	Pham et al. (1995)

($O_x - NO_y - HO_x$, $C_1 - C_3$ NMHCs (non-methane hydrocarbons), isoprene) in TOMCAT (Breider et al. 2010). The sulphur reaction scheme is presented in Table 2.1.

Aqueous Chemistry
Aqueous phase oxidation denotes the processes by which soluble gases such as SO_2 condense onto cloud droplets and subsequently become oxidised through the reaction with H_2O_2 or O_3 (see also Reactions 1.5 and 1.6 in Chap. 1). GLOMAP-mode treats aqueous phase oxidation (on aerosol that are considered to be activated into drops) in grid boxes that contain ISCCP-derived low-level stratiform clouds (see Sect. 2.6 for details). The dissolved sulphate mass produced by aqueous phase oxidation is then added to the soluble accumulation and coarse modes according to their fractional contribution (in terms of number) with respect to the total number concentration within these two modes (Mann et al. 2010).

Sulphuric Acid Vapour
Sulphuric acid vapour concentrations are crucial in determining the binary nucleation rate, and thus the rate of new particle formation. GLOMAP-mode accounts for the direct competition of nucleation and condensation (see Sect. 2.6) for the available H_2SO_4 vapour by introducing short competition sub-steps calling these routines within the normal model time-step (see Sect. 2.6 and Fig. 2.2, Spracklen et al. 2005a; Mann et al. 2010).

2.4 Aerosol Size Distribution

GLOMAP-mode uses a modal aerosol dynamics approach (e.g., Whitby and McMurry 1997) by parameterising the shape of the aerosol size distribution as a series of log-normal modes. GLOMAP-mode uses a two-moment aerosol scheme with the particle number concentration and mass concentration of each component prognosed in each mode (the width of each mode is fixed). The scheme can be run with any number of modes and components but generally (in its standard configuration) follows the framework of the M7 model (Vignati et al. 2004; Stier et al. 2005) carrying sulphate (SU), sea-salt (SS), black carbon (BC), organic carbon (OC) and dust (DU)

Table 2.2 Standard aerosol configuration for GLOMAP-mode with d_p = particle dry diameter; SU = sulphate; POM = particulate organic matter (i.e. POM = OC mass multiplied by 1.4 in order to account for molar mass of non-carbon atoms contributing to POM); BC = black carbon; SS = sea-salt; DU = mineral dust, and *sigma* referring to the geometric standard deviation of each of the respective modes

Mode	Size range	Sigma	Composition	Soluble?
Nucleation soluble	$d_p < 10\,\text{nm}$	1.59	SU, POM	Yes
Aitken soluble	$10 < d_p < 100\,\text{nm}$	1.59	SU, BC, POM	Yes
Accumulation soluble	$100 < d_p < 1\,\mu\text{m}$	1.59	SU, BC, POM, SS, DU	Yes
Coarse soluble	$d_p > 1\,\mu\text{m}$	2.0	SU, BC, POM, SS, DU	Yes
Aitken insoluble	$10 < d_p < 100\,\text{nm}$	1.59	BC, POM	No
Accumulation insoluble	$100 < d_p < 1\,\mu\text{m}$	1.59	DU	No
Coarse insoluble	$d_p > 1\,\mu\text{m}$	2.0	DU	No

Table modified after Mann et al. (2010)

in 4 soluble and 3 insoluble internally mixed modes. Table 2.2 lists properties and composition of each mode. For the work presented here, the component and mode setup used is stated in the methods section of each results chapter.

2.5 Primary Aerosol Emissions

Following recommendations of Dentener et al. (2006) a small fraction (2.5 %) of the total SO_2 flux is emitted as primary sulphate in order to account for sub-grid scale nucleation processes. The formation of new sulphate particles is known to occur in both volcanic and industrial plumes (Allen et al. 2002; Brock et al. 2002). In the model, primary sulphate originating from anthropogenic sources is emitted (in equal proportions) at two mean mode radii of 0.075 and 0.75 µm following Stier et al. (2005). Primary sulphate originating from volcanic and biomass burning sources is emitted at mean mode radii of 0.03 and 0.075 µm following Stier et al. (2005).

Wind speed dependent sea-salt emissions in GLOMAP-mode are calculated using the parameterisation of Gong (2003) which produces a size-resolved sea-salt flux into the soluble accumulation and soluble coarse modes. The version of GLOMAP-mode used here does not account for sub-micron sea-salt fluxes; however this is not regarded as a limitation given the aim of this study.

Annual mean BC and OC emissions from fossil fuel and biofuel sources are from Bond et al. (2004), and monthly-varying BC and OC emissions from vegetation fires are from Van der Werf et al. (2003). Fossil fuel and biofuel emissions are injected into grid boxes below 100 m and emissions from wildfires are injected into grid boxes between the surface and 6 km (depending on the vegetation type that is burning) following Dentener et al. (2006).

In Chap. 6 daily varying mineral dust emissions for the year 2000 are included following Dentener et al. (2006). Mineral dust is emitted into the insoluble accumulation and insoluble coarse modes.

2.6 Aerosol Microphysical Processes

Figure 2.1 depicts the aerosol microphysical processes that shape the aerosol size distribution and influence the lifetime and chemical composition of the aerosol. The following section provides a brief overview of the microphysical processes accounted for in GLOMAP-mode. An in-depth description of the mathematical and numerical representation of the aerosol processes in GLOMAP-mode has been provided by Mann et al. (2010).

Numerical Treatment

Figure 2.2 shows a flow chart of the order in which GLOMAP-mode treats advective, chemical and microphysical processes which follows the approach by Spracklen et al. (2005a). The differential equations determining particle number and mass concentrations are calculated by means of operator splitting. The version of GLOMAP-mode used here uses an advection time step of 1800 s, which is split into two chemical time steps (NCTS) during which chemistry and emissions are solved. Following that, a further split into two microphysical time steps (NMTS) solving the microphysics is utilised. In order to account for the competition between nucleation and condensation for available H_2SO_4 vapour, a further split of NMTS into five timesteps (NNTS) is utilised.

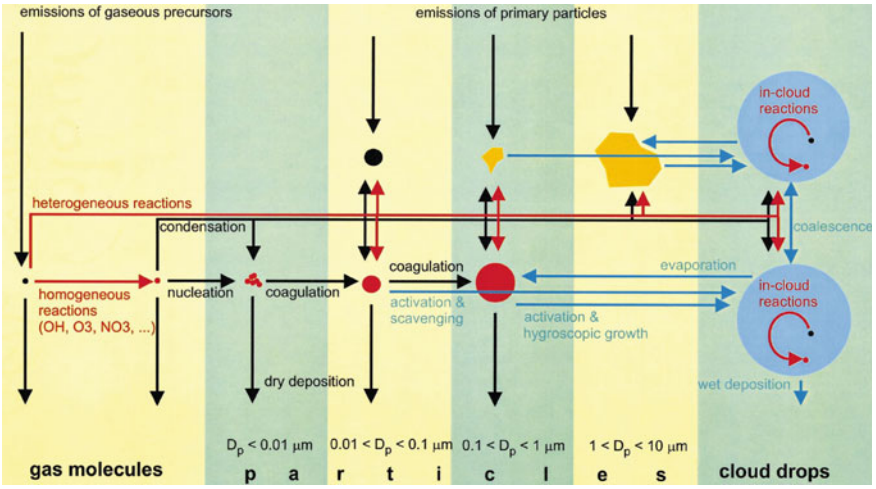

Fig. 2.1 The aerosol microphysical processes that shape the aerosol size distribution and influence the lifetime and chemical composition of atmospheric aerosol. Figure from Raes et al. (2000)

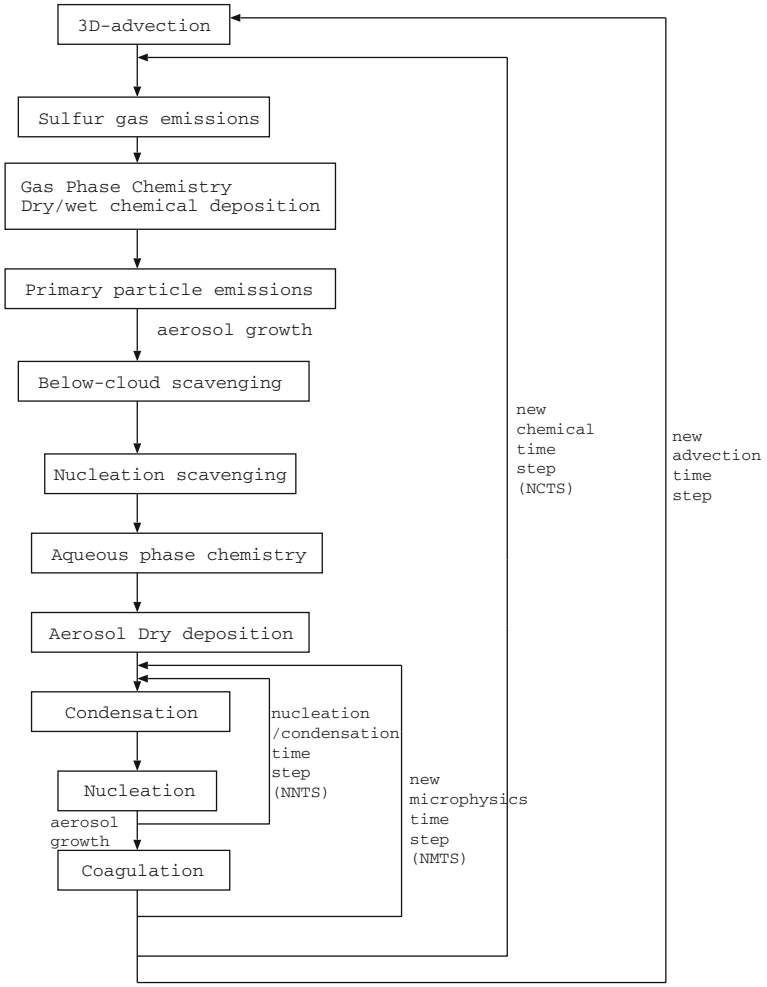

Fig. 2.2 Flow chart of the order in which GLOMAP-mode treats advective, chemical and microphysical processes with NCTS = chemical time step, NMTS = microphysical time step, and NNTS = nucleation/condensation time step. Figure from Spracklen et al. (2005a)

Nucleation

GLOMAP-mode simulates new particle formation in the free troposphere by using the binary H_2SO_4–H_2O nucleation scheme from Kulmala et al. (1998) with temperature, humidity and H_2SO_4 concentration being non-linearly related to the nucleation rate (and thus the change in nucleation mode number concentration). Favourable conditions for binary nucleation are a low temperature, a low particle surface area and a high relative humidity, thus the upper troposphere provides an ideal environment for new particle formation to take place (Spracklen et al. 2005a,b). Overall, the precise

mechanism inducing the formation of new particles remains poorly understood, and other mechanisms such as ternary (H_2SO_4–NH_3–H_2O) nucleation (e.g., Korhonen et al. 1999), and boundary layer nucleation (e.g., Kulmala et al. 2004) have been suggested.

Coagulation
Once new particles are formed, they are subject to coagulation and condensation which are important processes for the growth of newly formed sub-micron particles. GLOMAP-mode accounts for both intra-modal coagulation (i.e. collision of particles within the same mode) and inter-modal coagulation (i.e. collision of particles in different modes) using a simplified mass conserving scheme following Seinfeld and Pandis (1998) as described in Spracklen et al. (2005a) and Mann et al. (2010). Coagulation is an important growth mechanism for freshly nucleated particles as these small and often numerous particles move rapidly by Brownian motion leading to a high particle collision rate.

Condensation
Condensational growth of H_2SO_4 vapour (and secondary organics) onto existing aerosol follows Fuchs and Sutugin (1971) with condensation rates depending on the existing particle surface areas, the concentration of H_2SO_4 vapour and a mode-specific condensation coefficient. Sulphuric acid is a low volatility species, thus condenses easily onto existing aerosol.

Mode-Merging
In order to avoid growth of particles to sizes outside the specified mode-ranges (see Table 2.2) the geometric mean diameter is used for each mode, and particle number and mass are transferred between the modes if the upper limit of the geometric mean diameter is exceeded.

Removal Processes
Aerosol can be removed from the atmosphere by either dry deposition or wet deposition. In GLOMAP-mode, the parameterisation of dry deposition of aerosol follows the scheme of Zhang et al. (2001) accounting for gravitational settling, Brownian diffusion, impaction interception and particle rebound. In the model, the dry deposition rate depends on the size of particles, the land use category (e.g. forest, ocean) and the surface wind speed. Generally, the dry removal process is least efficient for particles with diameters of 1 μm and increases in efficiency for particles larger than 5 μm (as these gravitationally settle to the surface) and particles smaller than 0.05 μm (as these diffuse to the surface). Overall, dry deposition leads to the formation of the accumulation mode of an aerosol size distribution.

GLOMAP-mode treats nucleation scavenging (i.e. formation of a droplet around an aerosol nucleus) of in-cloud activated aerosol in grid boxes that are, according to ECMWF reanalyses, precipitating. In GLOMAP-mode large-scale rain removes 99.9 % of the aerosol number in the soluble accumulation and coarse modes at a constant removal rate over the course of 6 h. In contrast, convective rain is a sub-grid event for which the cloud-to-rainwater conversion rate is given by Tiedtke (1989) and removal of aerosol is assumed to occur in 30 % of the grid box.

GLOMAP-mode accounts for removal of aerosol via impaction scavenging (i.e. below-cloud scavenging or collection of aerosol particles by falling raindrops) using a size-dependent raindrop-aerosol collection efficiency look-up table which is calculated from the aerosol mean dry radius and an estimate of the rainfall size distribution (Sekhon and Srivastava 1971). In the model, impact scavenging is calculated for both dynamic and convective rain.

Cloud Processing
Here, the term "cloud processing" denotes the growth of already existing aerosol particles (as water droplets in non-precipitating clouds) by uptake and aqueous phase oxidation of SO_2. Cloud processing creates, after the evaporation of the drop, a minimum in the particle size distribution (referred to as Hoppel gap, e.g., Hoppel et al. 1994) which defines the Aitken and the accumulation modes. Cloud processing of aerosol in GLOMAP-mode follows Spracklen et al. (2005a) using a globally uniform activation dry radius that defines the smallest particles that are activated to cloud droplets. Throughout this thesis, an activation dry radius of 37.5 nm (corresponding to a cloud supersaturation of 0.2 % for sulphuric acid, which is typical for stratocumulus clouds) is assumed.

2.6.1 Aerosol Activation

Only a subset of the entire aerosol population acts as CCN. Throughout this thesis, CCN were counted as soluble particles with a dry radius larger than 35 nm, which is equivalent to the particles that would activate into cloud droplets at 0.22 % supersaturation (i.e. when considering H_2SO_4). Several microphysical processes lead to an increase in CCN concentrations:

(a) nucleation of H_2SO_4 vapour to SO_4 aerosol and its subsequent growth to CCN sizes by coagulation and condensation;
(b) growth to CCN sizes by condensation of H_2SO_4 onto existing particles; and
(c) cloud processing of Aitken mode-sized particles.

Once CCN are present in the atmosphere, water vapour can condense onto these particles and grow these particles to cloud drop size which is a hundred times larger when compared to the initial CCN-particle size. In this thesis, cloud drop number concentrations (CDNC) were calculated using a physically-based aerosol activation scheme, which is identical to Nenes and Seinfeld (2003) and evaluated for GLOMAP in Pringle et al. (2009). The Nenes and Seinfeld (2003) scheme predicts CDNC by means of calculating the maximum supersaturation for a given updraught velocity and aerosol distribution. Once the maximum supersaturation is obtained, the number of activated cloud drops is equal to the number of particles with a critical supersaturation less than the maximum supersaturation with the respective activation diameter being calculated using Köhler theory. The scheme has been shown to compare well with parcel model simulations (Nenes and Seinfeld 2003; Fountoukis and Nenes 2005)

and empirical schemes (Pringle et al. 2009). CDNC were calculated as a post-processing step using GLOMAP-mode output, thus there is no feedback with aerosol microphysical processes. CDNC were calculated in every grid box regardless of the presence of clouds, however when assessing the cloud-radiative effect a cloud mask was used. In this thesis, CDNC were calculated at the base of stratus clouds (approximately 1 km altitude or 920 hPa) using a globally uniform updraught velocity of $0.2\,\mathrm{ms}^{-1}$. Updraught velocities of $0.1–0.3\,\mathrm{ms}^{-1}$ are most commonly observed in stratus clouds (e.g., Gultepe and Isaac 1999; Peng et al. 2005). Fountoukis et al. (2007) showed that using an average updraught velocity provides a good approximation of mean CDNC. As with many other aerosol activation schemes (e.g., Chen and Penner 2005; Roelofs et al. 2006), the employed scheme does not account for droplet collision-coalescence (i.e. no droplet loss rate), thus the CDNC shown is representative of the cloud base.

2.7 Conclusions

GLOMAP-mode is a comprehensive global aerosol microphysics model embedded in the TOMCAT CTM. GLOMAP-mode uses a two-moment scheme in order to simulate the aerosol size distribution by carrying both aerosol mass and aerosol number. GLOMAP-mode accounts for microphysical processes such as nucleation, coagulation, condensation, cloud processing, and dry and wet deposition—all of which determine the evolution of the aerosol size distribution. GLOMAP-mode can be run using any combination of sulphate, sea-salt, black carbon, organic carbon and mineral dust components. Mann et al. (2010) provided a comprehensive overview of the processes treated in GLOMAP-mode, and of the models performance when compared to observational data sets and other numerical models. For the purpose of the work presented here, the coupled chemistry version of GLOMAP-mode has been employed.

References

Allen AG, Oppenheimer C, Ferm M, Baxter PJ, Horrocks LA, Galle B, McGonigle AJS, Duffell HJ (2002) Primary sulfate aerosol and associated emissions from Masaya Volcano, Nicaragua. J Geophys Res 107(D23):4682. doi:10.1029/2002JD002120

Andres RJ, Kasgnoc AD (1998) A time-averaged inventory of subaerial volcanic sulfur emissions. J Geophys Res 103:25251–25262

Atkinson R (2000) Atmospheric chemistry of VOCs and NOx. Atmos Environ 34:2063–2101

Bond TC, Streets DG, Yarber KF, Nelson SM, Woo JH, Klimont Z (2004) A technology-based global inventory of black and organic carbon emissions from combustion. J Geophys Res 109:D14203. doi:10.1029/2003JD003697

Breider TJ, Chipperfield MP, Richards NAD, Carslaw KS, Mann GW, Spracklen DV (2010) Impact of BrO on dimethylsulfide in the remote marine boundary layer. Geophys Res Lett 37:L02807. doi:10.1029/2009GL040868

Breider TJ (2010) Coupled halogen-sulfur-aerosol modeling in a 3D chemical transport model. Ph.D. thesis, School of Earth and Environment, University of Leeds

Brock CA, Washenfelder RA, Trainer M, Ryerson TB, Wilson JC, Reeves JM, Huey LG, Holloway JS, Parrish DD, Hübler G, Fehsenfeld FC (2002) Particle growth in the plumes of coal-fired power plants. J Geophys Res 107:4155. doi:10.1029/2001JD001062

Chen Y, Penner JE (2005) Uncertainty analysis for estimates of the first indirect aerosol effect. Atmos Chem Phys 5:2935–2948

Chipperfield MP (2006) New version of the TOMCAT/SLIMCAT off-line chemical transport model: intercomparison of stratospheric tracer experiments. Q J R Meteorol Soc 132:1179–1203

Cofala J, Amann M, Klimont Z, Schopp W (2005) Scenarios of world anthropogenic emissions of SO_2, NO_x and CO up to 2030. In: Internal report of the transboundary air pollution programme, International Institute of Applied Systems Analysis, Laxenburg, 2005

Dentener F, Kinne S, Bond T, Boucher O, Cofala J, Generoso S, Ginoux P, Gong S, Hoelzemann JJ, Ito A, Marelli L, Penner JE, Putaud JP, Textor C, Schulz M, van der Werf GR, Wilson J (2006) Emissions of primary aerosol and precursor gases in the years 2000 and 1750 prescribed data-sets for AeroCom. Atmos Chem Phys 6:4321–4344

Fountoukis C, Nenes A (2005) Continued development of a cloud droplet formation parameterization for global climate models. J Geophys Res 110:D11212

Fountoukis C, Nenes A, Meskhidze N, Bahreini R, Conant WC, Jonsson H, Murphy S, Sorooshian A, Varutbangkul V, Brechtel F, Flagan RC, Seinfeld JH (2007) Aerosol-cloud drop concentration closure for clouds sampled during the international consortium for atmospheric research on transport and transformation 2004 campaign. J Geophys Res 112:D10S30

Fuchs NA, Sutugin AG (1971) Topics in current aerosol research, International reviews in aerosol physics and chemistry, vol 2–3. Pergemon Press, New York

Gong SL (2003) A parameterization of sea-salt aerosol source function for sub- and super-micron particles. Glob Biogeochem Cycles 17(4):1097

Graf HF, Langmann B, Feichter J (1998) The contribution of earth degassing to the atmospheric sulfur budget. Chem Geol 147:131–145

Guenther A, Hewitt CN, Erickson D, Fall R, Geron C, Graedel T, Harley P, Klinger L, Lerdau M, Mckay WA, Pierce T, Scholes B, Steinbrecher R, Tallamraju R, Taylor J, Zimmerman P (1995) A global model of natural volatile organic compound emissions. J Geophys Res 100:8873–8892

Gultepe I, Isaac GA (1999) Scale effects on averaging of cloud droplet and aerosol number concentrations: observations and models. J Clim 12:1268–1279

Halmer M, Schmincke H, Graf HF (2002) The annual volcanic gas input into the atmosphere, in particular into the stratosphere, a global data-set for the past 100 years. J Volcanol Geotherm Res 115:511–528

Hoppel WA, Frick GM, Fitzgerald JW, Larson RE (1994) Marine boundary layer measurements of new particle formation and the effects nonprecipitating clouds have on aerosol size distribution. J Geophys Res 99:14443–14459

Kettle AJ, Andreae MO (2000) Flux of dimethylsulfide from the oceans: a comparison of updated data sets and flux models. J Geophys Res 105:26793–26808

Korhonen P, Kulmala M, Laaksonen A, Viisanen Y, McGraw R, Seinfeld JH (1999) Ternary nucleation of H_2SO_4, NH_3, and H_2O in the atmosphere. J Geophys Res 104:26349–26353

Kulmala M, Laaksonen A, Pirjola L (1998) Parameterization for sulfuric acid/water nucleation rates. J Geophys Res 108:8301–8307

Kulmala M, Vehkamäki H, Petäjä T, Dal Maso M, Lauri A, Kerminen VM, Birmili W, McMurry PH (2004) Formation and growth rates of ultrafine atmospheric particles: a review of observations. J Aerosol Sci 35:143–176

Loevblad G, Tarrason L, Torseth K, Dutchak S (2004) Sulphur. In: Loevblad G, Tarrason L, Torseth K, Dutchak S (eds) EMEP assessment, part I: European perspective, Norwegian Meteorological Institute, pp 15–46

Malm WC, Schichtel BA, Ames RB, Gebhart KA (2002) A 10-year spatial and temporal trend of sulfate across the United States. J Geophys Res 107:4627

Manktelow PT, Mann GW, Carslaw KS, Spracklen DV, Chipperfield MP (2007) Regional and global trends in sulfate aerosol since the 1980s. Geophys Res Lett 34:L14803

Mann GW, Carslaw KS, Spracklen DV, Ridley DA, Manktelow PT, Chipperfield MP, Pickering SJ, Johnson CE (2010) Description and evaluation of GLOMAP-mode: a modal global aerosol microphysics model for the UKCA composition-climate model. Geosci Model Dev 3:519–551

Merikanto J, Spracklen DV, Mann GW, Pickering SJ, Carslaw KS (2009) Impact of nucleation on global CCN. Atmos Chem Phys 9:8601–8616

Nenes, A, Seinfeld JH (2003) Parameterization of cloud droplet formation in global climate models. J Geophys Res 108(D14):4415. doi:10.1029/2002JD002911

Nightingale PD, Malin G, Law CS, Watson AJ, Liss PS, Liddicoat MI, Boutin J, Upstill-Goddard RC (2000) In situ evaluation of air-sea gas exchange—parameterizations using novel conservative and volatile tracers. Global Biogeochem Cycles 14(1):373–387

Peng Y, Lohmann U, Leaitch R (2005) Importance of vertical velocity variations in the cloud droplet nucleation process of marine stratus clouds. J Geophys Res 110:D21213

Pham M, Mueller JF, Brasseur GP, Granier C, Megie G (1995) A three-dimensional study of the tropospheric sulfur cycle. J Geophys Res 100(D12):26061–26092

Prather MJ (1986) Numerical advection by conservation of second-order moments. J Geophys Res 91:6671–6681

Pringle KJ, Carslaw KS, Spracklen DV, Mann GM, Chipperfield MP (2009) The relationship between aerosol and cloud drop number concentrations in a global aerosol microphysics model. Atmos Chem Phys 9:4131–4144

Raes F, Dingenen RV, Vignati E, Wilson J, Putaud JP, Seinfeld JH, Adams P (2000) Formation and cycling of aerosols in the global troposphere. Atmos Environ 34:4215–4240

Roelofs GJ, Stier P, Feichter J, Vignati E, Wilson J (2006) Aerosol activation and cloud processing in the global aerosol-climate model ECHAM5-HAM. Atmos Chem Phys 6:2389–2399

Seinfeld J, Pandis S (1998) Atmospheric chemistry and physics: from air pollution to climate change. Wiley, New York, p 1326

Sekhon RS, Srivastava RC (1971) Doppler radar observations of drop-size distributions in a thunderstorm. J Atmos Sci 28:983–994

Spracklen DV, Bonn B, Carslaw KS (2008b) Boreal forests, aerosols and the impacts on clouds and climate. Phil Trans R Soc A Math phys Eng Sci 366:4613–4626

Spracklen DV, Carslaw KS, Kulmala M, Kerminen VM, Sihto SL, Riipinen I, Merikanto J, Mann GW, Chipperfield MP, Wiedensohler A, Birmili W, Lihavainen H (2008a) Contribution of particle formation to global cloud condensation nuclei concentrations. Geophys Res Lett 35:L06808

Spracklen DV, Pringle KJ, Carslaw KS, Chipperfield MP, Mann GM (2005b) A global off-line model of size resolved aerosol processes: II. Identification of key uncertainties. Atmos Chem Phys 5:3437–3489

Spracklen DV, Pringle KJ, Carslaw KS, Chipperfield MP, Mann GW (2005a) A global off-line model of size-resolved aerosol microphysics: I. Model development and prediction of aerosol properties. Atmos Chem Phys 5:179–215

Stier P, Feichter J, Kinne S, Kloster S, Vignati E, Wilson J, Ganzeveld L, Tegen I, Werner M, Balkanski Y, Schulz M, Boucher O, Minikin A, Petzold A (2005) The aerosol-climate model ECHAM5-HAM. Atmos Chem Phys 5:1125–1156

Stockwell DZ, Chipperfield MP (1999) A tropospheric chemical-transport model: development and validation of the model transport schemes. Q J R Meteorol Soc 125:1747–1783

Textor C, Graf C, Timmreck HF, Robock A (2004) Emissions from volcanoes. In: Granier C, Artaxo P, Reeves C (eds) Emissions of chemical compounds and aerosols in the atmosphere. Kluwer, Dordrecht, pp 269–303

Textor C, Schulz M, Guibert S, Kinne S, Balkanski Y, Bauer S, Berntsen T, Berglen T, Boucher O, Chin M, Dentener F, Diehl T, Easter R, Feichter H, Fillmore D, Ghan S, Ginoux P, Gong S, Grini A, Hendricks J, Horowitz L, Huang P, Isaksen I, Iversen I, Kloster S, Koch D, Kirkevåg A, Kristjansson JE, Krol M, Lauer A, Lamarque JF, Liu X, Montanaro V, Myhre G, Penner J,

Pitari G, Reddy S, Seland Ø, Stier P, Takemura T, Tie X (2006) Analysis and quantification of the diversities of aerosol life cycles within AeroCom. Atmos Chem Phys 6:1777–1813
Tiedtke M (1989) A comprehensive mass flux scheme for cumulus parameterization in large-scale models. Mon Weather Rev 117:1779–1800
Van der Werf GR, Randerson JT, Collatz GJ, Giglio L (2003) Carbon emissions from fires in tropical and subtropical ecosystems. Glob Chang Biol 9:547–562
Vignati E, Wilson J, Stier P (2004) M7: An efficient size-resolved aerosol microphysics module for large-scale aerosol transport models. J Geophys Res 109:D22202
Whitby ER, McMurry PH (1997) Modal aerosol dynamics modeling. Aerosol Sci Technol 27:673–688
Woodhouse MT, Carslaw KS, Mann GW, Vallina SM, Vogt M, Halloran PR, Boucher O (2010) Low sensitivity of cloud condensation nuclei to changes in the sea-air flux of dimethyl-sulphide. Atmos Chem Phys 10:7545–7559
Woodhouse MT, Mann GW, Carslaw KS, Boucher O (2008) New directions: the impact of oceanic iron fertilisation on cloud condensation nuclei. Atmos Environ 42:5728–5730
Zhang L, Gong S, Padro J, Barrie L (2001) A size-segregated particle dry deposition scheme for an atmospheric aerosol module. Atmos Environ 35:549–560

Chapter 3
The Role of Time-Averaged Volcanic Sulphur Emissions in the Pre-industrial Era

3.1 Introduction

Volcanic degassing is an important natural source of sulphur to the atmosphere with estimates of the subaerial annual mean flux ranging from 0.75 Tg(S) per year (Kellogg et al. 1972) to 25.0 Tg(S) per year (Lambert et al. 1988). Andres and Kasgnoc (1998) compiled a time-averaged sulphur flux inventory for subaerial volcanoes, which is based on flux measurements from 49 continuously erupting and 25 sporadically erupting volcanoes between 1970 and 1997. The inventory by Andres and Kasgnoc (1998) has been used in the Aerosol Intercomparison Project (AEROCOM, Dentener et al. 2006) and accounts for an annual mean sulphur flux of 10.4 Tg(S) (with total SO_2 emissions accounting for 6.7 Tg(S) per year and emission of other sulphur species (H_2S, CS_2, carbonyl sulphide, SO_4^{2-} and particulate sulphur) accounting for 3.7 Tg(S) per year). For AEROCOM and in GLOMAP-mode, the Andres and Kasgnoc (1998) inventory is scaled by a factor of 1.21 and thus accounts for an annual mean sulphur flux of 12.58 Tg(S) (i.e. before any partitioning into SO_2 and primary SO_4).[1] The other natural sources of sulphur to the atmosphere are DMS (13–36 Tg(S) per year), biomass burning (1–6 Tg(S) per year), and land biota and soils (0.4–5.6 Tg(S) per year) (Penner et al. 2001). Thus, in the pre-industrial atmosphere volcanic degassing accounts for between 20 and 47 % of the total natural sulphur flux. In contrast, the modern-day atmosphere is dominated by anthropogenic sulphur emissions (i.e. around 58 Tg(S) per year, Smith et al. 2010) in which volcanic degassing accounts for around 10 % (Stevenson et al. 2003a) of the total present-day sulphur flux.

[1] As outlined in Chap. 2 the Andres and Kasgnoc (1998) inventory is commonly scaled by a factor of 1.21 (Dentener et al. 2006) following recommendations of Graf et al. (1998) and Textor et al. (2004), who highlighted that the original inventory is likely an underestimate. Note that throughout this thesis the scaled Andres and Kasgnoc (1998) inventory is used.

A. Schmidt, *Modelling Tropospheric Volcanic Aerosol*, Springer Theses,
DOI: 10.1007/978-3-642-34839-6_3, © Springer-Verlag Berlin Heidelberg 2013

Previous modelling studies have investigated the relative contribution of time-averaged volcanic sulphur emissions to the global sulphur budget (Chin and Jacob 1996; Stevenson et al. 2003a) and to the total SO_4 aerosol forcing (Graf et al. 1997, 1998) under modern-day conditions. Graf et al. (1997) found that time-averaged volcanic sulphur emissions are at least as important as anthropogenic sulphur emissions with regard to the global sulphur cycle and to their climate forcing potential. All previous studies neglected aerosol microphysical processes. In contrast, the simulations presented in this chapter explicitly account for aerosol microphysical processes such as nucleation, condensation and coagulation in order to determine the size and number concentration as well as the lifetime of climate-relevant particles.

Graf et al. (1998) hypothesized that the relationship between the source strength of time-averaged volcanic emissions and the tropospheric sulphur budget as well as the radiative effects is "quasi-linear" under the assumption that the source's spatial distribution remains fixed. However, Lohmann and Feichter (2005) highlighted that cloud-properties respond non-linearly to changes in aerosol loading, which is especially true when background aerosol concentrations are low (as is the case in the pre-industrial atmosphere).

Andres and Kasgnoc (1998) noted that their inventory is likely an underestimate as "only" 74 volcanoes are considered (i.e. the ones that featured flux measurements). For comparison, the Smithsonian's Global Volcanism Program lists more than 200 subaerial volcanoes that erupted during the twentieth century[2]—a criterion that could be used to declare a volcano as "active". In general, based on previous estimates of the volcanic source strength (see also review by Textor et al. (2004), Table 2) it seems reasonable to halve and double the Andres and Kasgnoc (1998) inventory for the purpose of a sensitivity study.

The chapter presented here, firstly aims to assess the contribution of time-averaged volcanic sulphur emissions to the global CCN budget in the pre-industrial era, building on previous studies that used mass-only schemes and neglected microphysical processes. Using a global aerosol microphysics model enables assessing the impact on CCN number concentration and cloud-radiative effect based on a size-resolved aerosol distribution. Secondly, this chapter investigates the sensitivity of the global sulphur and CCN budget with regards to the uncertainty in the strength of the volcanic sulphur flux. The sensitivity study is performed in relation to the time-averaged volcanic emission inventory of Andres and Kasgnoc (1998) by halving and doubling the inventory. Such information is important as the magnitude of the anthropogenic climate forcing is assessed with respect to the pre-industrial era. In other words, if the uncertainty in the magnitude of the volcanic sulphur flux leads to an uncertainty in the magnitude of the pre-industrial cloud-radiative effect, then estimates of the current radiative forcing are subject to uncertainty.

[2] http://www.volcano.si.edu/world/summary.xls

3.2 Data and Methods

In this study, GLOMAP-mode (Mann et al. 2010) is used together with the following natural emissions: 12.58 Tg(S) per year volcanic SO_2 using the Andres and Kasgnoc (1998) inventory[3]; 18.6 Tg(S) per year DMS (Kettle and Andreae 2000) assuming a sea-air transfer velocity parameterizations of Nightingale et al. (2000). Sea spray emissions are driven by wind speeds updated every 6 h using the emissions parameterizations of Gong (2003). Figure 3.1a shows the annual zonal mean SO_2 flux using the Andres and Kasgnoc (1998) inventory together with information on the injection height (which is then referred to as the GEIA inventory in the literature (e.g., Dentener et al. 2006). Figure 3.1b shows the spatial distribution of the volcanoes considered in the Andres and Kasgnoc (1998) inventory within GLOMAP-mode. The simulations also include sulphur emission from biomass burning representative for the year 1750 (total of 0.7 Tg(S) per year; provided by Jonahs Merchants using the same approach as described in Merikanto et al. (2010) but for 1750). All simulations are run for twelve months specifying the same meteorological fields from DECEM for the year 2004 in order to ensure consistency between the runs.

Table 3.1 lists the simulations that were conducted:

(a) excluding volcanic sulphur emissions;
(b) including the Andres and Kasgnoc (1998) inventory as is (hereafter referred to as AK1998);
(c) halving the Andres and Kasgnoc (1998) inventory (hereafter referred to as 0.5*AK1998); and
(d) doubling the Andres and Kasgnoc (1998) inventory (hereafter referred to as 2.0*AK1998).

The cloud-radiative effect was calculated off-line from monthly mean CDNC fields using a radiative transfer model (Edwards and Slingo 1996) together with monthly mean cloud and surface albedo fields from the International Satellite Cloud Climatology Project (ISCCP) for the years 1983–2007 (Rossow and Schiffer 1999). The cloud-radiative effect calculations were performed by Professor Piers Forester (University of Leeds) and were subsequently analyzed by the author. CDNC was calculated as a post-processing step using a physically based aerosol activation scheme (Pringle et al. 2009) as described in Sect. 2.6.1. Here, CDNC has been calculated at the base of stratus clouds (approximately 1 km altitude or 920 hPa above terrain or sea-level) using a globally uniform updraught velocity of 0.2 ms^{-1}, which provides a good approximation of mean CDNC (Fountoukis et al. 2007). It should be noted that, as with many other aerosol activation schemes (e.g., Chen and Penner 2005; Roelofs et al. 2006), the employed scheme does not account for droplet collision-coalescence (i.e. no droplet loss rate), thus the CDNC shown is representative of the cloud base.

[3] As outlined in Chap. 2 it is assumed that 2.5 % of the total volcanic sulphur flux is emitted as primary SO_4, hence after partitioning into SO_2 and primary SO_4 the annual mean volcanic SO_2 flux equates to 12.27 Tg(S).

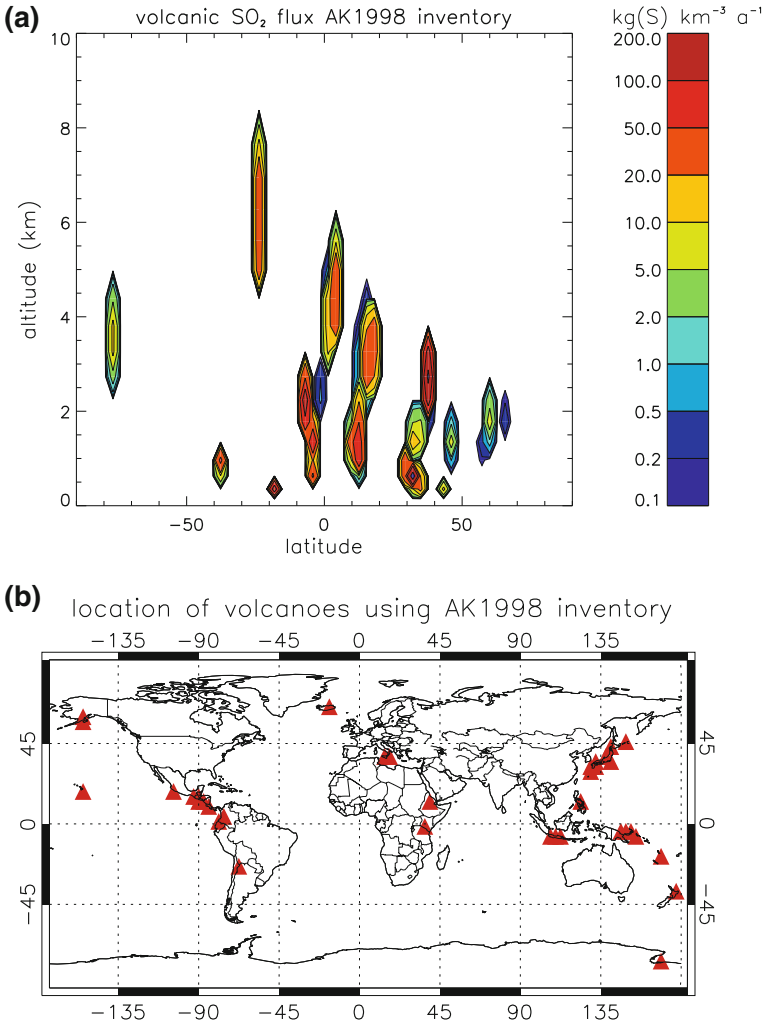

Fig. 3.1 Representation of the volcanic sulphur flux in GLOMAP-mode with (**a**) annual zonal mean volcanic SO_2 flux (kg(S) per km^3 per year) using the Andres and Kasgnoc (1998) inventory (referred to as AK1998), and (**b**) geographical location of the volcanic sources. Figure from Schmidt et al. (2012)

Two different baseline scenarios were considered in calculating the cloud-radiative effect:

(a) excluding the volcanic emissions; and
(b) using the AK1998 simulation as the baseline.

Table 3.1 Simulated global annual mean sulphur budget showing fluxes (Tg(S) per year) and lifetimes (days) with values in parentheses denoting relative changes (in %) for the simulations including volcanic emissions (AK1998) and for the simulations including half and double the volcanic emissions (0.5*AK1998 and 2.0*AK1998, respectively) with respect to the simulation without volcanic emissions

	Excluding volcanics	AK1998	0.5*AK1998	2.0*AK1998	Stevenson et al. (2003b)
SO_2 emissions (volcanic + biomass burning)	0.7	13.0	6.8	25.2	9.0
DMS to SO_2	17.1	17.1	17.1	17.1	12.2
SO_2 burden	0.05	0.14 (180)	0.09 (80)	0.24 (380)	0.09
SO_2 ddep	3.1	4.9 (56)	3.9 (25)	7.2 (129)	1.8
SO_2 wdep	1.7	4.8 (190)	3.2 (89)	8.5 (406)	2.2
SO_2 lifetime (days)	1.1	1.8 (65)	1.5 (37)	2.2 (99)	1.6
$SO_4 + OH$	1.6	4.6 (184)	3.0 (87)	7.9 (388)	1.9
Aq. phase SO_2 ox	10.2	14.1 (38)	12.4 (21)	16.8 (64)	15.5
$H_2SO_4 - H_2O$ nucleation	0.002	0.004 (100)	0.003 (50)	0.007 (250)	–
Condensation (all-modes)	1.5	4.5 (193)	2.9 (91)	7.7 (409)	–
Coagulation (all-modes)	0.04	0.12 (200)	0.08 (100)	0.20 (400)	–
SO_4 burden	0.14	0.28 (100)	0.21 (50)	0.41 (193)	0.28
SO_4 ddep	1.7	2.6 (56)	2.1 (30)	3.3 (102)	1.5
SO_4 wdep	11.4	18.2 (59)	15.0 (31)	24.1 (111)	15.8
SO_4 lifetime (days)	3.9	4.9 (27)	4.5 (17)	5.4 (41)	5.8

Abbreviations ddep = dry deposition; wdep = wet deposition

This approach allowed to investigate both the contribution of volcanic sulphur emissions to the cloud-radiative effect, and the importance of the uncertainty in the volcanic sulphur source strength, for assessing the pre-industrial aerosol-cloud state that is used as the baseline for present-day radiative forcing calculations. For the control (without volcanic emissions) and the volcanically perturbed runs, the cloud drop effective radius was calculated from the GLOMAP-mode monthly mean CDNC and ISCCP-derived liquid water paths, and only low-level clouds were modified. CDNC was calculated in every grid box, and for calculating the radiative effect a cloud mask was used. This approach, based on observed clouds, differs from that used in most coupled atmosphere-ocean GCMs in which marine stratocumulus cloud fields are calculated by the model, and often agree poorly with observations (e.g., Ramaswamy et al. 2001; Williams and Tselioudis 2007). For the baseline simulations, the liquid water paths for low-level clouds were calculated from ISCCP optical depth measurements assuming an effective drop radius of 10 μm. For the perturbed simulations, the liquid water path was assumed to remain unchanged and drop size is altered based on the fractional change in CDNC between the baseline and the perturbed simulations.

3.3 Results and Discussion

3.3.1 Global Sulphur Budget

Firstly, GLOMAP-mode is used to assess the effect of the time-averaged volcanic sulphur emissions on the global sulphur budget in the pre-industrial era. Figure 3.2 shows the annual zonal mean SO_2 mixing ratios for the simulation without volcanic emissions together with changes in the SO_2 mixing ratios for the three sensitivity simulations. For the simulation without volcanic emissions, annual zonal mean SO_2 mixing ratios range from 0.007 to 38.7 pptv and in the free troposphere south of 50° S the model predicts mixing ratios in excess of 20 pptv, which is a result of the updraught of DMS derived in the southern ocean and its subsequent oxidation to SO_2 in the free troposphere. The absolute changes in the annual zonal mean SO_2 mixing ratios for 0.5*AK1998, AK1998 and 2.0*AK1998 compared to the simulation excluding volcanic emissions are shown in Fig. 3.2b. GLOMAP-mode simulates absolute changes of up to 98.3, 201.0 and 415.1 pptv for 0.5*AK1998, AK1998 and for 2.0*AK1998, respectively. The spatial distribution of the SO_2 mixing ratios closely follows that of the volcanic source. However, at mid-latitudes, upper tropospheric SO_2 mixing ratios of up to 20 pptv are simulated for AK1998. In contrast, SO_2 mixing ratios are vertically more confined in the NH when compared to the SH, which is a result of the vertical distribution of the volcanic emissions as shown in Fig. 3.1.

Figure 3.3 shows the annual zonal mean mixing ratios and the absolute changes as in Fig. 3.2 but for SO_4 aerosol mixing ratios. Annual zonal mean SO_4 mixing ratios range from 0.82 to 111.0 pptv in the simulation without volcanic emissions. In the

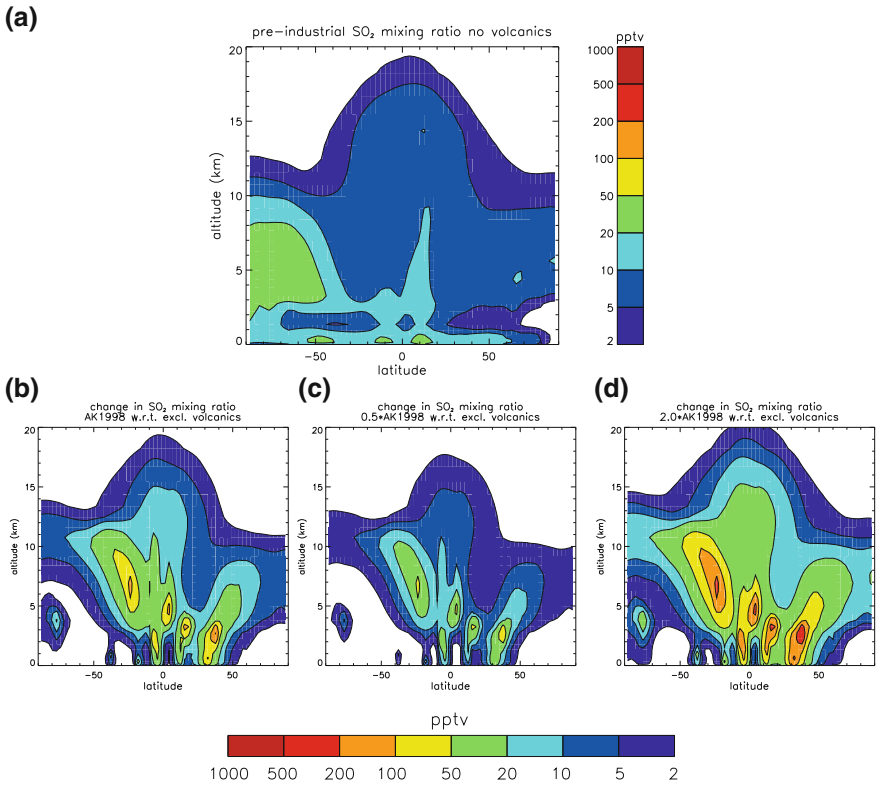

Fig. 3.2 Pre-industrial annual zonal mean SO_2 mixing ratios (pptv) with (**a**) the simulation without volcanic emissions. Change in annual zonal mean SO_2 mixing ratios for (**b**) the Andres and Kasgnoc (1998) inventory (AK1998); (**c**) the halved Andres and Kasgnoc (1998) inventory (0.5*AK1998); and (**d**) the doubled Andres and Kasgnoc (1998) inventory (2.0*AK1998) with respect to the simulation without volcanic emissions

latitude band ranging from 30° N to 50° S, SO_4 mixing ratios in excess of 50 pptv are simulated between the surface and around 2 km altitude (with the peak mixing ratio occurring at around 10° S). The model simulates peak absolute changes in the annual zonal mean SO_4 mixing ratios of 66.6, 121.5 and 217.7 pptv for 0.5*AK1998, AK1998 and 2.0*AK1998, respectively. Generally, the simulated SO_4 mixing ratios exhibit a vertically more widespread impact compared to the SO_2 mixing ratios (Fig. 3.2), which is a result of the longer lifetime of the SO_4 aerosol due to less efficient removal in the upper troposphere.

Table 3.1 shows the simulated global annual mean sulphur budgets together with the sulphur budgets obtained by Stevenson et al. (2003b) for an 1860 simulation as the latter can be used as a benchmark for the AK1998 simulation. In GLOMAP-mode, the annual mean SO_2 flux of 30.07 Tg(S) is a factor of ∼1.4 higher than that predicted by the STOCHEM-Ed CTM, which is a result of the differences in the magnitude

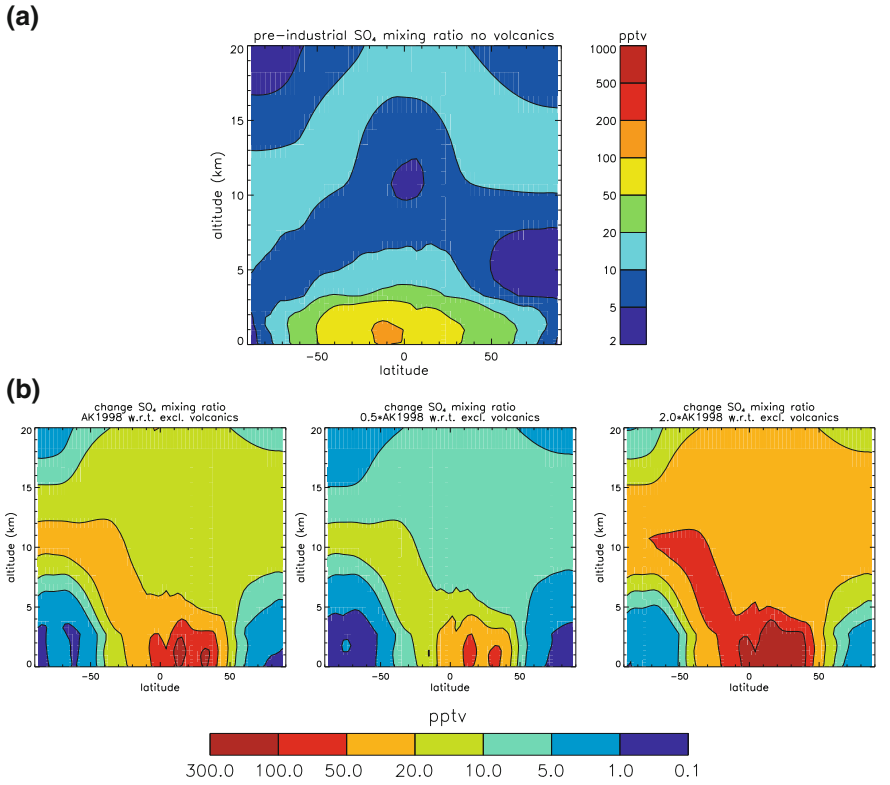

Fig. 3.3 As Fig. 3.2 but for SO_4 mixing ratios

of the annual mean DMS flux (i.e. 15.0 Tg(S) per year from DMS resulting in a DMS to SO_2 flux of 12.2 Tg(S) per year using the STOCHEM-Ed CTM compared to 18.6 Tg(S) per year from DMS resulting in a DMS to SO_2 flux of 17.1 Tg(S) per year using GLOMAP-mode), the annual mean volcanic sulphur flux (i.e. 8.7 Tg(S) per year using STOCHEM-Ed compared to 12.27 Tg(S) per year using GLOMAP-mode) and the annual mean sulphur flux from biomass burning (i.e. 0.3 Tg(S) per year using STOCHEM-Ed compared to 0.7 Tg(S) per year using GLOMAP-mode). For AK1998, GLOMAP-mode predicts a global annual mean SO_2 burden of 0.14 Tg(S) which is a factor of 1.6 higher than that found by Stevenson et al. (2003b). Both the Stevenson et al. (2003b) study and the study presented here find a global annual mean pre-industrial SO_4 burden of 0.28 Tg(S) (despite the differences in the magnitude of the SO_2 emissions) which can be explained by the fact that the SO_4 lifetime of 4.9 days predicted by GLOMAP-mode is shorter than the lifetime of 5.8 days found by Stevenson et al. (2003b). Furthermore, there are slight differences in the SO_2 removal processes in that GLOMAP-mode predicts a nearly equal contribution of SO_2 dry and wet deposition whereas the wet removal of SO_2 dominates over the dry removal

process in the STOCHEM-Ed model. Overall, both models predict SO_2 and SO_4 fluxes that compare reasonably well given that removal processes are parameterised differently in different models.

Furthermore, Table 3.1 indicates that in the AK1998 simulation around 32 % of the SO_2 is deposited before being oxidised to SO_4 whereas in the 0.5*AK1998 and 2.0*AK1998 simulations 30 % and 37 % of the SO_2 is deposited rather than oxidised to form SO_4. Thus, with increasing volcanic sulphur flux the ratio of deposition to oxidation of SO_2 increases, which means the relative amount of SO_4 formed drops. The latter is also apparent when comparing the SO_2 burden to SO_4 burden ratios of the 0.5*AK1998 (ratio of 0.43), AK1998 (ratio of 0.5) and 2.0*AK1998 (ratio of 0.59) simulations with each other. In all three simulations aqueous-phase oxidation of SO_2 (with H_2O_2 being the main oxidant) dominates over the gas-phase oxidation of SO_2; however the ratio of aqueous-phase to gas-phase oxidation (4.1 for 0.5*AK1998, 3.1 for AK1998 and 2.1 for 2.0*AK1998) reveals that the relative importance of gas-phase oxidations increases with increasing volcanic sulphur flux. Thus, the relative importance of nucleation and condensation of H_2SO_4 vapour increases as well.

Table 3.2 shows the relative contributions of the volcanic and the non-volcanic sulphur sources to the total global annual mean SO_2 emissions, the SO_2 and SO_4 burdens together with the SO_4 burden efficiency. The term "SO_4 burden efficiency" is defined as the fractional contribution of a sulphur source to the SO_4 burden divided by the fractional source strength, and is a useful measure for quantifying the efficiency of a sulphur source to form SO_4 (Graf et al. 1997). For 0.5*AK1998, AK1998 and 2.0*AK1998, volcanic emissions account for 26 %, 41 % and 58 % of the total SO_2 emissions, and contribute to 44 %, 64 % and 79 % to the SO_2 burden. The contribution to the pre-industrial SO_4 burden is found to be 33 % for 0.5*AK1998, 50 % for AK1998 and 66 % for 2.0*AK1998.

GLOMAP-mode predicts a pre-industrial SO_4 burden efficiency of 1.27 for 0.5*AK1998 (0.91 for non-volcanic source), 1.22 for AK1998 (0.85 for the non-volcanic sources) and 1.14 for 2.0*AK1998 (0.81 for non-volcanic source). Generally, volcanic sulphur emissions contribute more efficiently to the pre-industrial atmospheric SO_4 burden when compared to the other natural, non-volcanic sources. This finding is supported by previous studies investigating the SO_4 burden efficiency of different sulphur sources and can be explained by the longer lifetime of the volcanic SO_4 (due to the injection of SO_2 at higher altitudes) (Chin and Jacob 1996; Graf et al. 1997; Stevenson et al. 2003a). The results also suggest that an increase in the fractional contribution of the volcanic sulphur source results in a disproportional contribution to the SO_4 burden under pre-industrial conditions. The changes in the sulphur budgets (Table 3.1) show that the fraction of SO_2 being deposited, rather than oxidised to form SO_4, increases disproportionately with increasing volcanic sulphur flux, hence the atmospheric SO_4 burden does not increase proportionally.

Table 3.2 Total global annual mean SO_2 emissions (Tg(S) per year), SO_2 burden, SO_4 burden and percentage contribution of different sources to the total emissions and budgets. The term "SO_4 burden efficiency" denotes the fractional contribution of a sulphur source to the SO_4 burden divided by the fractional source strength (after Graf et al. 1997)

Pre-industrial	Contribution	Simulation		
		0.5*AK1998	AK1998	2.0*AK1998
SO_2 emissions	Total (Tg(S) a^{-1})	23.93	30.07	42.35
	Volcanic (%)	26	41	58
	Non-volcanic (%)	74	59	42
SO_2 burden	Total (Tg(S))	0.09	0.14	0.24
	Volcanic (%)	44	64	79
	Non-volcanic (%)	56	36	21
SO_4 burden	Total (Tg(S))	0.21	0.28	0.41
	Volcanic (%)	33	50	66
	Non-volcanic (%)	67	50	34
SO_4 burden efficiency	Volcanic	1.27	1.22	1.14
	Non-volcanic	0.91	0.85	0.81

3.3.2 Impact on CCN Number Concentrations

Natural sulphur emissions have a strong potential to impact CCN number concentrations throughout the atmosphere as the gas-phase oxidation of SO_2 increases atmospheric concentrations of H_2SO_4-vapour which subsequently nucleates to form new particles and condenses to grow newly nucleated and/or pre-existing particles to CCN sizes. A change in CCN number concentrations at low-level cloud altitude can subsequently mediate a cloud-radiative effect via the change in CDNC. Figure 3.4 shows the spatial distribution of the pre-industrial annual mean CCN number concentrations at 970 m altitude for the simulation without volcanic sulphur emissions and the AK1998 simulation. Without volcanic emissions, GLOMAP-mode simulates global annual mean CCN number concentrations at 970 m altitude of 60 cm^{-3} with peak concentrations of 379 cm^{-3} in biomass burning regions of South Africa. Without volcanic emissions, annual hemispheric mean CCN number concentrations of 58 and 62 cm^{-3} are simulated for the NH and SH, respectively, which compares to annual mean concentrations of 92 cm^{-3} in the tropics.

Figures 3.4b, c and 3.5 show the effect on annual mean CCN number concentrations at 970 m altitude when including volcanic sulphur emissions. Including volcanic sulphur emissions results in a 45 % increase in global mean CCN number concentrations at 970 m (i.e. to 87 cm^{-3}) when compared to an atmosphere without volcanic emissions. Halving and doubling the Andres and Kasgnoc (1998) inventory results in an increase of 28.3 % and 75 % in global mean CCN number concentrations (i.e. to 77 and to 105 cm^{-3}), respectively. Both AK1998 and 2.0*AK1998 exhibit the largest relative change in NH mean CCN number concentrations of 46.6 % and 75.0 %, respectively (i.e. increase to 85 and 104 cm^{-3}), whereas a change of 29.0 % in SH

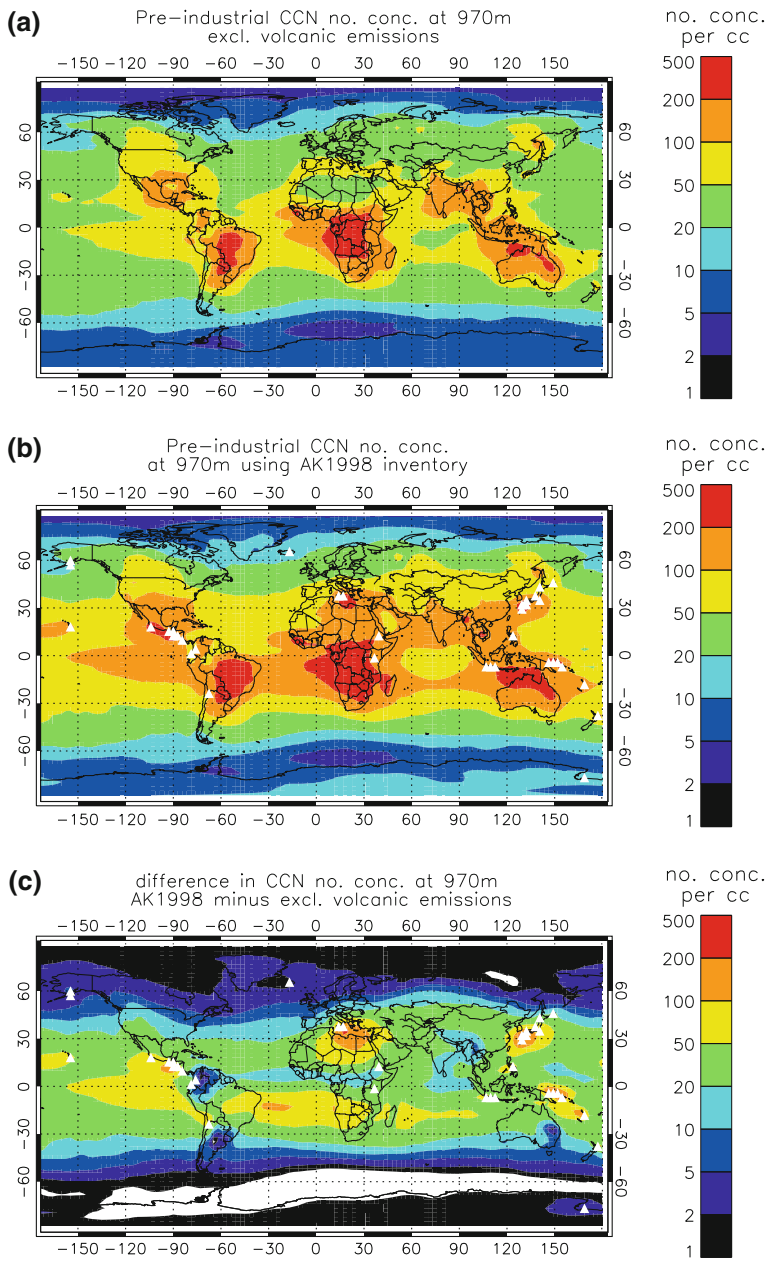

Fig. 3.4 Pre-industrial annual mean CCN number concentrations (per cm^3) at 970 m altitude for (**a**) the simulation without volcanic emissions; (**b**) the simulation using the AK1998 inventory. Panel (**c**) shows the difference in annual mean CCN number concentrations (i.e. AK1998 simulation minus simulation excluding volcanic emissions) at 970 m altitude. The *white triangles* denote the locations of volcanoes considered using the Andres and Kasgnoc (1998) inventory

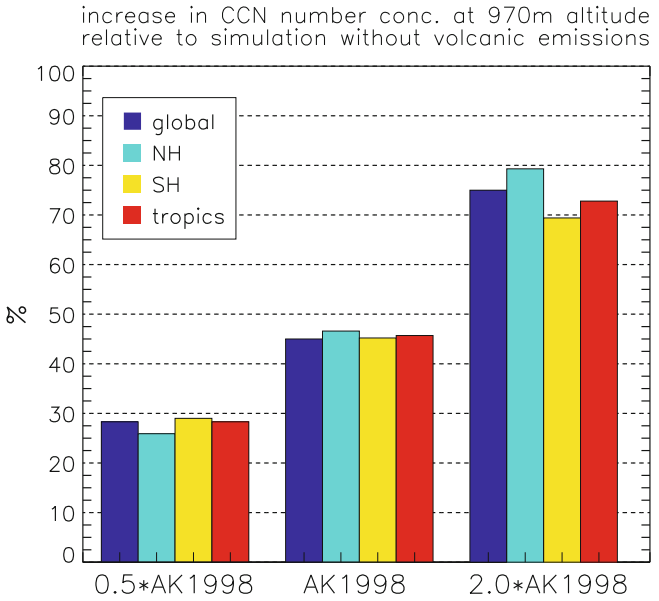

Fig. 3.5 Increase in CCN number concentrations at 970 m altitude due to including volcanic emissions relative to the simulation excluding volcanic emissions. CCN is counted as soluble particles with a dry radius larger than 35 nm, which is equivalent to the particles that would activate into cloud droplets at 0.22 % supersaturation. AK1998 denotes the Andres and Kasgnoc (1998) inventory, and 0.5*AK1998 and 2.0*AK1998 denote the halved and doubled Andres and Kasgnoc (1998) inventory, respectively

mean CCN number concentrations is simulated for 0.5*AK1998 (i.e. increase to $80\,\mathrm{cm}^{-3}$).

The response of CCN to changes in the magnitude of the volcanic flux can be compared in terms of a *relative CCN sensitivity*. The relative CCN sensitivity can be interpreted as the fractional change in CCN number concentrations for a fractional change in the flux of volcanic sulphur and is calculated as follows:

$$\Delta\,\mathrm{CCN_{rel}} = \frac{\sum_{i=1}^{N} \text{perturbed}\,\mathrm{CCN_i} - \sum_{i=1}^{N} \text{unperturbed}\,\mathrm{CCN_i}}{\sum_{i=1}^{N} \text{unperturbed}\,\mathrm{CCN_i}} * 100.0 \qquad (3.1)$$

where *perturbed CCN*$_i$ denotes the CCN number concentrations at 970 m altitude for the simulation in which the volcanic sulphur flux is halved or doubled; *unperturbed CCN*$_i$ denotes CCN number concentrations for the simulation using the volcanic sulphur flux from the AK1998 inventory; i denotes the grid box index in a given model domain (i.e. global, NH, SH, 21° S to 21° N domain, respectively).

$$\Delta\,\mathrm{SO_{2\,rel}} = \frac{\sum_{i=1}^{N} \text{perturbed } \mathrm{SO_{2\,i}} - \sum_{i=1}^{N} \text{unperturbed } \mathrm{SO_{2\,i}}}{\sum_{i=1}^{N} \text{unperturbed } \mathrm{SO_{2\,i}}} * 100.0 \tag{3.2}$$

where *perturbed* $SO_{2\,i}$ denotes the global column-integrated volcanic SO_2 flux for the simulation in which the volcanic sulphur flux is halved or doubled, *unperturbed* $SO_{2\,i}$ denotes the global column-integrated volcanic SO_2 flux in the simulation using the volcanic sulphur flux from the AK1998 inventory.

The relative CCN sensitivity at 970 m is then calculated as the fractional change in CCN number concentrations ($\Delta\,\mathrm{CCN_{rel}}$) divided by fractional change in volcanic sulphur flux ($\Delta\,\mathrm{SO_{2\,rel}}$):

$$\text{relative CCN sensitivity} = \frac{\Delta\,\mathrm{CCN_{rel}}}{\Delta\,\mathrm{SO_{2\,rel}}} \tag{3.3}$$

This definition of CCN sensitivity might at first be somewhat cumbersome; however it is more understandable than an absolute CCN sensitivity measure: $\Delta\,\mathrm{CCN_{abs}}/\Delta\,\mathrm{SO_{2\,abs}}$, which would have units of particles per cm^3 per Tg(S) per year.

Figure 3.6 shows the relative CCN sensitivity at 970 m altitude for emitting half or twice the amount volcanic sulphur of the Andres and Kasgnoc (1998) inventory.

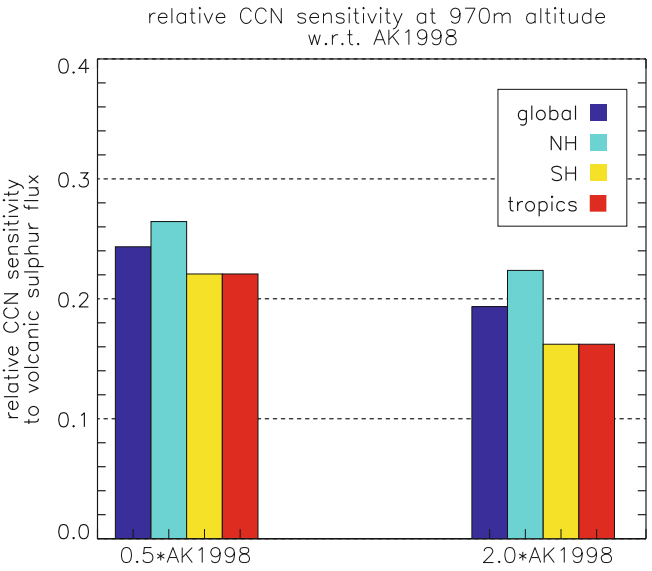

Fig. 3.6 Relative CCN sensitivity to volcanic sulphur flux at 970 m altitude for halving (0.5*AK1998) and doubling (2.0*AK1998) the Andres and Kasgnoc (1998) inventory with respect to the "standard" Andres and Kasgnoc (1998) inventory (AK1998)

Globally, the model predicts a relative CCN sensitivity of 0.24 and 0.19 for 0.5*AK1998 and for 2.0*AK1998, respectively. Firstly, it should be noted that CCN number concentrations at low-level cloud altitude are highly sensitive to changes in the magnitude of the volcanic sulphur flux. Moreover, the CCN sensitivity is disproportionally related to the strength of the volcanic sulphur flux. Considering a 100 % increase in volcanic sulphur flux would result in a 19 % increase in global annual mean CCN number concentrations at low-level cloud altitude when compared to the Andres and Kasgnoc (1998) inventory. In contrast, reducing the volcanic sulphur flux by 50 % would result in a 12 % reduction in global mean CCN number concentrations at low-level cloud altitude.

Using a size-resolving aerosol model, such as GLOMAP-mode reveals that the sensitivity of CCN to volcanic flux changes is driven by complex, non-linear interactions between chemical and microphysical processes (Table 3.1). The annual mean sulphur budgets reveal that, under pristine atmospheric conditions, aqueous-phase oxidation dominates over the gas-phase oxidation of SO_2 by a factor of 6.4 when excluding volcanic emissions, and by a factor of 3.1 when considering the simulation using the Andres and Kasgnoc (1998) inventory. In contrast, a 100 % change in the sulphur flux from volcanoes results in the gas-phase oxidation of SO_2 becoming more important relative to the aqueous-phase oxidation of SO_2 (i.e. factor of 2.1 between aqueous-phase and gas-phase oxidation). The majority of the volcanic sulphur is emitted well above the boundary layer into the free troposphere (Fig. 3.1) where OH is the dominant oxidant, thus explaining the shift towards gas-phase oxidation. The oxidation of SO_2 in the gas-phase produces H_2SO_4 vapour which subsequently nucleates to form new particles. A relative increase in nucleation leads to more numerous, small particles competing with pre-existing aerosol for the available H_2SO_4 vapour. Hence, more particles compete for condensational growth. As a result, fewer particles will grow to CC-sizes. Thus, the key microphysical processes that govern the formation of climate-relevant CC-sized particles are nucleation and condensation, which in turn are governed by the relative balance of gas-phase oxidation to aqueous-phase oxidation of SO_2. The results demonstrate that the balance between these chemical and microphysical processes shifts even under modest perturbations to the magnitude of the volcanic sulphur flux (Table 3.1).

Secondly, Fig. 3.6 reveals differences in the relative CCN sensitivity on a regional scale. For example, hemispheric mean relative CCN sensitivities of 0.26 and 0.22 (for the NH and SH, respectively) are calculated for 0.5*AK1998, whereas hemispheric mean CCN sensitivities of 0.22 and 0.16 are calculated for 2.0*AK1998. Both 2.0*AK1998 and 0.5*AK1998 exhibit the highest sensitivity between CCN number concentrations and volcanic sulphur flux in the NH. These differences in the regional CCN sensitivity can be explained with the spatial distribution of the volcanic sulphur flux as the majority of the sulphur is released in the NH (Fig. 3.1).

3.3.3 First Aerosol Indirect Effect

To assess the impact of volcanic emissions on the radiative balance at the top of the atmosphere (combined longwave and shortwave) the first aerosol indirect effect (AIE) for low-level cloud changes is calculated. Figure 3.7 shows the spatial distribution of the annual mean first AIE for the AK1998 simulation. A global annual mean first AIE of $-1.45\,\mathrm{W\,m^{-2}}$ is simulated when including volcanic emissions with a peak of $-10.9\,\mathrm{W\,m^{-2}}$ simulated in stratocumulus cloud regions along the western coast of south Africa. Annual NH and SH mean first AIEs of -1.29 and $-1.6\,\mathrm{W\,m^{-2}}$ are simulated, respectively. Figure 3.7 highlights that the first AIE is strongest in the southern tropics in regions that exhibit persistent stratocumulus cloud decks. Along the western coast of south America a first AIE in excess of $-6\,\mathrm{W\,m^{-2}}$ is simulated when including volcanic sulphur emissions.

Table 3.3 lists the magnitude of the annual mean first AIE when including volcanic emissions in the pre-industrial atmosphere (values denote first AIE in relation to simulation without volcanic emissions; values in parentheses denote first AIE in relation to AK1998 simulation). All three simulations exhibit the largest annual mean first AIE when averaged over the tropics with -1.46, -2.22 and $-3.14\,\mathrm{W\,m^{-2}}$ for 0.5*AK1998, AK1998, and 2.0*AK1998, respectively. Peaks in the annual mean first AIE of -7.46, -10.9 and $-13.88\,\mathrm{W\,m^{-2}}$ are simulated for 0.5*AK1998, AK1998, and 2.0*AK1998, respectively. For comparison, Graf et al. (1997) estimated that

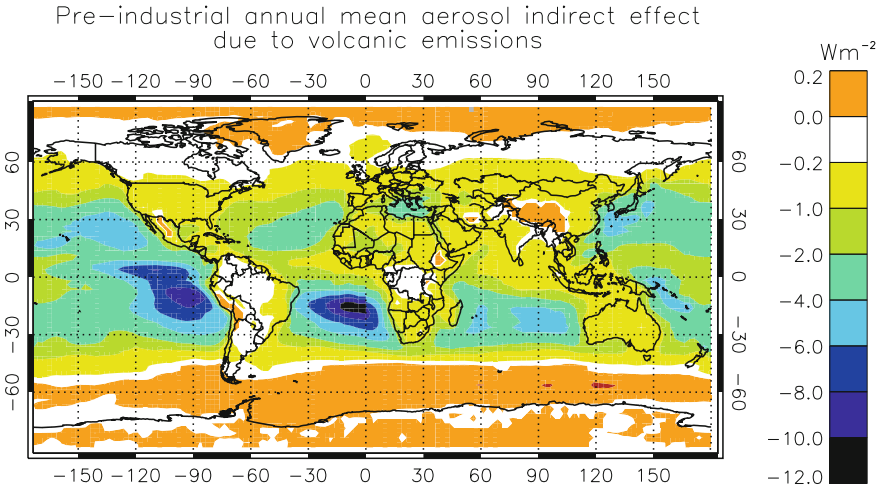

Fig. 3.7 Annual mean first AIE ($\mathrm{W\,m^{-2}}$) for the simulation using the AK1998 inventory in relation to the simulation excluding volcanic emissions. The first AIE is calculated for low-level cloud (approx. 970 m above terrain or sea-level) changes in the pre-industrial atmosphere

Table 3.3 Magnitude of the annual mean first AIE averaged over different regions

First AIE	AK1998	0.5*AK1998	2.0*AK1998
Global mean	−1.45	−0.94 [+0.45]	−2.09 [−0.58]
Peak	−10.9	−7.46 [+3.19]	−13.88 [−3.74]
SH mean	−1.6	−1.04 [+0.49]	−2.27 [−0.60]
NH mean	−1.29	−0.83 [+0.40]	−1.91 [−0.55]
Tropics mean	−2.22	−1.46 [+0.66]	−3.14 [−0.81]

Values in parentheses denote that the radiative effect is calculated in relation to the AK1998 simulation, whereas the values without parentheses denote that the radiative effect is calculated in relation to the simulation without volcanic emissions

in the present-day atmosphere, volcanic sulphur emissions regionally exert indirect aerosol radiative effects[4] in excess of $-3\,\mathrm{W\,m^{-2}}$.

When using the AK1998 simulation as the baseline case (Table 3.3, values in parentheses), non-linear differences in the magnitude of the first AIE arise. For example, a doubling of the volcanic source strength results in a global annual mean first AIE of $-0.58\,\mathrm{W\,m^{-2}}$ in relation to the AK1998 simulation. For comparison, the current total aerosol radiative forcing is estimated at $-1.2\,\mathrm{W\,m^{-2}}$ with the first AIE accounting for $-0.7\,\mathrm{W\,m^{-2}}$ (range of -1.1 to $+0.4\,\mathrm{W\,m^{-2}}$) of this total (Forster et al. 2007).

Graf et al. (1997) also highlighted that the cloud-radiative effects are particularly pronounced in tropical regions of the SH where the cloud amount is high. Comparing the results presented (Fig. 3.7) here to that presented in Graf et al. (1997, Fig. 7), differences in the spatial pattern of the first AIE become apparent. For example, the results presented in this chapter reveal a strong impact on stratocumulus cloud regions whereas the study of Graf et al. (1997) shows a much reduced first AIE in those regions. These differences can be attributed to the fact that observationally-derived cloud fields have been used for this chapter whereas Graf et al. (1997) parameterised cloud cover.

3.4 Conclusions

The results presented here, show that volcanic sulphur emissions are an important natural contributor to CCN number concentrations at low-level cloud altitude in the pre-industrial era. Without volcanic sulphur emissions, GLOMAP-mode predicts global annual mean CCN number concentrations at 970 m altitude of $60\,\mathrm{cm^{-3}}$, whereas concentrations of $87\,\mathrm{cm^{-3}}$ are predicted when including volcanic sulphur emissions (i.e. an increase of 45 %, Fig. 3.5). Thus, time-averaged volcanic sulphur emissions contribute around 31 % to the global mean CCN number concentrations at low-level cloud altitude in the pre-industrial era.

[4] Note that these authors did not provide a global mean value, which would have been more meaningful for the comparison.

Assuming the volcanic source strength is a factor of two greater than suggested by Andres and Kasgnoc (1998), results in a 19 % increase in global annual mean CCN number concentrations at 970 m altitude (Fig. 3.6). In contrast, reducing the annual mean volcanic sulphur flux by 50 % results in a 12 % reduction in global mean CCN number concentrations at low-level cloud altitude (Fig. 3.6). Thus, the relative sensitivity of CCN number concentrations to changes in the magnitude of the volcanic flux decreases disproportionally the higher the total volcanic sulphur flux. In other words, the higher the total volcanic sulphur flux the less effectively these additional emissions contribute to CC number concentrations of the pre-industrial atmosphere. However, it is important to realize that, despite the non-linearity, there is a substantial increase in climate-relevant CCN particle concentrations for a 100 % increase in the volcanic flux (i.e. 75 % increase when compared to global mean CCN at 970 m altitude of 60 cm^{-3} when excluding volcanic emissions) (Fig. 3.5). Moreover, the sensitivity of CCN number concentrations to changes in the strength of the volcanic sulphur flux appears to be much higher than that for global and regional changes in the flux of DMS (Woodhouse et al. 2010), or regional anthropogenic sulphur emissions (Manktelow et al. 2009). These difference can be explained with the injection height of the volcanic emissions and the subsequent oxidation of the volcanic sulphur in the gas-phase.

The ability of volcanic aerosol to act as CCN implies that the time-averaged volcanic sulphur emissions have a strong potential to induce changes in cloud microphysical properties thereby affecting the climate system. The results demonstrate that volcanic sulphur emissions exert a strong first AIE which is particularly pronounced in the stratocumulus cloud regions in the southern tropics. Using GLOMAP-mode, a global annual mean first AIE of $-1.45\,W\,m^{-2}$ is predicted with an annual mean peak of $-10.9\,W\,m^{-2}$ in the southern tropics. For comparison, Thomas et al. (2010) quantified DMS-derived changes in cloud microphysical properties and subsequently estimated a global annual mean first AIE of $-2.03\,W\,m^{-2}$ due to DMS under modern-day atmospheric conditions. Thomas et al. (2010) found peak values of $-16\,W\,m^{-2}$ in the extra-tropical southern ocean where biological activity is most prevalent. Thus, the results presented in this chapter highlight that volcanic emissions played an important role in modulating cloud microphysical properties and in subsequently inducing a significant cloud-radiative effect (see Table 3.3) in the pre-industrial era. The substantial impact of time-averaged volcanic sulphur emissions on stratocumulus clouds has not been reported previously; however such findings are corroborated by recent observational evidence suggesting that sulphur released from a continuously degassing volcano in Hawaii resulted in a modification of trade cumulus clouds (Yuan et al. 2011).

The strength of the volcanic sulphur source is highly uncertain which ultimately translates into an uncertainty regarding the first aerosol indirect effect induced by time-averaged volcanic sulphur emissions. Table 3.3 highlights that the uncertainty in the volcanic sulphur flux strength leads to an uncertainty in the magnitude of the first AIE which is non-linearly related to the source strength. Under pre-industrial atmospheric conditions, volcanic sulphur emissions induce a significant

global annual mean first AIE of $-1.45\,\mathrm{W\,m^{-2}}$ (Table 3.3). Assuming that the magnitude of the volcanic sulphur flux strength is twice as high as suggested by Andres and Kasgnoc (1998) leads to a difference in the global annual mean first AIE of $-0.58\,\mathrm{W\,m^{-2}}$, whereas a halving of the source strength results in $+0.45\,\mathrm{W\,m^{-2}}$ (Table 3.3).

3.5 Implications and Future Work

The results presented here have implications for studies addressing the link between CCN number concentrations and the state of the climate system of the pre-industrial atmosphere. Radiative forcing estimates are given in relation to pre-industrial which allows to separate the natural forcing component from the anthropogenic component. The magnitude of the radiative effect of uncertain volcanic sulphur emissions is likely to be larger under clean pre-industrial conditions than under polluted modern-day conditions. Therefore, even if the volcanic sulphur source strength did not change since the pre-industrial era, pre-industrial volcanic sulphur emissions could produce an aerosol radiative forcing that has to be accounted for in future radiative forcing assessments. Additional calculations assessing the magnitude of the first AIE under modern-day conditions need to be carried out in order to confirm this hypothesis.

Moreover, implications also arise for the assessment of the state of the climate system throughout Earth's history. For example, Kump and Pollard (2008) suggested that the mid-Cretaceous super-greenhouse climate could have been amplified by a diminished biological activity which subsequently led to a decrease in biological-derived CCN number concentrations, hence a lower cloud amount and albedo. However, volcanic activity varied spatially and temporally throughout Earth's history, thus potentially providing an important source of CCN and hence somewhat questioning the argumentation by Kump and Pollard (2008).

In summary, sulphur emissions from continuously degassing and sporadically erupting volcanoes are likely to have played a more important role than other, non-volcanic sulphur emissions throughout Earth's history. However, our understanding of the source-related differences in CCN sensitivity are far from complete (mainly because individual studies addressed individual source-related CCN sensitivities). Thus, future work should aim to investigate the CCN sensitivity of different sulphur sources using a common baseline.

References

Andres RJ, Kasgnoc AD (1998) A time-averaged inventory of subaerial volcanic sulfur emissions. J Geophys Res 103:25251–25262

Chen Y, Penner JE (2005) Uncertainty analysis for estimates of the first indirect aerosol effect. Atmos Chem Phys 5:2935–2948

Chin M, Jacob DJ (1996) Anthropogenic and natural contributions to tropospheric sulfate: a global model analysis. J Geophys Res 101:18691–18699

Dentener F, Kinne S, Bond T, Boucher O, Cofala J, Generoso S, Ginoux P, Gong S, Hoelzemann JJ, Ito A, Marelli L, Penner JE, Putaud JP, Textor C, Schulz M, van der Werf GR, Wilson J (2006) Emissions of primary aerosol and precursor gases in the years 2000 and 1750 prescribed data-sets for AeroCom. Atmos Chem Phys 6:4321–4344

Edwards JM, Slingo A (1996) Studies with a flexible new radiation code. I: choosing a configuration for a large-scale model. QJR Meteorol Soc 122:689–719

Forster P, Ramaswamy V, Artaxo P, Berntsen T, Betts R, Fahey D, Haywood J, Lean J, Lowe D, Myhre G, Nganga J, Prinn R, Raga G, Schulz M, van Dorland R (2007) Changes in atmospheric constituents and in radiative forcing. In: Solomon S, Qin D, Chen Z, Manning M, Marquis M, Averyt KB, Tignor M, Miller H (eds) Climate change 2007: the physical science basis. Cambridge University Press, Cambridge, Contribution of working group I to the fourth assessment report of the intergovernmental panel on climate change, pp 129–234

Fountoukis C, Nenes A, Meskhidze N, Bahreini R, Conant WC, Jonsson H, Murphy S, Sorooshian A, Varutbangkul V, Brechtel F, Flagan RC, Seinfeld JH (2007) Aerosol-cloud drop concentration closure for clouds sampled during the international consortium for atmospheric research on transport and transformation 2004 campaign. J Geophys Res 112:D10S30

Gong SL (2003) A parameterization of sea-salt aerosol source function for sub- and super-micron particles. Glob Biogeochem Cycles 17(4):1097

Graf HF, Feichter J, Langmann B (1997) Volcanic sulfur emissions: estimates of source strength and its contribution to the global sulfate distribution. J Geophys Res 102:727–738

Graf HF, Langmann B, Feichter J (1998) The contribution of Earth degassing to the atmospheric sulfur budget. Chem Geol 147:131–145

Kellogg WW, Cadle RD, Allen ER, Lazrus AL, Martell EA (1972) The sulfur cycle. Science 175:587–596

Kettle AJ, Andreae MO (2000) Flux of dimethylsulfide from the oceans: a comparison of updated data sets and flux models. J Geophys Res 105:26793–26808

Kump LR, Pollard D (2008) Amplification of cretaceous warmth by biological cloud feedbacks. Science 320:195

Lambert G, Le Cloarec MF, Pennisi M (1988) Volcanic output of SO_2 and trace metals: a new approach. Geochimica et Cosmochimica Acta 52:39–42

Lohmann U, Feichter J (2005) Global indirect aerosol effects: a review. Atmos Chem Phys 5:715–737

Manktelow PT, Carslaw KS, Mann GW, Spracklen DV (2009) Variable CCN formation potential of regional sulfur emissions. Atmos Chem Phys 9:3253–3259

Mann GW, Carslaw KS, Spracklen DV, Ridley DA, Manktelow PT, Chipperfield MP, Pickering SJ, Johnson CE (2010) Description and evaluation of GLOMAP-mode: a modal global aerosol microphysics model for the UKCA composition-climate model. Geosci Model Dev 3:519–551

Merikanto J, Spracklen DV, Pringle KJ, Carslaw KS (2010) Effects of boundary layer particle formation on cloud droplet number and changes in cloud albedo from 1850 to 2000. Atmos Chem Phys 10:695–705

Nightingale PD, Malin G, Law CS, Watson AJ, Liss PS, Liddicoat MI, Boutin J, Upstill-Goddard RC (2000) In situ evaluation of air-sea gas exchange–parameterizations using novel conservative and volatile tracers. Glob Biogeochem Cycles 14(1):373–387

Penner JE, Andrea M, Annegarn H, Barrie L, Feichter J, Hegg D, Jayaraman A, Leaitch R, Murphy D, Nganga J, Pitari GEA (2001) The scientific basis. Contribution of working group I to the third assessment report of the intergovernmental panel on climate change. In: Houghton JT, Ding YEA (eds) Climate change 2001. Cambridge University Press, Cambridge

Pringle KJ, Carslaw KS, Spracklen DV, Mann GM, Chipperfield MP (2009) The relationship between aerosol and cloud drop number concentrations in a global aerosol microphysics model. Atmos Chem Phys 9:4131–4144

Ramaswamy V, Boucher O, Haigh J, Hauglustaine D, Haywood J, Myhre J, Nakajima T, Shi G, Solomon S (2001) The scientific basis. Contribution of working group I to the third assessment report of the intergovernmental panel on climate change. In: Climate change (2001) Radiative forcing of climate. Cambridge University Press, Cambridge

Roelofs GJ, Stier P, Feichter J, Vignati E, Wilson J (2006) Aerosol activation and cloud processing in the global aerosol-climate model ECHAM5-HAM. Atmos Chemis Phys 6:2389–2399

Rossow WB, Schiffer RA (1999) Advances in understanding clouds from ISCCP. Bull Am Meteorol Soc 80:2261–2287

Schmidt A, Carslaw KS, Mann GW, Rap A, Pringle KJ, Spracklen DV, Wilson M, Forster PM (2012) Importance of tropospheric volcanic aerosol for indirect radiative forcing of climate. Atmos Chem Phys 12:7321–7339. doi:10.5194/acp-12-7321-2012

Smith SJ, van Aardenne J, Klimont Z, Andres R, Volke A (2010) Anthropogenic sulfur dioxide emissions: 1850–2005. Atmos Chem Phys Discuss 10:16111–16151

Stevenson DS, Johnson CE, Collins WJ, Derwent RG (2003a) The tropospheric sulphur cycle and the role of volcanic SO_2. Volcan Degassing 295–305

Stevenson DS, Johnson CE, Highwood EJ, Gauci V, Collins WJ, Derwent RG (2003b) Atmospheric impact of the 1783–1784 Laki eruption: part I chemistry modelling. Atmos Chem Phys 3:487–507

Textor C, Graf C, Robock A (2004) Emissions from volcanoes. In: Granier C, Artaxo P, Reeves C (eds) Emissions of chemical compounds and aerosols in the atmosphere. Kluwer, Dordrecht, pp 269–303

Thomas MA, Suntharalingam P, Pozzoli L, Rast S, Devasthale A, Kloster S, Feichter J, Lenton TM (2010) Quantification of DMS aerosol-cloud-climate interactions using the ECHAM5-HAMMOZ model in a current climate scenario. Atmos Chem Phys 10:7425–7438

Williams K, Tselioudis G (2007) GCM intercomparison of global cloud regimes: present-day evaluation and climate change response. Clim Dyn 29:231–250. doi:10.1007/s00382-007-0232-2

Woodhouse MT, Carslaw KS, Mann GW, Vallina SM, Vogt M, Halloran PR, Boucher O (2010) Low sensitivity of cloud condensation nuclei to changes in the sea-air flux of dimethyl-sulphide. Atmos Chem Phys 10:7545–7559

Yuan T, Remer LA, Yu H (2011) Microphysical, macrophysical and radiative signatures of volcanic aerosols in trade wind cumulus observed by the A-Train. Atmos Chem Phys Discuss 11:6415–6455

Chapter 4
Impact of the 1783–1784 AD Laki Eruption on Global Aerosol Formation Processes and Cloud Condensation Nuclei

4.1 Introduction

Chapter 3 dealt with moderate volcanic perturbations to the sulphur cycle, whereas the chapter presented here investigates the impact of the long-lasting, 1783–1784 AD Laki eruption, which is considered a volcanic "signature event" in recent history. Previous Laki studies have been conducted using GCMs with varying degrees of realism of the SO_2 emission scenario and the treatment of the aerosol processes. The Stevenson et al. (2003) study used various emission scenarios in terms of injection height of SO_2, although the scenarios are likely not to be representative of the assessed course of the Laki eruption (Thordarson et al. 1996; Thordarson and Self 1993, 2003). Chenet et al. (2005) injected 20 % of the SO_4 aerosol as smoothed monthly means at an altitude of 5 km and 80 % at an altitude of 10 km. The Oman et al. (2006) study is the most sophisticated in terms of an accurate representation of the SO_2 emission scenario based on the data of Thordarson et al. (1996) and Thordarson and Self (1993, 2003).

All previous Laki modelling studies treat aerosol microphysical processes and properties, such as size distribution, either not at all (Stevenson et al. 2003; Chenet et al. 2005) or in a simplified manner (Oman et al. 2006). However, explicitly simulating microphysical processes such as nucleation, condensation and coagulation is important in determining the size, the number concentration and the lifetime of climate-relevant particles. Stevenson et al. (2003) used the STOCHEM CTM in the Hadley Centre's Unified Model GCM which does not allow accounting for microphysical processes. Chenet et al. (2005) modelled the spatial and temporal distribution of 200 Tg of SO_4 aerosol (a theoretical value of the total SO_4 aerosol yield as derived from Stothers (1996) and Thordarson and Self (2003)) using the LMDZT-INCA GCM. Thus, Chenet et al. (2005) did not account for any chemical or microphysical processes. Oman et al. (2006) used the Goddard Institute for Space Studies (GISS) modelE GCM (Schmidt et al. 2006) coupled to a sulphur chemistry scheme (Koch et al. 2006) to simulate the chemical transformation of ~122 Tg of SO_2 and the subsequent SO_4 aerosol dispersal. The GISS modelE GCM (Schmidt et al. 2006)

A. Schmidt, *Modelling Tropospheric Volcanic Aerosol*, Springer Theses,
DOI: 10.1007/978-3-642-34839-6_4, © Springer-Verlag Berlin Heidelberg 2013

is an aerosol mass-only scheme thus a prescribed aerosol size-distribution is used in order to derive aerosol number concentrations. Consequently, the calculation of, for example, the direct radiative effects induced by the Laki eruption relies on an assumed size-distribution (Oman et al. 2006), despite observations of the aerosol size distribution following volcanic eruptions showing a great spatial and temporal variation (e.g., Hobbs et al. 1982). Recently, Timmreck et al. (2009, 2010) have suggested that it is important to use fully coupled chemistry and microphysics models in order to simulate the evolution and growth of stratospheric volcanic aerosol and to correctly constrain the climate effect of large explosive volcanic eruptions.

The study presented here aims to address the effect of the 1783–1784 AD Laki eruption microphysical processes and changes in tropospheric particle concentrations. In contrast to previous studies, this is the first study to use a dedicated global aerosol microphysics model (GLOMAP-mode) in order to simulate the driving aerosol processes, such as nucleation, condensation and coagulation, as well as the subsequent evolution of the aerosol size distribution in the troposphere. Using GLOMAP-mode allows assessment of the effect of the emitted SO_2 on the global budget of total particle number concentration and CCN number concentrations. Several studies (Mather et al. 2003, 2004; Gassó 2008) have shown that a detailed understanding of volcanically induced CCN is vital for assessing the potential ability of volcanic eruptions to alter cloud microphysical processes in the troposphere. In addition, a hypothetical Laki scenario commencing in December (as opposed to June) is simulated in order to investigate the role of the season in which such an eruption commences and its impact on the above-mentioned aerosol processes.

4.2 Experimental Design and Emissions

The simulations are conducted using GLOMAP-mode (Mann et al. 2010). The model is forced by reanalysed 2003 meteorology and large-scale atmospheric transport fields specified from the European Centre for Medium-Range Weather Forecasts (ECMWF) at six-hour intervals. Meteorological fields from the year 2003 are chosen as the summer of 1783 featured unusually hot July temperatures in western Europe and the presence of persistent anticyclones over central Europe (Thordarson and Self 2003 and references therein). The year 2003 was characterised by similar meteorological features during the summer months. However, as the model is not forced using meteorological fields for the year 1783 AD, the simulations here should be regarded as representing a "Laki-style" eruption.

The impact of the eruption is simulated in a pre-industrial setting (i.e. in the absence of anthropogenic emissions) using the same emissions as in Chap. 3 but aerosol formation due to biomass burning is excluded.[1]

[1] As the simulations for this chapter were performed at an earlier stage of the PhD project when those emissions were not available for GLOMAP-mode.

Two Laki simulations are conducted:

(a) a standard summer Laki scenario with the eruption commencing on 8 June (hereafter referred to as L-s) reproducing the actual eruption; and
(b) a hypothetical winter Laki scenario commencing on 8 December (hereafter referred to as L-w).

In order to define the magnitude, altitude and timing of the release of SO_2 into the atmosphere (Fig. 4.1) the data set of Thordarson et al. (1996) and Thordarson and Self (2003) is used. In order to represent emissions from the Laki vent system, a total of 94.3 Tg SO_2 is emitted into model grid boxes between 9 and 13 km above Iceland (17° W, 64° N) as 10 discrete SO_2 mass loadings (as suggested by Thordarson et al. 1996; Thordarson and Self 2003), each injected within one six-hour period. In addition, a total of 27.6 Tg SO_2 is continuously emitted into grid boxes between the surface and 1 km, representing passive degassing from the Laki lava flows (Thordarson et al. 1996; Thordarson and Self 2003). Both L-s and L-w use the same SO_2 mass loadings and the same temporal resolution, but L-s commences on 8 June and L-w on 8 December. The representation of the SO_2 mass loadings is identical to that used by Oman et al. (2006) but differs from that of Stevenson et al. (2003)

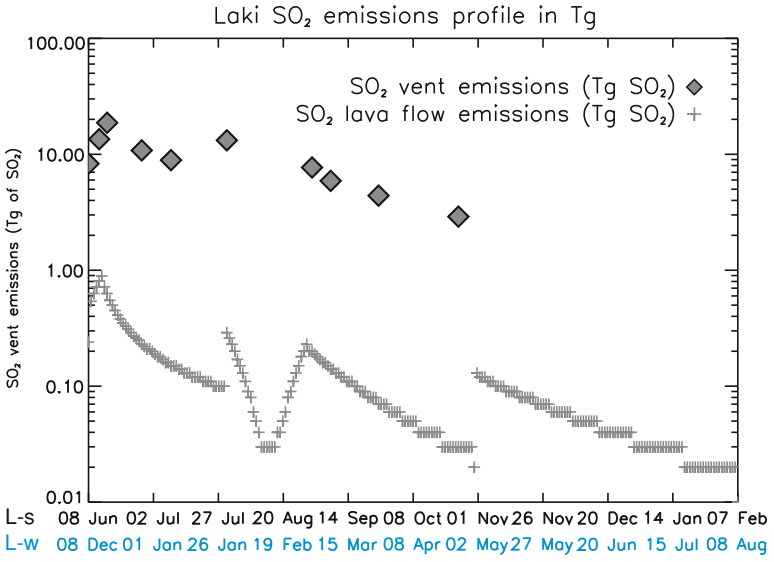

Fig. 4.1 Daily gas-phase SO_2 mass loadings in Tg for the L-s simulation commencing on the 8 June and for the hypothetical L-w simulation commencing on 8 December. Diamonds represent ten SO_2 mass loadings from the Laki vent system injected into the upper troposphere/lower stratosphere (i.e. between 9 and 13 km) and crosses represent daily SO_2 emissions from the Laki lava flows released into the boundary layer (i.e. between surface and 1 km). SO_2 mass loadings and temporal resolution are derived from Thordarson et al. (1996) and Thordarson and Self (2003), with L-w employing the same mass loadings and relative temporal resolution but commencing on 8 December. Figure after Schmidt et al. (2010)

in that discrete SO_2 mass loadings are used to represent degassing from the vent system instead of monthly mean SO_2 emissions or daily SO_2 emissions falling to 1/e of their initial value at the end of each eruption episode. No attempt is made to simulate the dispersal of volcanic ash injected into the atmosphere by the Laki eruption, nor does this study account for heterogeneous formation of H_2SO_4 on ash particles which could potentially modify the aerosol size distribution due to condensation and coagulation, and scavenge sulphur (e.g., Turco et al. 1983). However, these limitations only apply as long as ash is present in the atmosphere—commonly a lifetime on the order of days is assumed for fine volcanic ash resulting in a rather localised and small long-term effect, as shown for stratospheric volcanic aerosol by Niemeier et al. (2009).

4.3 Results and Discussion

4.3.1 SO_2 *and* SO_4 *Mixing Ratios and Burdens*

Figure 4.2 shows changes in zonal 3-month mean SO_2 and SO_4 aerosol mixing ratios for L-s and L-w. SO_2 mixing ratios increase by ∼140 ppbv (parts per billion by volume) and ∼96 ppbv at altitudes between 10 and 12 km for L-s and L-w, respectively. For both eruption scenarios elevated SO_2 mixing ratios of ∼5 ppbv are simulated in the boundary layer close to the eruption site due to continuous emission of SO_2 from the lava flows. In comparison, mean SO_2 mixing ratios of ∼1 ppbv are modelled in anthropogenically polluted regions over Europe using GLOMAP (Spracklen et al. 2005a). Thus the 1783–1784 AD Laki eruption would have been a strong pollutant in the pre-industrial atmosphere. Zonal 3-month mean SO_4 aerosol mixing ratios reach 17.8 ppbv during L-s and 2.9 ppbv during L-w at altitudes from 10 to 12 km. SO_4 mixing ratios in the boundary layer and middle troposphere from 30° N to 75° N are a factor of 4.4 higher for L-s than for L-w. SO_2 mixing ratios show a much greater difference than SO_2 mixing ratios when comparing L-s and L-w due to a faster photochemical conversion of SO_2 to SO_4 during L-s.

It is worth noting that a small fraction (up to ∼1 ppbv) of both SO_2 and SO_4 is transported into the southern hemisphere (SH). These results are consistent with those of Levine et al. (2007, 2008) who show that the TOMCAT CTM is capable of realistically simulating the relatively fast transport of tracers along isentropic surfaces and the efficient mixing process between the tropical upper troposphere and the lower stratosphere. The study presented here, finds a more efficient transport of SO_4 into the SH for L-s when compared to L-w which is in agreement with Chen (1995) who investigated tracer transport along isentropic surfaces using a semi-Lagrangian model together with ECMWF analysed winds. Chen (1995) found that a stratospheric tracer initialised in the extratropics of the northern hemisphere (NH) during northern summer is very efficiently transported into the troposphere along the 350 K isentropic surface and subsequently crosses the equator into the SH (within

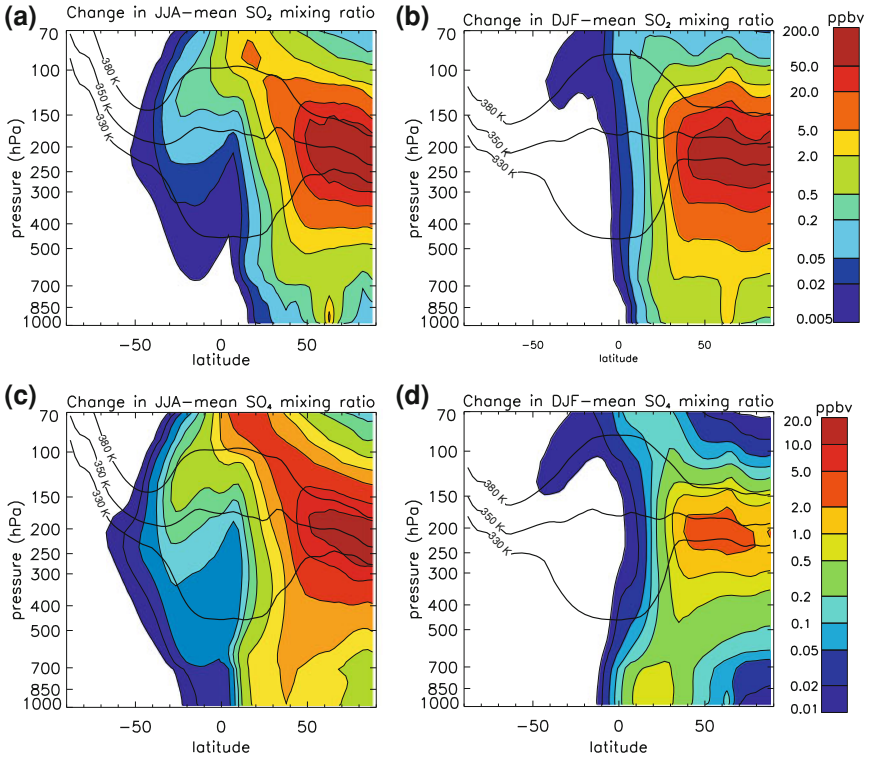

Fig. 4.2 Simulated changes (i.e. perturbed minus unperturbed) in zonal 3-month mean SO_2 and SO_4 aerosol mixing ratios in parts per billion by volume (ppbv) for L-s (**a** and **c**) and L-w (**b** and **d**). Heavy *black solid lines* represent the 380, 350 and 330 K isentropic surfaces. JJA = June–July–August; DJF = December–January–February. Figure after Schmidt et al. (2010)

three months of the initialisation). In contrast, cross-equatorial transport is much less efficient if the same tracer is initialised during NH winter (Chen 1995). Previous modelling studies (Chenet et al. 2005; Oman et al. 2006) suggested that the impact of the Laki eruption was confined to the NH. However, a recent compilation of historic observations (Trigo et al. 2010) supports a possible impact of the 1783–1784 AD Laki eruption in Brazil (20° S). Also, Stevenson et al. (2003) stated that the impact of the Laki eruption is basically confined to the NH, but mentioned the transport of a small amount of SO_4 into the SH. For the L-s simulation the descent of SO_2 gas and SO_4 aerosol into the SH troposphere starts two months after the onset of the eruption. Despite there being only relatively minor changes in mixing ratios, the additional SO_2 gas and SO_4 aerosol entrained into the SH will affect microphysical processes such as coagulation and direct growth of particles. As will be shown in Sect. 4.3.8, even small amounts of SO_4 can have a substantial effect on CCN, consistent with a previous study by Manktelow et al. (2009).

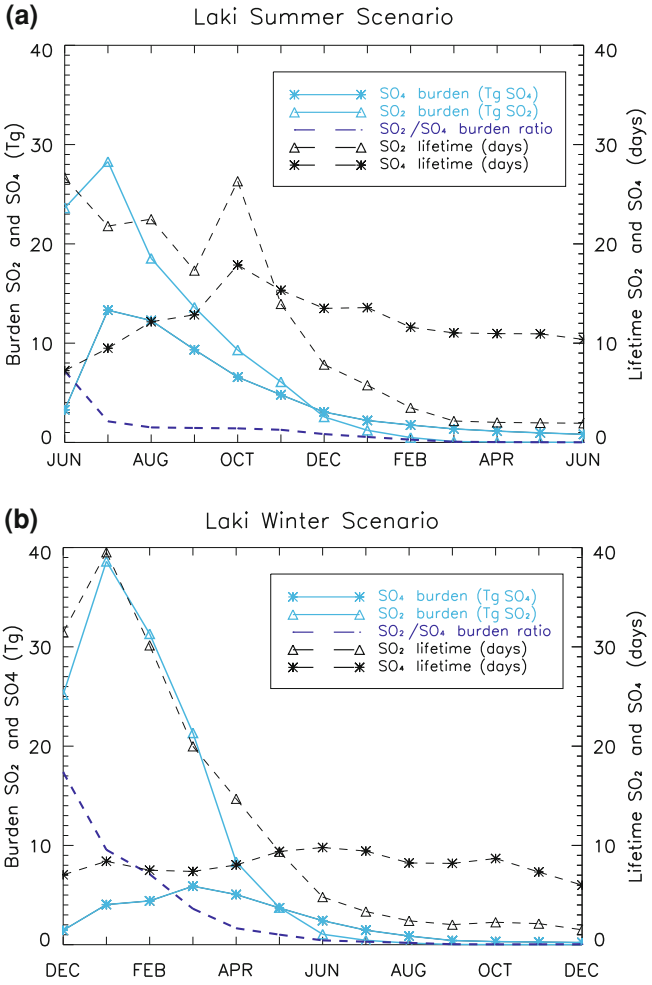

Fig. 4.3 Simulated global monthly mean SO_2 burden in Tg(SO_2) (*solid*, *light blue line* with *triangles*) and SO_4 burden in Tg(SO_4) (*solid*, *light blue line* with *asterisks*), SO_2 to SO_4 ratio (*dashed dark blue line*), and SO_2 residence time (*dashed black line* with *triangles*) and SO_4 aerosol residence time (*dashed black line* with *asterisks*) for L-s (**a**) and L-w (**b**), respectively. Figure from Schmidt et al. (2010)

Figure 4.3 shows the global monthly mean atmospheric SO_2 and SO_4 burdens (i.e. the amount of SO_2 and SO_4 in the atmosphere at a given time), the ratio of SO_2 to SO_4 burden, and global monthly mean SO_2 and SO_4 residence times for L-s and L-w, respectively. The most obvious differences between the summer and winter simulations are the higher SO_2 burden and the longer first 3-months mean SO_2 residence time of 34 days for L-w compared to 24 days for L-s. This compares to typical SO_2 residence times of ~2 days (e.g., Spracklen et al. 2005a) under current,

anthropogenically polluted atmospheric conditions. The significant increase in SO_2 residence times in the volcanically perturbed simulations is a result of the injection of SO_2 well above the boundary layer (where removal rates are low) as well as suppression of the oxidants (see Sect. 4.3.2). The higher wintertime SO_2 burden and residence time are a result of a less efficient oxidation of SO_2 to H_2SO_4 vapour when compared to the summertime eruption.

Figure 4.4 shows the simulated global 12-month mean sulphur species budget for the unperturbed run and for L-s (as an absolute difference from the unperturbed run) and Fig. 4.5 compares the same budgets for L-w. For L-s the gas-phase oxidation of SO_2 by OH to form SO_4 dominates the in-cloud oxidation pathway which corroborates the findings of Stevenson et al. (2003). In comparison, Manktelow et al. (2007) showed

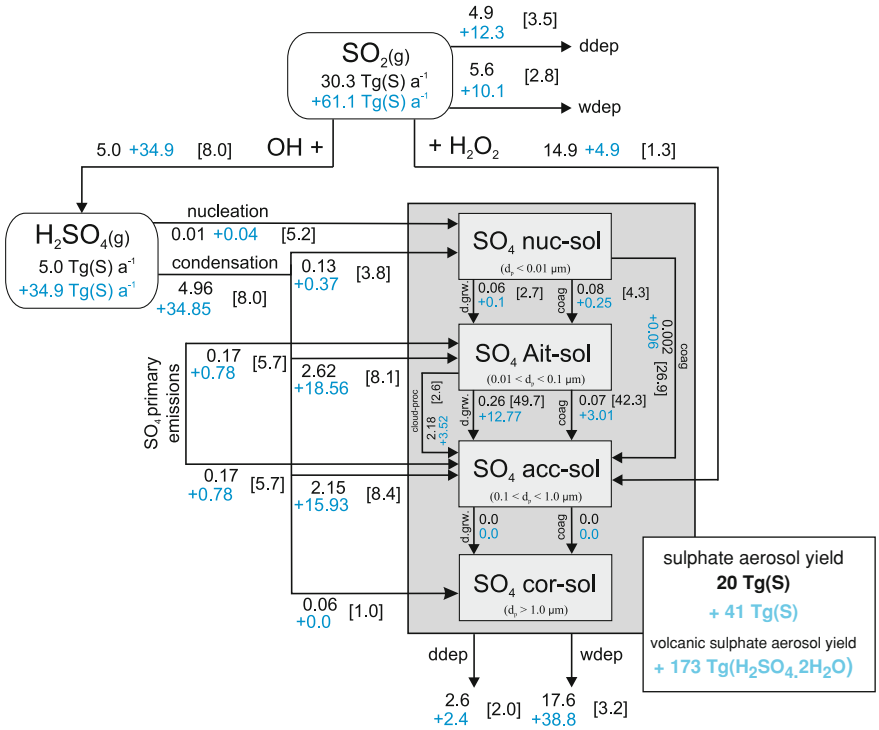

Fig. 4.4 Simulated global 12-month mean sulphur budget showing fluxes in Tg(S) a^{-1} with *blue colours* showing absolute changes for L-s, *black colours* showing the unperturbed run, and ratio of L-s to unperturbed in parentheses. Abbreviations: ddep = dry deposition; wdep = wet deposition; d.grw = direct growth; coag = coagulation; cloud-proc = cloud processing of Aitken mode-sized particles; nuc-sol = soluble nucleation mode; Ait-sol = soluble Aitken mode; acc-sol = soluble accumulation mode; cor-sol = soluble coarse mode; d_p = particle diameter. Volcanic SO_4 aerosol yield denotes the amount of SO_4 aerosol produced during the twelve months following the onset of the eruption assuming the volcanic aerosol is composed of $H_2SO_4 \cdot 2\,H_2O$. Figure after Schmidt et al. (2010)

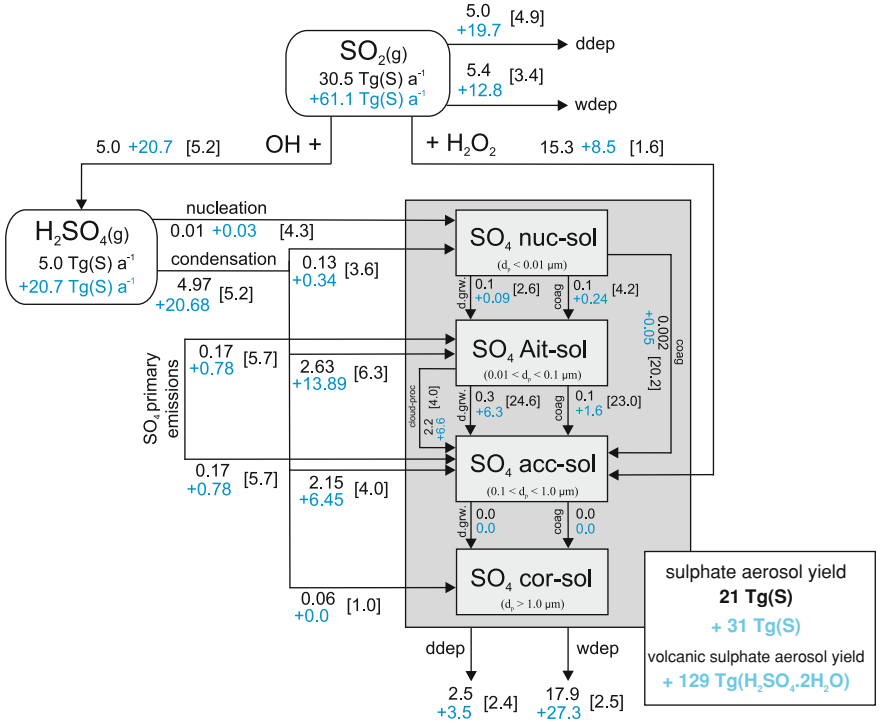

Fig. 4.5 As Fig. 4.4 but 12-month mean sulphur budget shown for L-w. Figure after Schmidt et al. (2010)

that in-cloud oxidation is the dominant SO_4 formation process under present-day atmospheric conditions. The reason for this difference is that most of the volcanic SO_2 is injected into the relative cloud-free upper troposphere. For L-w, however, in-cloud oxidation and dry oxidation are approximately equally important pathways to form SO_4. The different SO_4 production pathways significantly affect the aerosol microphysical processes (see Sect. 4.3.6 for more details). Production of H_2SO_4 vapour (and subsequently particulate SO_4) via gas-phase oxidation of SO_2 by OH is a factor of ∼1.6 lower in L-w than in L-s due to slower photochemistry. This summer–winter difference affects the timing of the peak SO_4 burden relative to the onset of the simulated eruption (see Fig. 4.3). In L-s, the peak SO_4 burden occurs in the month following the eruption, whereas the peak in L-w occurs almost four months after the onset of the eruption during spring. As a consequence SO_2 burdens and SO_2 removal rates during L-w remain higher than during L-s throughout the first five months. In L-w ∼32 % of the SO_2 is removed via dry deposition and ∼21 % via wet deposition. In contrast, L-s is characterised by lower SO_2 dry and wet deposition fluxes of ∼20 and ∼17 %, respectively. In comparison, Stevenson et al. (2003) found that 64–72 % of the SO_2 is deposited before the conversion to aerosol. During L-s, ∼94 % of the SO_4 aerosol is wet deposited (mainly via nucleation

scavenging of accumulation mode-sized ($0.1 < d_p < 1.0\,\mu m$) particles), and ~6 % is dry deposited. This compares to ~89 % of the SO_4 aerosol being wet deposited and ~11 % being dry deposited during L-w.

4.3.2 Depletion of Oxidants

The simulations reveal the significant impact of a Laki-style eruption on the principal oxidants (OH and H_2O_2) involved in the chemical conversion of SO_2 to SO_4 aerosol. Figure 4.6 shows the zonal 3-month mean change in H_2O_2 and OH concentrations while Figs. 4.7a, b and Figs. 4.8a, b show the spatial distribution of H_2O_2 and OH at altitudes where perturbations are largest. In the lowermost troposphere, H_2O_2 is the main oxidant of SO_2 in low-level cloud water, so it is depleted by the excess volcanic SO_2 emitted from the lava flows and re-entrained SO_2 from higher altitudes.

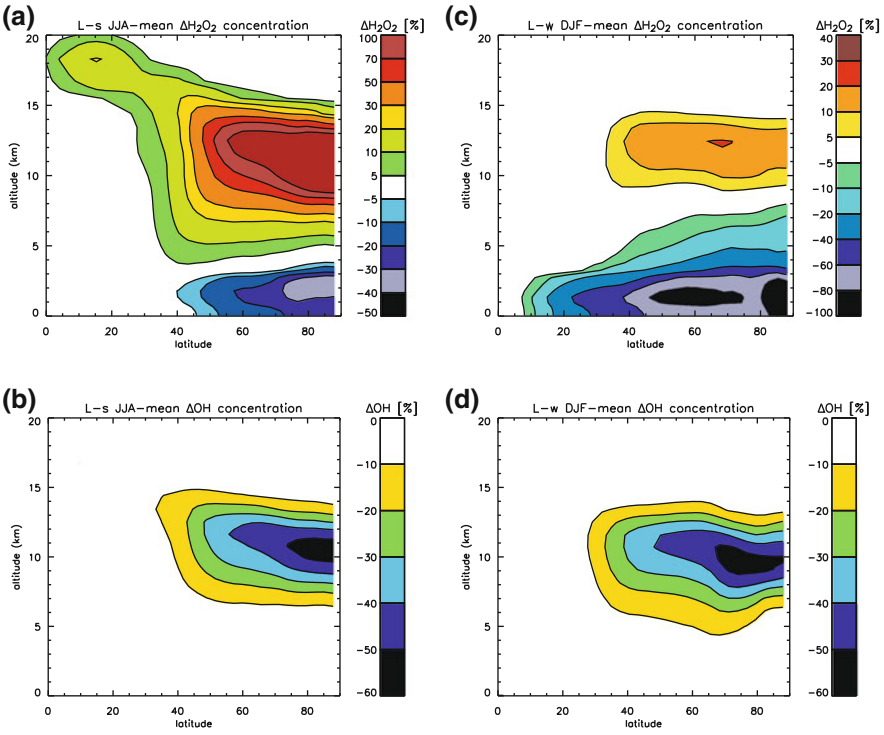

Fig. 4.6 Simulated relative changes in zonal 3-month mean H_2O_2 and OH concentrations averaged over the NH for (**a**) L-s relative change in JJA-mean H_2O_2 concentrations, (**b**) L-s relative change in JJA-mean OH concentrations; and (**c**) L-w relative change in DJF-mean H_2O_2 concentrations, and (**d**) L-w relative change in DJF-mean OH concentrations. JJA = June–July–August; DJF = December–January–February. Figure after Schmidt et al. (2010)

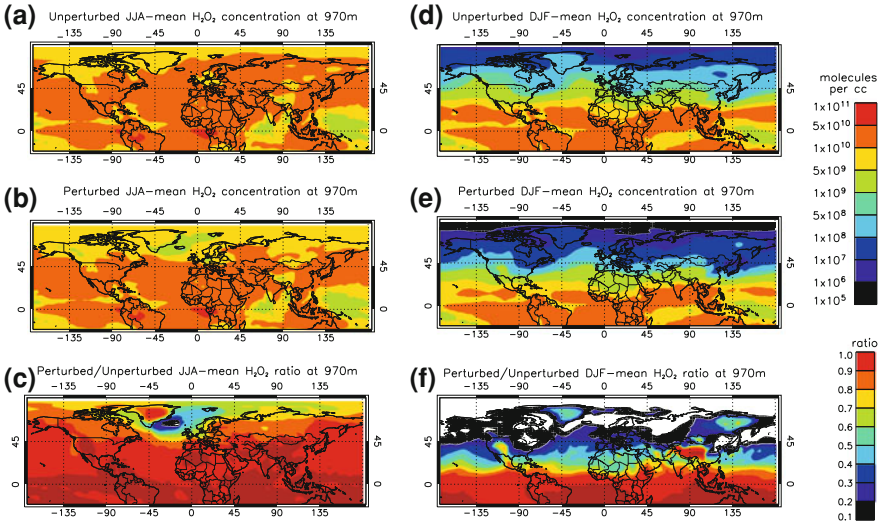

Fig. 4.7 Simulated 3-month mean H_2O_2 concentration at low-level cloud altitude (970 m) for (**a**) L-s unperturbed run, (**b**) L-s perturbed run, (**c**) L-s ratio perturbed to unperturbed run, (**d**) L-w unperturbed run, (**e**) L-w perturbed run, (**f**) L-w ratio perturbed to unperturbed run. JJA = June–July–August; DJF = December–January–February. Figure from Schmidt et al. (2010)

In contrast, OH is the principal oxidant above ∼3 km, so it is depleted by the excess volcanic SO_2 emitted from the vent system.

L-s and L-w have a similar impact on zonal 3-month mean OH concentrations compared to the unperturbed simulations, depleting them by up to ∼55 % at ∼10 km altitude at high-northern latitudes, where SO_2 concentrations are highest. In comparison, Stevenson et al. (2003) reported that OH depletion reaches 18 % during JJA. L-w exhibits a greater impact on OH at ∼10 km in the latitude band from 70° N to 90° N, which is a result of naturally lower OH production rates during wintertime.

Zonal 3-month mean H_2O_2 concentrations for L-s are depleted by up to 35 % in the lowermost troposphere which corroborates the findings by Stevenson et al. (2003). For L-s, H_2O_2 concentrations are enhanced by over 150 % in the Arctic free troposphere which is a result of the gas-phase reaction of SO_2 with OH:

$$OH + SO_2(+O_2 + H_2O) \rightarrow H_2SO_4 + HO_2 \tag{4.1}$$

followed by self-reaction of HO_2:

$$HO_2 + HO_2 \rightarrow H_2O_2 + O_2 \tag{4.2}$$

which is the only source of atmospheric H_2O_2.

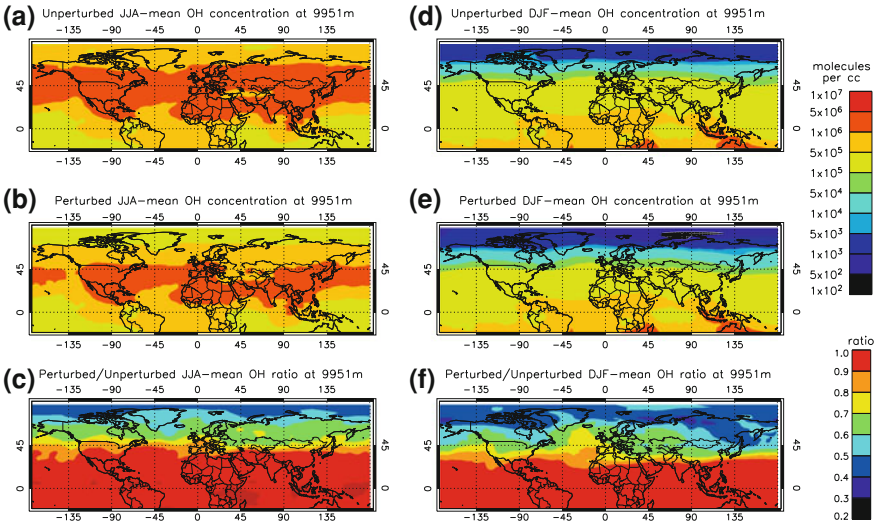

Fig. 4.8 Simulated 3-month OH concentration at 9951 m altitude for (**a**) L-s unperturbed run, (**b**) L-s perturbed run, (**c**) L-s ratio perturbed to unperturbed run, (**d**) L-w unperturbed run, (**e**) L-w perturbed run, (**f**) L-w ratio perturbed to unperturbed run. JJA = June–July–August; DJF = December–January–February. Figure from Schmidt et al. (2010)

For L-w, zonal 3-month mean boundary layer H_2O_2 concentrations exhibit a complete depletion at high-northern latitudes (>80° N), and are depleted by >80 % between 45° N and 75° N. In contrast, H_2O_2 depletion for L-s is generally latitudinally and vertically more confined when compared to L-w (i.e. average perturbed to unperturbed ratio of 0.75 in the latitude band 60° N to 90° N; see Fig. 4.7). The wider extent of H_2O_2 depletion in winter can be explained by the longer SO_2 residence time, which allows long-range transport of the SO_2 and depletion of H_2O_2 further away from the SO_2 source (Fig. 4.7).

4.3.3 Comparison with Previous Studies

Table 4.1 compares key diagnostics (from the L-s simulation) such as burden, residence times and yield (the integrated mass of volcanic aerosol produced in the year after the onset of the eruption) with previous modelling studies (Stevenson et al. 2003; Oman et al. 2006) and literature-based estimates and observations (Clausen and Hammer 1988; Mosley-Thompson et al. 2003; Thordarson and Self 2003). GLOMAP-mode predicts a similar peak global SO_2 burden when compared to previous modelling studies (Stevenson et al. 2003; Oman et al. 2006). In contrast, the peak SO_4 burden predicted by GLOMAP-mode is one quarter of that calculated by Oman et al. (2006), and up to a factor of 3.3 higher when compared to Stevenson et al.

Table 4.1 Comparison with previous modelling studies and literature-based estimates

Diagnostic	This study	S2003	O2006	Literature
Peak SO_2 burden (Tg of SO_2)	29; 23*	9–17*	37	–
Peak SO_4 burden (Tg of SO_4)	14	4.2–5.1	60	–
JJA-mean SO_2 residence time (days)	23	9–18	18[a]	–
JJA-mean SO_4 residence time (days)	9	7–8	27[a]	–
Greenland SO_4 dep. (kg SO_4 km^{-2})	190–1500	105–195	165–300	62–324[b,c]
Peak NH mean AOD	0.3	–	0.5	0.4–0.9[d]
Volcanic SO_4 aerosol yield (Tg)	173	71–92	163–166	46–374[e]; 175**

S2003 = Stevenson et al. (2003); O2006 = Oman et al. (2006); AOD = aerosol optical depth
Volcanic SO_4 aerosol yield = amount of sulphate aerosol produced during the twelve months following the onset of the eruption assuming volcanic aerosol is composed of $H_2SO_4 \cdot 2\,H_2O$
*June–July–August mean; **average
[a]L. Oman (personal communication, 2010)
[b]Clausen and Hammer (1988)
[c]Mosley-Thompson et al. (2003)
[d]Thordarson and Self (2003)
[e]Oman et al. (2006, Table 1)

(2003). The JJA-mean SO_2 residence times listed in Table 4.1 compare well between all three studies. However, the JJA-mean SO_4 residence times are at least a factor of three longer in the Oman et al. (2006) study when compared to both this study and the Stevenson et al. (2003) study. GLOMAP-mode predicts a total volcanic aerosol yield of 173 Tg for L-s (assuming $H_2SO_4 \cdot 2\,H_2O$ composition), which is remarkably close to the 163–166 Tg calculated by Oman et al. (2006) but higher than the 71–92 Tg found by Stevenson et al. (2003). In contrast to L-s, the total SO_4 aerosol yield for L-w is, with 129 Tg of volcanic aerosol, substantially lower, implying a less profound impact on radiation.

In summary, Table 4.1 shows that there is a fair amount of consistency between the results of the study presented here and previous modelling studies (Stevenson et al. 2003; Oman et al. 2006) with the differences between the models being within the range of uncertainty seen in previous model intercomparison studies (e.g., Textor et al. 2006). For example, the chemistry scheme employed here produces an amount of volcanic SO_4 aerosol similar to that of the GISS modelE used by Oman et al. (2006) but the JJA-mean SO_4 residence time and peak SO_4 burden predicted here are lower when compared to Oman et al. (2006). These differences indicate that either GLOMAP-mode tends to remove SO_4 too fast or that the assumption about the effective radius of the Laki aerosol used in the Oman et al. (2006) study is inconsistent when compared to the aerosol size distribution simulated using GLOMAP-mode (see Sect. 4.3.6).

4.3.4 Comparison with Sulphate Deposition Record in Ice-Cores

Several authors have measured acidity and total SO_4 in Greenland and Svalbard ice cores in order to reconstruct the total volcanic SO_4 deposition ($kg(SO_4)/km^2$) and the volcanic aerosol loading of the 1783–1784 AD Laki eruption (e.g., Clausen and Hammer 1988; Fiacco et al. 1994; Zielinski et al. 1997; Mosley-Thompson et al. 2003). The modelled total SO_4 deposition over twelve months following the onset of L-s (see Fig. 4.9a) is compared with measurements from Greenland (Clausen and Hammer 1988; Mosley-Thompson et al. 2003) and Svalbard (Kekonen et al. 2005). Generally, Greenland ice core measurements reveal a highly spatially variable amount of total SO_4 deposition, ranging from 62 to 294 $kg\,km^{-2}$ in eleven ice cores (Clausen and Hammer 1988) and from 80 to 324 $kg\,km^{-2}$ in six ice cores (Mosley-Thompson et al. 2003). GLOMAP-mode predicts a total SO_4 deposition ranging from $\sim$190 $kg\,km^{-2}$ over northernmost Greenland to $\sim$650 $kg\,km^{-2}$ over central Greenland with the majority being deposited during the first 3 months after the onset of the eruption. Up to $\sim$1500 $kg\,km^{-2}$ are deposited over Northwest Greenland and the south-westernmost tip. In order to compare the total SO_4 deposition predicted by GLOMAP-mode to ice-core measurements the normalised mean bias (NMB) is calculated as follows:

$$\mathrm{NMB} = \frac{\sum_{i=1}^{N} (M_i - O_i)}{\sum_{i=1}^{N} O_i} \tag{4.3}$$

where M_i represent the modelled values and O_i the observed values.

GLOMAP-mode predicts the total SO_4 deposition over Greenland with a NMB of 4.2 when comparing our results to measurements in 12 ice cores (Mosley-Thompson et al. 2003; Clausen and Hammer 1988, Table V). Generally, the lowest model biases (1.3 and 1.6) are calculated for central Greenland cores D3 and Milcent, and the highest biases (6.0 and 5.8) are calculated for the Raven core in the south west and the Humboldt core in northern Greenland (see Fig. 4.9b). For the Lomonosovfonna ice-core in Svalbard, the model predicts a total SO_4 deposition of 570 $kg\,km^{-2}$ with the majority being deposited during the first 6 months after the onset of the eruption. This compares to 390 $kg\,km^{-2}$ being preserved in the Lomonosovfonna ice-core (Kekonen et al. 2005).

Korhonen et al. (2008) have shown that GLOMAP may remove particles too efficiently over Arctic regions, which is most likely due to the simplified treatment of nucleation scavenging in frontal rain clouds. It is worth noting that, despite the model overpredicting the amount of SO_4 deposited on Greenland, the results presented in this chapter are thought to be reasonable as Table 4.1 shows that other diagnostics are in good agreement with previous modelling studies (Stevenson et al. 2003; Oman

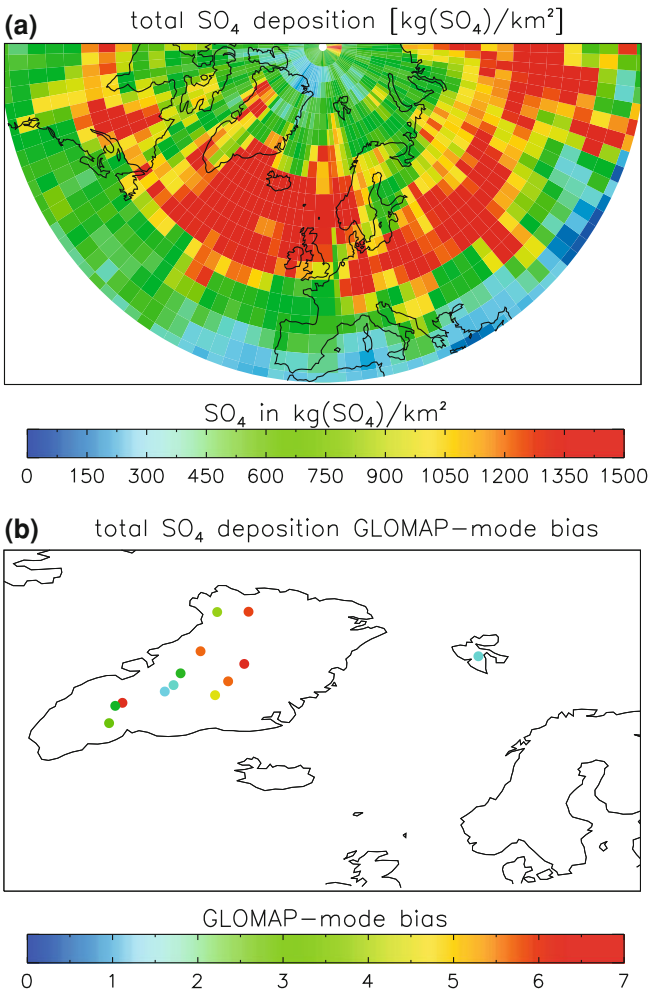

Fig. 4.9 **a** Total SO_4 deposition [kg(SO_4)/km^2] following the first 12 months after the onset of the Laki eruption shown for the NH. **b** Normalised mean bias of modelled total SO_4 deposition [kg(SO_4)/km^2] when compared to ice core measurements (*coloured circles*) in Greenland (Mosley-Thompson et al. 2003; Clausen and Hammer 1988, Table V) and Svalbard (Kekonen et al. 2005). Figure from Schmidt et al. (2010)

et al. 2006). Moreover, Mann et al. (2010) have shown that GLOMAP-mode performs well when compared to present-day observations. For example, present-day global annual mean surface SO_4 concentrations predicted by GLOMAP-mode are in very good agreement with a range of observational datasets (Mann et al. 2010, and references therein). Details on the performance of GLOMAP-mode can be found on

the AEROCOM model intercomparison website.[2] Moreover, the deposition of SO_4 to a particular location is strongly influenced by the meteorology used to force the model. For example, when forcing the model using ECMWF reanalysis for the year 2000 the deposition pattern is similar but the magnitude of the total SO_4 deposition between 2003 and 2000 ranges locally from 72 % less to 140 % more total deposition over Greenland and adjacent regions. Overall, these findings suggest that the SO_4 deposition to Greenland varies depending on atmospheric circulation patterns; thus only using the 1783 AD meteorology would be the a conclusive test for the model.

4.3.5 Comparison with Historical Records

Thordarson (1995) and Thordarson and Self (2003) have analysed historic weather logs from Grund (northern Iceland) and Mannheim (Germany) containing information on the first appearance of the Laki SO_4 aerosol haze and on the relative changes in haze opacity over the course of the eruption. The descriptive terminology of the haze's appearance was converted into an arbitrary index using values from 0 to 10, with 0 indicating "no haze" and 10 indicating "very intense and dark haze (visibility <2.5 km)" (Thordarson 1995). In order to compare the GLOMAP-mode output with that index, the aerosol optical depth (AOD) at 550 nm was simulated on a daily basis for the first three months following the onset of L-s.

In GLOMAP-mode the AOD is calculated as follows:

$$\mathrm{AOD} = \sum_{0}^{z_{\mathrm{top}}} \mathrm{b_{ext}} \times \mathrm{dz} \tag{4.4}$$

where b_{ext} is the extinction coefficient (m^{-1}) and dz is the height of each model level (m).

In order to calculate b_{ext} the particle number-size distribution is calculated for the dry-radius grid (i.e. the modes are "binned") followed by:

$$\mathrm{b_{ext}} = \pi \times \sum_{\mathrm{i}=0}^{\mathrm{n}} \mathrm{Q_{ext}} \times \mathrm{R_i^2} \times \frac{\mathrm{dN_i}}{\mathrm{d \ln R_i}} \times \Delta \ln \mathrm{R_i} \tag{4.5}$$

where n is the number of points on the dry-radius grid describing the distribution, N is the number density of particles in the dry-radius grid point i (cm^{-3}), Q_{ext} is the aerosol extinction efficiency, R_i is the average radius of particles in the dry-radius grid point i (m), and $\Delta \ln R_i$ is the width of the dry-radius grid point i. Q_{ext} is determined by means of a lookup table which is generated from the Mie scattering code developed by G. Thomas (University of Oxford).

[2] http://dataipsl.ipsl.jussieu.fr/cgi-bin/AEROCOM/aerocom/surfobs_annualrs.pl

Furthermore, daily outputs of b_{ext} simulated in the lowermost model grid box were then converted into visibility (V) at the surface.

Visibility can be defined as the change in intensity of light reflecting off an object as a function of the scattering of light by the atmosphere:

$$\frac{\Delta \mathrm{I}}{\mathrm{I}} = \mathrm{e}^{-\mathrm{b_{ext}V}} \tag{4.6}$$

where I is the intensity of light and V is the visibility in m or distance at which a large dark object can just be seen against the horizon. For the visibility calculations presented here a threshold contrast of 2 % is assumed (i.e. the visibility limit for the human eye is a 2 % change in intensity relative to the background), thus $\frac{\Delta I}{I} = 0.02$.

Note that the natural logarithm of 0.02 is about −3.9, thus Eq. 4.6 simplifies to:

$$\mathrm{V} = \frac{3.912}{\mathrm{b_{ext}}} \tag{4.7}$$

which is known as Koschmieder's equation (Koschmieder 1924). Figure 4.10 shows the simulated AOD, and the calculated visibility plotted together with the haze opacity index for grid boxes in Grund and Mannheim from the onset of L-s until the end of August. In Grund, GLOMAP-mode simulates a peak AOD of 2.9 on 13 June, shortly after the onset of eruption episode II. In Grund this is followed by a sharp drop in AOD and a subsequent increase of the AOD to 1.6 on 29 June; i.e. four days after the onset of eruption episode IV. Until the end of July the AOD in Grund exhibits large variations ranging from 0.3 to 2.6 with a drop to lower AOD values (0.5 on average) throughout August. It is not until 15 June that the AOD rises to 0.1 in Mannheim with AOD values of 0.3, 0.3 and 0.4 on 17, 21 and 30 June; that is each several days after the onset of the respective eruption episode. A peak AOD of 0.7 in Mannheim is simulated on 23 July, 13 days after the onset of eruption episode V. These findings are supported by documentations of the first appearance of the haze in western and southern Europe between 16 and 19 June (Thordarson and Self 2003) and its intensification from late June to mid-July.

GLOMAP-mode simulates a JJA-mean AOD of 0.65 in Grund and 0.26 in Mannheim, and a JJA-mean AOD of 0.23 when averaged over the NH, which is in good agreement with independent estimates of the AOD for Laki listed in Table 4.1.

In Grund, the first significant visibility reduction of under 20 km is calculated for 21 June, with the most severe visibility reductions of around 5 km occurring on the 29 June, and during mid-July. These changes in the transmission range of visible light compare well with historic records describing the appearance of a strong haze in northern and western Iceland 8–10 days after the onset of the eruption (Thordarson and Self 2003). JJA-mean visibility reductions to 99 km in Mannheim are much less severe than in Grund, where mean visibility is reduced to 47 km during JJA. The strongest impact on visibility in Mannheim is simulated for 8 July (visibility of around 11 km). The strongest visibility reduction in Grund occurs shortly after the onset of

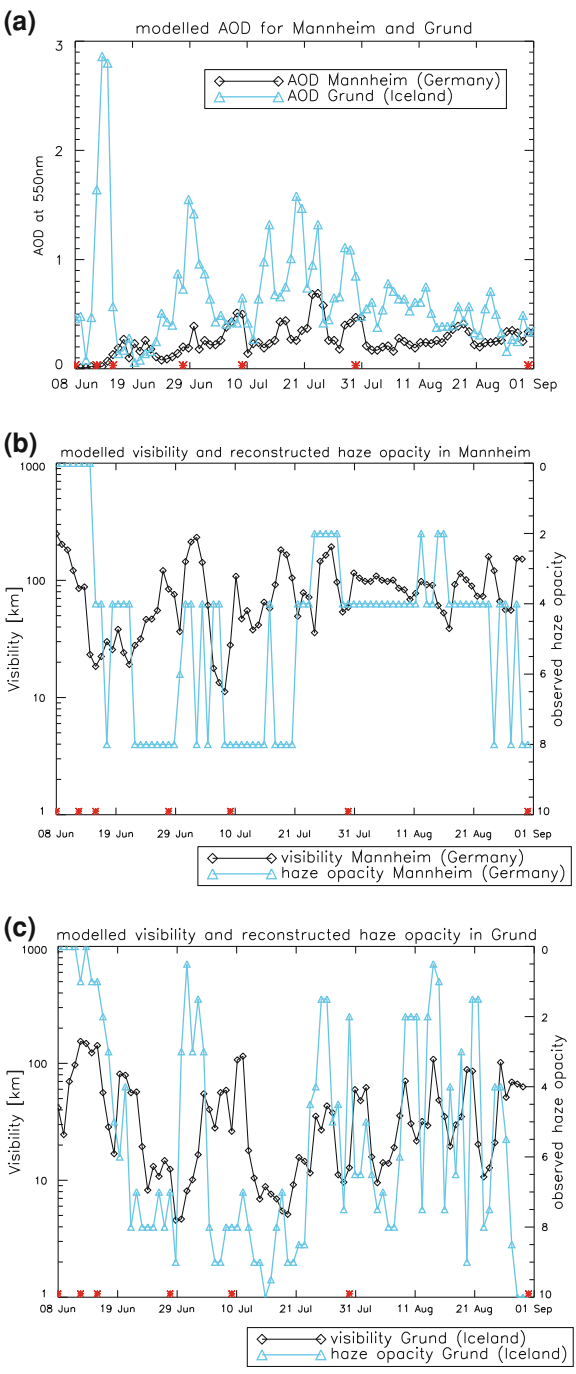

Fig. 4.10 (**a**) Simulated daily aerosol optical depth (AOD) at 550 nm from 8 June to 31 August for grid boxes above Grund (northern Iceland) (*blue line*) and Mannheim (Germany) (*black line*) (**b**) and (**c**) calculated daily visible range in km (*black line*) and haze opacity index (*blue line*) with 10 = very intense haze and 0 = no haze observed (Thordarson 1995; Thordarson and Self 2003) for Mannheim and Grund, respectively. *Red stars* indicate the onset of each of the ten eruption episodes.

eruption episode IV, however, in Mannheim there seems to be no straightforward correlation between the onset of an eruption episode and the timing of the visibility reduction. The results presented here are dependent on the meteorology used to force the model, hence conclusive comparison with historical records can only be achieved by using the exact 1783 meteorology (which is not possible). Nonetheless, the results presented here allowed quantification of the extent of the reductions in the transmission range of visible light during a Laki-style eruption.

4.3.6 *Aerosol Microphysical Processes and Size Distribution*

Figure 4.11 shows the simulated 3-month mean number-size distributions averaged over the NH for L-s and L-w, and the respective unperturbed simulations.

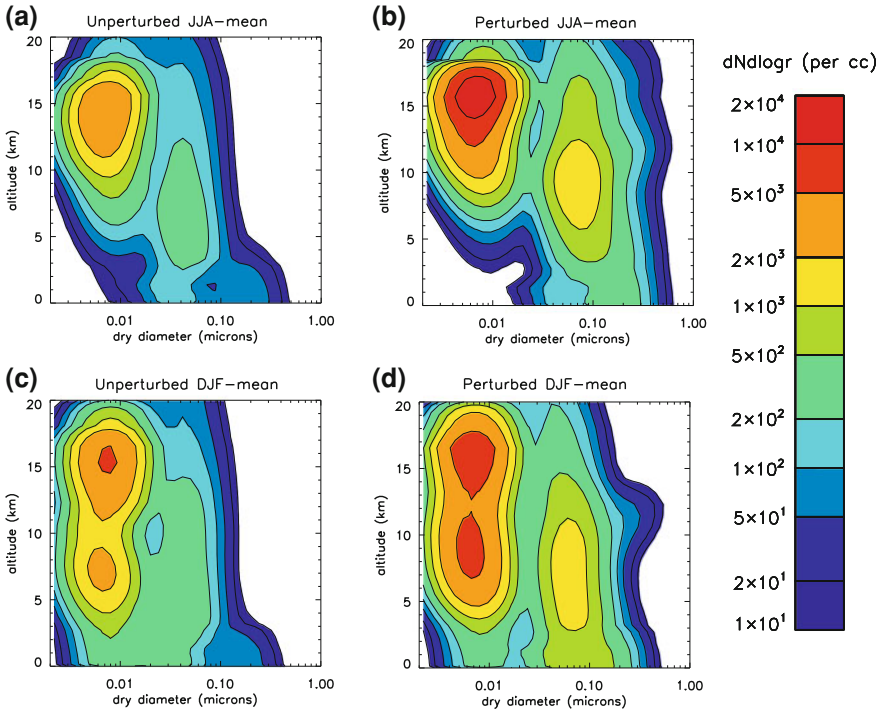

Fig. 4.11 Simulated 3-month mean number-size distribution averaged over the NH for (**a**) L-s unperturbed run, (**b**) L-s perturbed run, (**c**) L-w unperturbed run, (**d**) L-w perturbed run. JJA = June–July–August; DJF = December–January–February. With nucleation mode: ($d_p < 0.01\,\mu$m); Aitken mode: ($0.01 < d_p < 0.1\,\mu$m); accumulation mode: ($0.1 < d_p < 1.0\,\mu$m). JJA = June–July–August; DJF = December–January–February. Figure after Schmidt et al. (2010)

In both L-s and L-w there is a substantial effect on the sizes and number concentrations of particles throughout the atmosphere. Moreover, the aerosol processes controlling the evolution of the size distribution are noticeably different for the summer and winter scenarios when compared to the unperturbed atmosphere (see Figs. 4.4 and 4.5).

In both L-s and L-w the upper parts of the atmosphere are characterised by an increase in nucleation mode ($d_p < 0.01\,\mu m$) and Aitken mode ($0.01 < d_p < 0.1\,\mu m$) particle concentrations due to more favourable conditions for nucleation at high altitudes (Spracklen et al. 2005a). In L-s, zonal 3-month mean nucleation mode particle concentrations at 15 km are a factor of ~4 higher than in the unperturbed atmosphere, and they are a factor of ~2 higher in L-w.

Accumulation mode particles are the most relevant to climate, and below about 8 km the summer eruption increases their number concentration by a factor of ~9. The cause of the very substantial effects on Aitken and accumulation mode particle concentrations throughout the atmosphere is the combination of increased nucleation in the high free troposphere/upper troposphere and the availability of H_2SO_4 vapour for condensational growth to larger sizes. Nucleation mode particles in the free troposphere grow by H_2SO_4 condensation and coagulation as they descend. This in turn, leads to abundant Aitken mode particles with changes in concentration of up to $1695\,cm^{-3}$ at altitudes from 7 to 12 km for L-s.

Figure 4.4 highlights how much the microphysical processes change in response to the summertime eruption when compared to the unperturbed atmosphere. Condensation of H_2SO_4 onto Aitken particles rises by a factor of ~8 in the 12 months after the onset of L-s. The significant increase in Aitken particles also means that their coagulation adds a factor of ~42 more mass to the accumulation mode than in the unperturbed atmosphere. Moreover, the abundant H_2SO_4 vapour means that the direct growth of Aitken mode particles into the accumulation mode increases by a factor of ~50, accounting for around one-fifth of the accumulation mode SO_4 mass. Likewise, direct H_2SO_4 vapour condensation on to accumulation mode particles increases by a factor of ~8 and accounts for around one-third of the accumulation mode SO_4 mass.

The only process not greatly enhanced during the first 12 months after the onset of L-s is in-cloud SO_4 production (i.e. aqueous-phase oxidation of SO_2 by H_2O_2 to form SO_4 on Aitken and accumulation mode particles), which is enhanced by merely a factor of 1.5 compared to the unperturbed run. This small increase in in-cloud SO_4 production is due to the suppression of the main aqueous phase oxidant, H_2O_2 (see Fig. 4.6). Thus, in-cloud SO_4 production contributes only a small fraction of the accumulation mode mass in the perturbed atmosphere. In stark contrast, in-cloud SO_4 production is the main pathway for the increase of the accumulation mode in the unperturbed atmosphere and adds about a factor of 8 more SO_4 than the second most important process, condensation of H_2SO_4 vapour.

To summarise the budget for L-s: in the 12 months after the onset of the eruption, H_2SO_4 condensation on the accumulation mode and growth of Aitken mode particles

into the accumulation mode increase to such an extent (from 2.5 to 34 $Tg(S)\,a^{-1}$) that, alongside the small increase of in-cloud SO_4 production (from 17 to 25 $Tg(S)\,a^{-1}$), these processes become approximately equally important in determining the mass of the accumulation mode.

In contrast, in the 12 months after the onset of L-w, in-cloud SO_4 production is still the dominant process determining the mass of accumulation mode SO_4 due to less substantial increases in H_2SO_4 vapour condensation and direct growth of Aitken mode particles (from 2.5 to 16.0 $Tg(S)\,a^{-1}$) alongside a large increase in in-cloud SO_4 production (from 18 to 33 $Tg(S)\,a^{-1}$) (see Fig. 4.5). The dominance of in-cloud oxidation is a result of the less efficient conversion of SO_2 to SO_4 via OH during the winter months.

Chapter 3 highlighted that the key microphysical processes that govern the formation of climate-relevant CCN-sized particles are nucleation and condensation, which in turn are governed by the relative balance of gas-phase oxidation to aqueous-phase oxidation of SO_2. The results presented here demonstrate that both the chemical and the aerosol microphysical processes are fundamentally altered after the Laki eruption with the timing of the onset of the eruption playing an important role in determining the processes dominating the evolution of the aerosol size distribution.

4.3.7 Impact on Total Particle Number Concentration

Figure 4.12 shows zonal mean total particle number concentrations averaged over the first 3 months for L-s and L-w, together with the unperturbed runs and the ratio of the volcanically perturbed to the respective unperturbed period. In this study the total particle number concentration is defined in terms of the frequently used term condensation nuclei (CN), counted as all particles larger than 3 nm in diameter.

For L-s, GLOMAP-mode predicts an increase in CN number concentrations of up to a factor of 16 at high-northern latitudes at 8–10 km altitude (corresponding to increases of up to $\sim$4400 cm^{-3} in this region). CN number concentrations increase by as much as 16000 cm^{-3} at 15–18 km altitude at $\sim$10° N, however, given the high natural background concentrations, the increase in this region (factor of $\sim$11) is less than at higher northern latitudes. These results indicate that a fraction of the SO_2 emitted from the vents into the lower stratosphere enhances nucleation, and that new particles are transported over long distances. This result is consistent with findings from previous studies (Spracklen et al. 2005a,b) suggesting that the CN-formation potential is strongly enhanced in the cold upper troposphere where nucleation is most efficient. For L-w, the CN enhancement is a factor of $\sim$12, which is lower than for L-s. For L-w, maximum changes in CN number concentrations of 7800 cm^{-3} are simulated at $\sim$9 km at around 45° N. In the boundary layer, changes in CN number concentrations are on average a factor of $\sim$5 for both L-s and L-w, while L-s exhibits a local peak (factor of $\sim$16) at around 1 km above the eruption site.

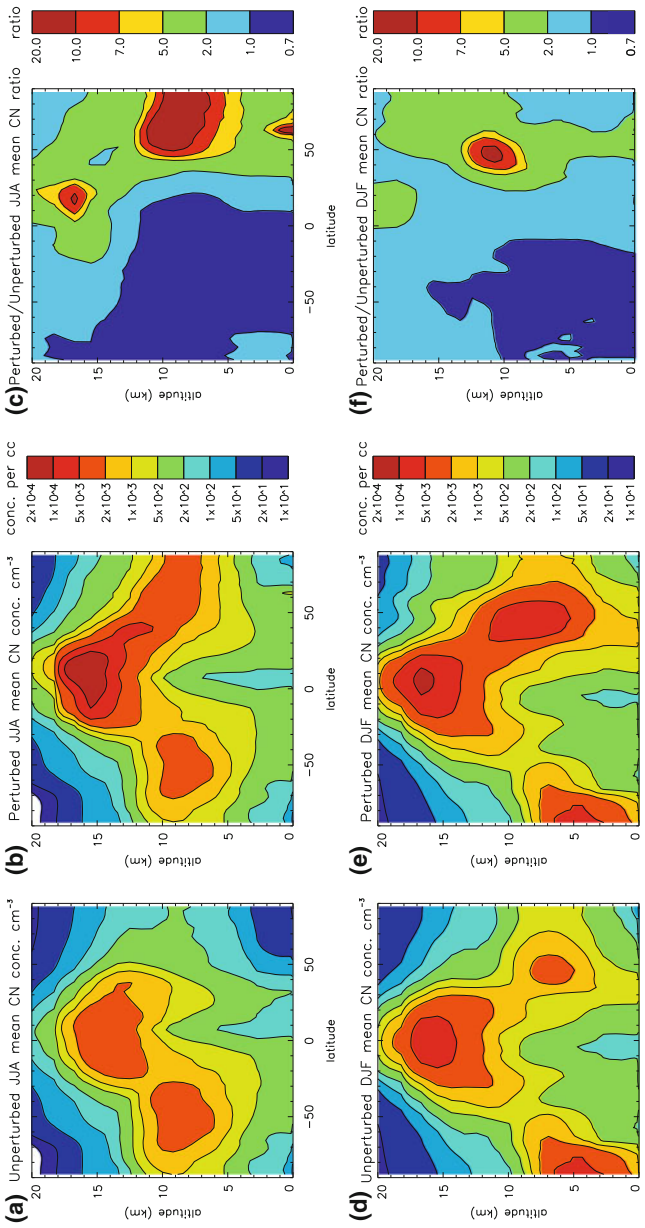

Fig. 4.12 Simulated zonal 3-month mean CN number concentrations per cubic centimeter (per cc) for L-s (**a**) unperturbed run, (**b**) perturbed run, (**c**) ratio of perturbed to unperturbed; and for L-w: (**d**) unperturbed run, (**e**) perturbed run, (**f**) ratio of perturbed to unperturbed. JJA = June–July–August; DJF = December–January–February. Figure after Schmidt et al. (2010)

Both L-s and L-w show reduced 3-month mean CN number concentrations in the SH relative to the unperturbed atmosphere, with the strongest reduction (factor of ~0.8) in the upper troposphere at 30° S. These reductions indicate that the net effect of the small increases in SH aerosol loading (see Sect. 4.3.1) is to enhance coagulation of existing and entrained particles. In the NH, closer to the emissions of SO_2, the net effect is to enhance nucleation of new particles from the produced H_2SO_4 vapour. However, the age of the pollution is older in the SH so most of the precursor gases have already been converted to aerosol.

Figure 4.13 shows the spatial distribution of 3-month mean CN number concentrations at low-level cloud altitude (~970 m) together with the ratio of the perturbed to the unperturbed simulations. Close to the eruption site, changes in concentrations reach a maximum of ~14000 cm^{-3} for L-s and ~12000 cm^{-3} for L-w. Enhanced CN number concentrations at the source are a result of nucleation of H_2SO_4 vapour from the gas-phase oxidation of SO_2 emitted from the lava flows. The change in NH 3-month mean CN number concentrations is greater in the winter (~328 cm^{-3}) than in the summer (~135 cm^{-3}). The main source of these additional low-level CN on a hemispheric scale is from nucleation in the free troposphere and upper troposphere, and in the winter, with lower temperatures and higher humidities, nucleation occurs at lower altitudes and has a greater impact lower down than in the summer. For L-s CN number concentrations increase on average to ~450 cm^{-3} over large parts of North America, Greenland, Europe, the Middle East and Asia (i.e. an enhancement in CN number concentration by a factor of ~2 to ~5 in those regions). This far-reaching impact on CN number concentrations is due to the long-range transport of nucleated particles as previously reported by Manktelow et al. (2009).

However, both eruptions have a relatively minor effect on CN number concentrations at low-level cloud altitude south of the equator with L-s having a more profound and latitudinally more widespread effect (down by a factor of 0.7) when compared to L-w (factor of 0.9) due to higher SO_2 and SO_4 aerosol mixing ratios in the SH atmosphere for L-s.

4.3.8 Impact on CCN Number Concentrations

The substantial change in the total CN population implies that both eruption scenarios have the potential to contribute significantly to the global CCN budget in the pre-industrial atmosphere, thus strongly impacting cloud microphysics. Here, CCN are counted as particles with a dry radius larger than 35 nm, which is equivalent to the particles that would activate into cloud droplets at 0.22 % supersaturation, which typically occurs in low-level stratocumulus clouds. Several microphysical processes lead to an increase in CCN concentrations: (a) nucleation of H_2SO_4 vapour to SO_4 aerosol and its subsequent growth to CCN sizes by coagulation and condensation; (b) growth to CCN sizes by condensation of H_2SO_4 onto existing particles; and (c) cloud

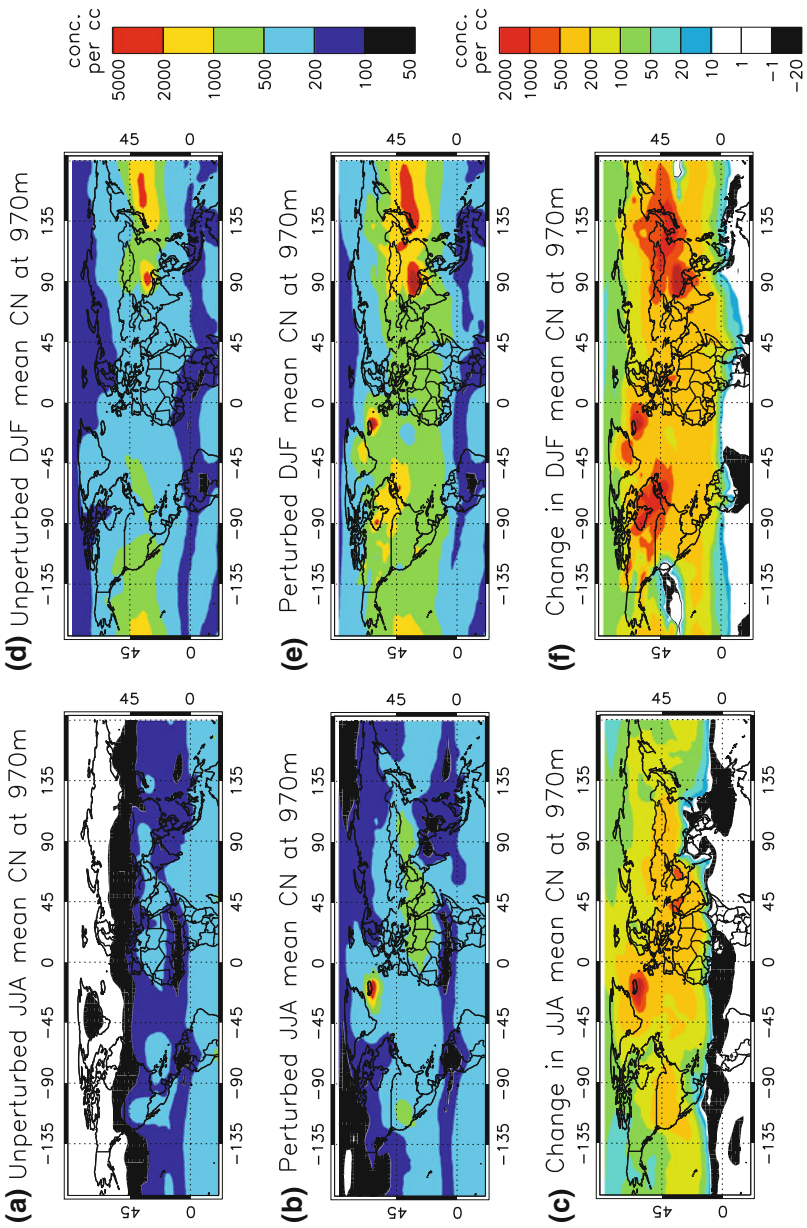

Fig. 4.13 Simulated 3-month mean CN number concentrations per cubic centimeter (per cc) at 970 m altitude for L-s: (**a**) unperturbed run, (**b**) perturbed run, (**c**) absolute change; and for L-w: (**d**) unperturbed run, (**e**) perturbed run, (**f**) absolute change. JJA = June–July–August; DJF = December–January–February. Figure after Schmidt et al. (2010)

processing of Aitken mode-sized particles. The balance of these pathways changes significantly in the volcanically perturbed simulations, as discussed in Sect. 4.3.6.

Figure 4.14 shows zonal mean concentrations of CCN-sized particles averaged over the first 3 months for L-s and L-w, together with the unperturbed run, and the change in CCN concentrations. GLOMAP-mode predicts an increase in CCN concentrations for L-s by a factor of >65 in the upper troposphere, giving a change in zonal mean concentrations at 10 km altitude of $\sim$1400 cm^{-3}. For comparison, following the Mt. St. Helens eruption, Rogers et al. (1981) measured CCN number concentrations (at 1 % supersaturation) ranging from 100 to 1000 cm^{-3} at an altitude of 13.6 km. Boundary layer zonal 3-month mean CCN concentrations increase up to a factor of $\sim$26 to $\sim$415 cm^{-3} during L-s. The impact of L-w on CCN concentrations at 10 km altitude is a factor of $\sim$24, so less profound than during L-s.

Figure 4.14 also shows the impact of the eruption on CCN number concentrations in the SH. In the L-s scenario zonal 3-month mean CCN number concentrations increase by up to a factor of 20 in the upper troposphere at $\sim$10° S where freshly nucleated particles subside in the general circulation and subsequently grow (by coagulation and condensation) to CCN sizes. Moreover, the model simulates an increase in boundary layer CCN number concentrations of up to 35 cm^{-3} (factor of 1.4) as far south as 20° S (see also Fig. 4.15). The increase in CCN number concentrations, together with the decrease in CN number concentrations in the SH (see Sect. 4.3.7), indicates a substantial impact of the eruption on microphysical processes leading to fewer, but larger-sized particles relative to the unperturbed atmosphere.

The main source of summertime CCN in the natural unperturbed lower troposphere in the pre-industrial period is from wind-dependent sea spray, which is rather weak during summer, and the formation of SO_4 aerosol from H_2SO_4 vapour derived from the oxidation of marine dimethylsulfide (Korhonen et al. 2008). At present, these processes typically account for CCN number concentrations of up to 100 cm^{-3} found in the lower troposphere in remote marine regions (Andreae 2009). In the NH, GLOMAP-mode predicts CCN number concentrations at 1 km altitude ranging from $\sim$5 to 450 cm^{-3} (see Fig. 4.15) with a mean of 55 cm^{-3} under unperturbed pre-industrial conditions. Thus, with changes in NH 3-month mean CCN number concentrations at low-level cloud altitude of $\sim$168 cm^{-3} for L-s and of $\sim$305 cm^{-3} for L-w, both eruptions would have completely dominated as a source of CCN in the pre-industrial atmosphere. Changes in peak 3-month mean CCN number concentrations of $\sim$8000 cm^{-3} for L-s and $\sim$5500 cm^{-3} for L-w are simulated close to the eruption site, representing an enhancement by factors of 543 and 594, respectively. Moreover, both eruptions significantly increase CCN number concentrations at the altitude of low-level clouds over North America (factor of $\sim$10 for L-s and factor of $\sim$17 for L-w), Europe (factor of $\sim$6 for L-s and factor of $\sim$8 for L-w), Asia (factor of $\sim$14 for L-s and factor of $\sim$11 for L-w) and Northern Africa (factor of $\sim$2 for L-s and factor of $\sim$5 for L-w), as well as over the Pacific (factor of $\sim$3 for L-s and factor of $\sim$10 for L-w).

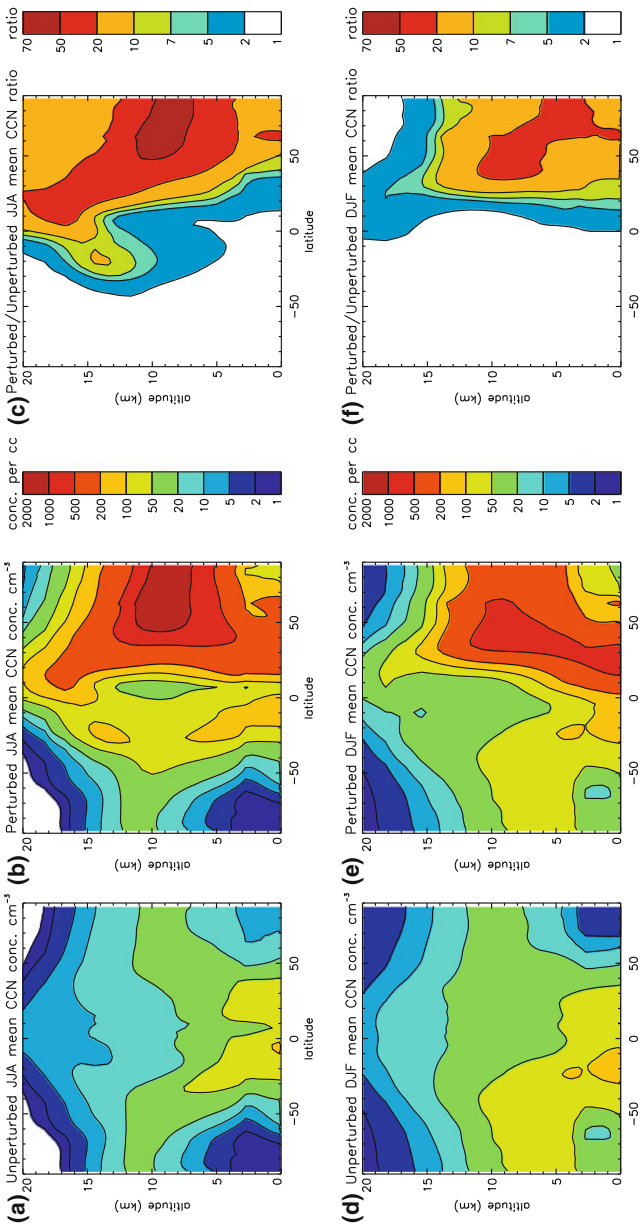

Fig. 4.14 Simulated zonal 3-month mean CCN concentrations (dry radius >35 nm, supersaturation $= 0.22\,\%$) per cubic centimeter (per cc) for L-s: (**a**) unperturbed run, (**b**) perturbed run, (**c**) ratio of perturbed to unperturbed; and for L-w: (**d**) unperturbed run, (**e**) perturbed run, (**f**) ratio of perturbed to unperturbed. JJA = June–July–August; DJF = December–January–February. Figure after Schmidt et al. (2010)

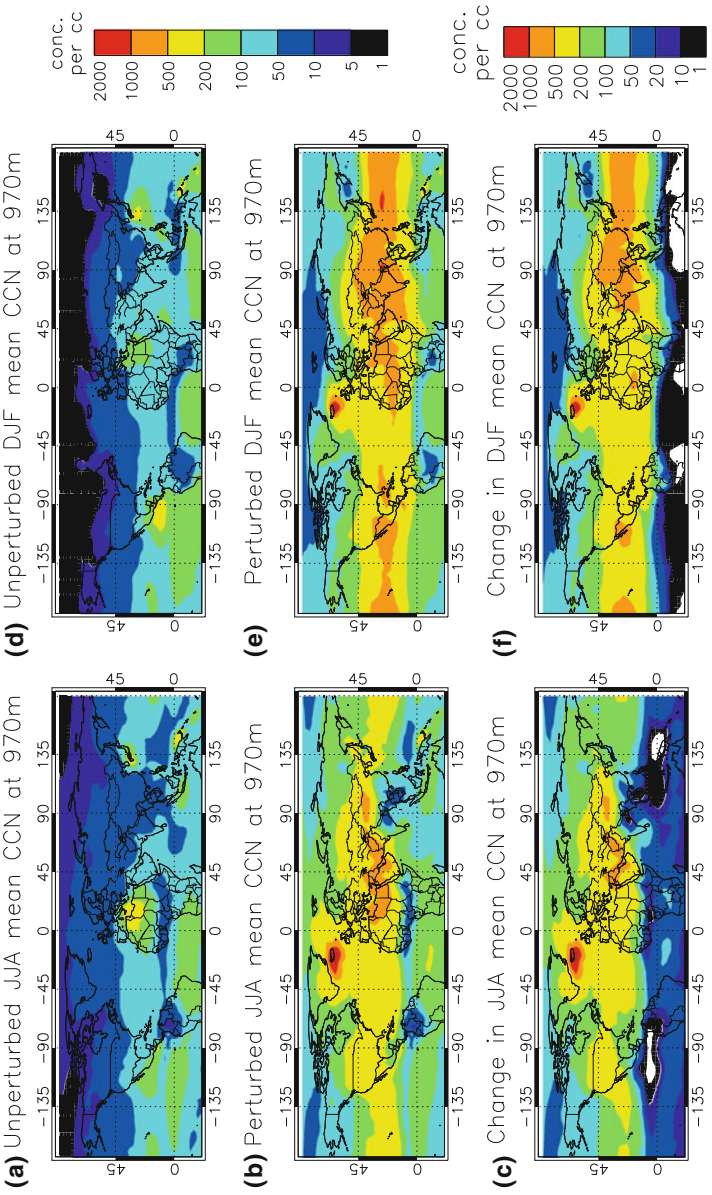

Fig. 4.15 Simulated 3-month mean CCN number concentrations (dry radius > 35 nm, supersaturation = 0.22 %) per cubic centimeter (per cc) for L-s: (**a**) unperturbed run, (**b**) perturbed run, (**c**) absolute change; and for L-w: (**d**) unperturbed run, (**e**) perturbed run, (**f**) absolute change. JJA = June–July–August; DJF = December–January–February. Figure after Schmidt et al. (2010)

The spatial distribution of CN and CCN changes will differ somewhat when forcing the model with different ECMWF reanalysis data. The analyses of a Laki simulation forced with ECMWF fields for the year 2000 shows that on climatologically relevant time-scales, the results are very similar for both CN and CCN number concentrations. For example, zonal JJA-mean CCN number concentrations increase by a factor of 74 in the upper troposphere (corresponding to maximum CCN changes of $1470\,cm^{-3}$) when using reanalysis for the year 2000. Northern Hemisphere JJA-mean CCN number concentrations at low-level cloud altitude reach $270\,cm^{-3}$ during the year 2003 and $290\,cm^{-3}$ during the year 2000. Moreover, similar to the year 2003, significant increases in CCN number concentrations are found far away from the eruption site (e.g., North America: factor of ∼11; Europe: factor of ∼5; Asia: factor of ∼12).

4.4 Conclusions

A comprehensive global aerosol microphysics model (GLOMAP-mode) has been used to study the impact of the 1783–1784 AD Laki eruption on aerosol microphysical processes, including the nucleation of new particles and their growth to CCN in a pre-industrial atmospheric setting. The SO_2 emission data set by Thordarson et al. (1996) and Thordarson and Self (2003) was used in order to simulate the eruption. This study also investigated the sensitivity of aerosol microphysical processes to the timing of the onset of such an eruption by additionally simulating a hypothetical Laki eruption commencing in December.

The principal finding of this study is that a Laki-style eruption had the potential to substantially impact global CN and CCN number concentrations. GLOMAP-mode predicts an increase of the total particle number concentration in the upper troposphere up to a factor of ∼16 over large parts of the NH during the first three months of the eruption. There are already several indications that particles released by volcanoes may act as CCN (e.g., Mather et al. 2004; Mather 2008; Gassó 2008) and thus potentially alter cloud microphysical properties. The study presented here shows that a Laki-style eruption had the potential to profoundly alter cloud microphysical properties and completely dominated as a source of CCN in the pre-industrial atmosphere. Zonal mean CCN number concentrations increase up to a factor of ∼65 in the upper troposphere and a factor of ∼26 in the boundary layer at high-northern latitudes during the first three months following the onset of the eruption.

Moreover, the simulations reveal that a Laki-style eruption has a spatially very widespread effect on CCN number concentrations. For example, CCN number concentrations at the altitude of low-level clouds are predicted to increase by a factor of ∼14 in Asia. Such a long-range effect is consistent with a previous study of regional air pollution transport (Manktelow et al. 2009). During a Laki-style eruption SO_2 is lofted into the free troposphere where the resultant H_2SO_4 vapour causes rapid nucleation of new particles at low temperatures. These particles grow by coagulation and condensation of further vapour during long-range transport. Although the

mass of SO_4 is quite small far from the eruption, it is present in a large number of small particles that are very effective CCN. Manktelow et al. (2009) have shown that Asian anthropogenic sulphur emissions are lofted higher into the free troposphere than other regional emissions and therefore have a high "CCN formation potential". The study presented here has shown that a similar high CCN formation potential applies to an eruption like Laki.

Furthermore, this study demonstrated that a Laki-style eruption that commences in June can affect CCN number concentrations in the SH. At 20° S, a summertime eruption is found to increase CCN number concentrations at the altitude of low level clouds by up to $35\,cm^{-3}$ (factor of 1.4). Although this is a small increase, the potential effects on cloud droplet concentrations and the radiative properties of marine stratocumulus clouds are significant and are quantified in Chap. 5.

So far, little work has been done comparing model output with historical records of the observed SO_4 aerosol haze opacity. The work presented here showed that the simulated reductions in the transmission range of visible light closely follow (in terms of the temporal pattern and their magnitude) reconstructions of the haze opacity (Thordarson and Self 2003). The comparison of the modelled SO_4 deposition over Greenland with ice-core measurements revealed a high model bias which warrants further investigation; however, other model diagnostics agree well with previous studies giving confidence in the model results. Future work could involve running multi-year simulations in order to investigate how well the ice-core measurements in Greenland compare to the multi-annual variability of the modelled deposition values.

One shortcoming of the present study is that the chosen model framework cannot account for feedbacks between the additional aerosol loading and cloud cover; however, substantial first-order effects on CCN have been identified (i.e. effects that are initially unaffected by any potential feedbacks). First-order effects on CCN have not been taken into account in any previous Laki modelling study and the data provided here can be used to investigate second-order feedback effects on CCN using an aerosol-chemistry-climate model.

Overall, the results presented here highlighted the importance of using a global aerosol model which treats microphysical processes such as nucleation and particle growth to CCN sizes when modelling the effects of volcanic eruptions. The simulations using GLOMAP-mode reveal that both the microphysical processes and the chemical processes controlling particle concentrations are fundamentally different when compared to an unperturbed atmosphere. Moreover, these processes are non-linear throughout the season; thus the effects of a high-latitude eruption such as Laki are strongly dependent on the season in which the eruption commences. For example, the simulations revealed that the impact of an equivalent wintertime eruption on upper tropospheric CCN is less than during a summertime eruption. The upper tropospheric zonal DJF-mean CCN number concentrations for a wintertime eruption are predicted to be only about one-third of those of a summertime eruption. However, a wintertime eruption is found to have a comparable or slightly larger effect on CCN number concentrations in the boundary layer.

Using a global aerosol microphysics model such as GLOMAP-mode advances our understanding of how long-lasting high-latitude volcanism influences natural background aerosol concentrations and microphysical processes. Moreover, the obtained data set enables the impact on cloud drop number concentrations to be calculated based on a fully resolved aerosol size distribution. In contrast, most GCMs use simplified schemes to derive cloud drop number concentrations (e.g., Lohmann and Feichter 2005) which do not account for microphysical processes controlling cloud drop number concentrations.

Chapter 5 investigates the impact of the 1783–1784 AD Laki eruption on cloud radiation using a physically-based aerosol activation scheme (Nenes and Seinfeld 2003; Pringle et al. 2009) together with a radiative transfer code (Edwards and Slingo 1996).

References

Andreae MO (2009) Correlation between cloud condensation nuclei concentration and aerosol optical thickness in remote and polluted regions. Atmos Chem Phys 9:543–556

Chen P (1995) Isentropic cross-tropopause mass exchange in the extratropics. J Geophys Res 100:16661–16673

Chenet AL, Fluteau F, Courtillot V (2005) Modelling massive sulphate aerosol pollution, following the large 1783 Laki basaltic eruption. Earth Planet Sci Lett 236:721–731

Clausen HB, Hammer C (1988) The Laki and Tambora eruptions as revealed in Greenland ice cores from 11 locations. Ann Glaciol 10:16–22

Edwards JM, Slingo A (1996) Studies with a flexible new radiation code. I: choosing a configuration for a large-scale model. QJR Meteorol Soc 122:689–719

Fiacco RJ, Thordarson T, Germani MS, Self S, Palais JM, Whitlow S, Grootes PM (1994) Atmospheric aerosol loading and transport due to the 1783–84 Laki eruption in Iceland, interpreted from ash particles and acidity in the GISP2 ice core. Quat Res 42:231–240

Gassó S (2008) Satellite observations of the impact of weak volcanic activity on marine clouds. J Geophys Res 113:D14S19

Hobbs P, Tuell J, Hegg D, Radke L, Eltgroth M (1982) Particles and gases in the emissions from the 1980–1981 volcanic eruptions of Mt. St. Helens. JGR Atmos 87:1062–1086

Kekonen T, Moore J, Perämäki P, Martma T (2005) The Icelandic Laki volcanic tephra layer in the Lomonosovfonna ice core, Svalbard. Polar Res 24:33–40

Koch D, Schmidt G, Field C (2006) Sulfur, sea salt and radionuclide aerosols in GISS ModelE. J Geophys Res 111:D06206

Korhonen H, Carslaw KS, Spracklen DV, Ridley DA, StrÃum J (2008) A global model study of processes controlling aerosol size distributions in the Arctic spring and summer. J Geophys Res 113:D08211

Koschmieder H (1924) Theorie der horizontalen Sichtweite. Beiträge zur Physik der Freien Atmosphäre 12:33–55 and 171–181

Levine JG, Braesicke P, Harris NRP, Savage NH, Pyle JA (2007) Pathways and timescales for troposphere-to-stratosphere transport via the tropical tropopause layer and their relevance for very short lived substances. J Geophys Res 112:D04308

Levine JG, Braesicke P, Harris NRP, Pyle JA (2008) Seasonal and inter-annual variations in troposphere-to-stratosphere transport from the tropical tropopause layer. Atmos Chem Phys 8:3689–3703

Lohmann U, Feichter J (2005) Global indirect aerosol effects: a review. Atmos Chem Phys 5:715–737

Manktelow PT, Mann GW, Carslaw KS, Spracklen DV, Chipperfield MP (2007) Regional and global trends in sulfate aerosol since the 1980s. Geophys Res Lett 34:L14803

Manktelow PT, Carslaw KS, Mann GW, Spracklen DV (2009) Variable CCN formation potential of regional sulfur emissions. Atmos Chem Phys 9:3253–3259

Mann GW, Carslaw KS, Spracklen DV, Ridley DA, Manktelow PT, Chipperfield MP, Pickering SJ, Johnson CE (2010) Description and evaluation of GLOMAP-mode: a modal global aerosol microphysics model for the UKCA composition-climate model. Geosci Model Dev 3:519–551

Mather TA (2008) Volcanism and the atmosphere: the potential role of the atmosphere in unlocking the reactivity of volcanic emissions. Philos Trans Royal Soc A Math Phys Eng Sci 366:4581–4595

Mather T, Pyle DM, Oppenheimer C (2003) Tropospheric Volcanic Aerosol. In: Volcanism and the Earth's atmosphere, vol 139 of Geophysical Monograph, American Geophysical Union (AGU) pp 189–212

Mather TA, Tsanev VI, Pyle DM, McGonigle AJS, Oppenheimer C, Allen AG (2004) Characterization and evolution of tropospheric plumes from Lascar and Villarrica volcanoes, Chile. J Geophys Res 109:D21303

Mosley-Thompson E, Mashiotta T, Thompson L (2003) High resolution ice core records of late Holocene volcanism: current and future contributions from the Greenland PARCA cores. In: Volcanism and the Earth's atmosphere, geophysical monograph series. American Geophysical Union (AGU), vol 139, pp 153–164

Nenes A, Seinfeld JH (2003) Parameterization of cloud droplet formation in global climate models. J Geophys Res 108(D14):4415. doi:10.1029/2002JD002911

Niemeier U, Timmreck C, Graf HF, Kinne S, Rast S, Self S (2009) Initial fate of fine ash and sulfur from large volcanic eruptions. Atmos Chem Phys Discuss 9:17531–17577

Oman L, Robock A, Stenchikov GL, Thordarson T, Koch D, Shindell DT, Gao C (2006) Modeling the distribution of the volcanic aerosol cloud from the 1783–1784 Laki eruption. J Geophys Res 111:D12209. doi:10.1029/2005JD006899

Pringle KJ, Carslaw KS, Spracklen DV, Mann GM, Chipperfield MP (2009) The relationship between aerosol and cloud drop number concentrations in a global aerosol microphysics model. Atmos Chem Phys 9:4131–4144

Rogers CF, Hudson JG, Kocmond WC (1981) Measurements of cloud condensation nuclei in the stratosphere around the plume of Mount St. Helens Sci 211:824–825

Schmidt GA, Ruedy R, Hansen JE, Aleinov I, Bell N, Bauer M, Bauer S, Cairns B, Canuto V, Cheng Y, Del Genio A, Faluvegi G, Friend AD, Hall TM, Hu YY, Kelley M, Kiang NY, Koch D, Lacis AA, Lerner J, Lo KK, Miller RL, Nazarenko L, Oinas V, Perlwitz J, Perlwitz J, Rind D, Romanou A, Russell GL, Sato M, Shindell DT, Stone PH, Sun S, Tausnev N, Thresher D, Yao MS (2006) Present-day atmospheric simulations using GISS ModelE: comparison to in situ, satellite, and reanalysis data. J Clim 19:153–192

Schmidt A, Carslaw KS, Mann GW, Wilson M, Breider TJ, Pickering SJ, Thordarson T (2010) The impact of the 1783–1784 AD Laki eruption on global aerosol formation processes and cloud condensation nuclei. Atmos Chem Phys 10:6025–6041

Spracklen DV, Pringle KJ, Carslaw KS, Chipperfield MP, Mann GW (2005a) A global off-line model of size-resolved aerosol microphysics: I. Model development and prediction of aerosol properties. Atmos Chem Phys 5:179–215

Spracklen DV, Pringle KJ, Carslaw KS, Chipperfield MP, Mann GM (2005b) A global off-line model of size resolved aerosol processes: II. Identification of key uncertainties. Atmos Chem Phys 5:3437–3489

Stevenson DS, Johnson CE, Highwood EJ, Gauci V, Collins WJ, Derwent RG (2003) Atmospheric impact of the 1783–1784 Laki eruption: Part I chemistry modelling. Atmos Chem Phys 3:487–507

Stothers RB (1996) Major optical depth perturbations to the stratosphere from volcanic eruptions: pyrheliometric period, 1881–1960. J Geophys Res Atmos 101:3901–3920

Textor C, Schulz M, Guibert S, Kinne S, Balkanski Y, Bauer S, Berntsen T, Berglen T, Boucher O, Chin M, Dentener F, Diehl T, Easter R, Feichter H, Fillmore D, Ghan S, Ginoux P, Gong S, Grini A, Hendricks J, Horowitz L, Huang P, Isaksen I, Iversen I, Kloster S, Koch D, Kirkevåg A, Kristjansson JE, Krol M, Lauer A, Lamarque JF, Liu X, Montanaro V, Myhre G, Penner J, Pitari G, Reddy S, Seland Ø, Stier P, Takemura T, Tie X (2006) Analysis and quantification of the diversities of aerosol life cycles within AeroCom. Atmos Chem Phys 6:1777–1813

Thordarson T (1995) Volatile release and atmospheric effects of basaltic fissure eruptions. Ph.D. thesis, University of Hawaii, Honolulu

Thordarson T, Self S (1993) The Laki (Skaftar Fires) and Grimsvatn eruptions in 1783–1785. Bull Volcanol 55:233–263

Thordarson T, Self S (2003) Atmospheric and environmental effects of the 1783–1784 Laki eruption: a review and reassessment. J Geophys Res Atmos 108(D1):4011. doi:10.1029/2001JD002042

Thordarson T, Self S, Oskarsson N, Hulsebosch T (1996) Sulfur, chlorine, and fluorine degassing and atmospheric loading by the 1783–1784 AD Laki (Skaftar fires) eruption in Iceland. Bull Volcanol 58:205–222

Timmreck C, Lorenz SJ, Crowley TJ, Kinne S, Raddatz TJ, Thomas MA, Jungclaus JH (2009) Limited temperature response to the very large AD 1258 volcanic eruption. Geophys Res Lett 36:L21708

Timmreck C, Graf HF, Lorenz SJ, Niemeier U, Zanchettin D, Matei D, Jungclaus JH, Crowley TJ (2010) Aerosol size confines climate response to volcanic super-eruptions. Geophys Res Lett 37:L24705

Trigo R, Vaquero J, Stothers R (2010) Witnessing the impact of the 1783–1784 Laki eruption in the Southern Hemisphere. Clim Change 99:535–546. doi:10.1007/s10584-009-9676-1

Turco RP, Toon OB, Whitten RC, Hamill P, Keesee RG (1983) The 1980 eruptions of Mount St. Helens: physical and chemical processes in the stratospheric clouds. J Geophys Res 88:5299–5319

Zielinski GA, Mayewski PA, Meeker LD, Grönvold K, Germani MS, Whitlow S, Twickler MS, Taylor K (1997) Volcanic aerosol records and tephrochronology of the Summit, Greenland, ice cores. J Geophys Res 102(C12):26625–26640

Chapter 5
Impact of the 1783–1784 AD Laki Eruption on Cloud Drop Number Concentrations and the First Aerosol Indirect Effect

5.1 Introduction

Low-level clouds have long been recognised as playing a major role in modulating the Earth's radiation budget (e.g., Klein and Hartmann 1993). Thus, fully understanding the impact of volcanic eruptions on the climate system requires the assessment of how volcanic aerosol might affect the microphysical properties of low-level clouds, which can subsequently mediate a cloud-radiative effect. The chapter presented here aims to assess the impact of the 1783–1784 AD Laki eruption on changes in cloud drop number concentration (CDNC) at low-level cloud altitude in order to quantify the magnitude of the first aerosol indirect effect (AIE). According to the IPCC, the first AIE is the largest aerosol radiative forcing of climate accounting for $-0.7\,\mathrm{W\,m^{-2}}$ (range of -1.1 to $+0.4\,\mathrm{W\,m^{-2}}$) of the total aerosol radiative forcing (i.e. direct and indirect effect) of $-1.2\,\mathrm{W\,m^{-2}}$ (Forster et al. 2007) under present-day conditions.

Table 5.1 provides an overview of the processes accounted for in previous Laki modelling studies compared to the study presented here. Stevenson et al. (2003b) used a CTM in order to assess the impact of the eruption on atmospheric composition. Highwood and Stevenson (2003) used output SO_4 fields from Stevenson et al. (2003b) in order to assess the direct and indirect radiative effects induced by the Laki SO_4 aerosol. Highwood and Stevenson (2003) accounted for the impact of surface temperature changes following the eruption on atmospheric dynamics; however, the changes in circulation were not fed back on to the aerosol distribution. In order to assess the first AIE on clouds, Highwood and Stevenson (2003) used an empirical relationship between SO_4 mass and CDNC (Boucher and Lohmann 1995) for the first month of the eruption. By modelling the spatial and temporal distribution of 200 Tg of SO_4 aerosol, Chenet et al. (2005) did not account for any impact of the SO_4 aerosol on atmospheric dynamics nor does their study account for chemical and microphysical processes. Oman et al. (2006a,b) addressed the direct radiative effect and the subsequent impact on atmospheric dynamics but did not account for microphysical processes that drive the evolution of the Laki SO_4 aerosol size distribution nor does their study account for the aerosol indirect effects on clouds and thus

A. Schmidt, *Modelling Tropospheric Volcanic Aerosol*, Springer Theses,
DOI: 10.1007/978-3-642-34839-6_5, © Springer-Verlag Berlin Heidelberg 2013

Table 5.1 Comparison of processes accounted for in previous Laki modelling studies and this study

Study	Dynamical feedbacks	Micro-physics	Aerosol activation	Radiative effect	SO_4 aerosol distribution	Comments
Stevenson et al. (2003b)	×	×	–	–	✓	Highwood and Stevenson (2003) used output sulphate fields
Highwood and Stevenson (2003)	✓	×	Empirical	Direct/ indirect	✓	Indirect effect calculated for first month of the eruption only
Chenet et al. (2005)	×	×	×	×	✓	
Oman et al. (2006a,b)	✓	×	×	Direct	✓	Prescribed aerosol size distribution
This thesis Chap. 4	×	✓	–	–	✓	Study presented here uses output aerosol fields
This study	×	✓	Physically	Indirect	✓	First full quantification of Laki first aerosol indirect effect

– Not applicable; × not considered; ✓ considered
"dynamical feedbacks" denotes feedbacks between aerosol-cloud changes and atmospheric circulation

climate. In Chap. 4 the impact of the Laki eruption on microphysical processes and particle number concentrations was addressed by means of a dedicated size-resolving global aerosol model.

Overall, none of the previous Laki modelling studies aimed to fully quantify the magnitude of the first AIE, which is mainly a result of the large uncertainties associated with aerosol-cloud interactions and their parameterisation in global models at the time these studies were conducted (e.g., Penner et al. 2001). Subsequently, the treatment of both aerosol microphysics and aerosol activation has greatly improved in global models, thus allowing investigation of the potential impact of the SO_4 aerosol on cloud microphysics and cloud radiative forcing. In this chapter, the magnitude of the AIE following the Laki eruption is assessed by using a physically-based aerosol activation scheme (Nenes and Seinfeld 2003; Pringle et al. 2009) together with a radiative transfer code (Edwards and Slingo 1996). This is an improvement on previous Laki studies as employing a physical based scheme mechanistically accounts for the physical and chemical properties of the aerosol size distribution when deriving CDNC. Additionally, the variability of the climate impact is investigated depending on the season during which such a high-latitude eruption commences.

5.2 Data and Methods

For this study, monthly mean aerosol number and size distribution fields as described in Chap. 4 are used. The model data sets for L-s and L-w cover one year following the onset of the eruption on 8 June and 8 December, respectively.

As already outlined in Chap. 2, CDNC is calculated using a physically-based aerosol activation scheme, which is identical to the Nenes and Seinfeld (2003) scheme and evaluated for GLOMAP in Pringle et al. (2009). In this study, CDNC is calculated at the base of stratus clouds (approximately 1 km altitude or 920 hPa) using a globally uniform updraught velocity of 0.2 ms^{-1}.

To calculate the first AIE due to the effect of the Laki SO_4 aerosol on CDNC and cloud albedo, a radiative transfer model (Edwards and Slingo 1996) is used, together with monthly mean cloud and surface albedo fields from the International Satellite Cloud Climatology Project (ISCCP) for the years 1983–2007 (Rossow and Schiffer 1999). The AIE calculations were performed by Professor Piers Forster (University of Leeds) and were subsequently analysed by the author. For the unperturbed and perturbed runs, the cloud drop effective radius is calculated from the GLOMAP-mode CDNC and ISCCP-derived liquid water paths, and only low-level clouds are modified. CDNC is calculated in every grid box, and for calculating the radiative effect a cloud mask is used. For the unperturbed simulations, the liquid water paths for low-level clouds are calculated from ISCCP optical depth measurements, assuming an effective drop radius of 10 μm. For the volcanically perturbed simulations, the liquid water path is assumed to remain unchanged and drop size is altered based on the fractional change in CDNC between the unperturbed and the perturbed simulations.

5.3 Results

5.3.1 *Widespread Impact on Cloud Drop Number Concentrations*

Figure 5.1 shows the temporal evolution of CDNC at low-level cloud altitude (i.e. ~970 m above sea-level or terrain) for the year following the onset of L-s and L-w. In the unperturbed pre-industrial atmosphere the model predicts global mean CDNC ranging from ~65 to ~91 cm^{-3} depending on the season (Fig. 5.1d, h), with a peak latitudinal mean of ~140 cm^{-3} between the equator and 30° S (Fig. 5.1a, e). In the first month of L-s, NH mean CDNC increases to ~110 cm^{-3} compared to ~66 cm^{-3} in the unperturbed simulation (Fig. 5.1d). For L-s, NH mean CDNC increases further to ~182 cm^{-3} during July and persists at around that level until November. Globally, elevated mean CDNC of ~125 cm^{-3} are maintained throughout the first seven months of L-s before steadily decreasing to unperturbed values. In the NH, the eruption commencing in June causes an increase in latitudinal

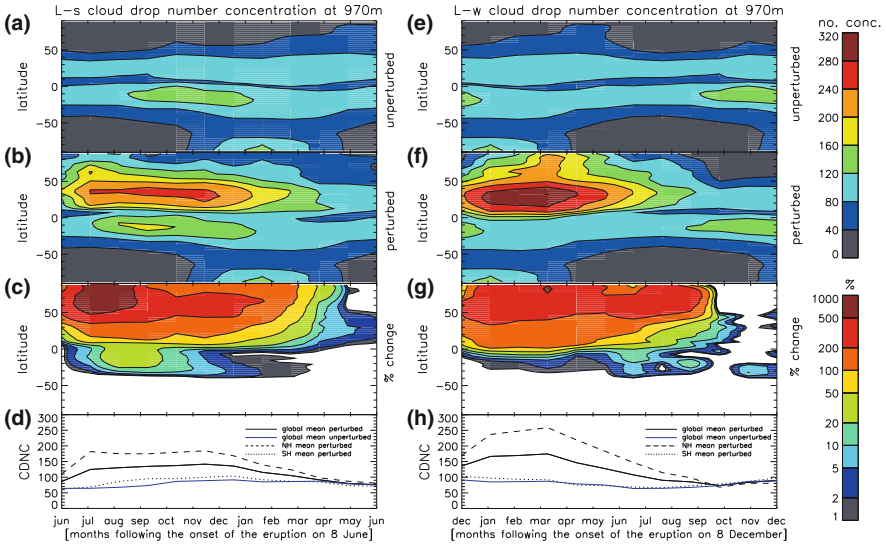

Fig. 5.1 Temporal evolution of latitudinal mean cloud drop number concentrations (CDNC) per cm^3 for L-s (commencing on 8 June) are shown on the *left-hand side* with (**a**) unperturbed simulation, (**b**) perturbed simulation, (**c**) relative changes. Latitudinal mean CDNC for L-w (commencing on 8 December) are shown on the *right-hand side* with (**e**) unperturbed simulation, (**f**) perturbed simulation, (**g**) relative changes. (**d**) and (**h**) show the temporal evolution of global perturbed and unperturbed mean (*solid black* and *blue lines*, respectively), NH perturbed mean (*dashed line*) and SH perturbed mean (*dotted line*) CDNC per cm^3 for L-s and L-w, respectively. In order to improve readability, hemispheric means for the unperturbed simulations are not shown because they closely resemble the global unperturbed mean

mean CDNC of at least 50 % lasting until April of the following year (Fig. 5.1c). The largest increase in latitudinal mean CDNC of up to a factor of 10 occurs at high-northern latitudes during July. For L-s, the model predicts an increase in CDNC of up to 37 % in southern tropical regions (corresponding to peak CDNC of $\sim$167 cm^{-3}) during September. The perturbation to CDNC in the SH peaks approximately two months after the onset of L-s and is not as long-lasting as it is in the NH. This comparatively rapid response of the SH aerosol to the NH source in GLOMAP-mode is consistent with previous studies of efficient transport of tracers along isentropic surfaces (Chen 1995) as discussed in Chap 4.

For L-w, latitudinal mean CDNC exhibit a maximum of $\sim$320 cm^{-3} during March; i.e. two months later than the peak increase simulated for L-s (relative to the onset of the respective eruption). For L-w, global mean CDNC in excess of $\sim$150 cm^{-3} are maintained until May (Fig. 5.1h) revealing that the impact of L-w on CDNC is larger than that of L-s. As for L-s, an increase in latitudinal mean CDNC of at least 50 % is maintained throughout the first ten months of L-w (Fig. 5.1g). In contrast to L-s, there is no significant impact on CDNC in the SH for L-w, which is consistent with Chen (1995) reporting a less efficient cross-equator transport during NH winter.

Figures 5.2 and 5.3 show the spatial distribution of July-August-September (JAS) and January-February-March (JFM) mean CDNC at low-level cloud altitude for the unperturbed and the perturbed simulations together with the absolute changes for L-s and L-w, respectively.

For L-s, changes in CDNC are widespread due to long-range transport of particles (see also Chap. 4) with mean perturbed concentrations reaching $\sim$247 and $\sim$237 cm^{-3} in regions as far from the eruption as Asia and North America (corresponding to absolute increases of $\sim$180 cm^{-3} in both regions). Perturbed NH JAS-mean CDNC reach $\sim$177 cm^{-3}; a factor of 2.7 increase when compared to unperturbed concentrations. The increases in JAS-mean CDNC are largest between 20 and 60° N with the peak change of $\sim$420 cm^{-3} simulated close to the source region at high-northern latitudes. For L-s, JAS-mean CDNC in tropical regions of the SH increase to $\sim$127 cm^{-3} (a factor of 1.2 larger than in the unperturbed simulation). Moreover, changes of up to $\sim$45 cm^{-3} are simulated along the western continental coasts of South America and South Africa, where marine stratocumulus decks are most persistent. In a few regions along the Intertropical Convergence Zone the model predicts CDNC changes of up to -13 cm^{-3} for L-s. These negative changes are the result of increased particle growth in the perturbed atmosphere resulting in larger-sized particles which are more efficiently removed.

For L-w, JFM-mean CDNC reach $\sim$248 cm^{-3} when averaged over the NH; that is a factor of 2.9 increase when compared to the respective unperturbed concentrations. For L-w, peak changes in JFM-mean CDNC of $\sim$380 cm^{-3} (which is a factor of 0.9 when compared to L-s) are simulated close to the source of the eruption. Overall, the impact on NH mean CDNC is a factor of 1.4 greater and latitudinally more confined (i.e. no significant impact on SH CDNC) during the first three months of an eruption that commences during NH winter when compared to an eruption that commences

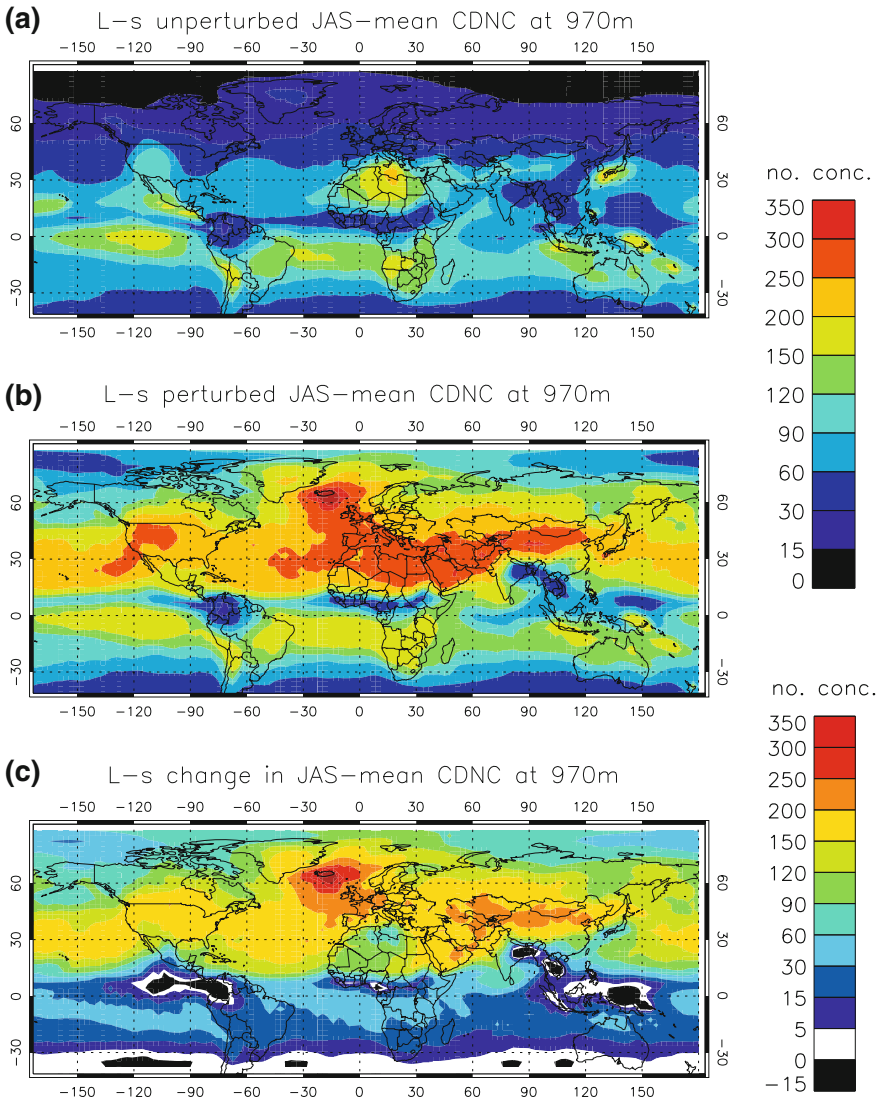

Fig. 5.2 July–August–September (JAS) mean cloud drop number concentrations (CDNC) per cm^3 for L-s at low-level cloud altitude (approx. 970 m above terrain) for (**a**) unperturbed simulation, (**b**) perturbed simulation, (**c**) difference perturbed minus unperturbed

during NH summer. However, as seen for L-s, the impact on CDNC is widespread concentrations reaching ∼309 and ∼264 cm^{-3} (corresponding to absolute increases of around ∼190 cm^{-3} in both regions) in Asia and North America, respectively.

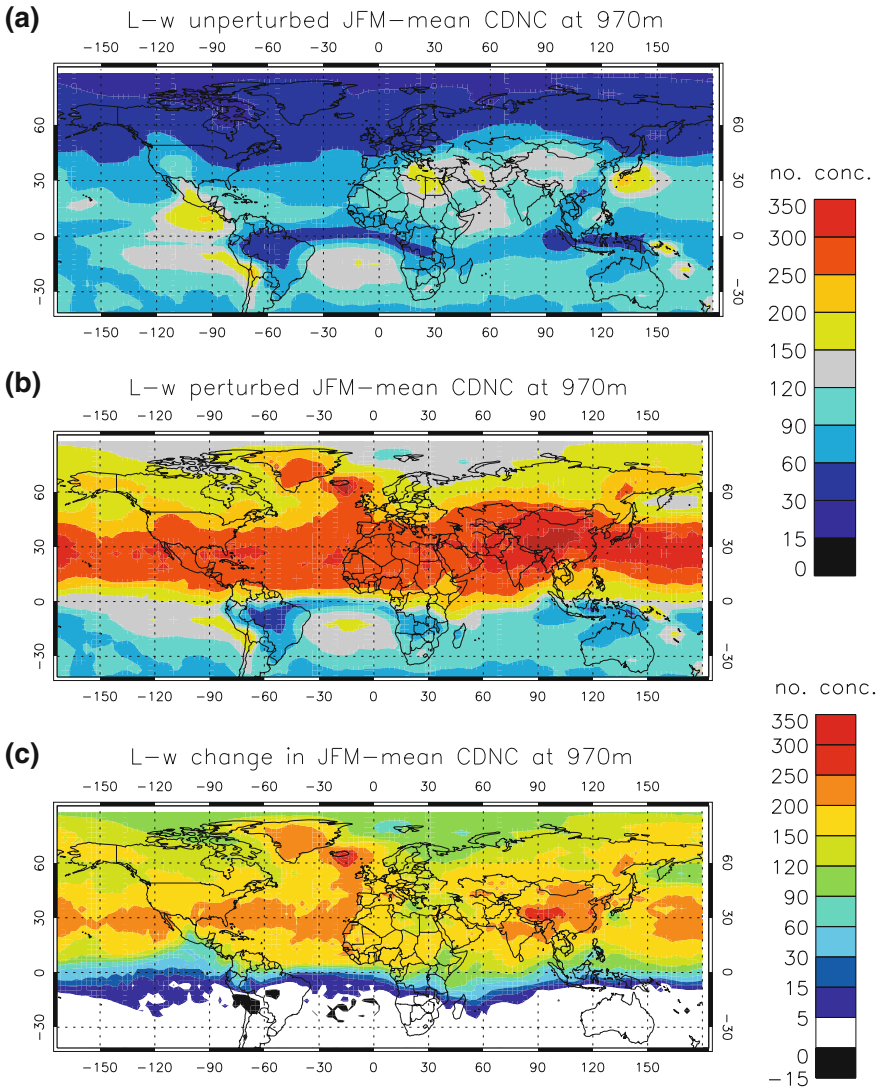

Fig. 5.3 January–February–March (JFM) mean cloud drop number concentrations (CDNC) per cm^3 for L-w at low-level cloud altitude (approx. 970 m above terrain) for (**a**) unperturbed simulation, (**b**) perturbed simulation, (**c**) difference perturbed minus unperturbed

5.3.2 Physically-Based Aerosol Activation Scheme Versus Empirically-Based Relationship

Here, a comparison of calculating changes in CDNC by means of a physically-based aerosol activation scheme and an empirically-based relationship (using the mass of

SO_4) is presented in order to provide insights in terms of the performance (i.e. with regards to similarities and differences) of these two approaches. Figure 5.4 shows the sensitivity of CDNC to SO_4 mass concentrations at low-level cloud altitude using the Nenes and Seinfeld (2003) aerosol activation scheme compared to a calculation using an empirical relationship of SO_4 mass and CDNC (Eq. 5.1) as suggested by Boucher and Lohmann (1995):

$$\log_{10}(\mathrm{CDNC}) = 0.410 \log_{10}(\mathrm{SO_4}) + 2.21 \tag{5.1}$$

where SO_4 is the mass of sulphate in $\mu g(SO_4)m^{-3}$. The CDNC sensitivity is subsequently calculated as follows:

$$\text{CDNC sensitivity} = \frac{\mathrm{CDNC_{perturbed}} - \mathrm{CDNC_{unperturbed}}}{\mathrm{SO_4\ mass_{perturbed}} - \mathrm{SO_4\ mass_{unperturbed}}} \tag{5.2}$$

Figure 5.4c shows the changes in the JAS-mean mass of SO_4 when comparing the perturbed to the unperturbed run for L-s. Changes in JAS-mean SO_4 mass concentrations are most significant in the NH with peak changes reaching $17.4\,\mu g(SO_4)m^{-3}$ close to the source region in Iceland. Averaged over the NH, changes in JAS-mean SO_4 mass concentrations of $2.2\,\mu g(SO_4)m^{-3}$ are simulated. GLOMAP simulates a change in JAS-mean SO_4 mass concentration of $0.06\ \mu g(SO_4)m^{-3}$ when averaged over the latitude band ranging from the equator to 30° S.

Figure 5.4a shows the sensitivity of CDNC to SO_4 mass concentrations for L-s using the mass-based empirical relationship by Boucher and Lohmann (1995). The sensitivity of CDNC using the physically-based aerosol activation scheme by Nenes and Seinfeld (2003) is shown in Fig. 5.4b, d shows the differences between the mass-based and the physically-based CDNC sensitivity. Tropical regions of the SH exhibit the most significant differences when comparing the CDNC sensitivity derived using the physically-based activation scheme to that derived using the mass-based relationship. In tropical regions of the SH the mass-derived CDNC sensitivity is on average ~260 CDN per μg of SO_4 lower when compared to the physically-based approach (Fig. 5.4d). Using a physically-based aerosol activation scheme reveals that CDNC is highly sensitive in regions where the change in the mass of SO_4 is small but particles with effective activation diameters become more numerous during the course of the eruption. Furthermore, over continental regions of the NH, the mass-based relationship exhibits a slightly higher CDNC sensitivity (factor of 1.1 when the sensitivity is averaged over continental regions in the latitude band from 90 to 30° N). The exceptions are Greenland and western Europe where the physically-based scheme predicts higher CDNC sensitivities of 185.1 and 44.6 CDN per μg of SO_4, respectively (factors of 1.2 and 1.04 higher when compared to mass-based relationship). Moreover, over marine regions such as the North Pacific, the physically-based scheme exhibits a factor of 1.5 higher CDNC sensitivity when compared to the mass-based relationship.

Figure 5.5 shows the JAS-mean perturbed and unperturbed number-size distributions at several locations in both hemispheres. For example, along the coast of South

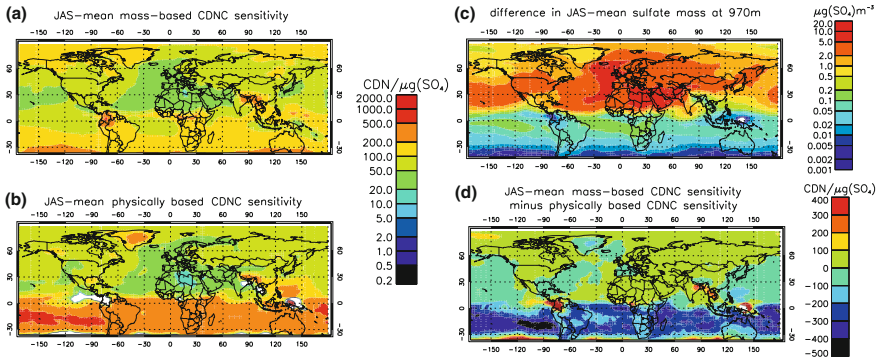

Fig. 5.4 Sensitivity of cloud drop number concentration (CDNC) to sulphate (SO_4) mass concentrations using an empirical relationship between CDNC and SO_4 mass, and using a physically-based aerosol activation scheme. All plots show June-July-August (JAS) averages for L-s with: (**a**) difference in SO_4 mass in microgram of SO_4 per m^3 at low-level cloud altitude following the onset of the eruption on 8 June; (**b**) mass-based CDNC to SO_4 mass sensitivity (see Eq. 5.2) using the empirical relationship from Boucher and Lohmann (1995); (**c**) CDNC to SO_4 mass sensitivity calculated using the physically-based aerosol activation scheme from Nenes and Seinfeld (2003); (**d**) difference (**a**) minus (**b**) highlighting that mass-based schemes are likely to underestimate changes in CDNC where the change in SO_4 mass is small

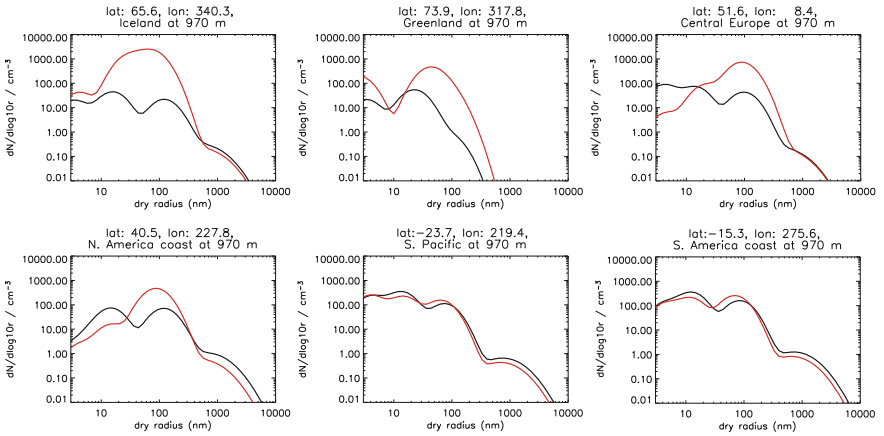

Fig. 5.5 Simulated July–August–September (JAS) mean number-size distribution for L-s at low-level cloud altitude (approx. 970 m above terrain) for several locations in both hemispheres with *black lines* showing the unperturbed number-size distributions and *red lines* showing the perturbed number-size distributions. d_r denotes dry radius with nucleation mode: $d_r < 5$ nm; Aitken mode: $5 < d_r < 50$ nm; accumulation mode: 50 nm $< d_r <$ 500 nm; coarse mode: $d_r > 500$ nm

America and in the South Pacific there are increases in the number of particles with dry radii between 30 and 100 nm. Even though the mass of SO_4 transported into the SH is relatively small, the number of particles in the formerly mentioned size range (i.e. above the activation diameter) increases to such an extent that particles become activated to form cloud drops.

5.3.3 First Aerosol Indirect Effect

To assess the impact of the simulated changes in CDNC for L-s and L-w on the radiative balance at the top of the atmosphere (combined longwave and shortwave) the first AIE for low-level clouds (i.e. at 970 m above terrain or sea-level) is calculated. Figure 5.6a shows the temporal evolution of the first AIE for the twelve months following the onset of L-s and L-w together with the temporal evolution of the global and the hemispheric first AIE means. For L-s, the first AIE is most significant in the latitude band 30–70° N with a latitudinal mean peak of $-9.6\,\mathrm{W\,m^{-2}}$ simulated during July. Averaged over the NH, the first AIE for L-s peaks at $-5.2\,\mathrm{W\,m^{-2}}$ during July with values declining steadily thereafter but remaining in excess of $-2\,\mathrm{W\,m^{-2}}$ until November, and in excess of $-0.5\,\mathrm{W\,m^{-2}}$ until March.

L-w exhibits a latitudinal mean peak of $-6.8\,\mathrm{W\,m^{-2}}$ simulated during June; i.e. seven months after the onset of L-w, which is in contrast to L-s where the peak in latitudinal mean first AIE occurs one month after the onset. It is worth noting that, for L-w, a secondary latitudinal mean maximum of $-6.5\,\mathrm{W\,m^{-2}}$ is simulated earlier during March and April between 20 and 30° N. Averaged over the NH, the first AIE for L-w peaks at $-3.8\,\mathrm{W\,m^{-2}}$ during April; that is 27 % lower when compared to the magnitude of the NH mean AIE peak for L-s. Figure 5.6b shows the spatial pattern of the JAS-mean first AIE due to changes in low-level clouds for L-s, and Fig. 5.6c shows the JFM-mean first AIE at low-level cloud altitude for L-w. For L-s, the strongest JAS-mean first AIE occurs over the North Atlantic and North Pacific oceans, with a peak radiative effect of $-29.4\,\mathrm{W\,m^{-2}}$ along the western continental margin of North America. This region features persistent marine stratocumulus decks which play a major role in modulating the Earth's radiation budget (e.g., Klein and Hartmann 1993). The other peak in JAS-mean first AIE of $-21.8\,\mathrm{W\,m^{-2}}$ occurs over the North Atlantic storm track region which also has extensive cloud cover. Furthermore, the L-s simulations reveal a substantial first AIE in regions far away from the eruption, reaching $-13.3\,\mathrm{W\,m^{-2}}$ in the western Pacific.

For L-w, a peak of $-14.2\,\mathrm{W\,m^{-2}}$ in JFM-mean first AIE is simulated along the western continental margin of North America; that is half the peak of the first AIE simulated for L-s. Averaged over the NH, a JFM-mean first AIE of $-3.1\,\mathrm{W\,m^{-2}}$ is simulated for L-w. Generally, for L-w the AIE is spatially more confined (i.e. to the latitude band ranging from the equator to 60° N) when compared to L-s.

Furthermore, in contrast to L-w, the L-s simulation also exhibits a substantial first AIE along the western continental margin of South America where the JAS-mean

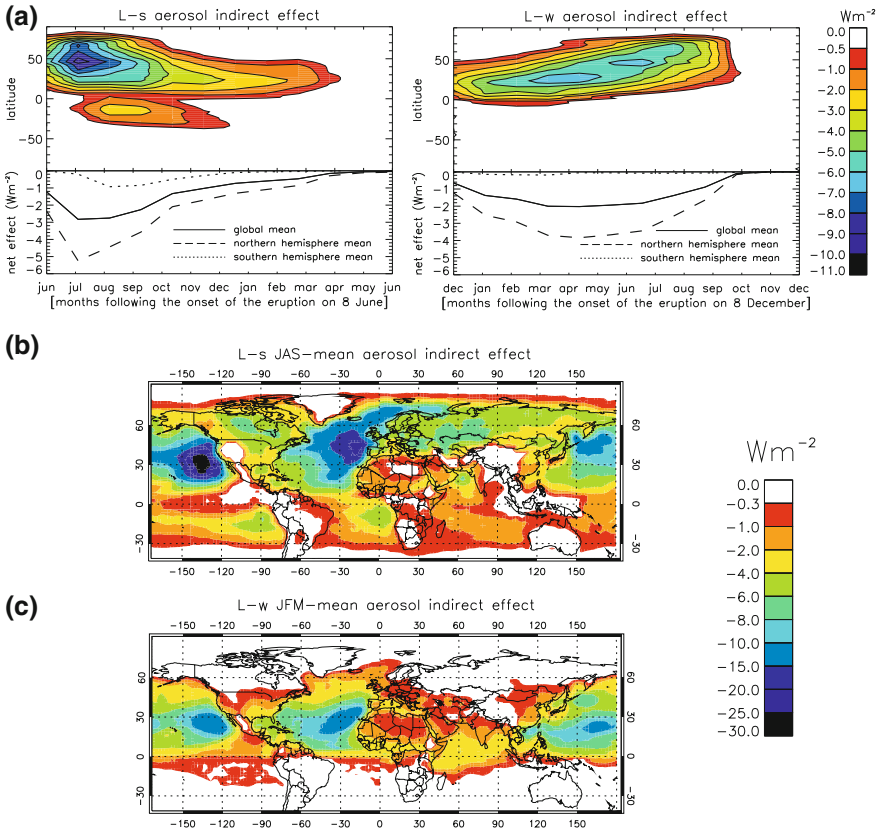

Fig. 5.6 (**a**) Temporal evolution of latitudinal mean first aerosol indirect effect (AIE) and mean first AIE (both in $\mathrm{W\,m^{-2}}$) for L-s (*left-hand side panel*) and L-w (*right-hand side panel*). (**b**) Spatial pattern of July–August–September (JAS) mean first AIE (in $\mathrm{W\,m^{-2}}$) for L-s calculated for low-level cloud (approx. 970 m above terrain or sea-level) changes, and (**c**) same as (**b**) but as January–February–March (JFM) mean for L-w

first AIE peaks at $-6.4\,\mathrm{W\,m^{-2}}$ (a factor of 4.6 lower than the peak observed for L-s along the western continental margin of North America). Marine stratocumulus decks along the western continental margin of West Africa are affected as well, with a JAS-mean first AIE averaged over the tropical SH of $-1.3\,\mathrm{W\,m^{-2}}$. For L-s, a peak in the latitudinal mean first AIE of $-2.6\,\mathrm{W\,m^{-2}}$ at $\sim$10° S during mid-August (Fig. 5.6a) is found; i.e. 1.5 months later than in the NH. Generally, the SH mean first AIE is of lower magnitude (peak of $-0.9\,\mathrm{W\,m^{-2}}$ during August) and not as long-lasting as the NH mean first AIE due to the dilution of aerosol during long-range transport.

5.4 Discussion

The study presented here tracks the microphysical evolution of the Laki SO_4 aerosol and finds that the magnitude of the first AIE is likely to have been comparable to that of the direct radiative effect calculated in previous studies (Highwood and Stevenson 2003; Oman et al. 2006a). The peak JAS-mean first AIE of $-29.4\,W\,m^{-2}$ calculated here for L-s is of similar magnitude as the peak direct effect of $-27\,W\,m^{-2}$ calculated by Oman et al. (2006a), and greater than the peak direct effect of $-17.5\,W\,m^{-2}$ calculated by Highwood and Stevenson (2003). The global mean first AIE calculated in this study for August is ~30 % lower than the global mean direct effect for August calculated by Oman et al. (2006a).

Highwood and Stevenson (2003) estimated a NH mean first AIE of -8 to $-14\,W\,m^{-2}$ for the first month of the eruption which is greater than the peak NH mean first AIE of $-5.2\,W\,m^{-2}$ calculated in this study (i.e. peak occurs during the second month for the L-s simulation). However, as suggested by Highwood and Stevenson (2003) the results presented here also show that there is a spatial difference between the peak direct and the peak indirect effects. The simulations presented here exhibit a substantial first AIE along regions that feature persistent stratocumulus cloud decks, thus it is important to comprehensively prognose or diagnose stratocumulus cloud fields in order to fully assess the spatial pattern of the first AIE.

Previous modelling studies assessing the radiative effects following Laki (Highwood and Stevenson 2003; Oman et al. 2006a) explain most of the observed surface temperature cooling following the eruption by means of the direct effect. The first AIE calculated here is large enough to have a potentially significant impact on surface temperatures. The combined magnitude of the peak global mean direct effect ($-4.0\,W\,m^{-2}$ calculated by Oman et al. 2006a) and the respective first AIE ($-2.8\,W\,m^{-2}$ calculated in this study for L-s) could be as large as $-6.8\,W\,m^{-2}$. Thus, the results presented have implications for modelling studies calculating the radiative effects and verifying the magnitude of the forcing with the observational record of the surface temperature cooling following the eruption. Generally, the calculation of the surface temperature response to historical aerosol and cloud perturbations is very uncertain. Firstly, there are inter-model differences in the volcanic aerosol loadings and distributions themselves (see Chap. 4). Furthermore, there are large uncertainties in the dynamic response of precipitating and non-precipitating clouds (not accounted for here) (Stevens and Feingold 2009) as well as in the response of regional surface temperatures to transient radiative effects which depend on surface moisture, among other factors. With these uncertainties it is not possible to use historical records of surface temperature cooling to verify calculations of the magnitude of the direct and indirect effects. Moreover, the background state of the climate system in 1783 AD could have played an important role. For example, the occurrence of an El Niño event during 1782–1783 AD (Ortlieb and Macharé 1993) could have dampened the surface cooling induced by the Laki SO_4 aerosol.

The simulations presented here also suggest that a long-lasting, high-northern latitude eruption such as Laki had the potential to induce widespread, interhemispheric changes in both CDNC and the first AIE if the eruption commences during NH summer. Previous studies suggested that the impact of high-northern latitude eruptions is mostly confined to the NH (Robock 2000; Oman et al. 2006a). The change in SH CDNC simulated here highlights the importance of simulating aerosol number and size as well as aerosol mass. Chapter 4 highlighted that an eruption commencing during NH summer can cause an increase in the number concentration of aerosol particles in regions south of the equator at sizes that are large enough (i.e. CCN size) to become activated as cloud droplets. Thus, according to our simulations a small change in SO_4 mass can have a relatively large impact on CCN, and hence on CDNC. The only other Laki study reporting a transport of SO_4 aerosol south of the equator is that of Stevenson et al. (2003b); however these authors did not elaborate on their results as the mass of SO_4 is presumably too small to induce a significant direct radiative effect (as shown in Highwood and Stevenson 2003). The chapter presented here also compared the sensitivity of CDNC to SO_4 mass using the Nenes and Seinfeld (2003) aerosol activation scheme to that using the empirical relationship by Boucher and Lohmann (1995) and it should be noted that the growth of new aerosol to CCN sizes due to direct growth and coagulation is a feature that mass-only aerosol schemes cannot capture. Thus, the results presented here suggest that GCMs using mass-based schemes will underestimate the change in CDNC and first AIE in regions remote from the eruption.

The simulations conducted here also highlight that the season in which a long-lasting flood lava eruption commences plays a critical role in determining the magnitude of the climate impact. The results show that a wintertime eruption is latitudinally more confined and thus has a slightly greater impact on CDNC than an equivalent summertime eruption. However, the peak first AIE occurring during a summertime eruption is a factor of two greater than that occurring during a wintertime eruption, which can be attributed to seasonal variations in insolation as well as to seasonal differences in the abundance of low-level stratocumulus clouds. Klein and Hartmann (1993) have shown that stratocumulus clouds along the western coast of California are most abundant during June. Moreover, Chap. 4 highlighted how seasonal differences in chemical and microphysical processes affect the magnitude of the volcanic SO_4 aerosol yield (i.e. a wintertime Laki-style eruption would produce about 20 % less SO_4 due to less effective photochemistry). Kravitz and Robock (2011) examined the role of the season a high-latitude eruption injecting 5 Tg of SO_2 into the upper troposphere/lower stratosphere commences, and found that an eruption commencing in June has the largest climatic impact when compared to one commencing in any other month of the year. In accordance with the study presented here, Kravitz and Robock (2011) also found that the volcanic aerosol formed during a June eruption is latitudinally more dispersed (i.e. reaching the tropics and subtropics) when compared to a wintertime eruption.

5.5 Conclusions

Overall, the model simulations using GLOMAP-mode suggest a substantial impact of the Laki eruption on cloud properties, in agreement with previous observational studies (e.g., Thordarson and Self 2003). The simulations suggest that the first AIE receded only after nine months of greatly elevated cloud drop concentrations if the eruption starts during northern hemisphere summer. Considering that the climatic impact will outlast the indirect effect, these results agree with previous numerical assessments suggesting that the climate response from the direct effect resulted in cooler surface temperatures for up to two years following the onset of the eruption (Highwood and Stevenson 2003; Oman et al. 2006a). Moreover, the work presented here highlights that the season in which a Laki-style eruption commences plays an important role with regard to the magnitude of the indirect effect and temporal occurrence of the peak effects. Moreover, the results presented here imply a less profound impact of the aerosol on cloud forcing if the eruption had commenced during NH winter. Thus, model simulations of large volcanic eruptions need to take into account that variabilities regarding the magnitude of the climate impact will arise depending on the season an eruption commences.

Studies of modern-day clouds and cloud systems suggest that very large changes in CDNC are likely to have caused substantial changes in precipitation and cloud dynamics (Levin and Cotton 2008). The substantial first aerosol indirect effect observed along stratocumulus cloud regions may have implications for the ocean heat-budget causing yet unknown atmosphere-ocean feedbacks far away from the source of the eruption. The presented study highlights the complexity of the impact high-latitude eruptions may exert on the atmosphere and subsequently the climate system.

Future work should aim to address the discrepancy between the observational records of surface temperature changes and the combined magnitude of the modelled transient direct and indirect effects. The results presented in this chapter suggest that either the observational records are incomplete or that numerical models overestimate the radiative effects induced by the eruption. Alternatively, Highwood and Stevenson (2003) highlighted that using a different Laki SO_2 profile with a lower injection height produces a less profound direct effect. It is worth noting that Timmreck et al. (2010) simulated a large Toba-style eruption using a dedicated microphysics scheme in an Earth System Model and found the climate impact of such an eruption to be a factor of three smaller when compared to previous GCM studies (Jones et al. 2005; Robock et al. 2009), which prescribed the aerosol size distribution. Thus, previous estimates of the direct effect due to Laki (using the best estimate of the Laki volatile release budget) might be too high. Furthermore, future work should also account for the potential ocean-atmosphere feedbacks resulting from the substantial indirect effect along stratocumulus cloud regions. The latter can be achieved by using fully coupled chemistry-aerosol-climate models such as the UK community atmospheric chemistry-aerosol (UKCA) global model, which allow

for aerosol size-resolved simulations and feedbacks between this aerosol distribution and, for example, atmospheric dynamics.

References

Boucher O, Lohmann U (1995) The sulfate-CCN-cloud albedo effect, a sensitivity study with two general circulation models. Tellus Ser B 47:281–300

Chen P (1995) Isentropic cross-tropopause mass exchange in the extratropics. J Geophys Res 100:16661–16673

Chenet AL, Fluteau F, Courtillot V (2005) Modelling massive sulphate aerosol pollution, following the large 1783 Laki basaltic eruption. Earth Planet Sci Lett 236:721–731

Edwards JM, Slingo A (1996) Studies with a flexible new radiation code. I: choosing a configuration for a large-scale model. Q J R Meteorol Soc 122:689–719

Forster P, Ramaswamy V, Artaxo P, Berntsen T, Betts R, Fahey D, Haywood J, Lean J, Lowe D, Myhre G, Nganga J, Prinn R, Raga G, Schulz M, Van Dorland R (2007) Changes in atmospheric constituents and in radiative forcing. In: Solomon S, Qin D, Chen Z, Manning M, Marquis M, Averyt KB, Tignor M, Miller H (eds) Climate change 2007: the physical science basis. Contribution of working group I to the fourth assessment report of the intergovernmental panel on climate change, Cambridge University Press, Cambridge, pp 129–234

Highwood EJ, Stevenson DS (2003) Atmospheric impact of the 1783–1784 Laki eruption: part II–climatic effect of sulphate aerosol. Atmos Chem Phys 3:1177–1189

Jones GS, Gregory JM, Stott PA, Tett SFB, Thorpe RB (2005) An AOGCM simulation of the climate response to a volcanic super-eruption. Clim Dyn 25:725–738

Klein SA, Hartmann DL (1993) The seasonal cycle of low stratiform clouds. J Clim 6:1587–1606

Kravitz B, Robock A (2011) Climate effects of high-latitude volcanic eruptions: role of the time of year. J Geophys Res 116:D01105

Levin Z, Cotton WR (eds) (2008) Aerosol pollution impact on precipitation: a scientific review. Springer, Berlin, p 386

Nenes A and Seinfeld JH (2003) Parameterization of cloud droplet formation in global climate models. J Geophys Res 108(D14):4415. doi:10.1029/2002JD002911

Oman L, Robock A, Stenchikov GL, Thordarson T, Koch D, Shindell DT, Gao C (2006a) Modeling the distribution of the volcanic aerosol cloud from the 1783–1784 Laki eruption. J Geophys Res 111:D12209. doi:10.1029/2005JD006899

Oman L, Robock A, Stenchikov GL, Thordarson T (2006b) High-latitude eruptions cast shadow over the African monsoon and the flow of the Nile. Geophys Res Lett 33:L18711. doi:10.1029/2006GL027665

Ortlieb L, Macharé J (1993) Former El Niño events: records from western South America. Global Planet Change 7:181–202

Penner JE, Andrea M, Annegarn H, Barrie L, Feichter J, Hegg D, Jayaraman A, Leaitch R, Murphy D, Nganga J, Pitari G et al (2001) The scientific basis. Contribution of working group I to the third assessment report of the intergovernmental panel on climate change. In: Houghton JT, Ding Y et al (eds) Climate change 2001. Cambridge University Press, Cambridge

Pringle KJ, Carslaw KS, Spracklen DV, Mann GM, Chipperfield MP (2009) The relationship between aerosol and cloud drop number concentrations in a global aerosol microphysics model. Atmos Chem Phys 9:4131–4144

Robock A (2000) Volcanic eruptions and climate. Rev Geophys 38:191–219

Robock A, Ammann CM, Oman L, Shindell D, Levis S, Stenchikov G (2009) Did the Toba volcanic eruption of ~74 ka B.P. produce widespread glaciation? J Geophys Res 114:D10107

Rossow WB, Schiffer RA (1999) Advances in understanding clouds from ISCCP. Bull Am Meteorol Soc 80:2261–2287

Stevens B, Feingold G (2009) Untangling aerosol effects on clouds and precipitation in a buffered system. Nature 461:607–613

Stevenson DS, Johnson CE, Highwood EJ, Gauci V, Collins WJ, Derwent RG (2003b) Atmospheric impact of the 1783–1784 Laki eruption: part I chemistry modelling. Atmos Chem Phys 3:487–507

Thordarson T and Self S (2003) Atmospheric and environmental effects of the 1783–1784 Laki eruption: a review and reassessment. J Geophys Res Atmospheres 108(D1):4011. doi:10.1029/2001JD002042

Timmreck C, Graf HF, Lorenz SJ, Niemeier U, Zanchettin D, Matei D, Jungclaus JH, Crowley TJ (2010) Aerosol size confines climate response to volcanic super-eruptions. Geophys Res Lett 37:L24705

Chapter 6
What if a Laki-Style Eruption were to Happen Tomorrow?

6.1 Introduction

Historical records show that the 1783–1784 AD Laki eruption caused severe environmental stress and posed a health hazard far beyond the borders of Iceland (e.g., Thordarson and Self 2003; Grattan et al. 2003; Witham and Oppenheimer 2005 and references therein). Given the reasonable likelihood of a recurrence of such a 'low-probability, high-impact' event it is important to assess the scale on which a future eruption could impact society.

Around 25 years ago, epidemiological studies revealed a statistical link between particulate matter (PM) air pollution and premature mortality (e.g., Ostro 1984). Subsequent research has confirmed a strong link between mortality and both acute and chronic exposure to PM (see reviews by Pope et al. 2006; Brook et al. 2010).

The awareness that exposure to air pollution could be associated with negative health effects led to the introduction of standards for improving air quality in Europe and other parts of the world. However, policies to improve air quality cannot account for unpredictable natural air pollution events such as volcanic eruptions. It is well known that volcanic eruptions can increase concentrations of for example SO_2 and H_2S which in turn can have a negative impact on health (e.g., Baxter 2000; Delmelle et al. 2002; Hansell and Oppenheimer 2004). Despite a range of pollutant measurements at several active volcanoes around the world, attempts to quantify the disease burden associated with exposure to volcanic air pollution are limited (Hansell and Oppenheimer 2004). However, historical records of some volcanic eruptions and their aftermaths clearly suggest a link between volcanic air pollution and severe negative health effects (e.g., Grattan et al. 2003; Witham and Oppenheimer 2005).

In summer 1783 AD, many countries in the NH witnessed an atmospheric phenomenon often referred to as the "great dry fog" or "haze" caused by a widespread sulphuric acid cloud linked to volcanic activity in Iceland (Thordarson and Self 2003 and references therein). Several historical reports from across Europe during the summer of 1783 clearly indicate an increase in air pollution, such as visibility

A. Schmidt, *Modelling Tropospheric Volcanic Aerosol*, Springer Theses,
DOI: 10.1007/978-3-642-34839-6_6, © Springer-Verlag Berlin Heidelberg 2013

reductions and the smell of sulphur/hydrogen sulphide. In Iceland around 21 % of the human population and 75 % of the livestock perished (Thordarson and Self 2003) and parish mortality records suggest that mortality in England in the summer of 1783 was 10–20 % (Grattan et al. 2003) above the 51-year moving mean (Wrigley and Schofield 1989). Historical accounts of increased mortality rates and/or respiratory disorders have also been found in France, The Netherlands, Italy and Sweden (Durand and Grattan 1999, 2001; Grattan et al. 2003; Grattan 2005; Witham and Oppenheimer 2005). Moreover, there are reports that the acidic air pollution during the Laki eruption posed a serious threat to remote ecosystems and vegetation such as crops and trees (Grattan and Pyatt 1994; Grattan 1998; Thordarson and Self 2003).

Large Icelandic flood lava events are not isolated occurrences. The distribution and frequency of volcanic events such as Laki suggests that four flood lava events have occurred in Iceland over the past 1150 years (Thordarson and Larsen 2007). Based on current knowledge (Thordarson and Larsen 2007), the probability of the recurrence of a Laki-style event is one event every 200–500 years with the size of such an eruption potentially ranging from one-quarter to twice the size of Laki. Thus, there is a likelihood that a Laki-style eruption may recur in the near future. A present-day Laki eruption would provide a very large source of gaseous SO_2 and acidic aerosol in close proximity to Europe, and thus has the potential to affect a very densely populated area.

Current evidence indicates that both short-term and long-term exposure to particulates with diameters smaller than 2.5 μm (PM2.5) is associated with all-cause and cardiopulmonary mortality (Brook et al. 2010). Several studies found strong associations between sulphate air pollution and premature mortality (Pope et al. 2002, 2006). Volcanic ash was only a minor constituent of the emissions (i.e. ~0.4 km^3 or 2.6 % of the total erupted volume) (Thordarson and Self 1993), thus the scope of this chapter is to assess the potential health effects arising from an increase in particulate matter air pollution due to the sulphate aerosol formed during such an event. Given the dominance of SO_2 released during the Laki eruption and the fact that the composition of the background particles is representative of present-day air pollution, it is regarded reasonable to apply the epidemiological evidence to the scenario presented here. Generally, following the onset of the eruption, the PM2.5 mass will exhibit a higher contribution from SO_4 when compared to the volcanically unperturbed situation.

This chapter assesses the impact of the SO_4 aerosol formed (due to the release of 122 Tg of volcanic SO_2) during a future Laki-style eruption on European air quality. Subsequently, potential negative health effects are quantified using concentration-response (C-R) functions from the epidemiological literature. Research investigating volcanic eruptions has often focused on the climatic and environmental impacts in general (which is especially true for Laki modelling studies). In contrast, the study presented here bridges the gap between volcanology, atmospheric science and epidemiology by quantifying the excess mortality from exposure to volcanic PM pollution that would arise in Europe if a Laki-style eruption occurred under present-day conditions.

6.2 Data and Methods

The course of the eruption was simulated as reconstructed for 1783–1784 AD but under present-day atmospheric conditions using the data set of Thordarson and Self (1993, 2003) and Thordarson et al. (1996) to define the magnitude, altitude and timing of the release of the volcanic SO_2 into the atmosphere. To drive the model, meteorological fields from the year 2003 were used because that summer was characterised by meteorological features similar to the summer of 1783—an unusually hot July in western Europe and the presence of persistent anticyclones over central Europe (Thordarson and Self (2003) and references therein).

Using GLOMAP-mode, PM2.5 mass concentrations over Europe were calculated for two scenarios: a baseline run using natural aerosol emissions and anthropogenic emissions, and a volcanically perturbed run which includes the Laki emissions. Both simulations were run for one year following the onset of the eruption on the 8th of June. Mann et al. (2010) evaluated GLOMAP-mode against a wide range of aerosol measurements around the world. To supplement this evaluation with a data set most relevant to human health, Fig. 6.1 provides a comparison of modelled PM2.5 data against 399 multi-annual measurements (for the years 2000–2006) at European ground stations (AirBase 2010). Here, a Pearson's correlation coefficient of 0.7 and a normalized mean bias of −0.14 (i.e. the model is 14 % biased low on average) is obtained giving confidence in the model's ability to simulate PM2.5 mass concentrations.

To quantify the negative health effects associated with a long-lasting Laki-style air pollution event C-R functions appropriate for PM2.5 were used (Pope et al. 2002; Ostro 2004). Generally, C-R functions are derived from epidemiological studies and link changes in pollutant concentrations to changes in health risk. The predicted number of deaths (i.e. excess mortality) depends on:

(a) the change in PM2.5 concentrations from a baseline;
(b) the population exposed;
(c) the excess risks from exposure (i.e. percent increase in mortality per $\mu g/m^3$ of PM2.5);
(d) the baseline mortality rates.

Data on the total exposed population (Fig. 6.2) were obtained from the HYDE 3.1 database (Klein Goldewijk et al. 2010) for the year 2004. The population data are provided on a $0.083° \times 0.083°$ grid and were subsequently re-gridded to GLOMAP-mode's model resolution ($2.8° \times 2.8°$). Baseline incidence rates for all-cause mortality and cardiopulmonary mortality in Europe were obtained for the year 2004 (see also Table 6.2 in Sect. 6.3.2) from the World Health Organization (WHO) (Mathers et al. 2008).

In this study, excess mortality resulting from both short-term and long-term exposure was calculated. These outcomes should not be added together since the effects of the long-term exposures should include most of those from the short-term as well (Ostro

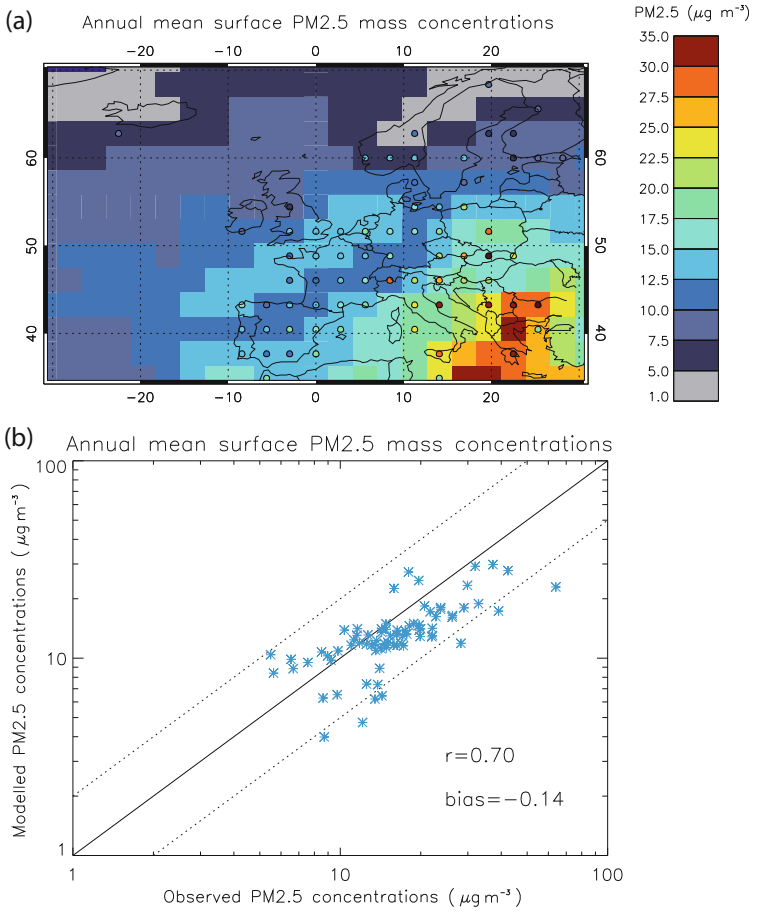

Fig. 6.1 Comparison of modelled annual mean surface PM2.5 mass concentrations against multi-annual measurements (for the years 2000–2006) at European ground stations (AirBase 2010) (*over-plotted circles* represent the mean of measurements in each grid box) in **(a)**, and Pearson's correlation coefficient and normalised mean bias stated in **(b)**. Figure after Schmidt et al. (2011)

2004). However, these alternatives represent two different methods of capturing the potential effects resulting from the exposure to volcanic air pollution.

To calculate cardiopulmonary excess mortality due to long-term exposure to PM2.5, the results of the American Cancer Society cohort study reported by Pope et al. (2002) have been applied to the modelled European 12-month mean PM2.5 data set. However, the Pope et al. (2002) study used a linear exposure function, which may not be appropriate for the very high concentrations that would occur after the eruption. Consequently, an adjusted function which assumes that mortality depends on the logarithm of exposure (Ostro 2004) was used here. Thus the C-R function flattens out at the higher concentrations. The relative risk (RR) is calculated as follows:

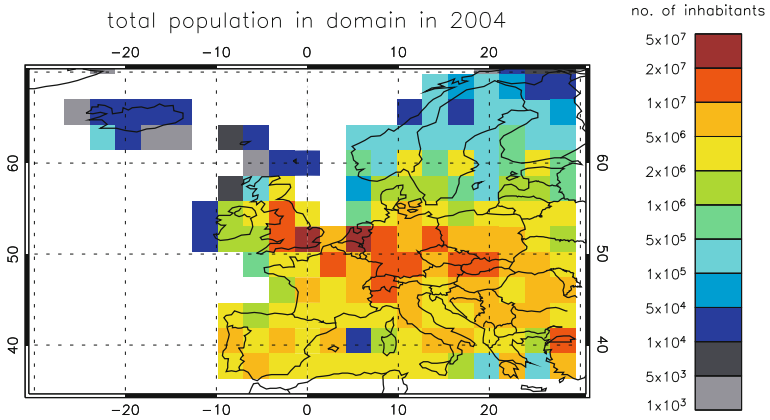

Fig. 6.2 Number of inhabitants in each grid box of the model's European domain for the year 2004. Population data were derived using the HYDE 3.1 database (Klein Goldewijk et al. 2010). Figure after Schmidt et al. (2011)

$$\mathrm{RR} = \frac{e^{[\alpha+\beta \ln(X_{\mathrm{Py}}+1)]}}{e^{[\alpha+\beta \ln(X_{\mathrm{Cy}}+1)]}} = \left[\frac{(X_{\mathrm{Py}}+1)}{(X_{\mathrm{Cy}}+1)}\right]^{\beta} \tag{6.1}$$

where X_{Cy} is the annual mean PM2.5 mass concentration ($\mu g/m^3$) in the baseline run; X_{Py} is the PM2.5 mass concentration ($\mu g/m^3$) in the volcanically perturbed run; and β is an estimated parameter for cardiopulmonary mortality: 0.1551 (95 % confidence interval (CI) = 0.05624, 0.2541); and α denotes a constant in the regression equation. The attributable fraction (AF) is calculated as follows:

$$\mathrm{AF} = \frac{(\mathrm{RR}-1)}{\mathrm{RR}} \tag{6.2}$$

and the total mortality effect due to long-term exposure to PM2.5 (E_{long}) (given as excess mortality per year) is given by:

$$E_{long} = \mathrm{AF} \times B_y \times P_{>30} \tag{6.3}$$

which simplifies to:

$$E_{long} = \left[1 - \left(\frac{(X_{\mathrm{Cy}}+1)}{(X_{\mathrm{Py}}+1)}\right)^{\beta}\right] \times B_y \times P_{>30} \tag{6.4}$$

where B_y is the baseline incidence rate (deaths/person/year) for the health effect under study (see also Table 6.2); and $P_{>30}$ represents the exposed population; i.e. persons that are older than 30 years.

Although PM2.5 concentrations vary substantially during the twelve months following the onset of the eruption, this is also the case with background air pollution on which the epidemiological evidence is based, thus justifying C-R functions that examine the impacts of long-term exposures. In addition, Puett et al. (2008) demonstrated that significant effects of cumulative exposure will be experienced during the first year of exposure. Thus, there is evidence for a very short latency period after the exposure.

To calculate excess all-cause mortality due to short-term exposure to PM2.5, the method of Ostro (2004) was applied using the modelled daily-mean PM2.5 data between 8 June 2003 and 28 February 2004. Here it is assumed that over the period of the eruption, there is a continuing pool of susceptible individuals, most likely individuals with pre-existing cardiovascular or respiratory disease. Wong et al. (2008) have shown that the C-R function for short-term exposure is basically linear without a threshold even if the PM mass concentrations are very high, as for example observed in cities in Asia. Thus it is reasonable to apply such a linear relationship in the study presented here. For calculating all-cause mortality due to short-term exposure (i.e. days to weeks) to PM2.5, the RR is calculated as follows:

$$\mathrm{RR} = \exp[\gamma(\mathrm{X_{Pd}} - \mathrm{X_{Cd}})] \tag{6.5}$$

where X_{Cd} and X_{Pd} denote the daily mean PM2.5 mass concentrations ($\mu g/m^3$) in the baseline and perturbed run, respectively; γ is an estimated parameter for all-cause mortality: 0.00096 (95 % CI = 0.00079, 0.00113) ($m^3/\mu g$) (see also Table 6.1 for percentage increase in mortality per 10 $\mu g/m^3$). By utilising the results of four recent time-series studies (i.e. performing a meta-analysis) which link acute exposure to PM2.5 with all-cause mortality (Klemm and Mason 2003; Ostro et al. 2006; Franklin et al. 2007; Zanobetti and Schwartz 2009) (see also Table 6.1), a mean effect was obtained by calculating the inverse-variance mean (see also Appendix A). In the study presented here a 10 $\mu g/m^3$ change in PM2.5 mass concentrations is associated with a 0.96 % increase in daily all-cause mortality.

Table 6.1 Excess risks (ER) from the four studies considered, and the inverse-variance weighted mean excess risk ($\overline{ER}$)

Study	ER	ER low	ER high
Klemm and Mason (2003)	1.2	0.8	1.6
Ostro et al. (2006)	0.6	0.2	1.0
Franklin et al. (2007)	1.2	0.3	2.1
Zanobetti and Schwartz (2009)	0.98	0.75	1.22
Meta estimate ($\overline{ER}$)	**0.96**	**0.79**	**1.13**

The lower and upper 95 % confidence intervals are given as percent increase in mortality per 10 $\mu g/m^3$ of PM2.5. Note that in order to obtain γ one divides the weighted mean excess risk by 1000 in order to move from percent change per 10 $\mu g/m^3$ to excess risk per 1 $\mu g/m^3$. Table after Schmidt et al. (2011)

The AF is calculated according to Eq. 6.2 and the total mortality effect due to short-term exposure to PM2.5 (E_{short}) (given as excess mortality per day) is given by:

$$E_{short} = AF \times B_d \times P_{tot} \tag{6.6}$$

where B_d is the baseline incidence rate (deaths/person/day) for the health effect under study. Equation 6.6 simplifies to:

$$E_{short} = \left[1 - \frac{1}{\exp[\gamma(X_{Pd} - X_{Cd})]}\right] \times B_d \times P_{tot} \tag{6.7}$$

where P_{tot} represents the exposed population; that is all-ages.

6.3 Results

6.3.1 Impact on European Air Quality

In the baseline run, GLOMAP simulates 12-month mean surface PM2.5 mass concentrations of about 12 $\mu g/m^3$ with peak concentrations reaching around 32 $\mu g/m^3$ over polluted regions in southern Europe (Fig. 6.3a). In the UK and Germany, background PM2.5 concentrations of around 13 and 14 $\mu g/m^3$ are simulated, respectively. These modelled PM2.5 concentrations agree well with multi-year observations across Europe (see also Fig. 6.1). Averaged over the first three months of the eruption, changes in European-mean PM2.5 concentrations equate to around 23 $\mu g/m^3$ (Fig. 6.3b) which is equivalent to a 120 % rise. The impact of the eruption on PM2.5 concentrations varies across Europe, ranging from a 320 % rise over northern Europe to a 60 % rise over southern Europe. Due to the eruption, European-mean PM2.5 concentrations changes equate to 8 $\mu g/m^3$ when averaged over twelve months with a peak change of 66 $\mu g/m^3$ close to the source region in Iceland (Fig. 6.3c).

Daily PM2.5 concentrations are temporally highly variable in the months after the onset of the eruption (Fig. 6.4). In the baseline run, European-mean PM2.5 concentrations vary between 4.4 and 25.5 $\mu g/m^3$, with highest concentrations occurring during the summer months. In the volcanically perturbed run European-mean PM2.5 concentrations exceed 30 $\mu g/m^3$ throughout the summer with a peak European-mean value of 62.1 $\mu g/m^3$ in mid-July which coincides with the end of the most vigorous stages of the eruption. The 95th percentile of the 24-hour mean PM2.5 concentration exceeds 160 $\mu g/m^3$ on three occasions, each several days after major eruption episodes (blue diamonds in Fig. 6.4). Note that the magnitude and the temporal pattern of the 95th percentiles for the volcanically perturbed PM2.5 concentrations closely mimic the changes in the haze opacity reconstructed for the summer of 1783 (Thordarson and Self 2003). By the end of October the European-mean PM2.5

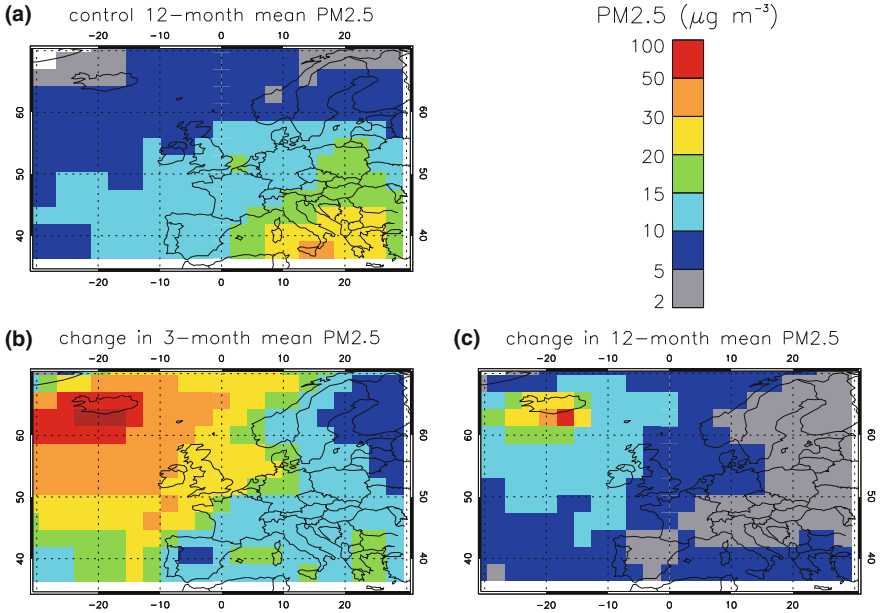

Fig. 6.3 Modelled PM2.5 mass concentrations at the surface. 12-month mean PM2.5 mass concentrations $\mu g/m^3$ for **(a)** baseline run without Laki emissions and for **(b)** absolute change between baseline run and perturbed run (the latter includes Laki emissions with the 3-month mean calculated for first three months following the onset of a Laki-style eruption on 8 June). **(c)** Shows the absolute change in 12-month mean PM2.5 concentrations (calculated for one year following the onset of the eruption)

concentrations steadily revert to background concentrations reflecting the reposing stages of the eruption.

The model data set allows estimation of the number of days (out of the 266 considered) that exceed the current WHO 24-hour mean PM2.5 guideline of 25 $\mu g/m^3$ (Fig. 6.5). Over land areas of Europe, the mean number of exceedances increases by 36 days (range 13–55 days) compared to a background mean of 38 days (i.e., corresponding to a 95 % rise due to the eruption). The highest number of exceedance days is simulated for Iceland (175 days, absolute difference 172 days).

6.3.2 Excess Mortality in Europe

Using 2004 population data together with long-term exposure to PM2.5, around 139,000 (95 % CI 51,200–224,1200) cardiopulmonary deaths are obtained from long-term exposure to PM2.5 in the year following the onset of the eruption (Table 6.2 and Fig. 6.6). Mortality densities vary spatially depending on the co-location of PM2.5 and the exposed population. The highest excess cardiopulmonary fatalities (Fig. 6.6)

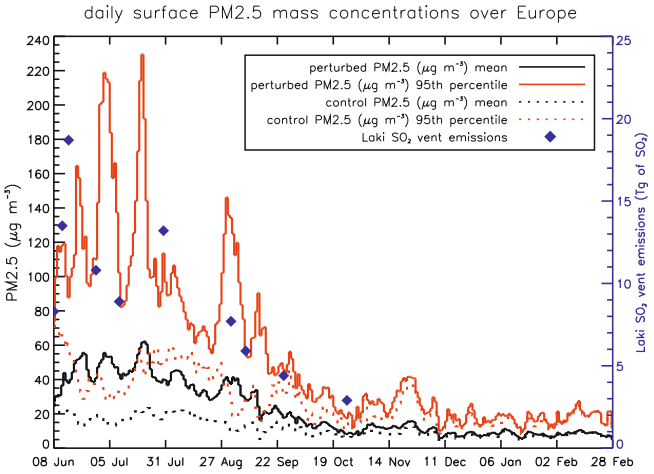

Fig. 6.4 Time-series of surface PM2.5 mass concentrations averaged over the European domain starting on 8 June 2003 and ending 28 February 2004 for both, the baseline run (*dotted black line*) and the perturbed run (*solid black line*) including the 95th percentiles for both baseline run (*dotted red line*) and perturbed run (*solid red line*). The temporal resolution and magnitude of the SO_2 emissions during the ten Laki eruption episodes are depicted by *blue diamonds* and the y-axis on the right-hand side

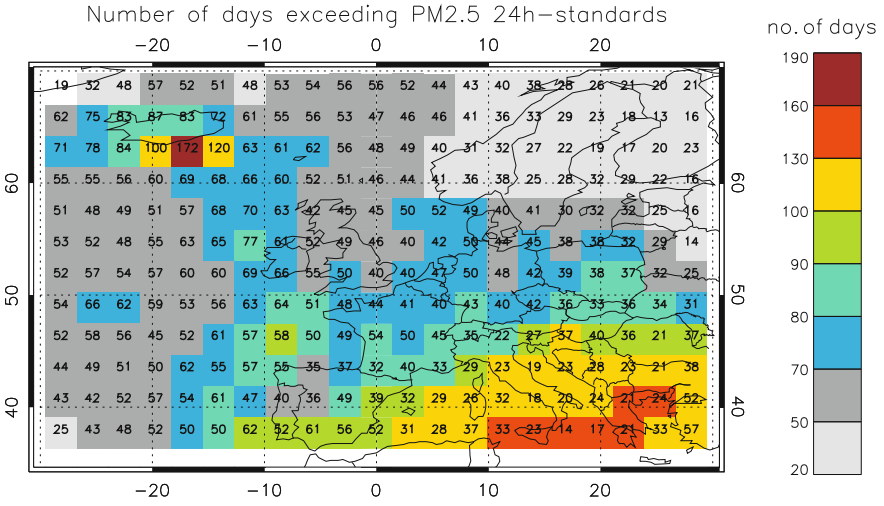

Fig. 6.5 Total number of days out of the 266 days considered (as shown in time-series in Fig. 6.4) exceeding the current WHO 24-h PM2.5 guideline of 25 μg/m^3. *Coloured boxes* depict the perturbed situation (including Laki emissions). Numbers in grid boxes denote the absolute differences (i.e. perturbed simulation minus baseline simulation)

Table 6.2 Excess mortality using 12-month mean and 24-h mean PM2.5 mass concentration ($\mu g/m^3$) data following the onset of a Laki-style eruption

Outcome and exposure metric	Sub-group	Mortality rate of disease group (deaths per year/100,000)	Population exposed (millions)	Deaths from exposure to volcanic pollution	Percent increase in mortality per 10 $\mu g/m^3$
All-cause mortality and short-term exposure to PM2.5	All ages	986	582	**27,483** (95 % CI = 22,671–32,273)	0.96 (95 % CI = 0.79, 1.13)*
Cardiopulmonary mortality and long-term exposure to PM2.5	Age >30 years	950	348	**139,018** (95 % CI = 51,221–224,165)	non-linear (see sect. 6.2)

* = Effect (given as percent increase in mortality per 10 $\mu g/m^3$ of PM2.5) based on meta analysis of existing studies (see Sect. 6.2). 95 % CI = lower and upper bounds of the 95 % confidence interval

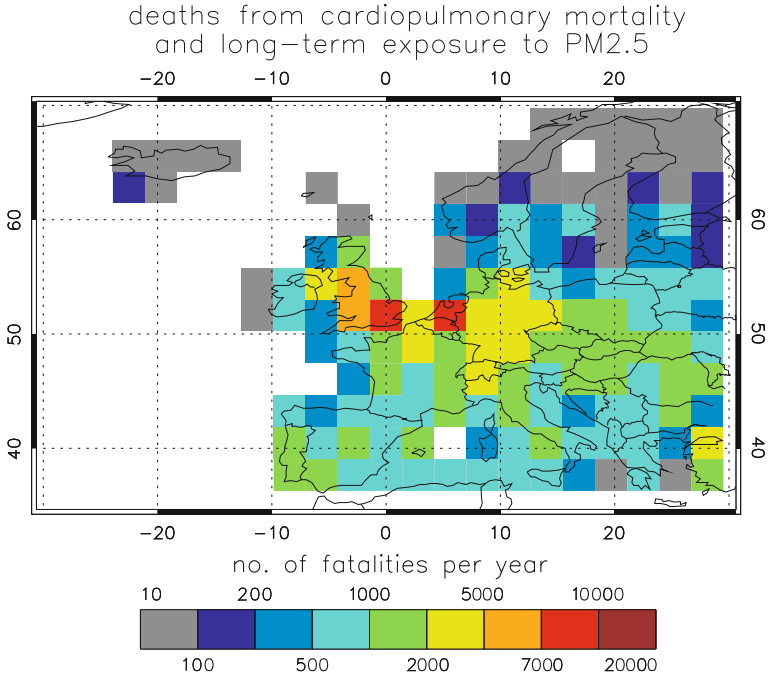

Fig. 6.6 Number of excess fatalities (i.e. due to Laki) in Europe resulting from cardiopulmonary mortality due to long-term exposure to PM2.5 in European domain in the year following the onset of a Laki-style eruption

of 8430 per year occur in the Netherlands and Belgium, 7307 in the south-east of the UK (total of 20,926 in the whole of the UK), 4690 in north-western Germany (total of 18,066 in the whole of Germany), and 3807 in northern France (total of 12,785 in the whole of France).

Using 2004 population data, some 27,000 additional all-cause fatalities from short-term exposure to PM2.5 are estimated over the course of 266 days following the onset of the eruption (Table 6.2 and Fig. 6.7). Peaks in daily all-cause mortality due to short-term exposure (Fig. 6.7a) of 664 (95 % CI 550–777) and 568 (95 % CI 470–665) deaths per day occur on 7 July and 21 June, respectively. Generally, daily all-cause mortality rates remain in excess of 100 deaths per day until mid-September. The highest cumulative total of all-cause mortality over the course of the 266 days (Fig. 6.7b) is simulated in the Netherlands and Belgium with 2,002 deaths and in southern parts of the UK with 1,515 deaths. The cumulative total of all-cause mortality from short-term exposure to PM2.5 over the course of 266 days equates to 4,083 deaths in the whole of the UK, 5,289 deaths in Germany, and 2,321 deaths in France.

Chapter 4 highlighted that the impact of the Laki eruption was not confined to Europe. Thus, it should be noted that excess mortality due to a future Laki-style eruption is likewise not restricted to Europe (the assessment of which is, however, outside the scope of the chapter presented here).

6.4 Discussion

The results showed that a future Laki-style volcanic air pollution event would be a severe health hazard. The estimated excess cardiopulmonary mortality in the year following such an eruption equates to a rise of 8 % (95 % CI 3–13) when considering the Netherlands, Belgium, UK, Ireland, Germany and France. That is an increase of around 78,000 (95 % CI 29,000–125,000) fatalities in these countries from a total of 950,000 cardiopulmonary deaths (i.e. due to all-causes) reported by the WHO for the year 2004 (Mathers et al. 2008). The study presented here also addressed all-cause mortality related to the short-term exposure to PM2.5 and has found an increase of 0.6 % when compared to the number of people who died in 2004 in the Netherlands, Belgium, UK, Ireland, Germany and France (i.e. an increase of 14,300 fatalities simulated from 2,240,000 baseline all-cause fatalities reported by the WHO (Mathers et al. 2008) for the beforehand mentioned countries).

The findings presented here can be compared with historical records of the aftermath of the 1783–1784 AD Laki eruption. Grattan et al. (2003) found a 10–20 % increase in summer mortality in 1783 in England (i.e. around 23,000 more deaths than 51-year mean deaths). Here, the UK is found to be one of the worst affected areas in Europe (after the Netherlands and Belgium), with an increase in mortality of 3.5 % (total of 20,926 additional cardiopulmonary fatalities due to eruption on top of 595,800 all-cause deaths in the UK in 2004). The results presented here also corroborate reports

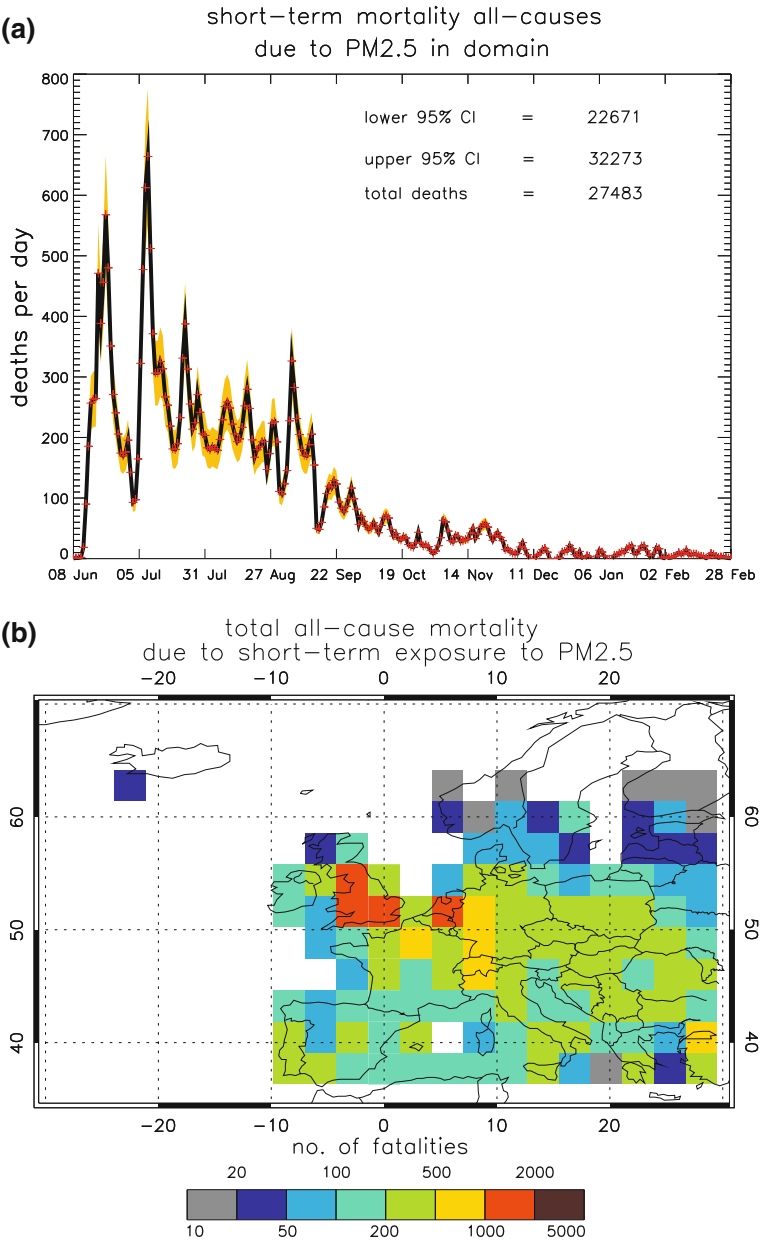

Fig. 6.7 (**a**) Time-series of daily all-cause excess mortality due to short-term exposure to PM2.5 mass concentrations starting with the onset of the Laki-style eruption on 8 June 2003 and ending 28 February 2004. The upper and lower 95 % confidence limits are shown in orange. (**b**) Cumulative total of all-cause excess mortality due to short-term exposure to PM2.5 in each grid box over the course of 266 days

of anomalously high mortality rates in France (i.e. in excess of 10,000) during the summer of 1783 (Grattan 2005). It is worth noting that the predicted excess mortality due to exposure to PM2.5 in Iceland is low despite the occurrence of peak pollutant mass concentrations over Iceland when compared to other regions such as the UK or Germany.

Why might the estimates of the percentage excess mortality be somewhat lower than the estimates based on historical records (e.g., Grattan et al. 2003), other than uncertainties in the historical reconstructions? First, there are other factors such as starvation associated with the eruption that certainly added to the number of deaths in Iceland. Second, due to a lack of C-R functions, the estimates presented here neglect the adverse health effects of exposure to elevated SO_2 concentrations, which is likely to exacerbate asthma (U.S. EPA 2008). Third, the modern population is likely to be healthier and more resilient to air pollution exposure than in the 1780s, so modern C-R functions are unlikely to extrapolate well to historical events. Fourth, only a subset of the adverse health outcomes associated with exposure to PM were considered here. Fifth, there is uncertainty regarding the precise C-R mortality functions to apply. While several recent studies generated much higher C-R functions for mortality (Brook et al. 2010 and references therein), here the study of Pope et al. (2002) was used since it involved the largest cohort and included a wide range of individual and city characteristics. Lastly, there may be inaccuracies in the model predictions for such a large volcanic event, although multi-model inter-comparisons of normal anthropogenic SO_4 pollution suggest that modelled SO_4 mass concentrations at the surface are generally predicted within 20 % of the observations (Barrie et al. 2001).

This study assessed one particular volcanic event in terms of the volatile release budget and its temporal evolution which commences at a certain time of the year. A future Laki eruption could occur in any season or in a different meteorological setting, which would alter the transport of volcanic aerosol towards Europe. In Chap. 4 it has been shown that a wintertime Laki-style eruption would yield about 20 % less SO_4 due to less effective photochemistry. Using ECMWF reanalysis, A. Simmons (unpublished data) calculated an annual mean index of the flow from Iceland to the UK for the years 1958–2010. The index presented in Fig. 6.8 highlights that the year

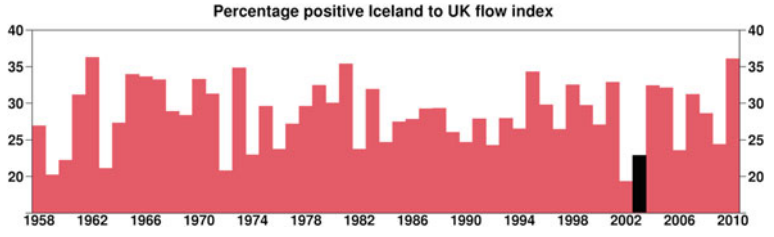

Fig. 6.8 Percentage positive (i.e. north-westerly flow) Iceland to UK flow index shown as annual means for the years 1958–2010 using ECMWF reanalysis (courtesy of Adrian Simmons). The year 2003 used for the simulations presented here is highlighted in *black colour*. Figure modified with permission from A. Simmons (unpublished data)

2003 was characterised by a low frequency of north-westerly flow (i.e. low percentage of "positive flow") from Iceland to the UK when compared to for example 2001, 2004 or 2005 during which a north-westerly flow was much more prevalent. Thus, the excess mortality rates calculated here using 2003 meteorology are likely to be a conservative estimate (as transport into Europe is regarded as one of the main factors determining the magnitude of excess mortality).

6.5 Implications

Given the historic records of the Laki eruption and the probability of a recurrence of such an event it is crucial to assess the scale on which a future Laki-style eruption could impact society. The work presented here agrees with historical records of the potential of Icelandic flood lava events to impact air quality and subsequently human health in Europe. Given the complex socio-economic framework we live in, it is important to further investigate the societal impacts of such "low-probability, high-impact" events. It should be noted that the impact of a future Laki-style eruption is not confined to human health but also has the potential to affect commercial aviation due to high SO_2 and SO_4 mass concentrations in upper parts of the atmosphere. Moreover, such an event has a huge potential to affect the environment in terms of, for example, crop failure.

The results presented here can be put in context with other major events. As part of the WHO Global Burden of Disease assessment, Cohen et al. (2004) estimated that globally 800,000 deaths in the year 2000 could be attributed to urban outdoor air pollution (in the form of PM2.5). These authors also estimate that of this total, 23,000 deaths (95 % CI = 10,000–43,000) would occur in western and central Europe. Thus, the results presented in this chapter are significant given that a total of around 139,000 additional deaths could occur in Europe due to a Laki-style eruption. Furthermore, between 250,000 and 500,000 persons die worldwide per year as a consequence of seasonal influenza (WHO 2003) and an estimated 41,000 per year in the United States, estimated to be associated with around 87 billion dollars economic burden (Molinari et al. 2007) (equivalent data are not available for Europe, although a direct scaling with population would equate to 1.6 times more deaths). The estimated excess mortality rate due to a future Laki-style Icelandic eruption is also larger than the death toll of most earthquake events. Only five earthquakes since 1900 killed more people in a single event than estimated here for Laki (USGS 2010). The number of deaths is also close to the total caused by all natural disasters in Europe over the last 100 years (142,000) (EM-DAT 2010). Investigating the negative health effects of such an eruption provides important evidence of its potential for significant public health impacts and the need to put in place appropriate risk reduction measures.

References

AirBase (2010). AirBase—the European AIR quality dataBASE. http://acm.eionet.europa.eu/databases/airbase/. Accessed Sept 2010

Baxter P (2000) Impacts of eruptions on human health. In: Stix J, Sigurdsson BF, Houghton SR (ed). Academic Press, Encyclopedia of Volcanoes, McNutt H Rymer, pp 1035–1043

Brook RD, Rajagopalan S, Pope I CA, Brook JR, Bhatnagar A, Diezroux AV, Holguin F, Hong Y, Luepker RV, Mittleman MA, Peters A, Siscovick D, Smith J, Sidney C, Whitsel L, Kaufman JD. On Behalf of the American Heart Association Council on Epidemiology, Prevention, C.O.T.K.I.C.D., Council on Nutrition, P.A. & Metabolism (2010) Particulate matter air pollution and cardiovascular disease: an update to the scientific statement from the american heart association. Circulation 121:2331–2378

Barrie LA, Yi Y, Leaitch WR, Lohmann U, Kasibhatla P, Roelofs GJ, Wilson J, McGovern F, Benkovitz C, MalliaRes MA, Law K, Prospero J, Kritz M, Bergmann D, Bridgeman C, Chin M, Christensen J, Easter R, Feichter J, Land C, Jeuken A, Kjellstrãüm E, Koch D & Rasch P (2001) A comparison of large-scale atmospheric sulphate aerosol models (COSAM): overview and highlights. Tellus B 53:615–645, ISSN: 1600–0889

Cohen AJ, Anderson HR, Ostro B, Pandey KD, Krzyzanowski M, Künzli N, Gutschmidt K, Pope III AC, Romieu I, Samet JM & Smith KR (2004) Urban air pollution. In M. Ezzati, A.D. Lopez, A. Rodgers & C.J.L. Murray, eds., Comparative Quantification of Health Risks, Global and Regional Burden of Disease Attributable to Selected Major Risk Factors, vol. 2, Chap. 17. World Health Organization, Geneva

Delmelle P, Stix J, Baxter P, Garcia-Alvarez J, Barquero J (2002) Atmospheric dispersion, environmental effects and potential health hazard associated with the low-altitude gas plume of Masaya volcano, Nicaragua. Bull Volcanol 64:423–434. doi:10.1007/s00445-002-0221-6

Durand M, Grattan J (1999) Extensive respiratory health effects of volcanogenic dry fog in 1783 inferred from european documentary sources. Environ Geochem Health 21:371–376. doi:10.1023/A:1006700921208

Durand M, Grattan J (2001) Effects of volcanic air pollution on health. Lancet 357:164–164

EM-DAT (2010). The OFDA/CRED International Disaster Database, Universite Catholique de Louvain, Brussels, Belgium. www.emdat.be. Accessed 13 Dec 2010

Franklin M, Zeka A, Schwartz J (2007) Association between PM2.5 and all-cause and specific-cause mortality in 27 US communities. J Expos Sci Environ Epidemiol 17:279–287

Grattan J (2005) Pollution and paradigms: lessons from Icelandic volcanism for continental flood basalt studies. Lithos 79:343–353

Grattan JP, Pyatt FB (1994) Acid damage to vegetation following the Laki Fissure Eruption in 1783—an historical review. Sci Total Environ 151:241–247

Grattan J (1998) The distal impact of Icelandic volcanic gases and aerosols in Europe: a review of the 1783 Laki Fissure eruption and environmental vulnerability in the late 20th century. Engineering Geology Special Publications, vol 15. Geological Society, London, pp 97–103

Grattan J, Durand M, Taylor S (2003) Illness and elevated human mortality in Europe coincident with the Laki Fissure eruption. Volcanic Degassing. In: Oppenheimer C, Pyle DM, Barclay J (eds) Special Publications, vol 213. Geological Society, London, pp 401–414

Hansell A, Oppenheimer C (2004) Health hazards from volcanic gases: a systematic literature review. Arch Environ Health 59:628–639

Klein Goldewijk K, Beusen A, Janssen P (2010) Long term dynamic modeling of global population and built-up area in a spatially explicit way, HYDE 3.1. The Holocene 20:565–573

Klemm R, Mason R (2003) Replication of reanalysis of Harvard six-city mortality study. In Revised Analyses of Time-Series of Air Pollution and Health, Health Effects Institute, Boston, Massachusetts

Mann GW, Carslaw KS, Spracklen DV, Ridley DA, Manktelow PT, Chipperfield MP, Pickering SJ, Johnson CE (2010) Description and evaluation of GLOMAP-mode: a modal global aerosol microphysics model for the UKCA composition-climate model. Geosci Model Dev 3:519–551

Mathers C, Fat DM, Boerma JT, Organization WH (eds) (2008) The global burden of disease: 2004 update. World Health Organization, Geneva, Switzerland

Molinari NAM, Ortega-Sanchez IR, Messonnier ML, Thompson WW, Wortley PM, Weintraub E, Bridges CB (2007) The annual impact of seasonal influenza in the US: Measuring disease burden and costs. Vaccine 25:5086–5096. doi:10.1016/j.vaccine.2007.03.046

Ostro B (1984) A search for a threshold in the relationship of air-pollution to mortality—a reanalysis of data on London winters. Environ Health Perspect 58:397–399

Ostro B (2004) Outdoor air pollution: assessing the environmental burden of disease at national and local levels. World Health Organization, Geneva, WHO Environmental Burden of Disease Series, No 5

Ostro B, Broadwin R, Green S, Feng WY, & Lipsett M (2006). Fine Particulate Air Pollution and Mortality in Nine California Counties: Results from CALFINE. Environ Health Perspect 114:29–33

Puett RC, Schwartz J, Hart JE, Yanosky JD, Speizer FE, Suh H, Paciorek CJ, Neas LM, Laden F (2008) Chronic particulate exposure, mortality, and coronary heart disease in the Nurses' health study. Am J Epidemiol 168:1161–1168

Pope I, Arden C (2006) Ischemic heart disease events triggered by short-term exposure to fine particulate air pollution. Circulation 114:2443–2448

Pope CA, Burnett RT, Thun MJ, Calle EE, Krewski D, Ito K, Thurston GD (2002) Lung cancer, cardiopulmonary mortality, and long-term exposure to fine particulate air pollution. Jama-J Am Med Assoc 287:1132–1141

Schmidt A, Ostro B, Carslaw KS, Wilson M, Thordarson T, Mann GW, Simmons AJ (2011) Excess mortality in Europe following a future Laki-style Icelandic eruption. Proc Nat Acad Sci 108:15710–15715

Thordarson T, Self S (2003) Atmospheric and environmental effects of the 1783–1784 Laki eruption: A review and reassessment. J Geophys Res-Atmospheres 108(D1):4011. doi:10.1029/2001JD002042

Thordarson T, Larsen G (2007) Volcanism in Iceland in historical time: Volcano types, eruption styles and eruptive history. J Geodyn 43:118–152

Thordarson T, Self S (1993) The Laki (Skaftar Fires) and Grimsvatn eruptions in 1783–1785. Bull Volcanol 55:233–263

Thordarson T, Self S, Oskarsson N, Hulsebosch T (1996) Sulfur, chlorine, and fluorine degassing and atmospheric loading by the 1783–1784 AD Laki (Skaftar fires) eruption in Iceland. Bull Volcanol 58:205–225

U.S. EPA (2008). Integrated Science Assessment (ISA) for Sulfur Oxides—Health Criteria (Final Report). U.S. Environmental Protection Agency, Washington, DC, EPA/600/R-08/047F

USGS (2010). USGS Earthquakes with 1,000 or More Deaths since 1900. http://earthquake.usgs.gov/earthquakes/world/, accessed 13 December 2010

Witham CS, Oppenheimer C (2005) Mortality in England during the 1783–1784 Laki Craters eruption. Bull Volcanol 67:15–26. doi:10.1007/s00445-004-0357-7

WHO (2003) World Health Organization— Influenza. http://www.who.int/mediacentre/factsheets/2003/fs211/en/. Accessed 13 Dec 2010

Wrigley EA, Schofield RS (1989) The population history of England 1541–1871: a reconstruction. Cambridge Univ. Press, p 794

Wong CM, Vichit-Vadakan N, Kan H, Qian Z, Teams TPP (2008) Public health and air pollution in Asia (PAPA): a multicity study of short-term effects of air pollution on mortality. Environ Health Perspect 116:1195–1202

Zanobetti A, Schwartz J (2009) The effect of fine and coarse particulate air pollution on mortality: A national analysis. Environ Health Perspect, p 117

Chapter 7
Conclusions

A comprehensive size-resolving global aerosol model (GLOMAP-mode) has been used to investigate the impact of the 1783–1784 AD Laki eruption on atmospheric chemistry, microphysical processes and the Earth's climate system. The study presented is the first to investigate the impact of the eruption on microphysical processes and the global cloud condensation nuclei budget. Moreover, in this thesis the potential impact of a future Laki-style eruption has, for the first time, been put quantitatively into a modern societal context. Furthermore, the sensitivity of the global pre-industrial CCN budget to time-averaged volcanic sulphur emissions has been investigated using GLOMAP-mode, which allowed identification of the key chemical and microphysical processes determining the subsequent cloud-radiative effect.

In response to the questions raised in Sect. 1.6, a summary of the major findings is presented below.

7.1 Summary of Major Findings

1. **GLOMAP-mode has been used to examine the role of time-averaged volcanic sulphur emissions in the pre-industrial era.**

   (a) The balance between chemical and microphysical processes shifts even under modest perturbations to the magnitude of the volcanic sulphur flux (Table 3.1). Using GLOMAP-mode allowed identification of the key microphysical processes that govern the formation of climate-relevant CCN-sized particles: nucleation and condensation, which in turn are governed by the relative balance of gas-phase oxidation to aqueous-phase oxidation of SO_2 (Sect. 3.3.1).

   (b) Volcanic sulphur emissions contribute around 31 % to the global mean CCN number concentrations at low-level cloud altitude in the pre-industrial era. Without volcanic sulphur emissions, GLOMAP-mode predicts global annual mean CCN number concentrations of 60 cm^{-3} at 970 m altitude,

A. Schmidt, *Modelling Tropospheric Volcanic Aerosol*, Springer Theses,
DOI: 10.1007/978-3-642-34839-6_7, © Springer-Verlag Berlin Heidelberg 2013

whereas concentrations of 87 $cm^{-3}s$ are predicted when including volcanic sulphur emissions (i.e. an increase of 45 %) (Sect. 3.3.2).

(c) Both globally and regionally, CCN number concentrations are more sensitive to the strength of the volcanic sulphur flux than to global and regional changes in the flux of other, non-volcanic sulphur sources (Sect. 3.3.2). Assuming that the volcanic source strength is a factor of two greater than suggested by Andres and Kasgnoc (1998), results in a 19 % increase in global annual mean CCN number concentrations at 970 m altitude (Sect. 3.3.2).

(d) Under pre-industrial atmospheric conditions, volcanic sulphur emissions induce a significant global annual mean first AIE of $-1.45\,W\,m^{-2}$ with a peak of $-10.9\,W\,m^{-2}$ in stratocumulus cloud regions of the southern tropics (Table 3.3). Assuming that the magnitude of the volcanic sulphur flux strength is twice as high as suggested by Andres and Kasgnoc (1998) leads to a difference in the global annual mean first AIE of $-0.58\,W\,m^{-2}$, whereas a halving of the source strength results in $+0.45\,W\,m^{-2}$ (Table 3.3). Based on this large aerosol indirect effect, it is shown that the uncertainty in the volcanic sulphur source strength leads to a substantial difference in the magnitude of the aerosol indirect effect in the baseline from which present-day aerosol radiative forcing is calculated. The magnitude of the indirect radiative effect of uncertain volcanic sulphur emissions is likely to be larger under clean pre-industrial conditions than under polluted modern-day conditions. Therefore, even if the volcanic sulphur source strength did not change since the pre-industrial era, pre-industrial volcanic sulphur emissions could produce an aerosol radiative forcing that has to be accounted for in future radiative forcing assessments.

2. GLOMAP-mode has been used to examine the impact of the 1783–1784 AD Laki eruption on chemical and microphysical processes and on the global CCN budget.

(a) The 1783–1784 AD Laki eruption provided a very large source of SO_2 to the pre-industrial atmosphere resulting in enhanced gas-phase oxidation of SO_2 and the subsequent nucleation of H_2SO_4 vapour forming new particles in the upper troposphere/lower stratosphere (Sects. 4.3.1 and 4.3.6). These newly formed particles grow by coagulation and condensation during long-range transport. Following Laki, chemical and microphysical processes controlling new particle formation and removal are fundamentally different when compared to the unperturbed pre-industrial atmosphere (Sect. 4.3.1).

(b) Laki had a strong potential to profoundly alter cloud microphysical properties and hence to exert substantial indirect climate effects. During the first three months, Laki became the dominant source of climate-relevant aerosol resulting in upper tropospheric CCN number concentrations in excess of $1{,}000\,cm^{-3}$ (factor of 65 increase), and boundary layer CCN of around $400\,cm^{-3}$ (factor of 26 increase) (Sect. 4.3.8). Due to long-range transport, CCN number concentrations are predicted to increase by a factor of $\sim$14 in Asia and by a factor of $\sim$10 in North America (Sect. 4.3.8).

(c) Both the microphysical and chemical processes controlling the change in the particle concentrations and particle size distribution display a non-linear response to the seasons in which the eruption commences (Sect. 4.3.6). For example, the simulations reveal that an equivalent wintertime eruption would yield around 20 % less SO_4 aerosol (Sect. 4.3.3) and, averaged over the first three months of the eruption, upper tropospheric CCN number concentrations are predicted to be only about one-third of these of a summertime eruption (Sect. 4.3.8).

(d) The simulated reductions in visibility closely follow (in terms of the temporal pattern and magnitude) reconstructions of the haze opacity (Thordarson and Self 2003). However, using GLOMAP-mode could not reproduce the SO_4 deposition observed in Greenland ice-cores which warrants further investigation. Nonetheless, other diagnostics such as the yield are in good agreement with both numerical and theoretical evidence (Table 4.1) corroborating the model's capabilities.

3. **A physically-based aerosol activation scheme has been used to investigate the impact of the 1783–1784 AD Laki eruption on cloud drop number concentrations (CDNC). Subsequently, a radiative transfer code has been used to quantify the magnitude of the first aerosol indirect effect (AIE) following the eruption.**

(a) For the first seven months of the summertime eruption, GLOMAP-mode predicts global mean CDNC of around 125 cm^{-3} compared with ~65 to ~91 cm^{-3} in the unperturbed pre-industrial atmosphere (Sect. 5.3.1). Studies of modern-day clouds and cloud systems suggest that these very large changes in CDNC are likely to have caused substantial changes in precipitation and cloud dynamics (Levin and Cotton 2008).

(b) Mass-only aerosol schemes cannot capture the growth of new aerosol to CCN (and hence cloud drop size) due to direct growth and coagulation. Thus, in order to adequately simulate the impact of such an eruption, the aerosol number, size and mass needs to be diagnosed.

(c) When averaged over the first three months of the eruption, a peak first AIE of $-29.4\ W\ m^{-2}$ is simulated using GLOMAP-mode together with a radiative transfer code (Sect. 5.3.3). The first AIE is substantial along regions that feature persistent stratocumulus cloud decks, highlighting that the impact of high-latitude eruptions on the atmosphere and subsequently the climate system is likely to have been more complex than previously thought.

(d) The magnitude of the first AIE (peak of $-29.4\ W\ m^{-2}$) is likely to have been comparable to that of the direct radiative effect calculated in previous studies (Highwood and Stevenson 2003; Oman et al. 2006a). However, the combined magnitude of the radiative effects (i.e. direct + indirect effect) would be too large to be in agreement with the observational evidence of temperature changes following the eruption, with implications for our understanding of the climate response to such an eruption. Either the observational records are incomplete or the numerical models used overestimate the radiative effects

induced by the eruption. Alternatively, there are uncertainties associated with the Laki SO_2 emission profile; both the injection height and the amount of SO_2 released will play an important role in determining the magnitude of the radiative effects. Reducing all uncertainties mentioned above might provide a more reasonable agreement between the observations and the model predictions.

(e) The season in which such an eruption commences plays a critical role in determining the magnitude of the climate impact. A wintertime eruption is latitudinally more confined and thus has a slightly greater impact on CDNC than an equivalent summertime eruption (Sect. 5.3.1). However, the peak first AIE during a summertime eruption is a factor of two greater than that during a wintertime eruption, which can be attributed to seasonal variations in insolation as well as to seasonal differences in the abundance of low-level stratocumulus clouds (Sect. 5.3.3).

4. **GLOMAP-mode has been used to explore the potential impact of a future Laki-style eruption on air pollution and mortality in Europe.**

(a) The concentration of particulate matter with diameters smaller than 2.5 μm (PM2.5) is predicted to double across central, western and northern Europe during the first three months of a future Laki-style eruption. Over land areas of Europe, the current World Health Organization 24 h air quality guideline for PM2.5 is exceeded on an additional 36 days on average (range 13–55 days) over the course of the eruption (Sect. 6.3.1).

(b) Based on the changes in particulate air pollution, an estimated 139,000 additional cardiopulmonary fatalities could occur in Europe (Sect. 6.3.2). Such a volcanic air pollution event would therefore be a severe health hazard, increasing excess mortality in Europe on a scale that likely exceeds excess mortality due to seasonal influenza. Moreover, the death toll of such an eruption would be larger than that of all but five of the world's earthquakes since 1900.

7.2 Future Work

Chapter 4 aimed to quantify first order effects of the Laki eruption on CCN number concentrations and is the first study showing that this effect was significant. However, the effects of these substantial changes in CCN number concentrations on atmospheric circulation and the subsequent feedback of dynamics-induced changes on CCN itself remain to be assessed. Nober et al. (2003) showed that such feedbacks are potentially important. For Laki, dynamics-induced changes on CCN are expected to be rather small—nonetheless, aerosol-climate-chemistry models such as UKCA should be used to explore this feedback.

The increase in upper tropospheric CCN-sized particle concentrations following the Laki eruption warrants investigating the impact on ice crystal concentrations. Sassen (1992) proposed that, following the 1991 Mt. Pinatubo eruption, the influx of large-sized volcanic aerosol particles from the stratosphere into cirrus-generating regions of the upper troposphere had the potential to perturb the microphysical properties of natural cirrus clouds. The link between volcanic aerosol and cirrus cloud modification would have significant implications for the climatic impact induced by volcanic eruptions because cirrus cloud modification could result in an increased cloud greenhouse effect (i.e. net warming due to absorption of terrestrial radiation) (Sassen 1992). To date, both observational-based (Wylie and Menzel 1999; Luo et al. 2002) and numerical-based (Jensen and Toon 1992; Kärcher and Lohmann 2002; Liu and Penner 2002; Lohmann et al. 2003) studies addressing the potential impact of the Mt. Pinatubo aerosol on cirrus clouds have been conducted; however, the results remain inconclusive. Future studies should investigate whether the substantial increase in upper tropospheric CCN number concentrations could have induced an aerosol-cirrus radiative effect or not. The data sets created for this thesis lend themselves for such a follow-up study.

Chapter 5 revealed a discrepancy between the observational record of surface temperature cooling following the Laki eruption and the combined magnitude of the modelled direct and indirect radiative effects. Thus, future work should investigate whether, for example, eruption-induced changes in the dynamics of the atmosphere result in lower radiative effects. Furthermore, by using a fully coupled chemistry-aerosol-climate models such as UKCA, both the direct and indirect radiative effect can be calculated on-line.

There is a wealth of contemporary accounts describing the impact of the Laki eruption. So far, relatively little work in relation to the amount of records has been done comparing model results with historical records or using numerical models for studying, for example, regional impacts. Moreover, none of the Laki modelling studies addressed the impact of the 15 Tg of HCl and the 7 Tg of HF released during the eruption on atmospheric chemistry.

Furthermore, with increasing computing power, future work could involve running multi-annual simulations in order to investigate the probability distribution of, for example, deposition to Greenland, impact on CCN number concentrations and total volcanic SO_4 aerosol yield.

The eruption of the Icelandic Eyjafjallajökull volcano in 2010 not only alerted European governments to the risks posed by volcanic ash but also to those that could arise from so-called "low probability, high-impact", sulphur-dominated volcanic events such as the 1783–1784 AD Laki eruption. Chapter 6 highlighted the potential of these events to affect human health due to increased air pollution, however, the full range of the impacts on modern society are virtually unknown. Thus, pursuing further inter-disciplinary research is paramount. For example, global models such as GLOMAP-mode could be used together with probabilistic descriptions of meteorological and volcanic variability in order to quantify the likelihood of the impacts of

SO_2 and SO_4 on human health, aviation and ecosystems. Such results will enable the European governments to take precautionary measures to mitigate the hazard from Icelandic eruptions. In particular, it should be noted that aviation could face drastic challenges as virtually nothing is known about the consequences of high SO_2 and particulate concentrations in flight cabins and the impact on aircraft in general.

References

Andres RJ, Kasgnoc AD (1998) A time-averaged inventory of subaerial volcanic sulfur emissions. J Geophys Res 103:25251–25262

Highwood EJ, Stevenson DS (2003) Atmospheric impact of the 1783–1784 Laki eruption: part II - climatic effect of sulphate aerosol. Atmos Chem Phys 3:1177–1189

Jensen EJ, Toon OB (1992) The potential effects of volcanic aerosols on cirrus cloud microphysics. Geophys Res Lett 19:1759–1762

Kärcher B, Lohmann U (2002). A parameterization of cirrus cloud formation: homogeneous freezing including effects of aerosol size. J Geophys Res 107(D23):4698. doi:10.1029/2001JD001429

Levin Z, Cotton WR (eds) (2008) Aerosol pollution impact on precipitation: a scientific review. Springer, Berlin, p 386

Liu X, Penner JE (2002) Effect of Mount Pinatubo H_2SO_4/H_2O aerosol on ice nucleation in the upper troposphere using a global chemistry and transport model. J Geophys Res 107(D12):4141. doi:10.1029/2001JD000455

Lohmann U, Kärcher B, Timmreck, C (2003) Impact of the Mount Pinatubo eruption on cirrus clouds formed by homogeneous freezing in the ECHAM4 GCM. J Geophys Res 108(D18):4568. doi:10.1029/2002JD003185

Luo Z, Rossow WB, Inoue T, Stubenrauch CJ (2002) Did the eruption of the Mt. Pinatubo volcano affect cirrus properties? J Clim 15:2806–2820

Nober FJ, Graf HF, Rosenfeld D (2003) Sensitivity of the global circulation to the suppression of precipitation by anthropogenic aerosols. Glob Planet Chang 37:57–80

Oman L, Robock A, Stenchikov GL, Thordarson T, Koch D, Shindell DT, Gao C (2006a) Modeling the distribution of the volcanic aerosol cloud from the 1783–1784 Laki eruption. J Geophys Res 111:D12209. doi:10.1029/2005JD006899

Sassen K (1992) Evidence for liquid-phase cirrus cloud formation from volcanic aerosols: climatic implications. Science 257:516–519

Thordarson T, Self S (2003) Atmospheric and environmental effects of the 1783–1784 Laki eruption: a review and reassessment. J Geophys Res-Atmos 108(D1):4011. doi:10.1029/2001JD002042

Wylie DP, Menzel WP (1999) Eight years of high cloud statistics using HIRS. J Clim 12:170–184

Appendix A

A.1 Inverse-Variance Mean Calculation

In order to obtain a combined effect for all-cause mortality due to short-term exposure to PM2.5, the four studies listed in the Table 6.1 were used to calculate the inverse-variance mean which assigns weight to each study based on the inverse of the variance. The weight assigned to each of the four studies was calculated as follows:

$$\mathrm{wt_i} = \frac{1}{\mathrm{var_i}} \tag{A.1}$$

where wt_i denotes the weight of each respective study and var_i denotes the variance of each respective study. The weighted mean excess risk ($\overline{ER}$) is then the sum of the products $wt_i ER_i$ (i.e. excess risk of each study multiplied by weight of each study) divided by the sum of the weights:

$$\overline{\mathrm{ER}} = \frac{\sum \mathrm{wt_i ER_i}}{\sum \mathrm{wt_i}} \tag{A.2}$$

The standard error of $\overline{ER}$ is then the square root of the variance which is equivalent to the reciprocal of the square root of the sum of the weights:

$$\mathrm{SE}_{\overline{\mathrm{ER}}} = \frac{1}{\sqrt{\sum \mathrm{wt_i}}} \tag{A.3}$$

The 95 % confidence interval for $\overline{ER}$ was calculated as follows:

$$\text{lower limit} = \overline{\mathrm{ER}} - 1.96 * \mathrm{SE}_{\overline{\mathrm{ER}}} \tag{A.4}$$

$$\text{upper limit} = \overline{\mathrm{ER}} + 1.96 * \mathrm{SE}_{\overline{\mathrm{ER}}} \tag{A.5}$$

A. Schmidt, *Modelling Tropospheric Volcanic Aerosol*, Springer Theses,
DOI: 10.1007/978-3-642-34839-6, © Springer-Verlag Berlin Heidelberg 2013

Appendix B

B.1 Index of the Atmospheric Flow Between Iceland and the UK

Adrian Simmons (ECMWF, unpublished data) investigated the variability of the atmospheric flow between Iceland and the United Kingdom (UK) using six-hourly wind fields between September 1957 to December 1998 (using ERA-40 reanalysis from Uppala et al. 2005) and January 1989 to December 2010 (using ERA-Interim reanalysis from Dee et al. 2011). Simmons (unpublished data) analysed the wind fields at three constant pressure levels of 300, 500 and 700 hPa corresponding to around 9, 5.5 and 3 km, respectively. The calculated flow index was designed to be positive for north-westerly flow (i.e. flow between Iceland and the UK) and was evaluated separately at ten locations (i.e. 20° W, 65° N; 15° W, 65° N; 20° W, 62.5° N; 15° W, 62.5° N; 10° W, 62.5° N; 15° W, 60° N; 10° W, 60° N; 10° W, 57.5° N; 5° W, 57.5°N). Subsequently, those ten locations were averaged by means of area weighting (i.e. cos(latitude) weighting).

The flow index has been calculated as follows:

$$|\mathrm{v}| \begin{cases} \cos(2\theta) & \text{if } |\theta| < \pi/2 \\ -1 & \text{if } |\theta| \geq \pi/2. \end{cases} \tag{B.1}$$

In Eq. B.1, $|\mathrm{v}|$ denotes the wind speed (ms^{-1}) and θ denotes the angular deviation of the flow direction from north-westerly.

A. Schmidt, *Modelling Tropospheric Volcanic Aerosol*, Springer Theses,
DOI: 10.1007/978-3-642-34839-6, © Springer-Verlag Berlin Heidelberg 2013

Glossary

The → symbol denotes a cross-reference to a related glossary entry.

Acid rain = Rain with a pH ranging from 2 to 4. Pure water in equilibrium with atmospheric CO_2 has a pH of 5.6 (Sigurdsson et al. 2000).

Aerosol = Suspension of solid or liquid particles in the air ranging in size from a few nanometres (nm) to around 100 micrometres (μm) in diameter (Seinfeld and Pandis 1998).

Aerosol microphysics model = A numerical model which is designed to simulate the → *aerosol* particle size distribution by means of representing the key microphysical processes (nucleation, coagulation, condensation and cloud processing) which control the evolution of the size distribution.

Aerosol optical depth (AOD) = Measure of the amount of light prevented from passing through the atmospheric column by airborne particles (Solomon et al. 2007).

Albedo = The term surface albedo refers to the reflectivity of the surface, ranging from 0 (perfectly absorbing) to 1 (perfectly reflecting), which is important in determining surface temperature. The Earth's planetary albedo is the fraction of the Sun's incoming radiation that reflects off the Earth and back into space (Sigurdsson et al. 2000).

Andesite = Volcanic rock with 53–63 % silica (SiO_2) content (Sigurdsson et al. 2000).

Ash = → *Pyroclasts* smaller than 2 mm in diameter (Sigurdsson et al. 2000).

Atmospheric lifetime = Also referred to as "residence time". The lifetime of a chemical species in the steady state is defined as the atmospheric → *burden* of the species divided by either the total loss rate or the total production rate (American Meteorological Society 2011).

A. Schmidt, *Modelling Tropospheric Volcanic Aerosol*, Springer Theses,
DOI: 10.1007/978-3-642-34839-6,

Attributable fraction (AF) = A measure of the public health impact of a causative factor; proportion of a disease in a group that is exposed to a particular factor which can be attributed to their exposure to that factor (Centre for Disease Control and Prevention 2011).

Basalt = Volcanic rock with SiO_2 (50 wt%), Al_2O_3 (15 wt%), CaO (12 wt%) and roughly equal amounts of FeO and MgO (10 wt%). The alkalis ($Na_2O + K_2O$) determine most of the composition differences (Sigurdsson et al. 2000).

Basaltic magma = is typically erupted at temperatures of 1,000–1,300 °C resulting in a relatively low viscosity of the → *magma* (Sigurdsson et al. 2000).

Burden = The amount of a gaseous substance or particulates in the atmosphere at a given time (Solomon et al. 2007).

Chemical lifetime = The time required for the concentration of a chemical species to decrease to 1/e of its original concentration (Solomon et al. 2007).

Chemical Transport Model (CTM) = Numerical model designed to simulate the chemical processing, transport, and deposition of various atmospheric species. CTMs normally use prescribed meterorology.

Cloud Condensation Nuclei (CCN) = Hygroscopic aerosol particles onto which water vapour can condense to form → *cloud drops* (American Meteorological Society 2011).

Cloud drop = Also referred to as "cloud droplet" (i.e. considered smaller and falling more slowly than a cloud drop). Spherical particle formed by condensation of water vapour on a → *cloud condensation nuclei*, ranging from a few micrometers to a few tens of micrometers in diameter (American Meteorological Society 2011).

Cloud-radiative forcing = Difference between the all-sky (i.e. with clouds) and the clear-sky (i.e. without clouds) Earth's radiation budget in units of Watts per square metre (W m^{-2}) (Solomon et al. 2007).

Cohort study = A type of observational analytic study in which participation is based on exposure characteristics or membership in a particular group. Disease, death, or other health outcomes are then assessed and compared (Centre for Disease Control and Prevention 2011).

Continental flood basalt (CFB) provinces = Large volumes of → *basalts* of predominantly tholeiitic (→ *Tholeiite*) composition forming extensive sheet flows with a few intervening sedimentary deposits. CFBs are thought to have been erupted in geologically short periods of time at high extrusion rates (Sigurdsson et al. 2000).

Degassing = The process by which → *magma* loses its dissolved → *volatile* species as pressure decreases (Sigurdsson et al. 2000).

Dose-response = Association between an exposure and a health outcome (Centre for Disease Control and Prevention 2011).

Effusive eruption = Non-explosive extrusion of → *magma* at the surface. However, effusive eruptions are clearly related to explosive activity in many instances (Sigurdsson et al. 2000).

Equilibrium vapour pressure = The pressure of a vapour in equilibrium with its condensed phase (liquid or solid) (American Meteorological Society 2011).

Explosive eruption = Any eruption in which the → *magma* is torn into fragments (→ *Fragmentation*) by gas pressure as it leaves the → *vent* (Sigurdsson et al. 2000).

Fire fountain = Also referred to as "lava fountain". A fire fountain is created when → *basaltic magma* exiting a → *fissure* is disrupted into a spray.

Fissure = A linear volcanic → *vent* (Sigurdsson et al. 2000).

Fissure eruption = An eruption that takes place along an elongated → *fissure*, rather than from a central → *vent* (Sigurdsson et al. 2000).

Flood lava volcanism = Basaltic effusive eruptions producing large (>1 km^3) lava volumes (Thordarson and Larsen 2007).

Fragmentation = The transition from a continuous melt with a dispersed gas phase to disconnected parcels of bubbly melt within a continuous gas phase (Sigurdsson et al. 2000).

General Circulation Model (GCM) = Numerical model that represents fundamental physical processes in the atmosphere, ocean, cryosphere and land surface (Solomon et al. 2007).

Glass inclusion = If a liquid is cooled very rapidly, it may harden to a glass and not crystallise. During crystallisation of magma, many crystals grow imperfectly, trapping small portions of silicate melt inside the crystals. If the magma cools rapidly, these trapped inclusions form a → *glass* (Sigurdsson et al. 2000).

Hawaiian-type eruption = A relatively gentle type of explosive eruption involving lava fountains and minor ash and → *scoria* production (Sigurdsson et al. 2000).

Holocene = Geological epoch which commenced around 11,700 years before present.

Hot spot = A large volcanic centre created by partial melting of the mantle due to the rise of deep, hot mantle material (Sigurdsson et al. 2000).

Insolation = Amount of solar radiation reaching the Earth by latitude and by season (Solomon et al. 2007).

Irradiance = Amount of radiant energy emitted from the Sun (Solomon et al. 2007).

Lava = Molten rock expelled at the Earth's surface by volcanic processes (Sigurdsson et al. 2000).

Lithic fragments = Pieces of the pre-existing volcanic system which are incorporated and ejected during an eruption (Sigurdsson et al. 2000).

Mafic rocks = Contain high proportions of minerals rich in MgO, FeO, and CaO, i.e. olivine, pyroxene, amphibole and biotite. → *Basalt* is a mafic rock (Sigurdsson et al. 2000).

Magma = Natural silicate melt with or without suspended crystals and bubbles (Sigurdsson et al. 2000).

Meta-analysis = Use of several statistical methods for integrating results from individual studies.

Mixed eruption = Volcanic eruption that features both, → *effusive eruption* and → *explosive eruption* styles (Thordarson and Larsen 2007).

Mixing ratio = The number of moles of a gas per mole of air (given in units of mole per mole, or equivalently in units of volume of gas per volume of air).

Mortality rate = A measure of the frequency of occurrence of death in a defined population during a specified time interval (Centre for Disease Control and Prevention 2011).

Petrological method = Difference between the → *volatile* component in a pre-eruptive melt (glassy melt inclusion) and in a post-eruptive melt (matrix glass) used to determine the amount of a → *volatile* component released per kg of erupted → *magma* (Devine et al. 1984).

Phreatomagmatic activity = → *Volcanic activity* resulting from the interactions between → *magma*/→ *lava* and groundwater, surface water or ice (Sigurdsson et al. 2000).

Pyroclast = A fragment of → *magma* (Sigurdsson et al. 2000).

Radiative effect = Used throughout this thesis to denote an unrelated measure of, for example, a change in cloud amount on the → *irradiance*.

Radiative forcing = Change in the net → *irradiance* (i.e. downward minus upward) at the → *tropopause* due to, for example, change in species concentration or the output of the Sun (Solomon et al. 2007). In IPCC reports defined as the change relative to the year 1750 (i.e. pre-industrial), thus the term → *radiative effect* has been used in this thesis.

Reanalysis = Analysis of atmospheric temperature, wind, pressure and other meteorological quantities that are created by using fixed numerical models and assimilation techniques to process past meteorological data (Solomon et al. 2007).

Relative risk (RR) = A comparison of the risk of a health-related event such as disease or death in two groups (Centre for Disease Control and Prevention 2011).

Residence time = → *Chemical lifetime*.

Scattering coefficient = A measure of the extinction due to scattering of monochromatic radiation as it traverses a medium containing scattering particles. Usually expressed as a volume scattering coefficient with units of reciprocal length (i.e., area per unit volume), but also as a mass scattering coefficient with units of area per unit mass (American Meteorological Society 2011).

Scoria = A → *pyroclast* containing bubbles that are typically several millimetres in diameter (Sigurdsson et al. 2000).

Stratocumulus clouds (Sc clouds) = Low level clouds usually below 2,400 m, characterised by large, dark grey or white cloud masses that are often broken in rolls and patches. Stratocumulus clouds cover around one-third of the oceans surface and have an → albedo of 0.3–0.7 (Klein and Hartmann 1993).

Subaerial volcanism = → *Volcanism* that occurs at the Earth's surface.

Submarine volcanism = → *Volcanism* that occurs underwater (mainly beneath the oceans).

(Sub-)Plinian activity = Majority of mass is discharged during phases characterised by the formation of high, convective eruption columns (Sigurdsson et al. 2000).

Strombolian eruption = Eruption with a low-viscosity → *basaltic magma* featuring a series (often rhythmical) of moderate explosions and/or fountaining of lava above a → *vent* or crater (Sigurdsson et al. 2000).

Stratosphere = The region of the atmosphere above the → *troposphere* between 10–17 and 50 km (i.e. base of the mesosphere) (American Meteorological Society 2011).

Tephra = Formed by → *fragmentation* of primarily silicic → *magma* during an → *explosive eruption* (Sigurdsson et al. 2000).

Tholeiite = A relatively silicic and iron-rich → *basalt* (Sigurdsson et al. 2000).

Troposphere = The lowermost portion of the atmosphere from the Earth's surface to the → *tropopause*. The troposphere is the portion of the atmosphere where most the clouds and weather occurs (American Meteorological Society 2011).

Tropopause = Boundary between the → *troposphere* and → *stratosphere* ranging from 9 km at high latitudes to around 16 km in the tropics (Sigurdsson et al. 2000).

Vent = Surface opening from which volcanogenic material is erupted (Sigurdsson et al. 2000).

Volatile = An element or compound such as H_2O or CO that forms a gas at relatively low pressure and magmatic temperatures. Volatiles can be dissolved in silicate melts, can occur as bubbles of exsolved gas, and can crystallise in minerals such as biotite and amphibole (Sigurdsson et al. 2000).

Volcanic activity = Includes → *magma* generation, its transport through the Earth's interior and its expulsion in form of → *lava* at the surface of a planet (Sigurdsson et al. 2000).

Volcanism = Processes linked to → *volcanic activity*.

Volcanic sulphate aerosol = Small droplets of sulphuric acid (H_2SO_4 formed in the atmosphere from oxidation of sulphur-rich gases (Sigurdsson et al. 2000). A composition of 75 wt% of H_2SO_4 and 25 wt% of H_2O is commonly assumed for volcanic sulphate → *aerosol* in the → *stratosphere* (Hamill et al. 1977). Throughout this thesis it is assumed that the volcanic aerosol exists as H_2SO_4. $2H_2O$ which is equivalent to 73 wt% of H_2SO_4 and 27 wt% of H_2O

Volcanic winter = Term used for the severe global and regional cooling that can be cause by large amounts of → *volcanic sulphate aerosol* in the atmosphere after very large volcanic eruptions (Sigurdsson et al. 2000).

Yield = The integrated mass of a substance (e.g. → *volcanic sulphate aerosol*) produced over a certain period of time.

References

American Meteorological Society (2011) Glossary of meteorology. http://amsglossary.allenpress.com/glossary. Accessed 19 Feb 2011

Centre for Disease Control and Prevention (2011) Epidemiology glossary. http://www.cdc.gov/reproductivehealth/EpiGlossary/glossary.htm. Accessed 19 Feb 2011

Dee D, Uppala SM, Simmons AJ, Berrisford P, Poli P, Kobayashi S, Andrae U, Balmaseda MA, Balsamo G, Bauer P, Bechtold P, Beljaars ACM, van de Berg L, Bidlot J, Bormann N, Delsol C, Dragani R, Fuentes M, Geer AJ, Haimberger L, Healy S, Hersbach H, Hólm EV, Isaksen L, Kallberg P, Köhler M, Matricardi M, McNally AP, Monge-Sanz BM, Morcrette JJ, Peubey C, de Rosnay P, Tavolato C, Thépaut JN Vitart F (2011) Configuration and performance of the data assimilation system. Q J R Meteorol Soc The ERA-Interim reanalysis (submitted)

Devine JD, Sigurdsson H, Davis AN, Self S (1984) Estimates of sulfur and chlorine yield to the atmosphere from volcanic eruptions and potential climatic effects. J Geophys Res 89:6309–6325

Hamill P, Toon OB, Kiang CS (1977) Microphysical processes affecting stratospheric aerosol particles. J Atmospheric Sci 34:1104–1119

Klein SA, Hartmann DL (1993) The seasonal cycle of low tratiform clouds. J Climate 6:1587–1606

Seinfeld J and Pandis S (1998). Atmospheric chemistry and physics: from air pollution to climate change. Wiley, New York, 1326 pp

Sigurdsson H, Houghton BF, McNutt SR, Rymer H, Stix J (eds) (2000). Encyclopedia of volcanoes. Academic Press, San Diego, 1417 pp

Solomon S, Qin D, Manning M, Chen Z, Marquis M, Averyt K, Tignor M, Miller H (eds) (2007) Contribution of Working Group I to the Fourth Assessment Report of the Intergovernmental Panel on Climate Change, 2007. Cambridge University Press, Cambridge, UK and New York, NY, USA 996 pp

Thordarson T, Larsen G (2007) Volcanism in Iceland in historical time: volcano types, eruption styles and eruptive history. J Geodyn 43:118–152

Uppala SM, KÃVllberg PW, Simmons AJ, Andrae U, Bechtold VDC, Fiorino M, Gibson JK, Haseler J, Hernandez A, Kelly GA, Li X, Onogi K, Saarinen S, Sokka N, Allan RP, Andersson E, Arpe K, Balmaseda MA, Beljaars ACM, Berg LVD, Bidlot J, Bormann N, Caires S, Chevallier F, Dethof A, Dragosavac M, Fisher M, Fuentes M, Hagemann S, HÃŞlm E, Hoskins BJ, Isaksen L, Janssen PAEM, Jenne R, Mcnally AP, Mahfouf JF, Morcrette JJ, Rayner NA, Saunders RW, Simon P, Sterl A, Trenberth KE, Untch A, Vasiljevic D, Viterbo P, Woollen J (2005) The ERA-40 re-analysis. Q J R Meteorol Soc 131:2961–3012